# CHEMICAL AND GENETIC MODIFICATION OF VIRUS-LIKE PARTICLES FOR APPLICATIONS IN VACCINE DESIGN AND DRUG DELIVERY

A Dissertation
Presented to
The Academic Faculty

By

Stephen Nicholas Crooke

In Partial Fulfillment
of the Requirements for the Degree
Doctor of Philosophy in Chemistry

Georgia Institute of Technology

August 2018

**CHEMICAL AND GENETIC MODIFICATION OF VIRUS-LIKE PARTICLES FOR APPLICATIONS IN VACCINE DESIGN AND DRUG DELIVERY**

Approved by:

Dr. M.G. Finn, Advisor
School of Chemistry and Biochemistry
*Georgia Institute of Technology*

Dr. Loren Williams
School of Chemistry and Biochemistry
*Georgia Institute of Technology*

Dr. Nicholas Hud
School of Chemistry and Biochemistry
*Georgia Institute of Technology*

Dr. Julia Babensee
Wallace H. Coulter Department of Biomedical Engineering
*Georgia Institute of Technology*

Dr. Susan Thomas
George W. Woodruff School of Mechanical Engineering
*Georgia Institute of Technology*

Date Approved: May 23, 2018

**Acknowledgments**

First and foremost, I would like to thank my parents and family. There is really not a way for me to describe in words how incredibly supportive they all have been over the years. Thanks for always believing in me and encouraging me to reach for my dreams.

A special thanks to my advisor, Professor M.G. Finn, who is far and beyond the nicest person I have ever met. He is perhaps the best boss you could have as he never demands work from you; rather, he stokes an intellectual fire that drives you to work hard of your own volition. His passion and enthusiasm for science is second-to-none and has been a true inspiration over the years.

I thank Dr. Jiri Schimer for being a fantastic labmate, a great gym partner (and motivator), and an even better friend. I look forward to sharing a cold beer and warm sauna in Prague someday.

Special thanks to Asheley Chapman and Jeff Noble for following me down the long and winding road of immunology. You made the lab and "mouse house" fun places to work, and I know that you will both have incredibly successful careers.

Thanks to all of the other members of the Finn lab who have been there along the course of my journey to provide aid, assistance, and support through the years: Igor Rupniewski, Cody Higginson, Allison Aioub, Nick Bruno, Zhishuai Geng, Robert Hincapie, Liangjun Zhao, Soumen Das, Breanne Hamlett, Kirstie Thompson, Srinivas Tekkam, Annika Yau,

Christian Scheibe, Craig McKay, Jenny Cheng, Hanna Wisniewska, Roman Valiulin, Lucrezia De Pascalis, Jessica Lloyd, Erin Whetzel, Ruyi Yang, Jennifer Beveridge, Robert Demont, Michael Baksh, Carlos Sanhueza-Chavez, Lindsay Dahora, Kelly Gamble, and Mark Garren. I am sure that I left someone off this long list, so if you ever read this and find your name missing, come and find me. A drink is certainly owed.

I have had the privilege of mentoring three very talented undergraduate students during my tenure at Georgia Tech, who all aided me tremendously. Robert Balaban, Areeba Abid, and Sophia Guldberg each made valuable contributions to the work presented in this thesis. I know that they will all go on to have long and successful careers in whatever endeavors they choose to pursue.

The results presented in these chapters could not have been obtained without the aid and collaboration of numerous individuals from a number of different departments and universities. Some very special thanks go out to Lingjun Zhang, Wen Qiu, Yan Li, Ben Xu, and Feng Lin of the Cleveland Clinic for their expertise in evaluating the complement vaccines in Chapter 2; Antonio Rampoldi, Marcela Preininger, Rajneesh Jha, Joshua Maxwell, Lingmei Ding, Paul Spearman, and Chunhui Xu of Emory University for their efforts in culturing and screening stem cells in Chapter 3; Idris Raji, Bocheng Wu, and Adegboyega Oyelere of Georgia Tech for their synthesis of macrolide derivatives and expertise on macrophage polarization for Chapter 4; Jukuan Zhang, Yogesh Dhande, Mitra Ganewatta, and Theresa Reineke of the University of Minnesota for the synthesis of polymers employed in Chapter 5; and Liangjun Zhao for introducing

the PP7 particle to the Finn lab and developing constructs for the exploratory studies in Chapter 6.

I would also like to thank the numerous staff members and managers of the Cellular Analysis and Cytometry Core, the Biopolymer Characterization Core, and the Physiological Research Laboratory at Georgia Tech for their assistance and use of instrumentation during the course of this work.

Finally, I dedicate this thesis to my fiancée, Samantha McGunigale, who has been my biggest supporter through this final push and has helped keep my sanity intact. I would be lost without you, and I count my blessings every day that I found you. I love you more than you could possibly know.

## Table of Contents

## List of Tables

## List of Figures

### Chapter 1



### Chapter 2



### Chapter 3

**Chapter 4**



**Chapter 5**

**Chapter 6**

## List of Abbreviations

| | |
|---|---|
| 5-FC | 5-fluorocytosine |
| 5-FU | 5-fluorouracil |
| AAV | adeno-associated virus |
| ADC | antibody-drug conjugate |
| AF488 | Alexa Fluor 488 |
| APC | antigen presenting cell |
| ATRP | atom-transfer radical polymerization |
| AZM | azithromycin |
| BCR | B-cell receptor |
| C5 | complement component 5 |
| CCMV | cowpea chlorotic mottle virus |
| CD | cytosine deaminase |
| CFA | complete Freund's adjuvant |
| CFPC | corrected fluorescence per cell |
| CLA | clarithromycin |
| CP | coat protein |
| CPMV | cowpea mosaic virus |
| CuAAC | copper-catalyzed azide-alkyne cycloaddition |
| DAPI | 4',6-diamidino-2-phenylindole dilactate |
| DC | dendritic cell |
| DLS | dynamic light scattering |

| | |
|---|---|
| DMSO | dimethyl sulfoxide |
| *E. coli* | *Escherichia coli* |
| EGFP | enhanced green fluorescent protein |
| EGFR | epidermal growth factor receptor |
| ELISA | enzyme-linked immunosorbent assay |
| EthD-1 | ethidium homodimer-1 |
| FPLC | fast protein liquid chromatography |
| HBcAg | hepatitis B core antigen |
| hDF | human dermal fibroblast |
| hESC | human embryonic stem cell |
| HER2 | human epidermal growth factor receptor 2 |
| hPSC | human pluripotent stem cell |
| hiPSC | human induced pluripotent stem cell |
| HPG | homopropargylglycine |
| HRP | horseradish peroxidase |
| IgG | immunoglobulin G |
| IgM | immunoglobulin M |
| IFN | interferon |
| IL-1α | interleukin-1α |
| IL-6 | interleukin-6 |
| IL-10 | interleukin-10 |
| IL-12 | interleukin-12 |
| IPTG | isopropyl β-D-1 thiogalactopyranoside |

| | |
|---|---|
| KLH | keyhole limpet hemocyanin |
| LPS | lipopolysaccharide |
| MΦ | macrophage |
| mAb | monoclonal antibody |
| MAC | membrane attack complex |
| MALS | multi-angle light scattering |
| MHC-I/II | major histocompatibility complex class I/II |
| MWCO | molecular weight cut-off |
| NHS | *N*-hydroxysuccinimide |
| PBS | phosphate-buffered saline |
| PEG | poly(ethylene glycol) |
| PMAG | poly(methacrylamido glucopyranose) |
| PNH | paroxysmal nocturnal hemoglobinuria |
| POEGMA | poly(oligo(ethylene glycol) methacrylate |
| PRR | pattern recognition receptor |
| PTFE | polytetrafluoroethylene |
| RAFT | reversible-addition fragmentation chain-transfer |
| RBC | red blood cell |
| RGD | arginine-glycine-aspartate |
| SIRPα | signal regulatory protein alpha |
| SSEA | stage-specific embryonic antigen |
| TBS | tris-buffered saline |
| THPTA | tris(3-hydroxypropyltriazolylmethyl)amine |

| | |
|---|---|
| TLR | Toll-like receptor |
| TMB | 3,3',5,5'-tetramethylbenzidine |
| TNF-α | tumor necrosis factor-alpha |
| UV | ultraviolet |
| VLP | virus-like particle |
| WGA | wheat germ agglutinin |
| WT | wild-type |

## Summary

Virus-like particles (VLPs) are multi-subunit protein assemblies that self-assemble into homogenous particles with periodic structure, making them ideal candidates for applications in biomedicine. This dissertation will discuss both the chemical and genetic modification of Qβ and PP7 VLPs for the design of vaccine platforms and drug delivery vehicles. Both the Qβ and PP7 VLPs are comprised of 180 copies of their respective coat protein (CP) monomers, which assemble to form icosahedral capsids of $T = 3$ geometry that are 28 and 30 nm in diameter, respectively. Herein, genetic engineering of the Qβ coat protein to introduce peptide and protein domains is described. First, these modifications were encoded as C-terminal extensions of the CP, and co-expression with unmodified subunits produced hybrid particles displaying the peptide or protein domains. These particles were successfully applied in both vaccination studies as well as the targeted delivery of prodrug-converting enzymes encapsulated within the VLP. To broaden the scope of targeting applications, the chemical conjugation of small molecules to the surface of Qβ VLPs was also used to direct cellular uptake and trafficking. The clearance of VLP delivery vehicles from circulation is an important factor governing their efficacy; to this effect, a survey of different polymer modifications and their effects on the immunological response to the Qβ VLP was undertaken. Lastly, PP7 VLPs were modified by genetically encoding extensions of a peptide implicated in mitigating phagocytic clearance to further explore strategies for prolonging circulation. All of the work presented here builds upon previous studies employing VLPs for drug delivery and vaccine development, while building upon

the knowledge of chemical and genetic modifications that can be used to develop these materials. This work is poised to bring together the power of chemical and genetic modification in the development of nanoparticle platforms with novel properties that are equipped for effective vaccination and cellular targeting with reduced clearance *in vivo*.

All work herein is adapted to varying degrees from manuscripts that are in preparation and/or manuscripts that have been submitted for publication. Chapters 2 and 3 detail experiments conducted in collaboration with several workers at Cleveland Clinic and Emory University – their contributions are presented here to give a full account of the work accomplished, and due credit is given to all those listed in the Acknowledgments.

# Chapter 1: Introduction to virus-like particles as biomedical platforms

## 1.1. Virus-like particle platforms

The development of systems for targeted drug delivery and vaccine design that combine efficacy concurrently with high margins of safety remains an elusive goal in biomedicine,[1] but advances within the past two decades have produced numerous nanoscale platforms that have been explored as candidates. Inorganic nanoparticles,[2] polymer assemblies,[3] dendrimers,[4] and liposomes[5] have all received attention as potential platforms for biomedical applications, but each have their own associated set of disadvantages. Inorganic materials are readily prepared but have raised concerns over their long-term accumulation in various tissues and associated toxicity.[6,7] Polymeric materials offer tunable stability but often at the cost of biocompatibility, while liposomes are often more biocompatible but are prone to rapid clearance.[8] Additionally, all of these platforms suffer from batch-to-batch variability in size distribution and structural composition.[9] In contrast, proteinaceous virus-like particles (VLPs) offer a more robust set of materials that allow for the union of chemistry and molecular biology in the generation of multifunctional platforms.

VLPs are structurally well-defined materials that are typically rod-like or icosahedral in shape with diameters ranging from 10-200 nm.[10] They are comprised of one or more repeating protein subunits derived from bacteriophages,[11–14] plant viruses,[15,16] or mammalian viruses,[17,18] that spontaneously assemble into particles which can be produced and isolated from recombinant expression systems in high yields. These particles are noninfectious, as they lack the native viral genome; however, VLPs do

nonspecifically encapsidate nucleic acids from the host cell.[10] In addition to their ease of production and homogeneity, VLPs are also remarkably stable structures, tolerant of a wide range of temperature,[19,20] pH,[19] and solvent compositions,[21] which allows for a broad scope of chemical modifications in the design of novel vaccines and delivery platforms. The inherent nature of VLPs as protein-based materials also permits modifications to be introduced at the genetic level prior to expression and assembly. Changes at the genetic level can vary from single point mutations[22,23] to incorporation of peptides[24] or protein domains[25] as extensions of the coat protein sequence, depending on the intended application.

The unique features of VLPs places them at the interface of chemistry, biology, and materials science, whereby combined techniques from each of these disciplines has the ability to generate novel platforms for medicine and biotechnology. The subsequent sections will discuss specific examples of nine different icosahedral, non-enveloped VLPs (CCMV, CPMV, HBcAg, AAV, P22, AP205, MS2, PP7, Qβ) (**Figure 1; Table 1**) that have been chemically or genetically engineered as vaccine carriers or targeted delivery vehicles. Modifications discussed will focus on the design principles of the resulting materials and their applications in vaccine development or drug delivery.

*1.1.1. Cowpea chlorotic mottle virus*

Cowpea chlorotic mottle virus (CCMV) is a positive-sense single-stranded RNA plant virus classified in the *Bromoviridae* family, but it is structurally similar to the bacteriophages in the *Leviviridae* family.[26] While it can be produced in high yields (1-2 mg/g) from infected plants, it can also be produced recombinantly in both bacteria and yeast.[27] The viral capsid is composed of 90 homodimers of the coat protein, which

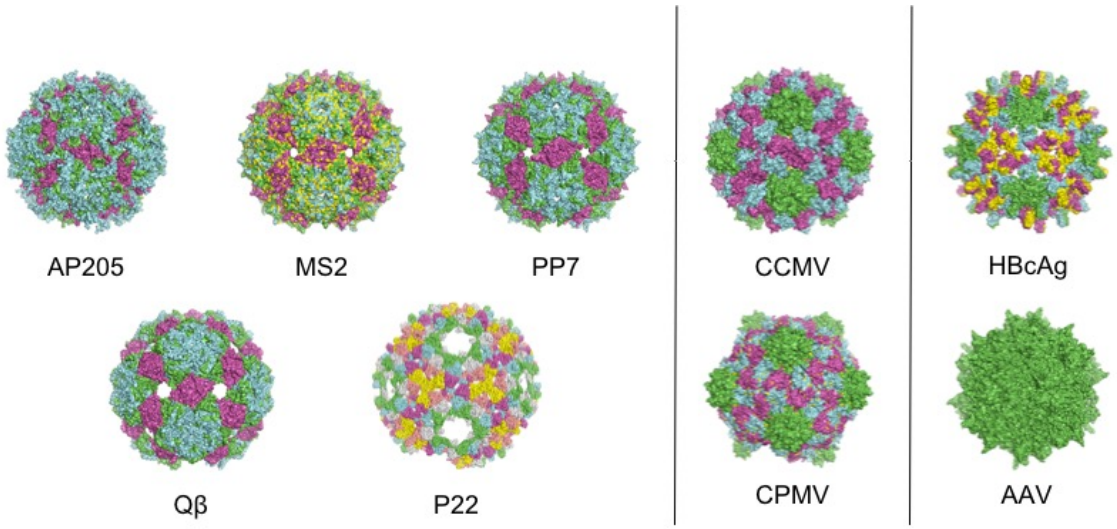


**Figure 1.** Three-dimensional structures of the virus-like particles discussed. Images were downloaded from viperdb.scripps.edu.[28] Structures not to scale.

**Table 1.** Relevant structural information of virus-like particles discussed. Viral geometry, size, and subunit composition are shown. Information compiled from viperdb.scripps.edu.[28]

| VLP | Classification | Outer Diameter (nm) | Inner Diameter (nm) | Triangulation Number | Subunits | References |
|---|---|---|---|---|---|---|
| AP205 | Bacteriophage | 28 | 18 | *T* = 3 | 180 | 61-64 |
| MS2 | Bacteriophage | 27 | 15 | *T* = 3 | 180 | 24, 65-69, 73, 83 |
| PP7 | Bacteriophage | 30 | 22 | *T* = 3 | 180 | 12, 24, 70-74 |
| Qβ | Bacteriophage | 28 | 21 | *T* = 3 | 180 | 14, 22, 75-87, 95, 96, 116, 118 |
| P22 | Bacteriophage | 58-64 | 48-50 | *T* = 7 | 420 | 54-60 |
| CCMV | Plant | 28 | 18 | *T* = 3 | 180 | 16, 26, 27, 29-33 |
| CPMV | Plant | 28-31 | 22 | *T* = 3 | 60 large + 60 small | 34-40 |
| HBcAg | Mammalian | 35 | 25 | *T* =3, 4 | 180, 240 | 17, 25, 41-45 |
| AAV | Mammalian | 29 | 17 | *T* = 1 | 60 | 46-53, 121-124 |

assemble into a 28 nm icosahedral particle possessing *T*=3 symmetry.[29] Reversible assembly of CCMV particles can be accomplished by tuning the ionic strength and pH of the solution, making them promising candidates for stimuli-responsive delivery.[30]

The Kormelink group engineered fusions of peptides from influenza A virus and foot-and-mouth disease virus as a proof-of-concept for epitope display.[16] Interestingly, insertion of the peptides into any loops on the CCMV coat protein surface abrogated particle assembly, but N- and C- terminal extensions were well-tolerated. Despite the incorporation of disease-associated peptides, no testing of the vaccine platforms was reported. Testing of the immune response was reported in a study by Pincus and colleagues, where a peptide mimitope of the group B streptococcal capsular polysaccharide was chemically conjugated to CCMV using a heterobifunctional maleimide cross-linker and shown to generate a Th1 response in mice.[31] The Th1 response bias was attributed to the encapsidated RNA within the CCMV particles, although this was not explored experimentally.

CCMV has also been explored for use as a drug delivery agent. Shin and colleagues developed a platform for applications in photothermal therapy by genetically encoding a tumor-homing peptide at the N-terminus of the coat protein.[32] After expression and purification, these particles were reversibly assembled in the presence of a near-infrared dye and directed against MCF-7 cancer cells. A separate study demonstrated covalent modification of CCMV with folic acid and doxorubicin via EDC coupling for selective targeting and killing of MCF-7 cancer cells.[33]

*1.1.2 Cowpea mosaic virus*

Unlike CCMV, cowpea mosaic virus (CPMV) is a member of the *Secoviridae* family and is formed from 60 copies of an asymmetric subunit comprised of a small (S) and large (L) domain.[34] The virions can be isolated in high yields (1 mg/g) from infected black-eyed pea plants (*Vigna unguiculata*) as approximately 30 nm particles with pseudo *T*=3 symmetry.[35,36] Interestingly, native CPMV particles have been shown to enter mammalian endothelial cells through interactions with surface vimentin,[37] but these VLPs can be directed against other cell types through chemical or genetic modification.

Hovlid and colleagues demonstrated selective targeting of cancer cells expressing $\alpha_V\beta_5$ integrins with CPMV that was chemically modified with a derivative of the cyclic arginine-glycine-aspartate (RGD) peptide Cilengitide using copper(I)-catalyzed azide-alkyne cycloaddition (CuAAC) chemistry.[38] In this same report, display of RGD peptide sequences through genetic insertion into loops on the particle surface was also accomplished to impart similar targeting function.[38] Steinmetz and coworkers demonstrated the capability of CPMV to serve as a drug delivery vehicle by covalently conjugating doxorubicin to the surface carboxylates for improved therapeutic efficacy relative to the free drug at similar concentrations.[39] The potential of CPMV as an agent for immunotherapy was assessed in a recent report by Fiering and coworkers where *in situ* vaccination of unmodified particles that were devoid of nucleic acid induced systemic anti-tumor immunity in metastatic breast, colon, and ovarian carcinoma models.[40] The broad efficacy of the CPMV platform in this context was linked to specific activation of neutrophils in the tumor microenvironment which mediate downstream anti-tumor immune responses.

*1.1.3. Hepatitis B virus*

The core antigen protein from hepatitis B virus (HBcAg) can be expressed in both bacterial and cell-free expression systems to yield two populations of *T*=3 and *T*=4 icosahedral particles comprised of 180 and 240 protein subunits, respectively.[17,41,42] These particles have been designed for both antigenic display as well as delivery of functional cargoes to cells. HBcAg has been shown to be incredibly stable towards the incorporation of extensions into the c/e1 loop region, ranging from large domains[25] to entire proteins.[43] Full-length green fluorescent protein (238 amino acids) was expressed in this manner as a model insert, and absorbance measurements revealed that ~ 50% of the displayed proteins were properly folded.[43] Khanna and colleagues expanded upon this technology by incorporating envelope domain III from dengue virus (104 amino acids) onto the HBcAg surface that was capable of generating cross-reactive antibody responses in mice.[25]

Modification of HBcAg VLPs for applications in therapeutic delivery has also been extensively explored. Particles designed for the selective encapsidation of plasmid DNA have been shown to be stable, yet their ability to deliver the DNA for expression in cells remains untested.[44] Strable and colleagues were the first to demonstrate successful incorporation of the unnatural amino acids azidohomoalanine and homopropargylglycine into the HBcAg capsid protein by expression in a methionine auxotroph strain of *E. coli*.[45] This allowed for the chemoselective conjugation of proteins and imaging agents to the capsid via CuAAC with near-perfect spatial control, although capsid stability was compromised by the formation of more than 120 triazole linkages on the capsid surface.[45]

*1.1.4. Adeno-associated virus*

Adeno-associated virus (AAV) is a small, non-enveloped virus of the *Parvoviridae* family that naturally encapsulates a single-stranded DNA genome and has received the lion's share of attention in the field of gene therapy. Engineered variants of AAV serotype 2 have been the most widely used vehicles for gene delivery applications, yet there has been relatively limited clinical success.[46–48] Delivery and expression of the cystic fibrosis transmembrane conductance regulator (CFTR) gene has been demonstrated in patients, but there was no clear therapeutic efficacy.[48] Several trials for the treatment of hemophilia B have also been conducted with varying levels of success. Kay and colleagues reported on an early trial of factor IX replacement using AAV that was halted due to cytotoxic T-cell responses against transduced hepatocytes in patients,[47] but Davidoff and coworkers later showed stable expression in patients over 6 months following treatment with a different AAV variant.[49] The lone example of an AAV-based therapeutic reaching market approval is Glybera®, which received approval for the treatment of lipoprotein lipase deficiency in the European Union in 2012, but it is being withdrawn due to the expensive price point and lack of demand.[50]

Neutralizing antibodies to AAV generated from previous asymptomatic exposures to adenovirus are the main challenge to therapeutic applications as they limit AAV transduction into certain tissues and hinder readministration of the vector.[46] Nakagawa and colleagues labeled AAV with varying degrees of polymer modifications and found that with higher levels of polymer loading, the antibody response against AAV was significantly diminished.[51] Directed evolution of the AAV capsid has also been employed to generate vectors capable of avoiding recognition by the neutralizing antibodies present

in a large portion of the population. Several studies have reported on the development of AAV variants capable of avoiding neutralization by AAV-specific antibodies both *in vitro*[52] and *in vivo*.[53] AAV variants prepared in this manner required 20-fold higher concentration of human antibodies for neutralization *in vitro* and could achieve significantly higher rates of transduction in mice that had been passively immunized with human antibodies.

*1.1.5. P22*

The bacteriophage P22 is a double-stranded DNA virus in the *Podoviridae* family that assembles from 420 identical copies of a coat protein subunit with the aid of ~ 300 scaffolding proteins.[54] P22 VLPs have the unique ability to undergo large morphological changes, with four distinct forms observed.[54,55] The procapsid is assembled as a 58 nm shell containing the scaffolding proteins; treatment of the procapsid with the chaotrope guanidinium chloride denatures the scaffolding protein and yields empty particles. Mild heating (65°C) of either the procapsid or empty particle induces a transition into an expanded from, measuring 64 nm in diameter. Further heating (75°C) leads to the formation of 10 nm pores at the fivefold symmetry axis, which is classified as the "wiffle-ball" formation.

Douglas and coworkers have shown that encapsulating protein antigens inside of P22-based VLPs promotes an antigen-specific $CD8^+$ T-cell response upon immunization.[56,57] Encapsulation of the conserved nucleoprotein from influenza resulted in a vaccine formulation that provided multi-strain protection against 100 times the lethal dose of the virus in a T-cell dependent manner.[56] Using the same VLP platform, Schwarz and colleagues were able to show that co-encapsidation of two different proteins from

respiratory syncytial virus (RSV) gave rise to robust CTL responses specific to both antigens that conferred protection against an RSV challenge.[57] Douglas and colleagues have also worked extensively in the area of encapsulating active proteins within P22 VLPs, demonstrating assembly of entire enzyme cascades for industrial applications[58] as well as the confinement of therapeutic proteins, such as cytochrome P450[59] and Cas9,[60] within the protein shell.

*1.1.6. AP205*

The single-stranded RNA bacteriophage AP205 is distantly related to the other viruses of the *Leviviridae* family but shares no sequence similarity other than two cysteine residues which form stabilizing inter-subunit disulfide bonds.[61] AP205 VLPs demonstrated variable tolerance to insertions at both the N- and C-termini when genetically fused with multiple disease-related antigens, with the largest fusion being a 55 amino acid peptide derived from HIV epitopes.[62] Additionally, Bachmann and colleagues combined genetic fusion with covalent attachment by encoding the SpyCatcher protein (~ 15 kDa) to the N-terminus of AP205 followed by covalent coupling to SpyTag-linked malaria antigens for VLP surface presentation.[63,64]

*1.1.7. MS2*

The bacteriophage MS2 is a positive-sense single-stranded RNA virus that bears structural homology to the Qβ bacteriophage. MS2 VLPs assemble from 180 identical protein subunits into a 28 nm capsid with *T*=3 geometry, and these particles bear pores at both the fivefold (1.7 nm) and threefold (1.4 nm) axes of symmetry. These particles have been investigated extensively for the development of both vaccines as well as targeted delivery platforms.

MS2 VLPs are known to spontaneously assemble in the presence of nucleic acids, which allowed Peabody and colleagues to package RNA-modified derivatives of doxorubicin, cisplatin, 5-fluorouracil, and ricin toxin A-chain inside of MS2 and selectively target cancer cells using a displayed peptide ligand.[65] All drug formulations tested with this platform resulted in selective cytotoxicity at sub-nanomolar drug concentrations. Building on the capacity of MS2 to encapsidate nucleic acids, this study further showed that delivery of an siRNA cocktail packaged within VLPs induced growth arrest and apoptosis of cancer cells.[65] Hall and colleagues showed that display of autoinducing peptide 4 from *Staphylococcus aureus* on a surface-exposed loop in the MS2 coat protein allowed for the affinity selection of VLP vaccine candidates that provided protection in a mouse model of *S. aureus*-induced dermonecrosis.[66]

Francis and colleagues have developed MS2-antibody conjugates using a covalent oxidative coupling strategy[67] that showed promising results *in vitro* but only moderate tumor uptake in a murine model of breast cancer.[68] Francis and coworkers had previously employed a similar coupling strategy for the attachment of DNA aptamers to the surface of MS2 VLPs for cancer-specific targeting applications, as well.[69]

*1.1.8. PP7*

PP7 is a single-stranded RNA phage that naturally infects *Pseudomonas aeruginosa*; these VLPs also bear structural as well as sequence homology with MS2 and Qβ.[70] PP7 capsids are comprised of 180 identical coat protein monomers that assemble into a 30 nm capsid bearing *T*=3 geometry and have been shown to be remarkably stable, in part due to the presence of inter-subunit disulfide bonds.[12] These particles have also

received considerable attention in the development of platforms for both vaccines and drug delivery.

Peabody and colleagues have engineered single-chain dimer variants of both MS2 and PP7 that were stable towards insertion of defined or random peptide sequences in the AB-loop region;[24,71] these platforms were employed in both rational vaccine design[71,72] as well as the generation of libraries for epitope discovery.[73] PP7 VLPs have also been investigated for the delivery of messenger RNA, with a proof-of-concept study showing the expression of fluorescent proteins in a target cell population.[74]

*1.1.9. Qβ*

Also a member of the *Leviviridae* family, bacteriophage Qβ is a single-stranded RNA virus with a 4.2-kilobase genome encoding for three genes (**Figure 2**).[75] The replicase and A2 protein are essential components for virulence, enabling replication of the viral genome and capsid maturation, respectively.[76] The A1 coat protein is the major structural element of the virion and can be expressed as either a full-length or truncated version. While most of the viral shell is comprised of the truncated variant, Qβ naturally incorporates 5-10 copies of the full-length coat protein.[77,78] This extended form of the A1 coat protein is produced through occasional read-through of an opal stop codon, and its incorporation into the capsid is vital for infectivity.

Qβ VLPs can be produced by recombinant expression of the truncated coat protein in both yeast[79] and bacteria,[80] as well as cell-free expression systems,[81] with high yields. The capsid assembles from 180 copies of the coat protein as a 28 nm icosahedral particle with $T$=3 symmetry.[82] Pores formed at the threefold (1.3 nm) and fivefold (0.7 nm) axes of symmetry allow for selective access of small molecules to the capsid interior,

and similar to other leviviruses, the coat protein forms tightly-associated noncovalent dimers.[83] Qβ VLPs are remarkably stable to changes in temperature, pH, and solvent composition, which has allowed for the engineering of platforms for numerous applications; this stability is largely attributed to the formation of inter-subunit disulfide bonds.[22]

The coat protein contains four solvent-exposed lysine residues, providing a total

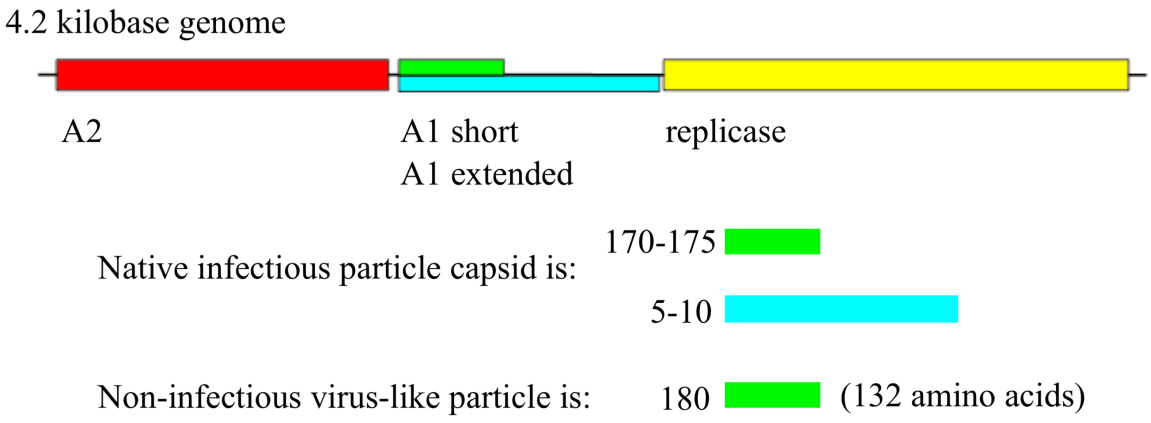


**Figure 2.** Cartoon representation of the Qβ genome.[76] Differences in the capsid composition for the native virion and non-infectious VLP are highlighted.

of 720 reactive amines per Qβ particle.[82] These residues have been addressed through *N*-hydroxysuccinimide ester chemistry to install numerous bifunctional linkers for biorthogonal conjugation to small molecules, peptides, polymers, and imaging agents. Rhee and colleagues demonstrated attachment of a modified sialic acid moiety to Qβ VLPs using CuAAC in order to target cells displaying CD22.[84] Pokorski and colleagues detailed the attachment of an atom-transfer radical polymerization (ATRP) initiator

moiety to the surface of Qβ VLPs followed by graft-from polymerizations to generate hybrid protein-polymer materials for use in drug delivery and imaging.[85]

The Qβ coat protein has also been shown to be stable to the genetic insertion of peptide or protein domains at the C-terminus. Taking advantage of the natural read-through process that produces the extended A1 coat protein, Pumpens and coworkers displayed foreign peptides on the surface of the assembled virion.[86] Building upon this approach, Brown and colleagues developed a system for displaying large protein domains on the surface in higher numbers by employing a two-plasmid system.[14] In this system, one plasmid harbors the gene for the truncated coat protein while the second harbors the coat protein plus a polypeptide extension at the C-terminus; co-expression in bacteria produces hybrid VLPs displaying these extensions on a greater number of subunits.

Functional therapeutic proteins can also be encapsulated within Qβ VLPs for delivery. Fiedler and colleagues used the propensity for Qβ to encapsidate endogenous cellular RNA to their advantage in designing a system to control the loadings of different proteins.[87] In this system, the cargo protein was engineered with an arginine-rich (Rev) terminal tag, and a bifunctional RNA was transcribed bearing an aptamer against the Rev peptide in combination with a hairpin that interacts with the interior of the Qβ capsid protein. Simultaneous expression of these factors in bacteria allows for the assembly of VLPs harboring the desired protein cargo.

### 1.2. Immunology of virus-like particles

As discussed in the preceding section, VLPs are structurally identical to the viruses from which they are derived, and it is their mimicry of viral structure that contributes to their interaction with both arms of the immune system. The specific

structural features contributing to the engagement of each component of innate and adaptive immunity will be discussed herein to provide an understanding of the immunogenicity of VLPs and to demonstrate their effectiveness as platforms for vaccine development. An understanding of the features that govern the interactions of VLPs with the immune system is also critical in guiding the design and implementation of VLPs as drug delivery platforms, which will be subsequently discussed in detail.

The innate immune system is comprised of a number of different proteins and cell types that circulate throughout the body and serve as a first line of defense against invading microorganisms and viruses.[88,89] As such, these molecules have evolved to be activated by structural features that are commonly associated with pathogenic organisms.[90] Pentraxins,[91] complement component 1q (C1q),[92] and IgM[93] are all multimeric proteins that perform critical roles in innate immunity by promoting the clearance of pathogens through activation of the complement cascade. These molecules are ideally suited for the recognition of highly repetitive structures, such as those of VLPs, due to their capacity for multivalent interactions. Although the affinity of the individual binding events may be low, the avidity of the interaction afforded by these multivalent structures may be quite high and promote strong binding.[94]

Not surprisingly, it has been shown that viral particles both bind natural IgM antibodies and trigger complement activation in mice. Bachmann and coworkers have shown that natural IgM antibodies recognize Qβ VLPs, and these particles are transported to B-cell follicles in a complement-dependent fashion by non-cognate B-cells.[95] These particles were subsequently transferred to follicular dendritic cells (FDCs) for prolonged retention and display, which is essential for B-cell activation and clonal selection within

the germinal center.[96] These observations were not recapitulated using the soluble Qβ coat protein, further supporting that the repetitive organization of the particle was necessitating activation of the complement system.[95]

The complement system has also been found to play a key role in the immune response to AAV vectors.[97] Binding of C3 proteins to the AAV capsid was shown to mediate uptake by macrophages, which promoted subsequent activation and expression of inflammatory cytokines.[97] Additionally, the binding of C3 proteins to AAV was shown to be essential for initiating the humoral response, either by promoting cross-linking of B-cell receptors (BCRs) with complement receptors on the B-cell surface or by an adjuvant effect to enhance the response to AAV.[97]

Activation of the complement system plays a significant role in the initial response to VLPs and AAV vectors, both in terms of initial clearance of the particles from circulation as well as initiating mechanisms for adaptive immune responses. The repetitive organization of VLPs serves to engage interactions with native IgM antibodies and other components of the innate immune system, which in turn gives rise to robust adaptive B-cell responses – a key component for the development of effective vaccines. Initiation of a strong adaptive response can undermine applications where multiple administrations of the therapeutic are necessary, however, as has been observed previously with AAV. Despite these observations, numerous strategies have been developed that allow VLPs to avoid immune recognition and serve as effective delivery vehicles.

Dendritic cells (DCs) and macrophages are the primary groups of antigen presenting cells (APCs) that serve to bridge the gap between the innate and adaptive

immune response. Macrophages are a diverse population of cells that perform various roles, from scavenging apoptotic cellular debris to regulating immune responses and antigen presentation.[98] The numerous subsets of macrophages that perform these tasks have been reviewed in excellent detail elsewhere.[99,100] Similarly, DCs are most well characterized as professional APCs that present processed antigens to lymphocytes for the initiation of adaptive immunity.[101]

Due to their size and repetitive structure, most VLPs are efficiently recognized for uptake by both DCs and macrophages.[10] As previously discussed, the binding of natural IgM antibodies and pentraxins to the VLP surface can result in the activation of the classical pathway in the complement cascade, facilitating uptake of the particles by interactions with both Fc and complement receptors on the APC surface.[102] Upon uptake, VLPs traffic to the endolysosomal compartment, where they are degraded into peptides and loaded onto major histocompatibility complex class II (MHC-II) molecules for presentation to $CD4^+$ T-cells (**Figure 3**). It should also be noted that cross-presentation of antigenic peptides on MHC class I (MHC-I) molecules occurs much more readily with particulate antigens than soluble proteins and can lead to the priming of $CD8^+$ T-cell responses, as well.[103]

Display of antigenic peptides on MHC-II is insufficient to fully activate helper T-cells, however; APCs must also be activated and express co-stimulatory signals.[104] Most VLPs and viral vectors package nucleic acid during assembly, either by design[105] or through non-specific interactions,[106] which serve as stimulatory Toll-like receptor (TLR)

ligands for APC activation once the particles are degraded in the endosome.[107] VLPs containing ssRNA stimulate TLR7/8,[108,109] while vectors or VLPs packaging CpG-rich

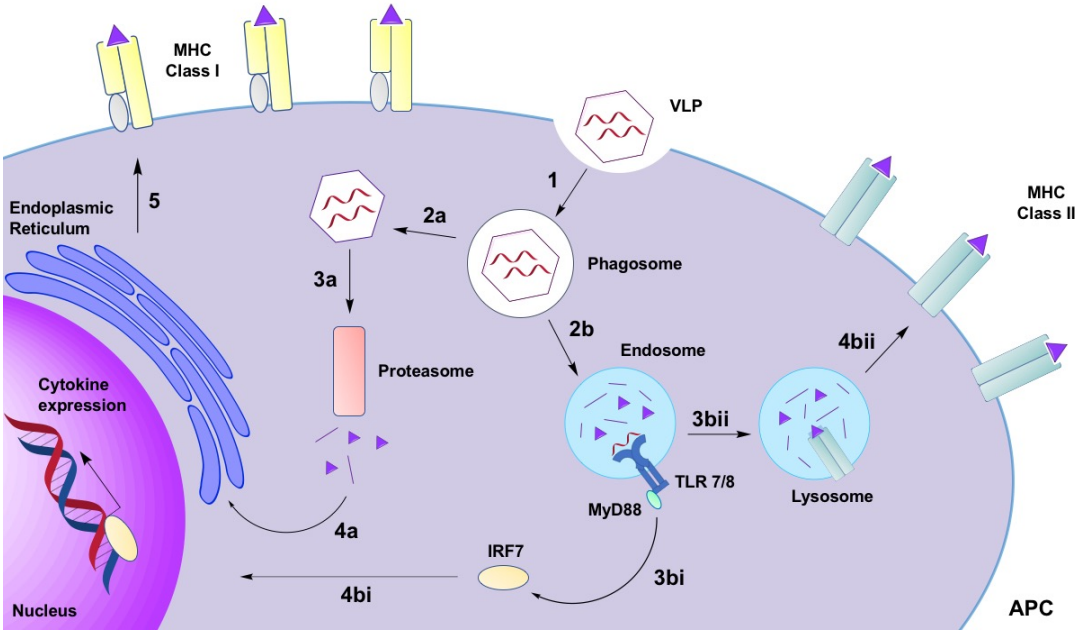


**Figure 3.** Uptake and processing of virus-like particles by antigen-presenting cells. VLPs are internalized by APCs through opsonin-mediated or passive phagocytosis (1) and are either released into the cytosol (2a) or retained and degraded as the phagosome matures into the endosome (2b). VLPs gaining access to the cytosol undergo degradation and processing by the proteasome (3a) and peptide antigens are trafficked into the endoplasmic reticulum (4a), where they are loaded onto MHC-I complexes and shuttled to the cell surface for cross-presentation (5). Nucleic acid released from VLPs in the endosome stimulate TLR7/8 and phosphorylation of IRF7 in a MyD88-dependent manner (3bi), which translocates to the nucleus (4bi) and induces inflammatory cytokine gene expression. Protein antigens retained in the endosome are degraded and loaded onto MHC-II following acidification to the lysosome (3bii), and MHC-II trafficks to the cell surface to present antigens for cellular recognition (4bii).

DNA activate TLR9.[110] Activation of these pathways results in the expression of inflammatory gene networks and the production of cytokines, such as interleukin-1β (IL-1β), interleukin-4, (IL-4), interleukin-6 (IL-6), transforming growth factor-β (TGF-β), and interleukin-12 (IL-12), which are key in initiating T-helper cell responses.[104,111]

In addition to priming signaling for innate immunity, the geometry and repetitive organization of VLPs are also the primary determinants of their interaction with and activation of B-cells.[112] The host-pathogen response has evolved to promote cross-linking of the BCR by repetitively organized antigens, which is the key activation signal for B-cells.[113] VLPs can directly interact with B-cells by virtue of their size; particles that are 20-200 nm in diameter efficiently drain into the lymphatic system and gain access to secondary lymphoid organs (**Figure 3**).[114] As shown for Qβ VLPs, complement fixation also played a key role in trafficking antigen to B-cell follicles and prolonging display for interactions in the germinal center.[95] Complement factors displayed on the VLP surface can also engage complement receptors on the cognate B-cell surface and provide further stimulation for activation.[115]

The B-cell response to VLPs is also influenced by TLR stimulation, both through TLR activation in DCs and direct TLR activation in B-cells that was independent of signaling from T-helper cells.[116,117] Delivery of ssRNA or CpG packaged inside of VLPs was found to significantly improve the IgG antibody response compared to the delivery of soluble TLR ligands mixed with VLPs.[118] Bachmann and colleagues further elucidated the role of direct TLR stimulation in B-cells by showing that activation of TLR9 was sufficient to induce isotype class switching to IgG2a in a T-bet-dependent manner that was irrespective of signaling in other cell types.[116] While VLPs are capable of stimulating B-cell activation and high titers of IgG antibodies even in the absence of TLR signaling, the quality of the immune response can be greatly influenced by TLR stimulation. An increase in the formation of antigen-specific germinal centers has been shown following

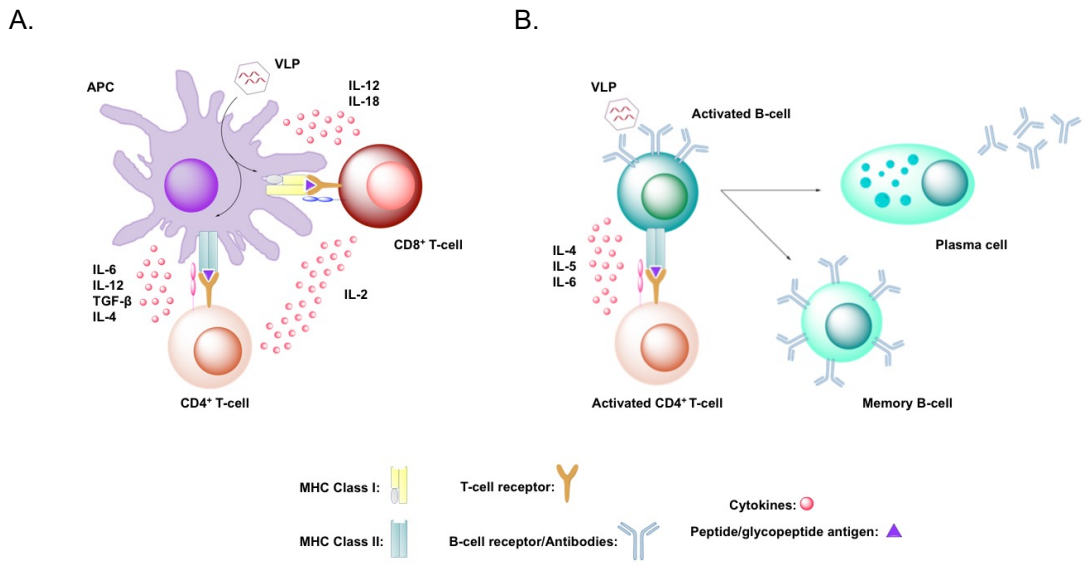


**Figure 4.** Key steps in the generation of humoral and cellular immune responses. (A) VLPs encounter antigen presenting cells in the periphery, where uptake is mediated by either passive phagocytosis or opsoninization by complement and other multivalent molecules involved in innate immune responses. Particles are degraded in the proteasome or endolysosome and peptide antigens are loaded onto MHC Class I (cross-presentation) or MHC-Class II for display on the mature APC surface and stimulation of T-cell activation. Maturation of APCs results in the secretion of cytokines that influence the differentiation of naïve lymphocytes into numerous classes of effector cells. Presentation of antigens on MHC-II promotes recognition by naïve $CD4^+$ T-cells, which can undergo differentiation into $T_H1$, $T_H2$, $T_H17$, or $T_{reg}$ lineages dependent upon the co-stimulatory signals received from the APC. In the absence of other signals, TGF-β favors the generation of $T_{reg}$ cells; however, the production of TGF-β in combination with IL-6 during early responses induces $T_H17$ differentiation. APCs can later produce cytokines favoring $T_H1$ (IL-12, IFN-γ) or $T_H2$ (IL-4) responses. Cross-presentation of antigens on MHC-I combined with production of IL-12 and IL-18 promotes proliferation of $CD8^+$ T-cells; activated $CD4^+$ helper cells also aid in stimulating this proliferation by producing IL-2. (B) Due to their size, VLPs can traffic to the lymph nodes and gain direct access to resident B-cells. Cross-linking of cognate BCRs by the repetitive structure of the particle, in combination with co-stimulatory signals from activated $CD4^+$ T-cells (IL-4, IL-5, IL-6), promote activation of the B-cells and differentiation into antibody-producing plasma cells. A subset of these activated cells undergoes further differentiation into memory cells that are critical for robust adaptive responses.

immunizations with antigens linked to TLR ligands, which directly governs the affinity and isotype switching of IgG antibodies produced.[118]

As VLPs are efficiently taken up and processed by DCs, they can also serve to stimulate robust $CD4^+$ and $CD8^+$ T-cell responses.[119,120] After uptake, DCs migrate to the lymph nodes and can present antigenic peptides loaded on MHC-II to $CD4^+$ T-cells (**Figure 4**); however, DCs can also cross-present antigens on MHC-I molecules for the activation of $CD8^+$ T-cells.[103] While $CD4^+$ T-cells feed back into promoting robust antibody responses by providing co-stimulatory signals to B-cells, the activation of cytotoxic $CD8^+$ T-cells promotes cellular immunity against cells displaying cognate antigens.

Priming cytotoxic T-lymphocyte (CTL) responses is a promising approach for vaccination against certain diseases, but it can also pose major limitations to certain therapeutic applications involving VLPs. Douglas and coworkers have shown that encapsulating protein antigens inside of P22-based VLPs promotes an antigen-specific $CD8^+$ T-cell response upon immunization.[56,57] On the other hand, $CD8^+$ T-cell responses have been identified as a significant hindrance to adenoviral gene delivery.[121] CTL responses have been found against both the AAV capsid and the transgene product,[122] which has been shown to compromise cells transduced by the vector and expressing the delivered gene product. Kay and colleagues reported on a clinical trial employing AAV for hemophilia B treatment that was halted due to CTL-mediated response against AAV-transduced hepatocytes,[47] but attempts to replicate the phenomenon in animal models for further study have proven unsuccessful.[123,124]

It is clear that the structural organization and composition of VLPs that are beneficial in the design of VLP-based vaccines can also hinder the development of VLP platforms for applications in targeted delivery. Thus, while native IgM antibodies and the complement system function as early effectors in stimulating adaptive memory responses, these systems can promote rapid clearance of VLPs from circulation and undermine their use as delivery agents. Uptake by APCs also serves to remove VLPs from circulation, but more importantly, begins to initiate adaptive B- and T-cell responses, which are ideal for effective vaccines but are detrimental for the long-term administration of VLPs for other applications.

Adaptive immune responses are the primary hindrance to repeat administrations of VLPs for delivery applications, as circulating antibody repertoires from previous exposures or treatments can function to neutralize VLPs. In the case of AAV, both B- and T-cell responses have been implicated in hindering clinical applications. Neutralizing antibody responses from previous exposures to AAV limit the capabilities for effective delivery and transduction of a gene product into target cells, while T-cell responses are more problematic, as they serve to eliminate transduced cells that are displaying peptides from either the protein cargo or the virus itself. In contrast, relatively little focus has been placed on studying the effects of adaptive immune responses on the clearance of other VLP platforms. A single study by Young and colleagues investigated the biodistribution and clearance of CCMV in both naïve and immunized mice, finding the distribution and trafficking of particles to be similar in both cases.[125]

Thus, while VLPs are now a generally accepted platform for immune activation, their general suitability for use as platforms for the directed delivery of therapeutics

remains an open question. Many of the same chemistries and design principles used for the generation of VLP-based vaccines can be employed for the development of delivery vehicles. For the remainder of this thesis, I will discuss the use of VLPs for both of these applications, with a focus on the key chemical and genetic modifications that can be leveraged for the development of both classes of functional nanoparticles.

### 1.3. Summary

In the preceding sections, I have described several examples of the chemical and genetic modifications of different virus-like particles and the applications of these platforms for vaccine development and drug delivery. These examples indicate that VLP systems hold considerable promise in biomedicine, but there are several inherent limitations to the current approaches. The immunogenicity of VLPs represents a substantial hindrance for applications in drug delivery, and the continuing development of new tools and methodologies to modify VLPs is critical. The following chapters of this thesis will discuss the chemical and genetic engineering of Qβ and PP7 VLPs for targeted delivery and shielding from the immune system, with a small focus on leveraging native VLP immunogenicity for vaccine development. Chapter 2 will describe the construction of hybrid Qβ VLPs displaying genetically encoded peptide extensions for applications as vaccines. Chapter 3 will detail the construction and application of hybrid Qβ VLPs displaying Fc-binding domains for antibody-directed targeting. In contrast to genetic strategies, Chapter 4 will discuss the chemical modification of Qβ VLPs with small molecules to alter trafficking and cellular uptake. Chapter 5 will detail the development of hybrid protein-polymer Qβ VLPs and an evaluation of their abilities to abrogate immune recognition, while Chapter 6 will detail the genetic modification of PP7 VLPs

with peptide extensions to mitigate uptake by immune cells. This body of work provides insights, tools, and techniques that will lead to the continued development of VLPs as platforms in biomedicine. The technologies developed here build towards the ultimate goal of engineering modular virus-like particle platforms that can be tailored for implementation as both vaccines as well as drug delivery vehicles.

### 1.4. References


(1) Strebhardt, K.; Ullrich, A. Paul Ehrlich's Magic Bullet Concept: 100 Years of Progress. *Nat. Rev. Cancer* **2008**, *8*, 473–480.

(2) Tonga, G. Y.; Moyano, D. F.; Kim, C. S.; Rotello, V. M. Inorganic Nanoparticles for Therapeutic Delivery: Trials, Tribulations and Promise. *Curr. Opin. Colloid Interface Sci.* **2014**, *19*, 49–55.

(3) Han, J.; Zhao, D.; Li, D.; Wang, X.; Jin, Z.; Zhao, K. Polymer-Based Nanomaterials and Applications for Vaccines and Drugs. *Polymers* , 2018, *10*.

(4) Madaan, K.; Kumar, S.; Poonia, N.; Lather, V.; Pandita, D. Dendrimers in Drug Delivery and Targeting: Drug-Dendrimer Interactions and Toxicity Issues. *J. Pharm. Bioallied Sci.* **2014**, *6*, 139–150.

(5) Allen, T. M.; Cullis, P. R. Liposomal Drug Delivery Systems: From Concept to Clinical Applications. *Adv. Drug Deliv. Rev.* **2013**, *65*, 36–48.

(6) McCarthy, J.; Inkielewicz-Stepmiak, I.; Corbalan, J. J.; Radomski, M. W. Mechanisms of Toxicity of Amorphous Silica Nanoparticles on Human Using Submucosal Cells in Vitro: Protective Effects of Fisetin. *Chem. Res. Toxicol.* **2012**, *25*, 2227–2235.

(7) Trouiller, B.; Reliene, R.; Westbrook, A.; Solaimani, P.; Schiestl, R. H. Titanium Dioxide Nanoparticles Induce DNA Damage and Genetic Instability in Vivo in Mice. *Cancer Res.* **2009**, *69*, 8784–8789.

(8) Mahato, R. I. Water Insoluble and Soluble Lipids for Gene Delivery. *Adv. Drug Deliv. Rev.* **2005**, *57*, 699–712.

(9) Desai, N. Challenges in Development of Nanoparticle-Based Therapeutics. *AAPS J.* **2012**, *14*, 282–295.

(10) Bachmann, M. F.; Jennings, G. T. Vaccine Delivery: A Matter of Size, Geometry, Kinetics and Molecular Patterns. *Nat. Rev. Immunol.* **2010**, *10*, 787–796.

(11) Yoshimura, H.; Edwards, E.; Uchida, M.; McCoy, K.; Roychoudhury, R.; Schwarz, B.; Patterson, D.; Douglas, T. Two-Dimensional Crystallization of P22 Virus-Like Particles. *J. Phys. Chem. B* **2016**, *120*, 5938–5944.

(12) Caldeira, J. C.; Peabody, D. S. Stability and Assembly in Vitro of Bacteriophage PP7 Virus-like Particles. *J Nanobiotechnology* **2007**, *5*.

(13) Legendre, D.; Fastrez, J. Production in Saccharomyces Cerevisiae of MS2 Virus-like Particles Packaging Functional Heterologous mRNAs. *J. Biotechnol.* **2005**, *117*, 183–194.

(14) Brown, S. D.; Fiedler, J. D.; Finn, M. G. Assembly of Hybrid Bacteriophage Q-Beta Virus-Like Particles. *Biochemistry* **2009**, *47*, 11155–11157.

(15) Wang, Q.; Kaltgrad, E.; Lin, T.; Johnson, J. E.; Finn, M. G. Natural Supramolecular Building Blocks: Wild-Type Cowpea Mosaic Virus. *Chem. Biol.* **2002**, *9*, 805–811.

(16) Hassani-Mehraban, A.; Creutzburg, S.; van Heereveld, L.; Kormelink, R. Feasibility of Cowpea Chlorotic Mottle Virus-like Particles as Scaffold for Epitope Presentations. *BMC Biotechnol.* **2015**, *15*, 80.

(17) Wynne, S. A.; Crowther, R. A.; Leslie, A. G. W. The Crystal Structure of the Human Hepatitis B Virus Capsid. *Mol. Cell* **1999**, *3*, 771–780.

(18) Clément, N.; Grieger, J. C. Manufacturing of Recombinant Adeno-Associated Viral Vectors for Clinical Trials. *Mol. Ther. - Methods Clin. Dev.* **2016**, *3*, 16002.

(19) Caldeira, J. C.; Peabody, D. S. Thermal Stability of RNA Phage Virus-Like Particles Displaying Foreign Peptides. *J. Nanobiotechnology* **2011**, *9*, 22.

(20) Ashcroft, A. E.; Lago, H.; Macedo, J. M.; Horn, W. T.; Stonehouse, N. J.; Stockley, P. G. Engineering Thermal Stability in RNA Phage Capsids via Disulphide Bonds. *J Nanosci Nanotechnol* **2005**, *5*, 2034–2041.

(21) Johnson, H. R.; Hooker, J. M.; Francis, M. B.; Clark, D. S. Solubilization and Stabilization of Bacteriophage MS2 in Organic Solvents. *Biotechnol. Bioeng.* **2007**, *97*, 224–234.

(22) Fiedler, J. D.; Higginson, C.; Hovlid, M. L.; Kislukhin, A. A.; Castillejos, A.; Manzenrieder, F.; Campbell, M. G.; Voss, N. R.; Potter, C. S.; Carragher, B.; *et al.* Engineered Mutations Change the Structure and Stability of a Virus-Like Particle. *Biomacromolecules* **2012**, *13*, 2339–2348.

(23) Peabody, D. S. A Viral Platform for Chemical Modification and Multivalent

Display. *J. Nanobiotechnology* **2003**, *1*, 5.

(24) Peabody, D. S.; Manifold-Wheeler, B.; Medford, A.; Jordan, S. K.; do Carmo Caldeira, J.; Chackerian, B. Immunogenic Display of Diverse Peptides on Virus-like Particles of RNA Phage MS2. *J Mol Biol* **2008**, *380*.

(25) Arora, U.; Tyagi, P.; Swaminathan, S.; Khanna, N. Virus-like Particles Displaying Envelope Domain III of Dengue Virus Type 2 Induce Virus-Specific Antibody Response in Mice. *Vaccine* **2013**, *31*, 873–878.

(26) Speir, J. A.; Munshi, S.; Wang, G.; Baker, T. S.; Johnson, J. E. Structures of the Native and Swollen Forms of Cowpea Chlorotic Mottle Virus Determined by X-Ray Crystallography and Cryo-Electron Microscopy. *Structure* **1995**, *3*, 63–78.

(27) Zeltins, A. Construction and Characterization of Virus-like Particles: A Review. *Molecular Biotechnology*, 2013, *53*, 92–107.

(28) Shepherd, C. M.; Borelli, I. a; Lander, G.; Natarajan, P.; Siddavanahalli, V.; Bajaj, C.; Johnson, J. E.; Brooks, C. L.; Reddy, V. S. VIPERdb: A Relational Database for Structural Virology. *Nucleic Acids Res.* **2006**, *34*, D386-9.

(29) Fox, J. M.; Wang, G.; Speir, J. A.; Olson, N. H.; Johnson, J. E.; Baker, T. S.; Young, M. J. Comparison of the Native CCMV Virion with in Vitro Assembled CCMV Virions by Cryoelectron Microscopy and Image Reconstruction. *Virology* **1998**, *244*, 212–218.

(30) Zhao, X.; Fox, J. M.; Olson, N. H.; Baker, T. S.; Young, M. J. In Vitro Assembly of Cowpea Chlorotic Mottle Virus from Coat Protein Expressed in Escherichia Coli and in Vitro-Transcribed Viral cDNA. *Virology*, 1995, *207*, 486–494.

(31) Pomwised, R.; Intamaso, U.; Teintze, M.; Young, M.; Pincus, H. S. Coupling Peptide Antigens to Virus-Like Particles or to Protein Carriers Influences the Th1/Th2 Polarity of the Resulting Immune Response. *Vaccines* , 2016, *4*.

(32) Wu, Y.; Li, J.; Yang, H.; Seoung, J.; Lim, H. D.; Kim, G. J.; Shin, H. J. Targeted Cowpea Chlorotic Mottle Virus-Based Nanoparticles with Tumor-Homing Peptide F3 for Photothermal Therapy. *Biotechnol. Bioprocess Eng.* **2017**, *22*, 700–708.

(33) Barwal, I.; Kumar, R.; Kateriya, S.; Dinda, A. K.; Yadav, S. C. Targeted Delivery System for Cancer Cells Consist of Multiple Ligands Conjugated Genetically Modified CCMV Capsid on Doxorubicin GNPs Complex. *Sci. Rep.* **2016**, *6*, 37096.

(34) Lomonossoff, G. P.; Johnson, J. E. The Synthesis and Structure of Comovirus Capsids. *Progress in Biophysics and Molecular Biology*, 1991, *55*, 107–137.

(35) Wellink, J. Comovirus Isolation and RNA Extraction BT - Plant Virology

Protocols: From Virus Isolation to Transgenic Resistance. In; Foster, G. D.; Taylor, S. C., Eds.; Humana Press: Totowa, NJ, 1998; pp. 205–209.

(36) Lin, T.; Chen, Z.; Usha, R.; Stauffacher, C. V.; Dai, J. B.; Schmidt, T.; Johnson, J. E. The Refined Crystal Structure of Cowpea Mosaic Virus at 2.8 Å Resolution. *Virology* **1999**, *265*, 20–34.

(37) Koudelka, K. J.; Destito, G.; Plummer, E. M.; Trauger, S. A.; Siuzdak, G.; Manchester, M. Endothelial Targeting of Cowpea Mosaic Virus (CPMV) via Surface Vimentin. *PLOS Pathog.* **2009**, *5*, e1000417.

(38) Hovlid, M. L.; Steinmetz, N. F.; Laufer, B.; Lau, J. L.; Kuzelka, J.; Wang, Q.; Hyypia, T.; Nemerow, G. R.; Kessler, H.; Manchester, M.; *et al.* Guiding Plant Virus Particles to Integrin-Displaying Cells. *Nanoscale* **2012**, *4*, 3698–3705.

(39) Aljabali, A. A. A.; Shukla, S.; Lomonossoff, G. P.; Steinmetz, N. F.; Evans, D. J. CPMV-DOX Delivers. *Mol. Pharm.* **2013**, *10*, 3–10.

(40) Lizotte, P. H.; Wen, A. M.; Sheen, M. R.; Fields, J.; Rojanasopondist, P.; Steinmetz, N. F.; Fiering, S. In Situ Vaccination with Cowpea Mosaic Virus Nanoparticles Suppresses Metastatic Cancer. *Nat. Nanotechnol.* **2016**, *11*, 295–303.

(41) Bundy, B. C.; Franciszkowicz, M. J.; Swartz, J. R. Escherichia Coli-Based Cell-Free Synthesis of Virus-like Particles. *Biotechnol. Bioeng.* **2008**, *100*, 28–37.

(42) Böttcher, B.; Wynne, S. A.; Crowther, R. A. Determination of the Fold of the Core Protein of Hepatitis B Virus by Electron Cryomicroscopy. *Nature* **1997**, *386*, 88.

(43) Kratz, P. A.; Böttcher, B.; Nassal, M. Native Display of Complete Foreign Protein Domains on the Surface of Hepatitis B Virus Capsids. *Proc. Natl. Acad. Sci. U. S. A.* **1999**, *96*, 1915–1920.

(44) Strods, A.; Ose, V.; Bogans, J.; Cielens, I.; Kalnins, G.; Radovica, I.; Kazaks, A.; Pumpens, P.; Renhofa, R. Preparation by Alkaline Treatment and Detailed Characterisation of Empty Hepatitis B Virus Core Particles for Vaccine and Gene Therapy Applications. *Sci. Rep.* **2015**, *5*.

(45) Strable, E.; Prasuhn, D. E.; Udit, A. K.; Brown, S. D.; Link, A. J.; Ngo, J. T.; Lander, G.; Quispe, J.; Potter, C. S.; Carragher, B.; *et al.* Unnatural Amino Acid Incorporation into Virus-like Particles. *Bioconjug. Chem.* **2008**, 866–875.

(46) Daya, S.; Berns, K. I. Gene Therapy Using Adeno-Associated Virus Vectors. *Clin. Microbiol. Rev.* **2008**, *21*, 583–593.

(47) Manno, C. S.; Arruda, V. R.; Pierce, G. F.; Glader, B.; Ragni, M.; Rasko, J.;

Ozelo, M. C.; Hoots, K.; Blatt, P.; Konkle, B.; *et al.* Successful Transduction of Liver in Hemophilia by AAV-Factor IX and Limitations Imposed by the Host Immune Response. *Nat Med* **2006**, *12*, 342–347.

(48) Flotte, T.; Carter, B.; Conrad, C.; Guggino, W.; Reynolds, T.; Rosenstein, B.; Taylor, G.; Walden, S.; Wetzel, R. A Phase I Study of an Adeno-Associated Virus-CFTR Gene Vector in Adult CF Patients with Mild Lung Disease. Johns Hopkins Children's Center, Baltimore, Maryland. *Hum. Gene Ther.* **1996**, *7*, 1145–1159.

(49) Nathwani, A. C.; Tuddenham, E. G. D.; Rangarajan, S.; Rosales, C.; McIntosh, J.; Linch, D. C.; Chowdary, P.; Riddell, A.; Pie, A. J.; Harrington, C.; *et al.* Adenovirus-Associated Virus Vector–Mediated Gene Transfer in Hemophilia B. *N. Engl. J. Med.* **2011**, *365*, 2357–2365.

(50) Senior, M. After Glybera's Withdrawal, What's next for Gene Therapy? *Nat Biotech* **2017**, *35*, 491–492.

(51) Eto, Y.; Yoshioka, Y.; Ishida, T.; Yao, X.; Morishige, T.; Narimatsu, S.; Mizuguchi, H.; Mukai, Y.; Okada, N.; Kiwada, H.; *et al.* Optimized PEGylated Adenovirus Vector Reduces the Anti-Vector Humoral Immune Response against Adenovirus and Induces a Therapeutic Effect against Metastatic Lung Cancer. *Biol. Pharm. Bull.* **2010**, *33*, 1540–1544.

(52) Perabo, L.; Endell, J.; King, S.; Lux, K.; Goldnau, D.; Hallek, M.; Büning, H. Combinatorial Engineering of a Gene Therapy Vector: Directed Evolution of Adeno-Associated Virus. *J. Gene Med.* **2006**, *8*, 155–162.

(53) Maheshri, N.; Koerber, J. T.; Kaspar, B. K.; Schaffer, D. V. Directed Evolution of Adeno-Associated Virus Yields Enhanced Gene Delivery Vectors. **2006**, *24*, 198.

(54) Bazinet, C.; King, J. Initiation of P22 Procapsid Assembly in Vivo. *J. Mol. Biol.* **1988**, *202*, 77–86.

(55) Kang, S.; Lander, G. C.; Johnson, J. E.; Prevelige, P. E. Development of Bacteriophage P22 a Platform for Molecular Display: Genetic and Chemical Modifications of the Procapsid Exterior Surface. *ChemBioChem* **2008**, *9*, 514–518.

(56) Patterson, D. P.; Rynda-Apple, A.; Harmsen, A. L.; Harmsen, A. G.; Douglas, T. Biomimetic Antigenic Nanoparticles Elicit Controlled Protective Immune Response to Influenza. *ACS Nano* **2013**, *7*, 3036–3044.

(57) Schwarz, B.; Morabito, K. M.; Ruckwardt, T. J.; Patterson, D. P.; Avera, J.; Miettinen, H. M.; Graham, B. S.; Douglas, T. Viruslike Particles Encapsidating Respiratory Syncytial Virus M and M2 Proteins Induce Robust T Cell Responses. *ACS Biomater. Sci. Eng.* **2016**, *2*, 2324–2332.

(58) Patterson, D. P.; Schwarz, B.; Waters, R. S.; Gedeon, T.; Douglas, T. Encapsulation of an Enzyme Cascade within the Bacteriophage P22 Virus-Like Particle. *ACS Chem. Biol.* **2014**, *9*, 359–365.

(59) Sánchez-Sánchez, L.; Tapia-Moreno, A.; Juarez-Moreno, K.; Patterson, D. P.; Cadena-Nava, R. D.; Douglas, T.; Vazquez-Duhalt, R. Design of a VLP-Nanovehicle for CYP450 Enzymatic Activity Delivery. *J. Nanobiotechnology* **2015**, *13*, 66.

(60) Qazi, S.; Miettinen, H. M.; Wilkinson, R. A.; McCoy, K.; Douglas, T.; Wiedenheft, B. Programmed Self-Assembly of an Active P22-Cas9 Nanocarrier System. *Mol. Pharm.* **2016**, *13*, 1191–1196.

(61) Shishovs, M.; Rumnieks, J.; Diebolder, C.; Jaudzems, K.; Andreas, L. B.; Stanek, J.; Kazaks, A.; Kotelovica, S.; Akopjana, I.; Pintacuda, G.; *et al.* Structure of AP205 Coat Protein Reveals Circular Permutation in ssRNA Bacteriophages. *J. Mol. Biol.* **2016**, *428*, 4267–4279.

(62) Tissot, A. C.; Renhofa, R.; Schmitz, N.; Cielens, I.; Meijerink, E.; Ose, V.; Jennings, G. T.; Saudan, P.; Pumpens, P.; Bachmann, M. F. Versatile Virus-Like Particle Carrier for Epitope Based Vaccines. *PLoS One* **2010**, *5*, e9809.

(63) Leneghan, D. B.; Miura, K.; Taylor, I. J.; Li, Y.; Jin, J.; Brune, K. D.; Bachmann, M. F.; Howarth, M.; Long, C. A.; Biswas, S. Nanoassembly Routes Stimulate Conflicting Antibody Quantity and Quality for Transmission-Blocking Malaria Vaccines. *Sci. Rep.* **2017**, *7*, 3811.

(64) Brune, K. D.; Leneghan, D. B.; Brian, I. J.; Ishizuka, A. S.; Bachmann, M. F.; Draper, S. J.; Biswas, S.; Howarth, M. Plug-and-Display: Decoration of Virus-Like Particles via Isopeptide Bonds for Modular Immunization. *Sci. Rep.* **2016**, *6*, 19234.

(65) Ashley, C. E.; Carnes, E. C.; Phillips, G. K.; Durfee, P. N.; Buley, M. D.; Lino, C. A.; Padilla, D. P.; Phillips, B.; Carter, M. B.; Willman, C. L.; *et al.* Cell-Specific Delivery of Diverse Cargos by Bacteriophage MS2 Virus-like Particles. *ACS Nano* **2011**, *5*, 5729–5745.

(66) O'Rourke, J. P.; Daly, S. M.; Triplett, K. D.; Peabody, D.; Chackerian, B.; Hall, P. R. Development of a Mimotope Vaccine Targeting the Staphylococcus Aureus Quorum Sensing Pathway. *PLoS One* **2014**, *9*, e111198.

(67) ElSohly, A. M.; Netirojjanakul, C.; Aanei, I. L.; Jager, A.; Bendall, S. C.; Farkas, M. E.; Nolan, G. P.; Francis, M. B. Synthetically Modified Viral Capsids as Versatile Carriers for Use in Antibody-Based Cell Targeting. *Bioconjug. Chem.* **2015**, *26*, 1590–1596.

(68) Aanei, I. L.; ElSohly, A. M.; Farkas, M. E.; Netirojjanakul, C.; Regan, M.; Taylor Murphy, S.; O'Neil, J. P.; Seo, Y.; Francis, M. B. Biodistribution of Antibody-MS2 Viral Capsid Conjugates in Breast Cancer Models. *Mol. Pharm.* **2016**, *13*, 3764–3772.

(69) Tong, G. J.; Hsiao, S. C.; Carrico, Z. M.; Francis, M. B. Viral Capsid DNA Aptamer Conjugates as Multivalent Cell-Targeting Vehicles. *J. Am. Chem. Soc.* **2009**, *131*, 11174–11178.

(70) Tars, K.; Fridborg, K.; Bundule, M.; Liljas, L. Structure Determination of Bacteriophage PP7 from Pseudomonas Aeruginosa: From Poor Data to a Good Map. *Acta Crystallogr. Sect. D* **2000**, *56*, 398–405.

(71) Caldeira, J. D.; Medford, A.; Kines, R. C.; Lino, C. A.; Schiller, J. T.; Chackerian, B.; Peabody, D. S. Immunogenic Display of Diverse Peptides, Including a Broadly Cross-Type Neutralizing Human Papillomavirus L2 Epitope, on Virus-like Particles of the RNA Bacteriophage PP7. *Vaccine* **2010**, *28*.

(72) Tumban, E.; Peabody, J.; Tyler, M.; Peabody, D. S.; Chackerian, B. VLPs Displaying a Single L2 Epitope Induce Broadly Cross-Neutralizing Antibodies against Human Papillomavirus. *PLoS One* **2012**, *7*, e49751.

(73) Chackerian, B.; Caldeira, J. D.; Peabody, J.; Peabody, D. S. Peptide Epitope Identification by Affinity Selection on Bacteriophage MS2 Virus-Like Particles. *J Mol Biol* **2011**, *409*.

(74) Sun, Y.; Sun, Y.; Zhao, R.; Gao, K. Intracellular Delivery of Messenger RNA by Recombinant PP7 Virus-like Particles Carrying Low Molecular Weight Protamine. *BMC Biotechnol.* **2016**, *16*, 46.

(75) van den Worm, S. H. E.; Koning, R. I.; Warmenhoven, H. J.; Koerten, H. K.; van Duin, J. Cryo Electron Microscopy Reconstructions of the Leviviridae Unveil the Densest Icosahedral RNA Packing Possible. *J. Mol. Biol.* **2006**, *363*, 858–865.

(76) Karnik, S.; Billeter, M. The Lysis Function of RNA Bacteriophage Qbeta Is Mediated by the Maturation (A2) Protein. *EMBO J.* **1983**, *2*, 1521–1526.

(77) Kozlovska, T. M.; Cielens, I.; Dreilinna, D.; Dišlers, A.; Baumanis, V.; Ose, V.; Pumpens, P. Recombinant Rna Phage Qβ Capsid Particles Synthesized and Self-Assembled in Escherichia Coli. *Gene* **1993**, *137*, 139–143.

(78) Rumnieks, J.; Tars, K. Crystal Structure of the Read-through Domain from Bacteriophage Qbeta A1 Protein. *Protein Sci.* **2011**, *20*, 1707–1712.

(79) Freivalds, J.; Dislers, A.; Ose, V.; Skrastina, D.; Cielens, I.; Pumpens, P.; Sasnauskas, K.; Kazaks, A. Assembly of Bacteriophage Qβ Virus-like Particles in

Yeast Saccharomyces Cerevisiae and Pichia Pastoris. *J. Biotechnol.* **2006**, *123*, 297–303.

(80) Engelberg-Kulka, H.; Israeli-Reches, M.; Dekel, L.; Friedmann, A. Q Beta-Defective Particles Produced in a Streptomycin-Resistant Escherichia Coli Mutant. *J. Virol.* **1979**, *29*, 1107–1117.

(81) Patel, K. G.; Swartz, J. R. Surface Functionalization of Virus-Like Particles by Direct Conjugation Using Azide−Alkyne Click Chemistry. *Bioconjug. Chem.* **2011**, *22*, 376–387.

(82) Golmohammadi, R.; Fridborg, K.; Bundule, M.; Valegard, K.; Liljas, L. The Crystal Structure of Bacteriophage QB at 3.5A Resolution. *Structure* **1996**, *4*, 543–554.

(83) Lima, S. M. B.; Vaz, A. C. Q.; Souza, T. L. F.; Peabody, D. S.; Silva, J. L.; Oliveira, A. C. Dissecting the Role of Protein-Protein and Protein-Nucleic Acid Interactions in MS2 Bacteriophage Stability. *FEBS J.* **2006**, *273*, 1463–1475.

(84) Rhee, J.-K.; Baksh, M.; Nycholat, C.; Paulson, J. C.; Kitagishi, H.; Finn, M. G. Glycan-Targeted Virus-like Nanoparticles for Photodynamic Therapy. *Biomacromolecules* **2012**, *13*, 2333–2338.

(85) Pokorski, J. K.; Breitenkamp, K.; Liepold, L. O.; Qazi, S.; Finn, M. G. Functional Virus-Based Polymer-Protein Nanoparticles by Atom Transfer Radical Polymerization. *J. Am. Chem. Soc.* **2011**, *133*, 9242–9245.

(86) Vasiljeva, I.; Kozlovska, T.; Cielens, I.; Strelnikova, A.; Kazaks, A.; Ose, V.; Pumpens, P. Mosaic Qβ Coats as a New Presentation Model. *FEBS Lett.* **1998**, *431*, 7–11.

(87) Fiedler, J. D.; Brown, S. D.; Lau, J.; Finn, M. G. RNA-Directed Packaging of Enzymes within Virus-Like Particles. *Angew. Chemie Int. Ed.* **2010**, *49*, 9648–9651.

(88) Vivier, E.; Tomasello, E.; Baratin, M.; Walzer, T.; Ugolini, S. Functions of Natural Killer Cells. *Nat Immunol* **2008**, *9*, 503–510.

(89) Sarma, J. V.; Ward, P. A. The Complement System. *Cell Tissue Res.* **2011**, *343*, 227–235.

(90) Akira, S.; Uematsu, S.; Takeuchi, O. Pathogen Recognition and Innate Immunity. *Cell* **2006**, *124*, 783–801.

(91) Bottazzi, B.; Garlanda, C.; Salvatori, G.; Jeannin, P.; Manfredi, A.; Mantovani, A. Pentraxins as a Key Component of Innate Immunity. *Curr. Opin. Immunol.* **2006**,

*18*, 10–15.

(92) Sontheimer, R. D.; Racila, E.; Racila, D. M. C1q: Its Functions within the Innate and Adaptive Immune Responses and Its Role in Lupus Autoimmunity. *J. Invest. Dermatol.* **2005**, *125*, 14–23.

(93) Grönwall, C.; Vas, J.; Silverman, G. J. Protective Roles of Natural IgM Antibodies. *Front. Immunol.* **2012**, *3*, 66.

(94) Varner, C. T.; Rosen, T.; Martin, J. T.; Kane, R. S. Recent Advances in Engineering Polyvalent Biological Interactions. *Biomacromolecules* **2015**, *16*, 43–55.

(95) Link, A.; Zabel, F.; Schnetzler, Y.; Titz, A.; Brombacher, F.; Bachmann, M. F. Innate Immunity Mediates Follicular Transport of Particulate but Not Soluble Protein Antigen. *J. Immunol.* **2012**, *188*, 3724–3733.

(96) Vinuesa, C. G.; Linterman, M. A.; Goodnow, C. C.; Randall, K. L. T Cells and Follicular Dendritic Cells in Germinal Center B-Cell Formation and Selection. *Immunol. Rev.* **2010**, *237*, 72–89.

(97) Zaiss, A.-K.; Cotter, M. J.; White, L. R.; Clark, S. A.; Wong, N. C. W.; Holers, V. M.; Bartlett, J. S.; Muruve, D. A. Complement Is an Essential Component of the Immune Response to Adeno-Associated Virus Vectors. *J. Virol.* **2008**, *82*, 2727–2740.

(98) Lavin, Y.; Mortha, A.; Rahman, A.; Merad, M. Regulation of Macrophage Development and Function in Peripheral Tissues. *Nat Rev Immunol* **2015**, *15*, 731–744.

(99) Mosser, D. M.; Edwards, J. P. Exploring the Full Spectrum of Macrophage Activation. *Nat. Rev. Immunol.* **2008**, *8*, 958–969.

(100) Martinez, F. O.; Gordon, S. The M1 and M2 Paradigm of Macrophage Activation: Time for Reassessment. *F1000Prime Rep.* **2014**, *6*.

(101) Mildner, A.; Jung, S. Development and Function of Dendritic Cell Subsets. *Immunity 40*, 642–656.

(102) Bottazzi, B.; Doni, A.; Garlanda, C.; Mantovani, A. An Integrated View of Humoral Innate Immunity: Pentraxins as a Paradigm. *Annu. Rev. Immunol.* **2010**, *28*, 157–183.

(103) Kovacsovics-Bankowski, M.; Clark, K.; Benacerraf, B.; Rock, K. L. Efficient Major Histocompatibility Complex Class I Presentation of Exogenous Antigen upon Phagocytosis by Macrophages. *Proc. Natl. Acad. Sci. U. S. A.* **1993**, *90*, 4942–4946.

(104) Curtsinger, J. M.; Schmidt, C. S.; Mondino, A.; Lins, D. C.; Kedl, R. M.; Jenkins, M. K.; Mescher, M. F. Inflammatory Cytokines Provide a Third Signal for Activation of Naive CD4+ and CD8+ T Cells. *J. Immunol.* **1999**, *162*, 3256.

(105) Fang, P.-Y.; Gómez Ramos, L. M.; Holguin, S. Y.; Hsiao, C.; Bowman, J. C.; Yang, H.-W.; Williams, L. D. Functional RNAs: Combined Assembly and Packaging in VLPs. *Nucleic Acids Res.* **2017**, *45*, 3519–3527.

(106) Speir, J. A.; Johnson, J. E. Nucleic Acid Packaging in Viruses. *Curr. Opin. Struct. Biol.* **2012**, *22*, 65–71.

(107) Barton, G. M. Viral Recognition by Toll-like Receptors. *Semin. Immunol.* **2007**, *19*, 33–40.

(108) Lund, J. M.; Alexopoulou, L.; Sato, A.; Karow, M.; Adams, N. C.; Gale, N. W.; Iwasaki, A.; Flavell, R. A. Recognition of Single-Stranded RNA Viruses by Toll-like Receptor 7. *Proc. Natl. Acad. Sci. U. S. A.* **2004**, *101*, 5598–5603.

(109) Forsbach, A.; Nemorin, J.-G.; Montino, C.; Müller, C.; Samulowitz, U.; Vicari, A. P.; Jurk, M.; Mutwiri, G. K.; Krieg, A. M.; Lipford, G. B.; *et al.* Identification of RNA Sequence Motifs Stimulating Sequence-Specific TLR8-Dependent Immune Responses. *J. Immunol.* **2008**, *180*, 3729.

(110) Hemmi, H.; Takeuchi, O.; Kawai, T.; Kaisho, T.; Sato, S.; Sanjo, H.; Matsumoto, M.; Hoshino, K.; Wagner, H.; Takeda, K.; *et al.* A Toll-like Receptor Recognizes Bacterial DNA. *Nature* **2000**, *408*, 740–745.

(111) O'Shea, J. J.; Paul, W. E. Mechanisms Underlying Lineage Commitment and Plasticity of Helper CD4+ T Cells. *Science (80-. ).* **2010**, *327*, 1098 LP-1102.

(112) Zabel, F.; Kundig, T. M.; Bachmann, M. F. Virus-Induced Humoral Immunity: On How B Cell Responses Are Initiated. *Curr. Opin. Virol.* **2013**, *3*, 357–362.

(113) Bachmann, M. F.; Rohrer, U. H.; Kundig, T. M.; Burki, K.; Hengartner, H.; Zinkernagel, R. M. The Influence of Antigen Organization on B Cell Responsiveness. *Science (80-. ).* **1993**, *262*, 1448.

(114) Swartz, M. A. The Physiology of the Lymphatic System. *Adv. Drug Deliv. Rev.* **2001**, *50*, 3–20.

(115) Jegerlehner, A.; Storni, T.; Lipowsky, G.; Schmid, M.; Pumpens, P.; Bachmann, M. F. Regulation of IgG Antibody Responses by Epitope Density and CD21-Mediated Costimulation. *Eur. J. Immunol.* **2002**, *32*, 3305–3314.

(116) Jegerlehner, A.; Maurer, P.; Bessa, J.; Hinton, H. J.; Kopf, M.; Bachmann, M. F.

TLR9 Signaling in B Cells Determines Class Switch Recombination to IgG2a. *J. Immunol.* **2007**, *178*, 2415–2420.

(117) Hemmi, H.; Akira, S. TLR Signalling and the Function of Dendritic Cells. *Chem. Immunol. Allergy* **2005**, *86*, 120–135.

(118) Hou, B.; Saudan, P.; Ott, G.; Wheeler, M. T.; Ji, M.; Kuzmich, L.; Lee, L. M.; Coffman, R. L.; Bachmann, M. F.; DeFranco, A. L. Selective Utilization of Toll-like Receptor and MyD88 Signaling in B Cells for Enhancement of the Antiviral Germinal Center Response. *Immunity* **2011**, *34*, 375–384.

(119) Braun, M.; Jandus, C.; Maurer, P.; Hammann-Haenni, A.; Schwarz, K.; Bachmann, M. F.; Speiser, D. E.; Romero, P. Virus-like Particles Induce Robust Human T-Helper Cell Responses. *Eur. J. Immunol.* **2012**, *42*, 330–340.

(120) Schwarz, K.; Meijerink, E.; Speiser, D. E.; Tissot, A. C.; Cielens, I.; Renhof, R.; Dishlers, A.; Pumpens, P.; Bachmann, M. F. Efficient Homologous Prime-Boost Strategies for T Cell Vaccination Based on Virus-like Particles. *Eur. J. Immunol.* **2005**, *35*, 816–821.

(121) Nayak, S.; Herzog, R. W. Progress and Prospects: Immune Responses to Viral Vectors. *Gene Ther.* **2010**, *17*, 295–304.

(122) Jooss, K.; Yang, Y.; Fisher, K. J.; Wilson, J. M. Transduction of Dendritic Cells by DNA Viral Vectors Directs the Immune Response to Transgene Products in Muscle Fibers. *J. Virol.* **1998**, *72*, 4212–4223.

(123) Mingozzi, F.; Maus, M. V; Hui, D. J.; Sabatino, D. E.; Murphy, S. L.; Rasko, J. E. J.; Ragni, M. V; Manno, C. S.; Sommer, J.; Jiang, H.; *et al.* CD8+ T-Cell Responses to Adeno-Associated Virus Capsid in Humans. *Nat Med* **2007**, *13*, 419–422.

(124) Li, H.; Murphy, S. L.; Giles-Davis, W.; Edmonson, S.; Xiang, Z.; Li, Y.; Lasaro, M. O.; High, K. A.; Ertl, H. C. J. Pre-Existing AAV Capsid-Specific CD8+ T Cells Are Unable to Eliminate AAV-Transduced Hepatocytes. *Mol. Ther.* **2007**, *15*, 792–800.

(125) Kaiser, C. R.; Flenniken, M. L.; Gillitzer, E.; Harmsen, A. L.; Harmsen, A. G.; Jutila, M. A.; Douglas, T.; Young, M. J. Biodistribution Studies of Protein Cage Nanoparticles Demonstrate Broad Tissue Distribution and Rapid Clearance in Vivo. *Int. J. Nanomedicine* **2007**, *2*, 715–733.

## Chapter 2: Design of Qβ VLPs displaying peptide epitopes for vaccination

### 2.1. Abstract

The complement system is emerging as a new target for treating many diseases. For example, eculizumab, a humanized monoclonal antibody against complement component 5 (C5), has been approved for paroxysmal nocturnal hemoglobinuria (PNH) in which patient erythrocytes are lysed by complement. In this study, we developed vaccines to elicit autologous anti-C5 antibody production in mice for complement inhibition. Immunization of mice with a conservative C5 xenoprotein raised high titers of IgGs against the xenogenous C5, but these antibodies did not reduce C5 activity in the blood. In contrast, an autologous mouse C5 vaccine containing multiple predicted epitopes together with a tolerance-breaking peptide was found to induce anti-C5 autoantibody production *in vivo*, resulting in decreased hemolytic activity in the blood. We further validated a peptide epitope within this C5 vaccine and created recombinant virus-like particles displaying this epitope fused with the tolerance-breaking peptide. Immunizing mice with these novel nanoparticles elicited strong humoral responses against recombinant mouse C5, reduced hemolytic activity, and protected the mice from complement-mediated intravascular hemolysis in a model of PNH. This proof-of-concept study demonstrated that autologous C5-based vaccines could be an effective alternative or supplement for treating complement-mediated diseases such as PNH.

### 2.2. Introduction

Therapeutic vaccination has recently emerged as a potential strategy for the treatment of numerous autoimmune disorders.[1–3] In contrast to viral or bacterial infections,

it is inherently difficult to treat autoimmune disorders using vaccination strategies due to the evolution of immunological tolerance against self-antigens.[4] Virus-like particles (VLPs) have provided a particularly useful vaccine platform in this respect. While VLPs resemble viruses in most ways relevant to the generation of an immune response (repetitive structure, lymphatic trafficking, B-cell recognition, T-cell stimulation, packaged bacterial RNA),[5,6] they are non-infectious and can act as self-adjuvants capable of breaking immune tolerance.[7–9]

The bacteriophage Qβ is a highly effective and easily-modified VLP platform for these purposes.[10,11] It has been reported that the direct attachment of antigens to the surface of Qβ VLPs using chemical cross-linkers is effective in eliciting strong immune responses against self-antigens for vaccine development. Bachmann and colleagues have worked extensively in this area, designing Qβ-based vaccines against several cytokines that have been implicated in autoimmune disorders, with several candidates advancing to clinical trials.[12–14] Conjugation of full-length IL-1β to Qβ VLPs generated vaccines that were well-tolerated and gave rise to neutralizing antibody responses which correlated with improved glucose tolerance in both pre-clinical[1] and clinical trials.[2] Interleukin-17 (IL-17) has been implicated in the pathology of rheumatoid arthritis[15] and multiple sclerosis,[16] and chemical conjugation of recombinant IL-17 to Qβ VLPs produced vaccines that ameliorated disease progression in murine models of both collagen-induced arthritis and experimental autoimmune encephalomyelitis.[3,17] Immunization of mice deficient in apolipoprotein E with full-length IL-1α conjugated to Qβ VLPs was shown to be effective at reducing inflammation and plaque progression, suggesting that vaccination may be an effective treatment for atherosclerosis.[18]

Despite the promising results of these studies, the display of full-length proteins on the VLP surface still presents challenges in construct design, safety, and efficacy. The ligation of two large biomolecules is relatively inefficient using all but the most robust conjugation strategies, and the systemic delivery of cytokines and other bioactive proteins is often associated with acute off-target toxicity.[19] Furthermore, delivery of full-length protein conjugates may not present antigens in a context capable of overcoming immunological tolerance. The technology developed by Brown and Fiedler for the genetic incorporation and display of peptide antigens on the Qβ VLP surface[11] could provide useful strategies for overcoming these hurdles but has remained relatively unexplored. Introduction of antigenic peptides at the genetic level overcomes the limitations of challenging conjugations, while also eliminating toxicity concerns associated with delivery of the full-length protein. Introducing minimized domains and peptides could also allow for presentation in a more unnatural context on the VLP surface, favoring the development of a specific immune response. The work presented in this chapter will detail the application of this technology in developing vaccines to treat complement-mediated hemolytic disorders.

The complement system is an important part of the innate immune system, consisting of multiple proteins present at varying levels in the blood.[20] When complement is activated through any of three general pathways (by antibody-antigen complexes through the classical pathway, by certain carbohydrates through the lectin pathway, or spontaneously through the alternative pathway), C3 is activated to form C5 convertase and cleaves C5 into C5b and C5a. When C5 is activated in this way, membrane attack complexes (MACs) consisting of C5b-9 are assembled and form pores through the cell

membrane, resulting in lysis or damage of the target cell. At the same time, the small fragment C5a is released into the fluid phase and binds to its receptor (C5aR) on nearby immune cells to promote inflammatory reactions. Activated complement cannot distinguish self from foreign cells, but self-cells express cell surface complement inhibitors, including CD55 and CD59, which confer protection from complement-mediated attack.[20] Aberrant complement activation is integrally involved in many diseases, and many complement components are currently being tested as new targets for drug development.[21] C5 is a promising example because its concentration in blood is relatively low (~100 μg/mL for C5 versus ~1500 μg/mL for C3), and C5 inhibition should theoretically inhibit both the formation of MACs, which damage tissue cells, and suppress the release of C5a, a potent inflammation initiator that is involved in many pathological conditions.

Indeed, eculizumab, a humanized anti-human C5 monoclonal antibody (mAb) has been successfully employed to treat complement-mediated diseases including paroxysmal nocturnal hemoglobinuria (PNH)[22] and atypical hemolytic uremic syndrome (aHUS).[23] In most patients with PNH, inactivation of the gene for phosphatidylinositol glycan A in the glycosyl phosphatidylinositol (GPI) pathway in hematopoietic stem cells results in red blood cells (RBCs) lacking the GPI-anchored cell surface complement inhibitors CD55 and CD59, rendering these cells highly susceptible to complement-mediated lysis.[24] Eculizumab binds to C5 and inhibits the formation of MACs, thereby preventing complement-mediated hemolysis in PNH. Although highly effective, eculizumab is the most expensive drug on the market with an annual cost of more than $400,000/patient, and in most of the patients, life-long drug administration is required.[25,26] Clearly, the

development of an effective and affordable C5-targeting therapy for treating PNH is a worthwhile goal.

We describe here our first exploration of the idea that eliciting a moderate immune response against the C5 protein may represent a cost-effective treatment of diseases such as PNH caused by excess complement activity. To explore the feasibility of eliciting anti-C5 antibody production from the host immune system to prevent complement-mediated hemolysis, we combined the identification of C5 epitopes using previously reported data and computational prediction with a modular strategy of VLP functionalization to produce candidate immunogens. These vaccine candidates were able to elicit anti-C5 autoantibodies and protect mice in a model of intravascular hemolysis. Our data suggest that autologous C5 vaccines could be developed as an alternative or supplement to eculizumab for treating complement-mediated diseases such as PNH.

## 2.3. Materials and Methods

*Mice and complement reagents*

C57BL/6 WT mice were purchased from the Jackson Laboratory and maintained in the animal facility of Cleveland Clinic. All animal care and experimental procedures were approved by the Institutional Animal Care and Use Committee of Cleveland Clinic. Purified human C5 protein and pooled human C5-depleted serum were purchased from Complement Technology Inc. (Tylor, TX).

*Mouse C5 vaccine design*

The mouse C5 protein sequence was analyzed using OptimumAntigen Design™ software (Genscript, NJ) which utilizes an advanced antigen design algorithm based on several protein databases. The identified epitopes were compared with the published C5

protein crystal structure[27] to check for surface exposure. These steps provided twelve potential immunogenic epitopes that are likely present on the surface of the native mouse protein. An artificial gene was designed coding for a polypeptide comprised of these twelve potential epitopes interspersed in three places with a copy of the nonnatural pan-DR epitope (PADRE) sequence (a linear peptide that improves humoral responses against antigens and helps break immune tolerance[28,29]) and capped at the C-terminus with a 6XHis tag.

*Mouse C5 vaccine expression and purification*

The artificial gene (obtained from Genscript, NJ) was cloned into the PET-21b expression vector and transformed into *E. coli* strain BL21. Expression of the desired protein, intended to be a recombinant mouse C5 vaccine, was induced using the Overnight Express™ Autoinduction System (EMD Millipore, MA) following manufacturer-provided protocols. The protein formed inclusion bodies and was isolated using the B-PER® Bacterial Protein Extraction Reagent (Thermo Fisher, IL), denatured in 8 M urea, and refolded by dialysis against PBS containing gradually reduced concentrations of urea. The refolded recombinant C5 was then affinity-purified using HisPur™ Cobalt Resin (Thermo Fisher, IL) following our previously published and manufacturer-provided protocols. The purity of the resultant protein was checked by SDS-PAGE and then purified again using a C8 reversed-phase HPLC (Beckman, CA). The single major protein peak was collected for sequential experiments.

*Mouse immunizations*

C57BL/6 WT mice (8-12 weeks old) were used in all *in vivo* experiments. The amounts administered per mouse were as follows: human C5, 25 μg; recombinant mouse C5, 100 μg; VLP-based C5, 200 μg. For immunization, vaccines were emulsified with

complete Freund's adjuvant (CFA) (Difco Laboratories, MI), then administered subcutaneously. For human C5 and recombinant mouse C5 vaccine studies, mice immunized with CFA alone were included as controls; for VLP-based C5 vaccine studies, mice immunized with the same amount of wild-type VLPs (lacking the C5 epitope) were used as controls. The immunized mice were boosted 2 weeks after the initial immunization with the same amount of antigens in incomplete Freund's adjuvant (IFA) (Difco Laboratories, MI) once or twice after every other week.

*Serum anti-C5 antibody titer measurements by ELISA*

One week after the last boost, serum was collected from the tail vein and the anti-C5 IgG titers were measured by ELISA. Briefly, the ELISA plate was coated with 5 μg/mL purified full-length human C5 or recombinant mouse C5. After blocking, diluted serum samples were added to the plate and incubated for 2h. After washing, HRP-anti-mouse IgG was added as a detection antibody. The absorbance was read at 450 nm using a microtiter plate reader (Molecular Devices, CA).

*Ex vivo mouse complement-mediated hemolysis assay*

Antibody-sensitized sheep erythrocytes ($E^{shA}$) were used in the *ex vivo* mouse complement-mediated hemolysis assay following previously published protocol with modifications.[30] In brief, 15 μL mouse serum and 5 μL human C5 depleted serum were added to $GVB^{+2}$ (5 mM Barbital, 145 mM NaCl, 0.5 mM $MgCl_2$, 0.15 mM $CaCl_2$ and 0.1% Gelatin, pH 7.4) in a total volume of 90 μL, then 10 μL of $E^{shA}$ (~ $5x10^6$) suspended in $GVB^{+2}$ were added to each sample and incubated in 37℃ for 5mins. For negative control, 5 mM EDTA was added to the $GVB^{+2}$ to inhibit the complement activation. After incubation, samples were centrifuged, and the absorbance of the supernatant was measured

at 414 nm using a microtiter plate reader. To calculate the percentage of hemolysis rate, the following equation was used: Hemolysis rate (%) = [(A-B)/(C-B)] x100%. A= $OD_{414}$ reading of sample in $GVB^{+2}$, B= $OD_{414}$ reading of sample in $GVB^{+2}$ with 5mM EDTA, C= $OD_{414}$ reading of maximum hemolysis induced by $H_2O$.

*In vivo complement-mediated intravascular hemolysis and hemoglobinuria*

Complement-induced intravascular hemolysis was induced followed by published protocols with modifications.[31] In brief, each mouse was injected with 200 μL human C5-depleted serum intraperitoneally, and 1 hour later, blood was collected through retro-orbital bleeding (to minimize bleeding-related hemolysis). Sera were diluted at a 1:10 ratio in PBS in a total volume of 100 μL and hemolysis was quantitated by OD reading at 414 nm. At the same time of blood collection, the mouse abdomen was gently pressed to collect urine, which was diluted at a ratio of 1:10 before hemoglobin levels were measured by OD reading at 414 nm.

*Epitope mapping of the recombinant mouse C5 vaccine*

A library of 15-mer oligopeptides overlapping each other by 6 amino acids, spanning the entire sequence of the recombinant mouse C5 vaccine, was custom-synthesized (GenScript, NJ) and used to map the dominant epitope(s) by ELISA. In brief, each peptide (20 μg/mL) was used to coat a plate at 4°C overnight. After blocking with 1% BSA in PBS for two hours, the plate was incubated (room temperature, 2 h) with 1:500 diluted sera collected from the recombinant C5 vaccine-immunized mice. After washing, the plate was incubated with HRP-labeled anti-mouse IgG at RT for 1 h, followed by color development by adding the HRP substrate TMB and $OD_{450}$ reading using a microplate reader (Molecular Devices, CA).

*Mouse C5 protein structure modeling and peptides epitope localization*

A structural homology model of mouse C5 was generated using the Phyre2 protein recognition server following an established protocol.[32] The X-ray crystal structure of human C5 protein was used as the template (PDB access code: 3cu7).[27] Sequence identity and homology between human and mouse C5 proteins is 89% respectively. A normal modeling mode was used. Major steps of modeling include gathering homologous sequences, fold library scanning, loop modeling, and side-chain placement. The PyMOL visualization program (Schrödinger, LLC, MA) was used to display all the structural models in this work.

*Construction of plasmids for VLP-C5 vaccine*

The previously described pCDF-CP plasmid[33] has a multiple cloning site (containing NdeI and XhoI restriction sequences) immediately downstream of the viral coat protein (CP) gene. The DNA sequence for the mC5 cleavage domain and the PADRE peptide, codon optimized for *E. coli* expression, were inserted at this site to generate plasmids pCDF-CP-mC5 and pCDF-CP-PADRE, respectively. The pCDF-CP-PADRE vector was further elaborated with the codon-optimized DNA for the identified C5 epitope (ASYKPSKEESTSGS, designated P2) or a scrambled variant (SPAGSEETSKSYSK, designated scrP2) downstream of the PADRE sequence, resulting in the plasmids pCDF-CP-PADRE-P2 or pCDF-CP-PADRE-scrP2.

*VLP-C5 vaccine production and characterization*

The VLP-C5 vaccines were produced and characterized following previously published protocols.[33] In brief, electrocompetent ClearColi BL21(DE3) E. coli cells (Lucigen) were co-transformed with both pCDF-CP-mC5/pCDF-CP-PADRE-P2 and

pET28-CP to produce VLP-C5 particles. The control VLP particles were produced using only cells transformed with pET28-CP. Cells were plated on selective SOB agar. After 24 h, isolated colonies were selected into autoclaved SOB media (1% NaCl; 25 mL) containing appropriate antibiotics and grown overnight at 37°C. Cultures were diluted into autoclaved selective SOB media (1% NaCl; 500 mL) the following day. Cultures were grown at 37°C until the cultures reached mid-log phase ($O.D._{600}$ ~ 0.9), at which time protein expression was induced by the addition of IPTG to a final concentration of 1 mM. Cultures were maintained at 30°C for 16 h, after which cells were pelleted by centrifugation at 6,000 rpm for 10 min. Cells were lysed with a probe sonicator (10 min total, 5 s intervals) in an ice bath. Cell debris was removed by centrifugation at 14,000 rpm for 10 min, and supernatant collected. VLPs were precipitated by the addition of 30% $(NH_4)_2SO_4$ (*w/v*) at 4°C for 2 h, and samples were pelleted at 14,000 rpm for 10 min. The pellet was dissolved in 1x TBS and extracted with *n*-BuOH:$CHCl_3$ (1:1, *v/v*) to remove lipids and aggregates. The samples were centrifuged at 3,500 rpm for 10 min, and the aqueous phase was collected and subsequently loaded onto 10-40% sucrose density gradients. VLPs purified on gradients by centrifugation at 28,000 rpm for 4 h, and VLP bands were isolated via syringe. Particles pelleted by centrifugation at 68,000 rpm for 2 h, and subsequent pellets dissolved in 0.1M phosphate buffer and characterized.

The resulting VLPs were characterized by FPLC size-exclusion chromatography (Superose 6, monitored by absorbance at 280 nm), dynamic light scattering (Wyatt Dynapro plate reader), and microfluidic gel electrophoresis (Agilent 2100 Bioanalyzer with Series II Protein 80 chips). The average number of CP and CP-C5 subunits per particle was determined by integrating the electropherogram peaks in the instrument

software. Levels of endotoxin contamination were found to be less than 0.1 EU/mL using Pierce LAL Chromogenic Endotoxin Quantitation Kit (Thermo Fisher, IL).

## 2.4. Results and Discussion

### *2.4.1. Epitope discovery and vaccine design*

Because 1) autoantigens are generally immune tolerized, 2) previous studies suggest that conservative antigens from different species could elicit the production of antibodies that cross-react with the autoantigens,[34–38] and 3) mouse and human C5 protein share >80% homology,[39] we initially immunized mice with purified human C5 protein, hoping that the developed polyclonal antibodies could cross-react with mouse C5, therefore inhibiting mouse C5 activity *in vivo*. Indeed, mice immunized with human C5 protein developed high titers of antibodies against human C5 (**Figure 1A**); however, sera from

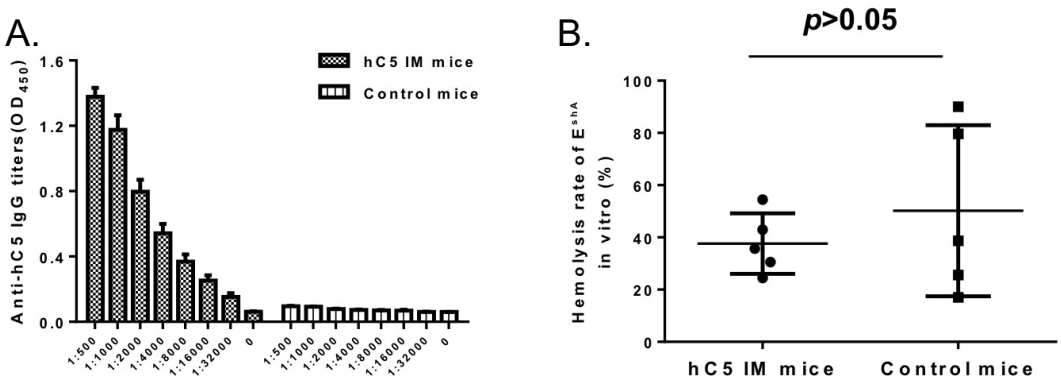


**Figure 1.** Immunization of mice with purified human C5 (hC5) generating anti-hC5 IgG's that do not reduce mouse C5 (mC5) activity. WT C57BL/6 mice were immunized with purified hC5 in CFA or CFA alone (control) and boosted 2 weeks later. One week after the boost, serum samples were collected. (A) Serum samples were tested for anti-hC5 IgG antibody titers using a hC5 ELISA, showing high titers of anti-hC5 antibodies developed in the hC5 immunized (IM) mice (detectable at a 1:32 000 dilution), but not control mice (not detectable even at a 1:500 dilution). (B) C5 activity in the serum samples were assessed by a modified $E^{shA}$ hemolysis assay, and no significant difference was found between the hC5-immunized mice and the control mice. $n = 7$ in each group.

these immunized mice had similar potency as sera from control mice in lysing sensitized sheep erythrocytes *ex vivo* (**Figure 1B**). These results demonstrated that immunizing mice with human C5 did not develop cross-reacting antibodies to reduce mouse C5 activity *in vivo*.

We next sought to minimize a domain from the mouse C5 protein for recombinant display on the Qβ VLP platform with the goal of reducing or blocking C5 activity as in patients receiving eculizumab A large domain (60 amino acids) of the mC5 protein containing the cleavage site was encoded as a C-terminal extension of the viral coat protein; flanking regions of the cleavage site were included in the construct design to ensure the cleavage site maintained the context of its native structure in order to generate effective neutralizing antibody responses. These particles were prepared according to a well-established method[33] in which a mixture of truncated and extended capsid proteins are co-expressed in *E. coli* and self-assemble into a hybrid particle. Notably, only 15 copies of the extension were displayed per capsid in this case. The resultant VLP-mC5 vaccine was characterized using dynamic light scattering, size-exclusion chromatography, and gel electrophoresis, showing intact particles of the expected size (~ 30 nm) and composition. Mice immunized with these particles developed robust IgG titers against the Qβ capsid (**Figure 2A**) but failed to develop a response against the C5 protein (**Figure 2B**). Furthermore, sera from immunized mice possessed similar activity as sera from control mice in lysing sheep erythrocytes (**Figure 2C**).

After failing to generate a cross-reactive immune response with the first generation VLP vaccine, we next planned to immunize the mice with an autologous mouse C5 mosaic protein to systematically identify immunodominant epitopes. Analysis of the mouse C5

protein sequence identified 12 potential immunogenic epitopes that are likely to be on the surface of the protein (important so that the generated antibodies can have access to them

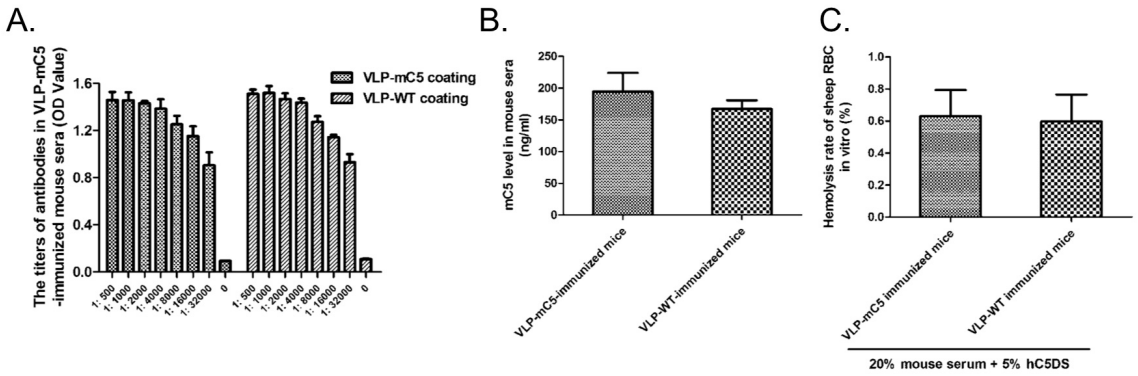


**Figure 2.** Immunizing mice with VLPs displaying the mouse C5 (mC5) cleavage site domain did not generate anti-mC5 antibody responses. WT C57BL/6 mice were immunized with VLP-mC5 in CFA or wild-type VLP in CFA (control) and boosted 2 weeks later. One week after the boost, serum samples were collected. **(A)** Serum samples were tested for anti-mC5 and anti-Qβ IgG antibody titers by ELISA, showing high titers of anti-Qβ antibodies developed in both cohorts (detectable at a 1:32 000 dilution), but no detectable anti-mC5 antibodies. **(B)** C5 levels in the serum samples from both cohorts as measured by anti-mC5 ELISA. **(C)** C5 activity in the serum samples were assessed by a modified hemolysis assay using C5-depleted human serum, and no significant difference was found between the VLP-mC5 immunized mice and the control mice. $n = 5$ in each group

under native conditions; **Table 1**). We designed an artificial gene coding for all of these identified epitopes in a linear sequence together with three copies of a previously published tolerance-breaking peptide, PADRE (**Figure 3A**).[28,29] This polypeptide was expressed in *E. coli*, isolated from inclusion bodies, denatured, refolded, affinity purified via a 6XHis tag (**Figure 3B**), and finally purified by reversed-phase HPLC (**Figure 3C**).

Mice that were immunized and boosted with the purified C5 multi-epitope polypeptide showed high IgG antibody titers against full-length recombinant mouse C5 protein by ELISA (**Figure 4A**). Therefore, this C5 vaccine was able to break immune tolerance and develop a significant immune response to the autologous C5 epitopes.

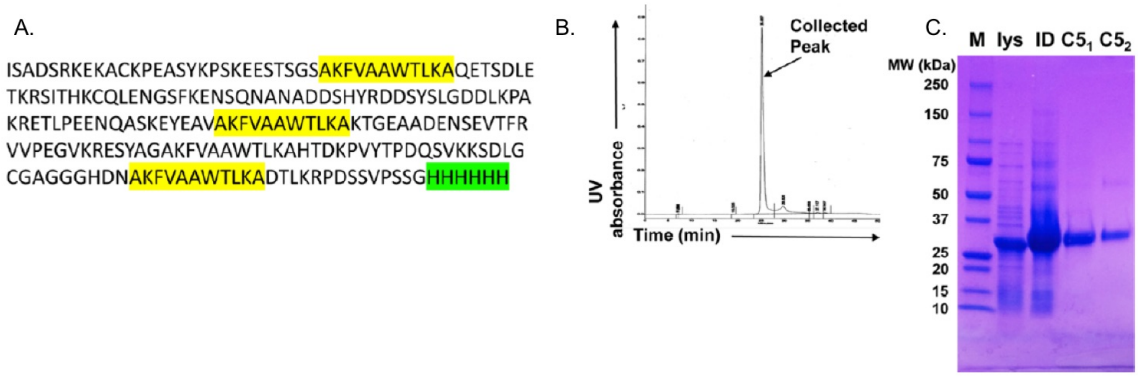


**Figure 3.** Design, expression, and purification of the recombinant mouse C5 vaccine. **(A)** Amino acid sequence of the recombinant C5 vaccine, consisting of 12 computer-identified mouse C5 surface epitopes (non-highlighted amino acids), three copies of the PADRE peptide (highlighted in yellow), and a 6XHis-tag (highlighted in green). **(B)** Reversed-phase HPLC to further purify the recombinant C5P after affinity chromatography. **(C)** SDS-PAGE analysis of the purified recombinant C5 vaccine. M = markers; lys = whole E. coli lysate; ID = inclusion bodies; C51 = 60 µg of purified recombinant C5 vaccine; C52 = 20 µg of purified recombinant C5 vaccine.

**Table 1.** Computer-predicted immunogenic C5 protein surface epitopes.

| peptide no. | start | antigenic determinant | length | antigenicity/ surface/ hydrophilicity |
|---|---|---|---|---|
| P1 | 1547 | ISADSRKEKACKPE | 14 | 2.66/0.79/1.14 |
| P2 | 1410 | ASYKPSKEESTSGS | 14 | 2.56/0.86/0.69 |
| P3 | 399 | QETSDLETKRSITH | 14 | 2.42/0.86/0.85 |
| P4 | 1114 | KCQLENGSFKENSQ | 14 | 2.38/0.79/0.43 |
| P5 | 657 | NANADDSHYRDDS | 14 | 2.32/0.79/0.86 |
| P6 | 146 | YSLGDDLKPAKRET | 14 | 2.29/0.71/0.73 |
| P7 | 442 | LPEENQASKEYEAV | 14 | 2.22/0.71/0.76 |
| P8 | 1590 | KTGEAADENSEVTF | 14 | 2.19/0.86/0.65 |
| P9 | 932 | RWPEGVKRESYAG | 14 | 2.17/0.71/0.43 |
| P10 | 630 | KSDLGCGAGGGHDN | 14 | 1.86/0.93/0.38 |
| P11 | 129 | HTDKPVYTPDQSVK | 14 | 1.80/0.86/0.22 |
| P12 | 1234 | DTLKRPDSSVPSSG | 14 | 1.73/0.86/0.58 |

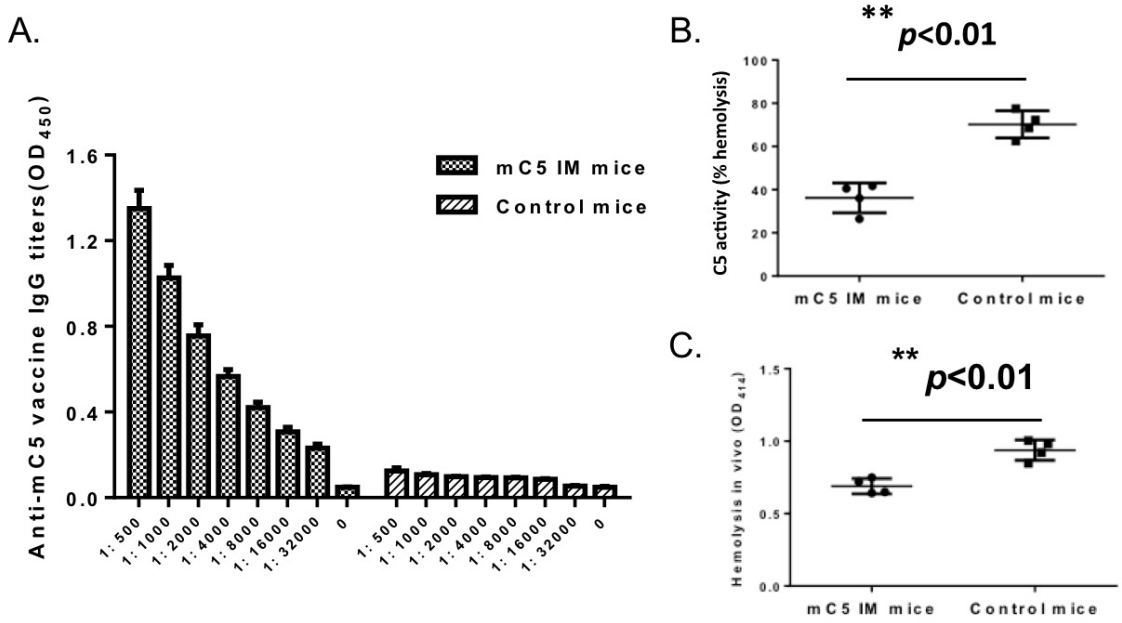


**Figure 4.** Recombinant mouse C5 vaccine reducing mouse C5 (mC5) levels and activity in the blood and significantly reducing hemolysis in these mice in a model of PNH. **(A)** After the last immunization of the recombinant mouse C5 vaccine or CFA alone, serum samples were collected and tested for their anti-mC5 vaccine IgG titers by ELISA ($n = 4$ in each group). **(B)** Mouse C5 activity in these samples was compared using the modified EshA-based hemolytic assay ($n = 12$ in each group). **(C)** The recombinant C5 vaccine-immunized mice and control mice were intravenously injected with 200 μL of C5-deficient human serum per mouse and then, 1 h later, were bled retro-orbitally using a heparinized capillary tube, and *in vivo* intravascular hemolysis was assessed by measuring the $OD_{414}$ of the plasma samples ($n = 4$ in each group). IM, immunized.

Furthermore, the mice receiving the C5-based polypeptide vaccine showed less complement-mediated hemolytic activity than the control mice (**Figure 4B,C**). This suggests that the recombinant autologous C5 vaccine is effective in eliciting functional anti-C5 autoantibodies that have the intended outcome of inhibiting C5 activity.

To identify which of the 12 C5 peptide sequences were most effective in inducing the above immune response, we designed a library of overlapping 15-mer oligopeptides spanning the entire sequence of the recombinant C5 vaccine (**Table 2**). Using these individual peptides as ELISA probes, we assessed the IgG composition of the serum from

the C5 vaccine-immunized mice and found that the sera contained high titers of IgG against the peptide ACKPEASYKPSKEES, suggesting that this sequence contains a dominant surface epitope within the vaccine that elicited strong humoral responses.

The C5 peptide P2 (ASYKPSKEESTSGS) is predicted by the computer algorithms to be an immunogenic epitope exposed on the C5 protein surface and it contains the peptide sequence identified in the above-described epitope mapping experiments. To verify that this peptide is indeed on C5 protein surface for our future VLP-C5 vaccine development, we constructed a mouse C5 three-dimensional homology model based on the published human C5 crystal structure[27] using the Phyre2 protein recognition program following published protocols.[32] Mouse C5 protein shares 89% homology with the human C5 sequence, providing a model with high confidence (100%) and sequence coverage (98%). Visualization of the location of the P2 peptide in the mouse C5 structure model showed it to be exposed on the solvent-exposed surface (**Figure 5**, in red), further supporting the hypothesis that it represents a suitable epitope for development of VLP-C5 vaccines.

A recombinant VLP bearing a linear peptide composed of the putative dominant C5 surface epitope P2 and the PADRE peptide (separated by a short spacer) was expressed as a C-terminal extension of the VLP coat protein (**Figure 6A**). These particles were produced by a well-established method[33] in which a mixture of truncated and extended capsid proteins are co-expressed in *E. coli* and self-assemble into a hybrid particle in which an average of 50 copies of the extension were incorporated per capsid. The resultant VLP-C5 vaccine was characterized using dynamic light scattering, size-exclusion chromatography, and gel electrophoresis (**Figure 6B-D**), showing intact particles of the expected size (~ 30 nm) and composition.

**Table 2.** Peptide library for C5 epitope mapping.

| | peptide |
|---|---|
| 1 | ISADSRKEKACKPEA |
| 2 | ACKPEASYKPSKEES |
| 3 | PSKEESTSGSAKFVA |
| 4 | SAKFVAAWTLKAQET |
| 5 | LKAQETSDLETKRSI |
| 6 | ETKRSITHKCQLENG |
| 7 | CQLENGSFKENSQNA |
| 8 | ENSQNANADDSHYRD |
| 9 | DSHYRDDSYSLGDDL |
| 10 | SLGDDLKPAKRETLP |
| 11 | KRETLPEENQASKEY |
| 12 | QASKEYEAVAKFVAA |
| 13 | AKFVAAWTLKAKTGE |
| 14 | KAKTGEAADENSEVT |
| 15 | ENSEVTFRVVPEGVK |
| 16 | VPEGVKRESYAGAKF |
| 17 | YAGAKFVAAWTLKAH |
| 18 | WTLKAHTDKPVYTPD |
| 19 | PVYTPDQSVKKSDLG |
| 20 | KKSDLGCGAGGGHDN |
| 21 | GGGHDNAKFVAAWTL |
| 22 | VAAWTLKADTLKRPD |
| 23 | TLKRPDSSVPSSG |
| 24 | DTLKRPDSSVPSSG |

*2.4.2. Evaluation of protection in PNH disease model*

WT mice were immunized with either the VLP-C5 vaccine or the same amount of control VLP lacking the extended capsid component. Using the same analyses as described

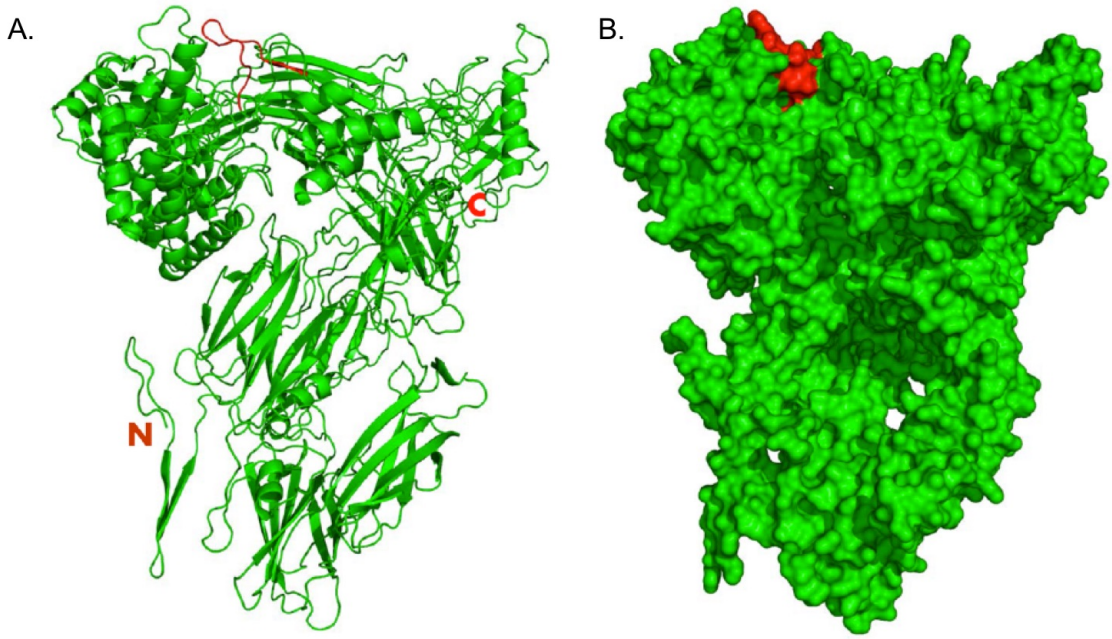


**Figure 5.** Verification of the P2 peptide on the surface of mouse C5 protein by homology modeling. A three-dimensional model of mouse C5 was constructed based on the published human C5 X-ray crystal structure. Mouse C5 protein shares 89% sequence homology with human C5 protein. The P2 epitope (red) was found to be exposed on mouse C5 surface based on this model. (A) Ribbon representation of the mouse C5 structure model. Amino (N) and carboxy (C) terminus of the protein are also labeled. (B) Surface representation of the mouse C5 structure model.

above, we found that mice receiving the control VLP produced no detectable recombinant mouse C5-reactive IgG (**Figure 7A**), whereas the VLP-C5 vaccine immunized mice developed high titers of IgG antibodies against intact recombinant mouse C5. Mice immunized with VLPs displaying the scrambled P2 peptide also failed to generate cross-reactive antibodies (**Figure 8**). Most importantly, the complement-mediated hemolytic activity of these VLP-C5 vaccine-immunized mice was also significantly reduced (**Figure**

**7B**), indicating that this VLP-based vaccine is effective in eliciting C5-reactive autoantibody production and reducing C5 activity.

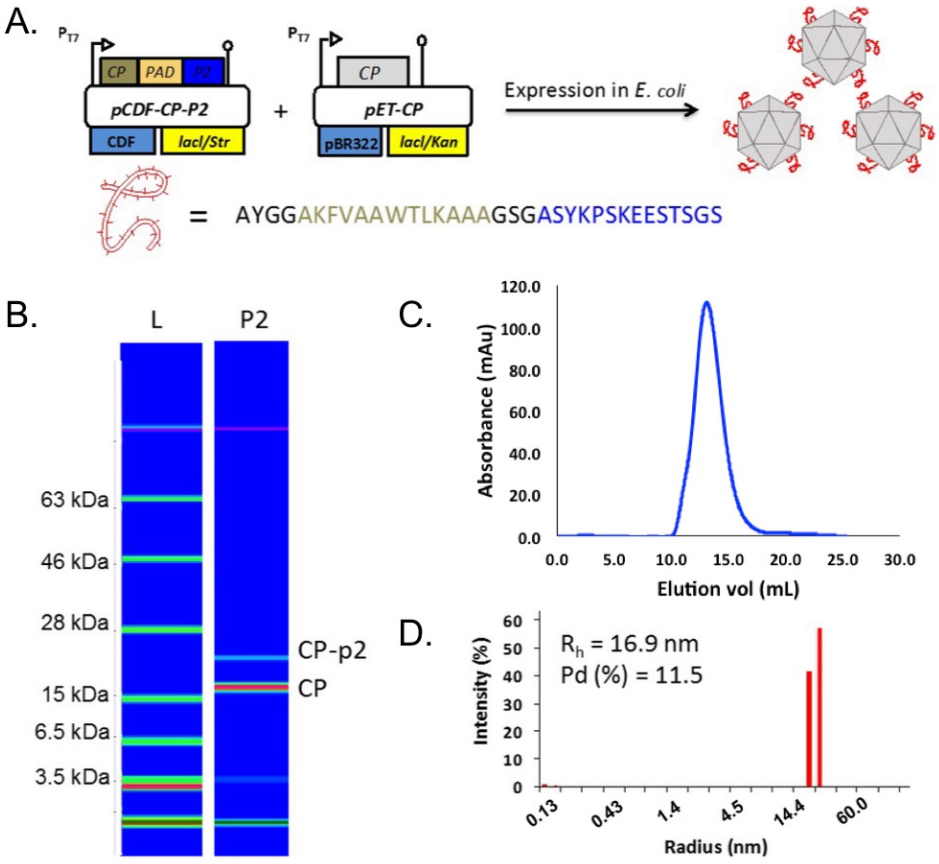


**Figure 6.** Expression and characterization of hybrid Qβ VLPs. **(A)** Schematic representation of plasmids used for particle expression. PADRE sequence highlighted in gold; C5 P2 peptide highlighted in blue. CP: coat protein. **(B)** Denaturing electrophoretic analysis of VLPs displaying the P2 peptide. Bands for the wild-type CP and the CP-P2 fusion are indicated. Particle composition calculated using densitometry. **(C)** FPLC elution profile for Qβ-P2 VLPs showing particles are intact and greater than 95% pure. **(D)** Dynamic light scattering histogram of Qβ-P2 VLPs showing particles are monodisperse in size with a hydrodynamic radius of 16.9 nm.

To test whether the C5 vaccine approach is effective in protecting mice from complement-mediated intravascular hemolysis, as found in patients with PNH, we modified a previously established complement-mediated intravascular hemolytic anemia model.[31] In brief, we introduced 200 µL of C5-depleted human serum into each of the VLP-

C5 vaccine-immunized mice and control mice by i.p. injection. After one hour, each mouse was bled retro-orbitally to collect sera to measure intravascular hemolysis, and urine was also collected to measure hemoglobinuria. We found that injection of C5-depleted human serum-induced much less severe hemolysis and hemoglobinuria in the VLP-C5 vaccine-immunized mice compared to the control mice (**Figure 9**). This suggests that mouse C5 can replace human C5 to form functional MAC and that the VLP-C5 vaccine is effective in protecting mice from complement-mediated cell damage *in vivo*.

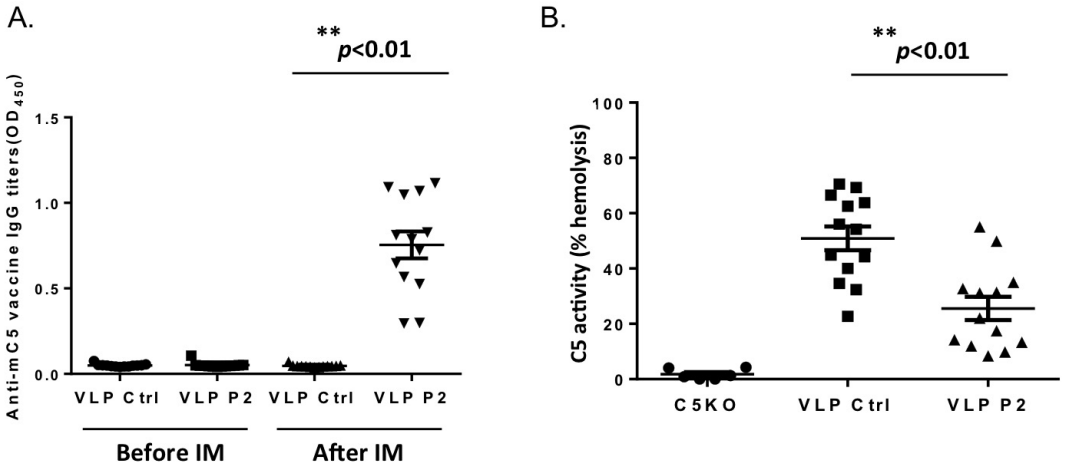


**Figure 7.** VLP-C5 vaccine eliciting high titers of anti-C5 autoantibodies and significantly decreasing mouse C5 hemolytic activity. WT mice were immunized subcutaneously with the VLP-C5 vaccine or empty VLP as controls and boosted once or twice after every other week. IgG titers of the anti-recombinant mouse C5 in the sera were measured before the immunization and after the last boost. (A) Before immunization, anti-C5 antibodies were not detectable in both groups of mice. After the last boost, anti-mouse C5 IgGs were highly detectable in sera from VLP-C5 vaccine immunized mice but not in sera from the control mice. (B). In the modified *ex vivo* hemolysis assays, sera from the same VLP-C5 vaccine immunized mice and control mice were incubated with antibody-sensitized sheep RBCs ($E^{shA}$) to quantitate mouse C5 activity. Sera from C5 KO mice were used as negative controls. $n = 13$ in each group.

*2.4.3. Discussion*

Aberrant activity of the complement system is emerging as a target for treating certain inflammatory and autoimmune diseases.[40] While excess complement activity can

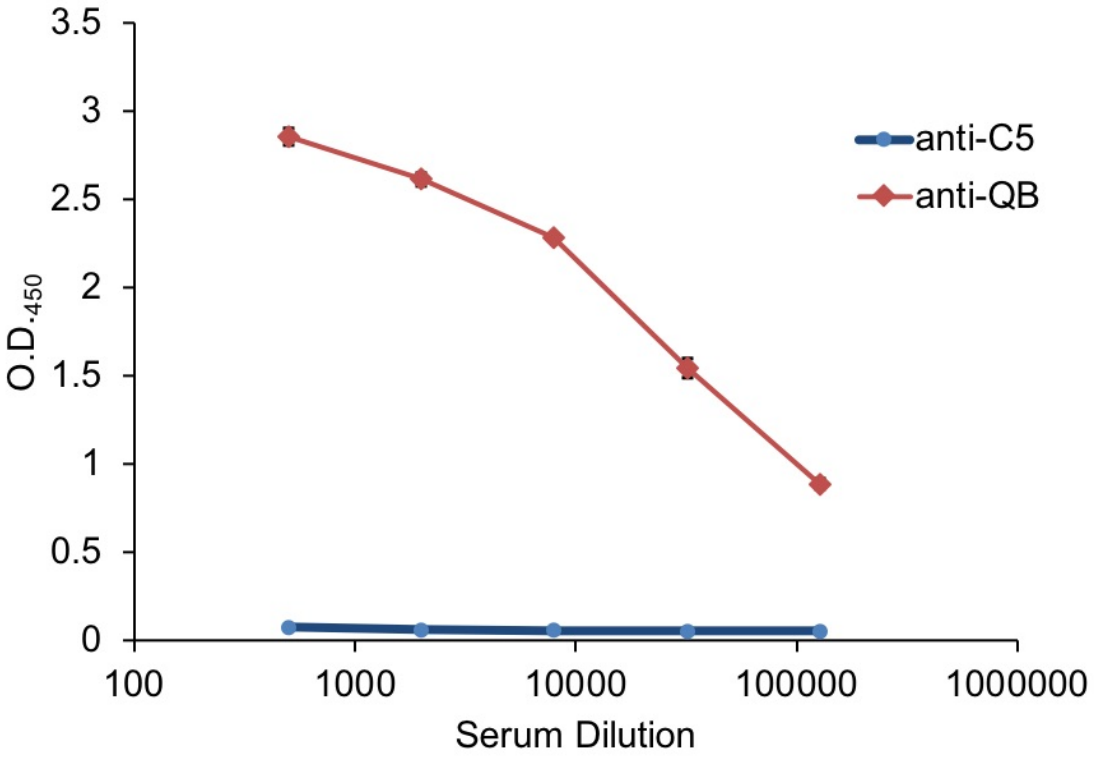


**Figure 8.** Scrambled peptide display fails to elicit cross-reactive antibody responses in mice. WT mice were immunized subcutaneously with the VLP-scrambled peptide vaccine and boosted once every other week. IgG response of anti-C5 and anti-Qβ antibodies in the sera were measured after the final boost by ELISA ($n = 4$).

have many potential causes, a choke point of the system is the C5 protein, responsible for the penultimate step in the induction of hemolytic function. Most of the complement-targeted reagents that have been approved or under development are mAbs;[41] others are based on aptamers,[42] peptides,[43,44] and small molecules.[45] Given the life-long complement inhibition required in most of these patients, all currently available complement inhibition therapies suffer from limited half-life, high costs, and compliance issues. This is especially true in the case of the anti-C5 antibody eculizumab, which many PNH patients have to receive by i.v. infusion every two weeks for life, at a current price of almost a half million dollars a year per patient.[22,46] Interest in C5 as a target has recently expanded to other

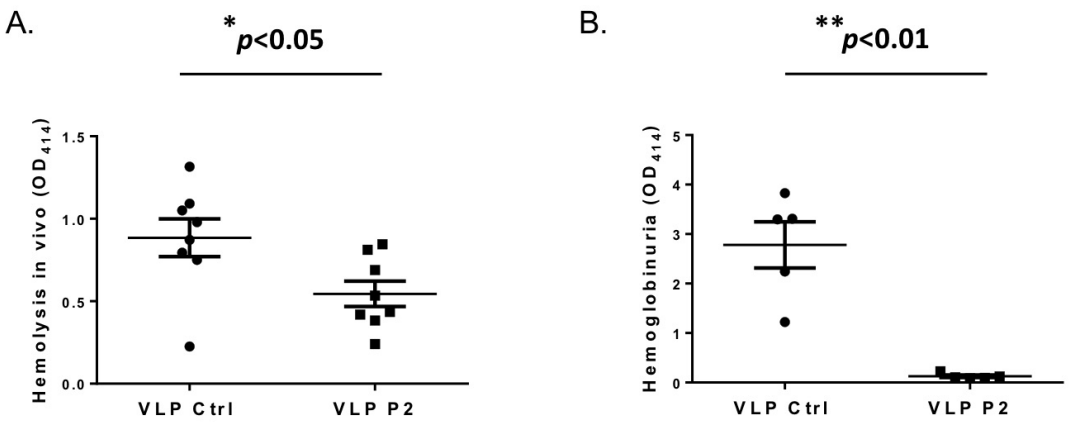


**Figure 9.** VLP-C5 vaccine immunization protecting mice from complement-mediated hemolysis and hemoglobinuria in a model of PNH. (A) VLP-C5 vaccine immunized mice and empty VLP-immunized control mice were injected with 200 μL of human C5- depleted serum intraperitoneally. One hour later, blood was collected through the venous sinus of the eye, and the resultant sera were diluted at a ratio of 1:10 using PBS before OD values were measured at 414 nm. $n = 8$ in each group. (B) Urea samples were collected from the VLP-C5 vaccine immunized mice and empty VLP-immunized control mice, and hemoglobinuria were measured by reading $OD_{414}$ after 1:10 dilution with PBS. $n = 5$ in each group.

diseases, with eculizumab in late-stage clinical trials for conditions such as myasthenia gravis[47] and cold agglutinin disease[48] that involve excessive complement activation.

We show here proof-of-concept examples of C5 vaccine-based approaches for the production of autologous C5-reactive antibodies to reduce C5 activity for the treatment of complement-mediated diseases, mimicking the effect of eculizumab. Vaccination with a homologous C5 from a different species (human) did not confer anti- mouse C5 function in mouse, although it did elicit a strong antibody response against the immunized human C5. This stands in contrast to many examples of the use of conservative xeno-antigens in antitumor vaccines, in which immunization elicited T- and/or B-cell responses that cross-react with their mouse counterparts on tumor cells.[35–38] In our case, we suggest that the overlapping epitopes between mouse and human C5 (which are more than 80%

homologous) are well-tolerated in mice and that all the antibodies produced were likely against the epitopes that are unique in the human C5.

We further explored the display of a large protein domain from the mouse C5 protein on Qβ VLPs as a potential vaccine. These particles also failed to elicit cross-reactive C5 antibodies in immunized mice, although all mice responded to the viral coat protein. In this case, we hypothesize that the truncated domain maintained the native conformation of the C5 cleavage site and was unable to stimulate a robust immune response and overcome tolerance against the self-antigen.

Instead, we were able to break tolerance in mice using a linear polypeptide composed of computer-predicted strong immunogenic epitopes along with the PADRE sequence. We identified a potential dominant C5 peptide within these 12 computer-predicted immunogenic peptides by epitope mapping using an overlapping peptide library and constructed a mouse C5 structure model to ensure that this identified C5 peptide is exposed on the mouse C5 protein surface. We then developed VLP nanoparticles that display this dominant C5 surface peptide together with the PADRE sequence as a new autologous C5 vaccine. The VLP-based C5 vaccine proved to be especially effective at eliciting autologous anti-C5 antibody production, inhibiting C5 activity, and protecting the vaccinated mice from intravascular hemolysis and hemoglobinuria in a model that mimics PNH. Our results suggest that autologous C5 vaccines may hold potential as a supplement and/or alternative for eculizumab for treating complement-mediated diseases. Of course, whether the human counterparts of the identified mouse C5 epitopes work in humans needs to be confirmed in assays such as *in vitro* immunization using human peripheral blood

mononuclear cells[49] followed by human C5 blocking experiments and, eventually, in human clinical studies.

Although numerous studies have extensively explored the development of Qβ vaccines for the display of self-antigens, these have all focused on the chemical conjugation of full-length proteins to the particle surface.[2,12,13,18] Peptide display through genetic extension has been explored using both PP7 and MS2 VLPs; however, these studies have focused on insertions into the AB loop on the VLP surface and remained limited to targets in infectious disease.[50–53] The work presented in this chapter represents the first study to explore the rational design and assembly of hybrid Qβ VLPs displaying genetically-encoded peptide epitopes as terminal extensions for the development of vaccines against self-antigens.

Vaccination against C5 to have the immune system produce its own anti-C5 antibodies could represent a cost- and compliance-effective alternative to antibody infusion, with therapeutic effects prolonged by booster immunizations. Indeed, one publication has appeared testing the potential of a vaccination approach against complement in treating/preventing diseases.[54] In that work, a peptide of undisclosed sequence was designed to mimic one or more mouse C5a epitopes, and immunization of this peptide conjugated to carrier protein KLH elicited anti-C5a autoantibodies and protected the vaccinated mice from chronic neuroinflammation and neuropathologic alterations in a model of Alzheimer's disease.[54] This work supports the concept of complement-targeted vaccination for treating complement-mediated diseases, but it also significantly differs from the work presented here. The vaccine tested in the prior report was specific to C5a, which is a complement activation product released from activated C5,

and therefore does not have an effect on C5b-9 (MAC) formation. In contrast, the C5 vaccines developed here do not target C5a, but are specific for the C5b part of C5, which is the essential component to initiate the assembly of the MAC to lyse RBCs and to damage other tissues in pathological conditions.

Another important difference in these approaches is the relative concentrations of the target. The C5a protein exists in blood at very low levels (~0.5-50 ng/mL),[55,56] whereas C5 concentration is approximately 100-200 μg/mL in the blood. It requires strong vaccines to break the tolerance to produce enough anti-C5 antibodies to significantly reduce C5 activity *in vivo*. By combining multiple epitopes and the PADRE peptide, and by using a VLP as a carrier, our approaches did indeed develop high titers of anti-C5 autoantibodies and decreased C5 activity. However, C5 activity was not completely eliminated in the immunized mice. This is significant because of the dangers inherent in the complete elimination of complement function. An eventual therapeutic application of this vaccine strategy would require a moderation, but not elimination, of C5 activity, which seems to be possible on the basis of this initial study.

Our use of the PADRE peptide was stimulated by its known ability to help break immune tolerance and to improve humoral responses against immunized antigens both in humans and in C57BL/6 mice.[28,29] PADRE works by strongly binding to 15 of 16 of the most common HLA-DR types tested to date in humans and I-$A^b$ molecules in mice to boost T-helper responses to improve immune responses against both T-cell and B-cell epitopes. Tests to support or refute the assumption that these mechanistic factors are important in the present application must await further studies.

It should also be noted that the use of human C5-depleted serum to induce intravascular hemolysis is a new model of situations found in PNH patients. Mouse complement is much weaker than human complement in hemolytic activity. The severe intravascular hemolysis and hemoglobinuria induced by injecting mice with C5-depleted serum, which does not have any hemolytic activity by itself, shows that mouse C5 can replace human C5 to form "hybrid" MAC to lyse mouse RBCs in vivo. We believe this method will be useful in other proof-of-concept studies testing mouse C5 targeted therapies in treating complement-mediated hemolysis or tissue damage.

**2.5. Conclusions**

In summary, we found that immunization of the conservative human C5 did not raise cross-reactive antibodies that reduced mouse C5 activity. We showed that immunization of a recombinant mouse C5 vaccine composed of multiple potential protein surface B-cell epitopes and the PADRE peptides broke immune tolerance of C5 in mice and decreased C5 activity. Finally, we demonstrated that immunization of a VLP vaccine displaying one of the identified strong mouse C5 surface epitopes together with the PADRE peptide elicited strong humoral responses against mouse C5, reduced C5 activity and protected mice from complement-mediated hemolysis and hemoglobinuria in a model of intravascular hemolysis, which closely mimic the situations found in PNH patients. Furthermore, this study serves as a proof-of-concept for the genetic display of peptide epitopes on Qβ VLPs in the development of vaccines, particularly in the context of self-antigens. Our results suggest that C5 auto-vaccines, especially the ones on the Qβ VLP platform, could be developed as a supplement and/or alternative for eculizumab for treating

complement-mediated diseases, especially those in which complement activation needs to be controlled for the rest of the life.

### 2.6. References


(1) Spohn, G.; Schori, C.; Keller, I.; Sladko, K.; Sina, C.; Guler, R.; Schwarz, K.; Johansen, P.; Jennings, G. T.; Bachmann, M. F. Preclinical Efficacy and Safety of an Anti-IL-1β Vaccine for the Treatment of Type 2 Diabetes. *Mol. Ther. - Methods Clin. Dev.* **2014**, *1*, 14048.

(2) Cavelti-Weder, C.; Timper, K.; Seelig, E.; Keller, C.; Osranek, M.; Lassing, U.; Spohn, G.; Maurer, P.; Muller, P.; Jennings, G. T.; *et al.* Development of an Interleukin-1B Vaccine in Patients with Type 2 Diabetes. *Mol. Ther.* **2016**, *24*, 1003–1012.

(3) Röhn, T. A.; Jennings, G. T.; Hernandez, M.; Grest, P.; Beck, M.; Zou, Y.; Kopf, M.; Bachmann, M. F. Vaccination against IL-17 Suppresses Autoimmune Arthritis and Encephalomyelitis. *Eur. J. Immunol.* **2006**, *36*, 2857–2867.

(4) Saupe, F.; Huijbers, E. J. M.; Hein, T.; Femel, J.; Cedervall, J.; Olsson, A. K.; Hellman, L. Vaccines Targeting Self-Antigens: Mechanisms and Efficacy-Determining Parameters. *FASEB J.* **2015**, *29*, 3253–3262.

(5) Bachmann, M. F.; Jennings, G. T. Vaccine Delivery: A Matter of Size, Geometry, Kinetics and Molecular Patterns. *Nat. Rev. Immunol.* **2010**, *10*, 787–796.

(6) Chackerian, B. Virus-like Particles: Flexible Platforms for Vaccine Development. *Expert Rev. Vaccines* **2007**, *6*, 381–390.

(7) Handisurya, A.; Gilch, S.; Winter, D.; Shafti-Keramat, S.; Maurer, D.; Schätzl, H. M.; Kirnbauer, R. Vaccination with Prion Peptide-Displaying Papillomavirus-like Particles Induces Autoantibodies to Normal Prion Protein That Interfere with Pathologic Prion Protein Production in Infected Cells. *FEBS J.* **2007**, *274*, 1747–1758.

(8) Spohn, G.; Schwarz, K.; Maurer, P.; Illges, H.; Rajasekaran, N.; Choi, Y.; Jennings, G. T.; Bachmann, M. F. Protection against Osteoporosis by Active Immunization with TRANCE/RANKL Displayed on Virus-Like Particles. *J. Immunol.* **2005**, *175*, 6211–6218.

(9) Li, Q.; Cao, C.; Chackerian, B.; Schiller, J.; Gordon, M.; Ugen, K. E.; Morgan, D. Overcoming Antigen Masking of Anti-Amyloidbeta Antibodies Reveals Breaking of B Cell Tolerance by Virus-like Particles in Amyloidbeta Immunized Amyloid Precursor Protein Transgenic Mice. *BMC Neurosci.* **2004**, *5*.

(10) Bachmann, M. F.; Jennings, G. T. Therapeutic Vaccines for Chronic Diseases: Successes and Technical Challenges. *Philos. Trans. R. Soc. B Biol. Sci.* **2011**, *366*, 2815–2822.

(11) Brown, S. D.; Fiedler, J. D.; Finn, M. G. Assembly of Hybrid Bacteriophage Q-Beta Virus-Like Particles. *Biochemistry* **2009**, *47*, 11155–11157.

(12) Ambühl, P. M.; Tissot, A. C.; Fulurija, A.; Maurer, P.; Nussberger, J.; Sabat, R.; Nief, V.; Schellekens, C.; Sladko, K.; Roubicek, K.; *et al.* A Vaccine for Hypertension Based on Virus-like Particles: Preclinical Efficacy and Phase I Safety and Immunogenicity. *J. Hypertens.* **2007**, *25*.

(13) Tissot, A. C.; Maurer, P.; Nussberger, J.; Sabat, R.; Pfister, T.; Ignatenko, S.; Volk, H. D.; Stocker, H.; Müller, P.; Jennings, G. T.; *et al.* Effect of Immunisation against Angiotensin II with CYT006-AngQb on Ambulatory Blood Pressure: A Double-Blind, Randomised, Placebo-Controlled Phase IIa Study. *Lancet* **2008**, *371*, 821–827.

(14) Senti, G.; Johansen, P.; Haug, S.; Bull, C.; Gottschaller, C.; Müller, P.; Pfister, T.; Maurer, P.; Bachmann, M. F.; Graf, N.; *et al.* Use of A-Type CpG Oligodeoxynucleotides as an Adjuvant in Allergen-Specific Immunotherapy in Humans: A Phase I/IIa Clinical Trial. *Clin. Exp. Allergy* **2009**, *39*, 562–570.

(15) Chabaud, M.; Durand, J. M.; Buchs, N.; Fossiez, F.; Page, G.; Frappart, L.; Miossec, P. Human Interleukin-17: A T Cell–derived Proinflammatory Cytokine Produced by the Rheumatoid Synovium. *Arthritis Rheum.* **1999**, *42*, 963–970.

(16) Matusevicius, D.; Kivisäkk, P.; He, B.; Kostulas, N.; Özenci, V.; Fredrikson, S.; Link, H. Interleukin-17 mRNA Expression in Blood and CSF Mononuclear Cells Is Augmented in Multiple Sclerosis. *Mult. Scler. J.* **1999**, *5*, 101–104.

(17) Dallenbach, K.; Maurer, P.; Rohn, T.; Zabel, F.; Kopf, M.; Bachmann, M. F. Protective Effect of a Germline, IL-17-Neutralizing Antibody in Murine Models of Autoimminue Inflammatory Disease. *Eur. J. Immunol.* **2015**, *45*, 1238–1247.

(18) Tissot, A. C.; Spohn, G.; Jennings, G. T.; Shamshiev, A.; Kurrer, M. O.; Windak, R.; Meier, M.; Viesti, M.; Hersberger, M.; Kundig, T. M.; *et al.* A VLP-Based Vaccine against Interleukin-1a Protects Mice from Atherosclerosis. *Eur. J. Immunol.* **2013**, *43*, 716–722.

(19) Röhn, T. A.; Bachmann, M. F. Vaccines against Non-Communicable Diseases. *Current Opinion in Immunology*, **2010**, *22*, 391–396.

(20) Ricklin, D.; Hajishengallis, G.; Yang, K.; Lambris, J. D. Complement: A Key System for Immune Surveillance and Homeostasis. *Nature Immunol.*, **2010**, *11*, 785–797.

(21) Ricklin, D.; Lambris, J. D. Progress and Trends in Complement Therapeutics. In *Adv. Exp. Med. Biol.*; **2013**; *734*, 1–22.

(22) Hillmen, P.; Hall, C.; Marsh, J. C. W.; Elebute, M.; Bombara, M. P.; Petro, B. E.; Cullen, M. J.; Richards, S. J.; Rollins, S. A.; Mojcik, C. F.; *et al.* Effect of Eculizumab on Hemolysis and Transfusion Requirements in Patients with Paroxysmal Nocturnal Hemoglobinuria. *N. Engl. J. Med.* **2004**, *350*, 552–559.

(23) Zuber, J.; Fakhouri, F.; Roumenina, L. T.; Loirat, C.; Frémeaux-Bacchi, V. Use of Eculizumab for Atypical Haemolytic Uraemic Syndrome and C3 Glomerulopathies. *Nat. Rev. Nephrol.*, **2012**, *8*, 643–657.

(24) DeZern, A. E.; Brodsky, R. A. Paroxysmal Nocturnal Hemoglobinuria. A Complement-Mediated Hemolytic Anemia. *Hematology/Oncology Clinics of North America*, **2015**, *29*, 479–494.

(25) Coyle, D.; Cheung, M. C.; Evans, G. A. Opportunity Cost of Funding Drugs for Rare Diseases: The Cost-Effectiveness of Eculizumab in Paroxysmal Nocturnal Hemoglobinuria. *Med. Decis. Mak.* **2014**, *34*, 1016–1029.

(26) Murphy, R. M. Rare Diseases Mean Big Profits. *Fortune*, 2012, *166*, 24.

(27) Fredslund, F.; Laursen, N. S.; Roversi, P.; Jenner, L.; Oliveira, C. L. P.; Pedersen, J. S.; Nunn, M. A.; Lea, S. M.; Discipio, R.; Sottrup-Jensen, L.; *et al.* Structure of and Influence of a Tick Complement Inhibitor on Human Complement Component 5. *Nat. Immunol.* **2008**, *9*, 753–760.

(28) Alexander, J.; del Guercio, M.-F.; Maewal, A.; Qiao, L.; Fikes, J.; Chesnut, R. W.; Paulson, J.; Bundle, D. R.; DeFrees, S.; Sette, A. Linear PADRE T Helper Epitope and Carbohydrate B Cell Epitope Conjugates Induce Specific High Titer IgG Antibody Responses. *J. Immunol.* **2000**, *164*, 1625–1633.

(29) Del Guercio, M. F.; Alexander, J.; Kubo, R. T.; Arrhenius, T.; Maewal, A.; Appella, E.; Hoffman, S. L.; Jones, T.; Valmori, D.; Sakaguchi, K.; *et al.* Potent Immunogenic Short Linear Peptide Constructs Composed of B Cell Epitopes and Pan DR T Helper Epitopes (PADRE) for Antibody Responses in Vivo. *Vaccine* **1997**, *15*, 441–448.

(30) Tu, Z.; Bu, H.; Dennis, J. E.; Lin, F. Efficient Osteoclast Differentiation Requires Local Complement Activation. *Blood* **2010**, *116*, 4456–4463.

(31) Ino, Y.; Sato, T.; Suzuki, S.; Iwaki, M.; Yoshikawa, T. Inhibitory Effects of FUT-175, a New Synthetic Protease Inhibitor, on Intravascular Hemolysis by Human Serum in Mice. *Int. J. Immunopharmacol.* **1987**, *9*, 533–537.

(32) Kelley, L. A.; Mezulis, S.; Yates, C. M.; Wass, M. N.; Sternberg, M. J. E. The Phyre2 Web Portal for Protein Modeling, Prediction and Analysis. *Nat. Protoc.*

**2015**, *10*, 845–858.

(33) Fiedler, J. D.; Higginson, C.; Hovlid, M. L.; Kislukhin, A. A.; Castillejos, A.; Manzenrieder, F.; Campbell, M. G.; Voss, N. R.; Potter, C. S.; Carragher, B.; *et al.* Engineered Mutations Change the Structure and Stability of a Virus-Like Particle. *Biomacromolecules* **2012**, *13*, 2339–2348.

(34) Fattori, E.; Cappelletti, M.; Lo Surdo, P.; Calzetta, A.; Bendtsen, C.; Ni, Y. G.; Pandit, S.; Sitlani, A.; Mesiti, G.; Carfí, A.; *et al.* Immunization against Proprotein Convertase Subtilisin-Like/kexin Type 9 Lowers Plasma LDL-Cholesterol Levels in Mice. *J. Lipid Res.* **2012**, *53*, 1654–1661.

(35) Fong, L.; Brockstedt, D.; Benike, C.; Breen, J. K.; Strang, G.; Ruegg, C. L.; Engleman, E. G. Dendritic Cell-Based Xenoantigen Vaccination for Prostate Cancer Immunotherapy. *J. Immunol.* **2001**, *167*, 7150–7156.

(36) Su, J. M.; Wei, Y. Q.; Tian, L.; Zhao, X.; Yang, L.; He, Q. M.; Wang, Y.; Lu, Y.; Wu, Y.; Liu, F.; *et al.* Active Immunogene Therapy of Cancer with Vaccine on the Basis of Chicken Homologous Matrix Metalloproteinase-21. *Cancer Res.* **2003**, *63*, 600–607.

(37) Wei, Y. Q.; Huang, M. J.; Yang, L.; Zhao, X.; Tian, L.; Lu, Y.; Shu, J. M.; Lu, C. J.; Niu, T.; Kang, B.; *et al.* Immunogene Therapy of Tumors with Vaccine Based on Xenopus Homologous Vascular Endothelial Growth Factor as a Model Antigen. *Proc. Natl. Acad. Sci. U. S. A.* **2001**, *98*, 11545–11550.

(38) Wei, Y. Q.; Wang, Q. R.; Zhao, X.; Yang, L.; Tian, L.; Lu, Y.; Kang, B.; Lu, C. J.; Huang, M. J.; Lou, Y. Y.; *et al.* Immunotherapy of Tumors with Xenogeneic Endothelial Cells as a Vaccine. *Nat. Med.* **2000**, *6*, 1160–1166.

(39) Havilands, D. L.; Haviland, J. C.; Fleischer, D. T.; Wetsels, R. a. Structure of the Murine Fifth Complement Component (C5) Gene. *J. Biol. Chem.* **1991**, *266*, 11818–11825.

(40) Ricklin, D.; Lambris, J. D. New Milestones Ahead in Complement-Targeted Therapy. *Seminars in Immunology*, **2016**, *28*, 208–222.

(41) Ricklin, D.; Lambris, J. D. Complement in Immune and Inflammatory Disorders: Pathophysiological Mechanisms. *J. Immunol.* **2013**, *190*, 3831–3838.

(42) Hoehlig, K.; Maasch, C.; Shushakova, N.; Buchner, K.; Huber-Lang, M.; Purschke, W. G.; Vater, A.; Klussmann, S. A Novel C5a-Neutralizing Mirror-Image (L-)Aptamer Prevents Organ Failure and Improves Survival in Experimental Sepsis. *Mol. Ther.* **2013**, *21*, 2236–2246.

(43) Sharp, J. A.; Whitley, P. H.; Cunnion, K. M.; Krishna, N. K. Peptide Inhibitor of

Complement C1, a Novel Suppressor of Classical Pathway Activation: Mechanistic Studies and Clinical Potential. *Front. Immunol.* **2014**, *5*.

(44) Sahu, A.; Morikis, D.; Lambris, J. D. Compstatin, a Peptide Inhibitor of Complement, Exhibits Species-Specific Binding to Complement Component C3. *Mol. Immunol.* **2003**, *39*, 557–566.

(45) Ames, R. S.; Lee, D.; Foley, J. J.; Jurewicz, A. J.; Tornetta, M. A.; Bautsch, W.; Settmacher, B.; Klos, A.; Erhard, K. F.; Cousins, R. D.; *et al.* Identification of a Selective Nonpeptide Antagonist of the Anaphylatoxin C3a Receptor That Demonstrates Antiinflammatory Activity in Animal Models. *J. Immunol.* **2001**, *166*, 6341–6348.

(46) Risitano, A. M.; Marotta, S. Therapeutic Complement Inhibition in Complement-Mediated Hemolytic Anemias: Past, Present and Future. *Seminars in Immunology*, 2016, *28*, 223–240.

(47) Howard, J. F.; Barohn, R. J.; Cutter, G. R.; Freimer, M.; Juel, V. C.; Mozaffar, T.; Mellion, M. L.; Benatar, M. G.; Farrugia, M. E.; Wang, J. J.; *et al.* A Randomized, Double-Blind, Placebo-Controlled Phase II Study of Eculizumab in Patients with Refractory Generalized Myasthenia Gravis. *Muscle Nerve* **2013**, *48*, 76–84.

(48) Shapiro, R.; Chin-Yee, I.; Lam, S. Eculizumab as a Bridge to Immunosuppressive Therapy in Severe Cold Agglutinin Disease of Anti-Pr Specificity. *Clin. Case Reports* **2015**, *3*, 942–944.

(49) Tomimatsu, K.; Shirahata, S. Antigen-Specific in Vitro Immunization: A Source for Human Monoclonal Antibodies. *Methods Mol. Biol.* **2014**, *1060*, 297–307.

(50) Chackerian, B.; Caldeira, J. D.; Peabody, J.; Peabody, D. S. Peptide Epitope Identification by Affinity Selection on Bacteriophage MS2 Virus-Like Particles. *J Mol Biol* **2011**, *409*.

(51) O'Rourke, J. P.; Daly, S. M.; Triplett, K. D.; Peabody, D.; Chackerian, B.; Hall, P. R. Development of a Mimotope Vaccine Targeting the Staphylococcus Aureus Quorum Sensing Pathway. *PLoS One* **2014**, *9*, e111198.

(52) Tumban, E.; Peabody, J.; Tyler, M.; Peabody, D. S.; Chackerian, B. VLPs Displaying a Single L2 Epitope Induce Broadly Cross-Neutralizing Antibodies against Human Papillomavirus. *PLoS One* **2012**, *7*, e49751.

(53) Peabody, D. S.; Manifold-Wheeler, B.; Medford, A.; Jordan, S. K.; do Carmo Caldeira, J.; Chackerian, B. Immunogenic Display of Diverse Peptides on Virus-like Particles of RNA Phage MS2. *J Mol Biol* **2008**, *380*.

(54) Landlinger, C.; Oberleitner, L.; Gruber, P.; Noiges, B.; Yatsyk, K.; Santic, R.;

Mandler, M.; Staffler, G. Active Immunization against Complement Factor C5a: A New Therapeutic Approach for Alzheimer's Disease. *J Neuroinflammation* **2015**, *12*, 150.

(55) Mocco, J.; Wilson, D. A.; Komotar, R. J.; Sughrue, M. E.; Coates, K.; Sacco, R. L.; Elkind, M. S. V; Connolly, E. S. Alterations in Plasma Complement Levels after Human Ischemic Stroke. *Neurosurgery* **2006**, *59*, 28–32.

(56) Gressner, O. a; Koch, A.; Sanson, E.; Trautwein, C.; Tacke, F. High C5a Levels Are Associated with Increased Mortality in Sepsis Patients--No Enhancing Effect by Actin-Free Gc-Globulin. *Clin. Biochem.* **2008**, *41*, 974–980.

# Chapter 3: Genetic display of Fc-binding domains on Qβ VLPs

## 3.1. Abstract

Structurally-defined protein nanoparticles are attractive platforms for the polyvalent display of targeting ligands or other bioactive molecules for applications in biomedicine. Virus-like particles (VLPs) represent a particularly promising scaffold due to their chemical and genetic malleability, which allows for the installation of targeting motifs as well as the delivery of functional payloads. In this work, we genetically incorporated protein domains on the surface of Qβ VLPs capable of binding Fc-domains with high affinities and decorated the surface of these particles with targeting antibodies to direct cytotoxic payloads against specific cell populations. The co-expression of wild-type Qβ coat proteins and coat protein fusions resulted in the assembly of hybrid VLPs that were structurally homogenous and displayed the Fc-binding domain on their surface. The interior of these particles could be simultaneously loaded with active proteins for applications in imaging or pro-drug therapy. As a proof-of-concept, these particles were employed for the selective removal of undifferentiated human pluripotent stem cells (hPSCs). After labeling with antibodies against the hPSC-specific surface glycan SSEA-5, particles containing enhanced green fluorescent protein (EGFP) were shown to specifically bind undifferentiated cells in culture, and cytosine deaminase (CD)-containing particles were able to eliminate undifferentiated hPSCs with virtually no cytotoxicity to differentiated cells upon treatment with the prodrug 5-fluorocytosine (5-FC). We further tested the modularity of this system by replacing the displayed antibody in order to direct VLPs against validated cancer cells expressing varying levels of human

epidermal growth factor receptor 2 (HER2) on their surface. Particles displaying the antibody selectively targeted cells expressing HER2; furthermore, these cells could be selectively killed upon incubation with CD-containing particles followed by dosing with 5-FC. Both of these proof-of-concept studies established the efficacy and modularity of this technology, which has tremendous potential for the development of a targeted chemotherapeutic platform with improved margins of safety.

### 3.2. Introduction

One of the primary challenges facing the field of biomedicine is the lack of suitable strategies for the delivery of therapeutic molecules (i.e., drugs, proteins, nucleic acids) to specific sites of disease.[1] The ability to selectively deliver therapeutics to specific cellular populations, such as tumors, would offer increased drug efficacy at lower dosing while reducing the debilitating off-target effects commonly associated with the systemic administration of chemotherapeutics. Monoclonal antibody-drug conjugates (ADCs) offer a high degree of selectivity but have limited payload capacity.[2,3] Therefore, combining the specificity of antibody-based therapeutics with platforms that can carry larger payloads represents a promising goal in biomedical research.

Nanoscale platforms are of particular interest in the development of next-generation therapeutics as several modalities can be simultaneously engineered into a single platform over a large surface area, providing for high degrees of functionalization. Numerous nanoparticle platforms have been developed for the delivery of drug payloads to cellular environments that are marked by the dysregulated expression of cell-surface receptors as a consequence of disease.[4–6] In particular, proteinaceous nanoparticles offer novel platforms that can be engineered at the genetic level with both targeting and

effector functions. Although VLPs and other protein nanoparticles have been well-established as carrier proteins for vaccine development, their broad applicability as delivery agents remains to be fully surveyed; however, this class of biomaterials has been explored previously for antibody-mediated delivery.

Francis and colleagues developed an oxidative coupling strategy for the covalent modification of MS2 VLPs with antibodies and successfully targeted cancer cells expressing epidermal growth factor receptor (EGFR) or human epidermal growth factor receptor 2 (HER2) with this platform.[7] Despite these promising results *in vitro*, only moderate tumor uptake was observed when the biodistribution of this platform was investigated in a murine model of breast cancer.[8] It should be noted here that penetration of the particle into the tumor is not a necessary requirement for effective delivery of a therapeutic, as will be discussed later in this chapter. Vault nanoparticles have also been engineered to display antibody-binding peptides (Z domains) derived from *Staphylococcus aureus* protein A and, after labeling with anti-EGFR antibodies, could specifically localize to A431 cancer cells.[9] Although these constructs demonstrated selective targeting, their ability to deliver a cytotoxic payload was not tested.

In the work presented in this chapter, we sought to build on the technology developed by Fiedler and Brown[10–12] by simultaneously encapsulating active prodrug-converting enzymes within Qβ VLPs while incorporating ZZ domains on the particle surface to mediate targeting antibody display. A dimeric variant of the Z domain (approximately 200 amino acids) first reported by Nilsson *et al.*[13]was chosen for incorporation, hence the "ZZ" designation. As a proof-of-concept, we first explored the

utility of our system for the targeted removal of human pluripotent stem cells (hPSCs) in cardiomyocyte differentiation cultures.

Due to their virtually unlimited self-renewal capacity and differentiation potential *in vitro*, hPSCs—comprising human induced pluripotent stem cells (hiPSCs) and human embryonic stem cells (hESCs)—remain leading candidates for cell-based regenerative therapies.[14–18] Despite substantial advances in protocol efficiencies, directed differentiation of hPSCs to a desired cell type usually yields a population containing residual undifferentiated and potentially tumorigenic cells. Before widespread clinical adoption of hPSC-based therapies can be achieved, effective strategies for the removal of hPSCs are needed to eliminate the risk of post-transplantation teratoma formation.[19–21] To this end, making potentially tumorigenic hPSCs sensitive to prodrugs via expression of suicide-inducing genes is considered a promising approach.[22–27] Transgenic expression of the bacterial gene encoding cytosine deaminase (CD), which enables the conversion of the negligibly toxic prodrug 5-fluorocytosine (5-FC) to the highly cytotoxic 5-fluorouracil (5-FU), has been used to selectively eradicate pluripotent stem cells derived from mice[25] and primates.[27] However, since transgenic modification of cells poses the risk of deleterious mutagenesis, we explored our system for specific intracellular delivery of suicide-inducing macromolecules such as CD to viable hPSCs as a safer alternative for clinical applications.

Targeted therapeutics have also emerged in recent years as promising approaches for the treatment of certain cancers.[28] Overexpression of ErbB2/HER2 has been reported in ~ 25% of all breast, gastric, and ovarian cancers, where its expression level correlates with the aggressiveness of the disease.[29–31] Trastuzumab is an FDA-approved monoclonal

antibody therapeutic that is employed against HER2+ cancers in combination therapies, as it can inhibit growth but is primarily ineffective at eliminating tumors on its own.[30] We further sought to explore the modular utility of our system by targeting cancer cells expressing HER2 by simply replacing the surface-displayed antibody.

Our data shows that the antibody-guided delivery of VLPs to specific cell populations is highly efficient even at low nanomolar concentrations and is highly selective at delivering cytotoxic payloads only to the target cells with no detectable levels of off-target toxicity. This extends the engineering of hybrid VLPs presented in Chapter 2 to much larger protein domains that mediate markedly different functional outcomes (cellular targeting vs. epitope presentation). While the work presented here is not the first example of cellular targeting mediated by protein domain display on hybrid Qβ particles,[32] it is by far the most modular. Furthermore, it is one of the few examples to simultaneously investigate both antibody-mediated targeting as well as delivery of a cytotoxic effector using a nanoparticle platform. The ability to develop a single platform and alter its tissue tropism by simple exchange of the surface-displayed antibody provides for a system that can be directed against multiple disease targets in a "plug-and-play" fashion, which is demonstrated by the two studies presented herein.

### 3.3. Materials and Methods

*Cell culture*

Human induced pluripotent stem cells [iPS(IMR90)-1, WiCell][33] and human embryonic stem cells (H7, WiCell)[34] were cultured either on a feeder layer of irradiated mouse embryonic fibroblasts (MEF), where they were maintained in hPSC medium (KnockOut DMEM, 20% KnockOut Serum Replacement, 2 mM L-glutamine, 0.1 mM

non-essential amino acids, 0.1 mM β-mercaptoethanol, 100 U/mL Penicillin-Streptomycin) supplemented with 8 ng/mL human basic fibroblast growth factor (bFGF), or in feeder-free hPSC conditions as previously described.[35] Primary human dermal fibroblasts (hDFs) were obtained with informed consent from a patient skin biopsy in a safe and ethical manner as approved by the Emory University Institutional Review Board (IRB). Isolated hDFs were cultured in fibroblast growth medium (DMEM, 10% FBS, 4 mM L-glutamine, 100 U/mL Penicillin-Streptomycin). MDA-MB-435, MDA-MB-231, HT-29, and HEK-293 cells were all cultured in standard growth medium (DMEM, 10% FBS, 2 mM GlutaMAX™, 1 mM sodium pyruvate, 100 U/mL Penicillin-Streptomycin). All cell culture reagents were from Fisher Scientific unless specified.

*Protein expression and purification of Qβ(ZZ) VLPs*

The hybrid VLP constructs were produced and characterized as previously described.[10] Briefly, ClearColi® BL21(DE3) electrocompetent *E. coli* cells (Lucigen) were co-transformed with one of the following plasmid combinations: pET28-CP@EGFP/pCDF-CP(ZZ) or pET28-CP(ZZ)/pCDF-CP@CD according to the manufacturer's recommended protocol. The ZZ domain was connected to the C-terminal end of the Qβ capsid sequence by an 8-amino acid linker; the full sequence of the extended coat protein [(Qβ)(linker)(Z)(Z)] was as follows, noting that the N-terminal methionine required for bacterial expression is processed off the capsid structure by cellular proteases:

(AKLETVTLGNIGKDGKQTLVLNPRGVNPTNGVASLSQAGAVPALEKRVTVSVS
QPSRNRKNYKVQVKIQNPTACTANGSCDPSVTRQAYADVTFSFTQYSTDEERAF
VRTELAALLASPLLIDAIDQLNPAY)(GGASESGA)(AMVDNKFNKEQQNAFYEIL
HLPNLNEEQRNAFIQSLKDDPSQSANLLAEAKKLNDAQAPKNLNEEQRNAFIQSL

KDDPSQSANLLAEAKKLNDAQAPK)(AMVDNKFNKEQQNAFYEILHLPNLNEEQ RNAFIQSLKDDPSQSANLLAEAKKLNDAQAPKNLNEEQRNAFIQSLKDDPSQSA NLLAEAKKLNDAQAPK)

Cells were plated on selective super optimal broth (SOB) agar; after 24 h, single colonies were isolated and transferred to selective SOB media (1% NaCl; *w/v*) for overnight growth at 37°C. The following morning, cultures were diluted under the same conditions and growth was monitored via optical density (600 nm) until the cultures reached mid-log phase (i.e., $O.D._{600} \sim 0.9$). Protein expression was induced by the addition of IPTG at a final concentration of 1 mM. Cultures were maintained at 30°C for 24 h, after which time cells were harvested by centrifugation (6,000 rpm, 10 min). Cell pellets were suspended in 1X Tris-buffered saline (TBS; pH 7.06), and cells were lysed with a probe sonicator in an ice bath (10 min total, 5 s pulse intervals). Cell debris was removed by centrifugation (14,000 rpm, 10 min) and the supernatant was collected. VLPs were precipitated by the addition of 30% $(NH_4)_2SO_4$ (*w/v)* for 2 h at 4°C, and the precipitate was pelleted by centrifugation (14,000 rpm, 10 min). The pellet was dissolved in 1x TBS and extracted with a solution of *n*-BuOH:$CHCl_3$ (1:1, *v/v*) to remove lipids and aggregates. The aqueous phase was collected following centrifugation (14,000 rpm, 10 min) and VLPs were further purified on 10-40% sucrose density gradients (28,000 rpm, 4 h). VLP bands were isolated via syringe and pelleted by ultracentrifugation (68,000 rpm, 2 h). Subsequent pellets were dissolved in 0.1M potassium phosphate buffer and characterized.

*Characterization of Qβ(ZZ) VLPs*

VLP concentration was quantified using Bradford assay with BSA standards according to the manufacturer's protocol (Thermo Fisher) with average yields of 10-20

mg/L. Particle purity was assessed by fast protein liquid chromatography (FPLC) with a Superose 6 GL column and monitored by absorbance (280 nm). Size of the VLPs was determined by dynamic light scattering (DLS) using a Dynapro II plate reader (Wyatt Technology), and particle composition was determined by microfluidic gel electrophoresis using an Agilent 2100 Bioanalyzer with Series II Protein 80 chips. The relative particle composition was determined by comparing peak integrations from the electropherograms using the Bioanalyzer software. Due to overlap of the CP(ZZ) and EGFP bands, EGFP concentration was calculated by measuring the sample absorbance at 488 nm and using the Beer-Lambert law (Abs = $\varepsilon cl$; $\varepsilon_{EGFP}$ = 56,000 $M^{-1}cm^{-1}$). On average, 4-8 molecules of EGFP were packaged, 13-18 molecules of CD were packaged, and 40-60 ZZ-domain subunits were incorporated per particle, respectively.

*Antibody-labeling of Qβ(ZZ) VLPs*

Qβ(ZZ)@EGFP or Qβ(ZZ)@CD VLPs were labeled with anti-SSEA-5 or anti-ErbB2/HER2 antibodies. Briefly, VLPs were diluted to 0.1 mg/mL and 20 μg VLP was incubated with 50 μg purified anti-human SSEA-5 mouse IgG1, κ antibody (Clone 8e11, BioLegend) or 50 μg purified anti-human ErbB2/HER2 rat IgG2a (Clone ICR55, Thermo Fisher) for 2 h at 37°C. A antibody: ZZ-domain mole ratio of 0.75 was used for all labeling reactions and was sufficient for uniform labeling of the particles. To serve as a control, the same procedure was repeated with purified mouse IgG1, κ isotype control antibody (Clone MG1-45, BioLegend).

*Quantification of antibody loading by multi-angle light scattering*

Empty Qβ(ZZ) VLPs were split into two samples at 0.1 mg/mL, and one sample was labeled with mouse IgG1, κ isotype control antibody as previously described. Samples

were separated over a Superose 6 10/300 GL size exclusion column (GE Healthcare) using an Agilent HPLC to maintain a 0.2 mL/min flow rate of 0.1M $KPO_4$ buffer (pH 7.4). Samples of 100 μL were injected onto the column. Samples were detected using a UV-vis detector (Agilent), a Viscotek SEC-MALS 20 multi-angle light scattering detector (Malvern), and a Viscotek VE3580 refractometer (Malvern). The number-average molecular weight, $M_n$, was calculated with OmniSEC 5.0 software and plotted across the elution peak. The increase in molecular weight for the antibody-labeled sample was related to the number of bound antibodies using the average molecular weight for IgG antibodies (~150 kDa).

*Cardiomyocyte differentiation*

hPSCs were induced for cardiac differentiation as described previously.[36,37] hPSCs were first dissociated using Versene and plated on Matrigel-coated wells plate at density of $1.6x10^5$ cells/$cm^2$. Cells were cultured in conditioned medium from MEF (MEF-CM) for 2 days and treated with 100 ng/mL activin A (R&D Systems) from differentiation day 0 till day 1 and 10 ng/mL bone morphogenic protein-4 (BMP4, R&D Systems) from day 1 till day 5 in RPMI/B27 insulin-free medium. Cells were cultured successively with RPMI/B27 medium with insulin and the medium was changed on alternate days. Cardiomyocytes showed beating activity at day 9/10 of differentiation.

*Treatment of Cardiac Progenitors with VLPs*

One day before the treatment of cardiac progenitors derived from hPSCs (at day 7 or 8), the medium was replaced with a blocking solution (medium with 20% KnockOut Serum Replacement) to prevent non-specific binding of VLPs. After cultured for 24 h (at day 8 or 9), the cells were then treated for 1 h with medium containing 8 nM SSEA-5-

labeled Qβ(ZZ)@CD VLPs or vehicle (PBS as a control) followed by 24 h incubation with 100 μM 5-FC.

*Treatment of co-culture of hPSCs and cardiomyocytes with VLPs*

Cardiomyocytes at day 14 were plated on a Matrigel-coated plate at density of $1.6x10^5$ cells/$cm^2$ and cultured in RPMI/B27 medium until they regained beating activity. Undifferentiated hPSCs were then plated at density of 1-5% compared to cardiomyocytes ($1.6x10^3$ to $8x10^3$ cells/$cm^2$) and cultured in MEF-CM medium. Cells were treated for 1 h with medium containing 8 nM SSEA-5-labeled Qβ(ZZ)@CD VLPs or PBS (vehicle as a control) followed by 24 h incubation with 100 μM 5-FC.

*Live-cell microscopy and fluorescence imaging*

*Procedure for SSEA-5 targeting*. For standard live-cell microscopy, cultured cells were imaged using a phase contrast and epifluorescence inverted microscope (Zeiss AxioVert A1) equipped with Zeiss AxioCam digital camera system. Images were processed and exported using Zeiss AxioVision LE imaging software and image merging was performed in Adobe Photoshop. For live-cell deconvolution microscopy, undifferentiated hPSC colonies were seeded onto a Matrigel-coated glass-bottom chamber slide and allowed to adhere overnight before imaging. The following day, the cells were incubated for 30 min at 37°C in 25 μL of cell culture medium containing 8 nM of $Qβ(ZZ)_{60}$@$EGFP_4$+$SSEA\text{-}5_{30}$ particles, 5 μg/mL membrane-specific wheat germ agglutinin, Alexa Fluor 594 conjugate (Invitrogen) and 2 drops/mL of NucBlue® Live ReadyProbes® (Life Technologies) in accordance with the manufacturer's instructions. After 30 min, the particle and nuclear probe-containing medium was removed and the cells were rinsed twice with cell culture medium before imaging. Live cells were imaged at 37°C

using an Olympus® IX71/IX51 temperature-controlled wide-field deconvolution fluorescence microscope. Optical sections were acquired using an automated stage and deconvolution algorithms. Cells were first imaged in the XY plane at 60X magnification, where EGFP and DAPI were excited at 495 nm and 358 nm, respectively, and emission was collected at 519 nm, and 461 nm, respectively. Z-series orthogonal image stacks were captured using 50 steps at a size of 0.2 μm per step. Pictures were taken using SoftWoRx microscopy software (DeltaVision) and files were exported and analyzed using Volocity 6.3 3D image analysis software (Perkin Elmer).

*Procedure for ErbB2/HER2 targeting*. For standard fluorescence microscopy, cultured cells were imaged on an Eclipse Ti-U fluorescence microscope (Nikon) equipped with a 60x oil immersion objective and a CoolSNAP™ MYO CCD camera system (Photometrics). Prior to imaging, $5x10^5$ cells (MDA-MB-435, MDA-MB-231, and HEK-293) were seeded onto 8-chambered microscope slides and allowed to adhere overnight. The following day, cells were incubated for 2 h at 4°C with 200 μL cell culture media containing 10 nM $Q\beta(ZZ)_{32}$(Alexa Fluor $488)_{20}$ + anti-ErbB2/$HER2_{16}$ or 10 nM $Q\beta(ZZ)_{32}$(Alexa Fluor $488)_{20}$. Following incubation, cells were rinsed twice with 1x PBS and fixed with 2% paraformaldehyde for 15 min at room temperature. Cells were subsequently rinsed twice with 1x PBS and imaged immediately. Pictures were taken using NIS Elements imaging software (Nikon) and files were exported and analyzed using ImageJ software.

*Cytotoxicity and viability assays*

*Procedure for SSEA-5 targeting*. The cytotoxic range of 5-fluorocytosine (5-FC) in the presence of $Q\beta(ZZ)_{42}@CD_{13}$+$SSEA\text{-}5_{21}$ and 5-fluorouracil (5-FU) in hPSCs was

determined using Cell Counting Kit-8 (CCK-8; Dojindo) pursuant to the manufacturer's instructions. CCK-8 is a tetrazolium salt-based calorimetric assay which measures the amount of formazan dye generated by cell dehydrogenases, whereby the optical density of the dye is directly proportional to the number of living cells. Each condition was performed with triplicate wells containing ~ 10,000 cells per well. Cells were incubated for 4 h in culture media with a 1:10 dilution of CCK-8 and absorbance was measured at 450 nm with a Synergy 2 microplate reader and Gen5 software (BioTek). The $EC_{50}$ was generated and calculated using GraphPad statistical analysis software. The specificity of killing hPSCs in a feeder layer co-culture was assessed via microscopy after a 30 min incubation with 4 μM fluorescence-dependent ethidium homodimer-1 (EthD-1; Molecular Probes). Dead cells are detectable when the cell-impermeable dye EthD-1 enters cells with damaged membranes and binds intracellular nucleic acids to emit bright red fluorescence. To identify hPSCs, fluorescent StainAlive (DyLight 488) TRA-1-60 anti-human antibody (Stemgent) was added directly to the culture media (1:100 dilution) and incubated for 30 min. Fluorescent antibodies were excited and captured in accordance with the manufacturer's instructions.

*Procedure for ErbB2/HER2 targeting.* Targeted killing of MDA-MB-435 cells was assessed using a standard MTT assay to assess cell viability post-treatment. Each condition was performed in duplicate wells containing $5x10^4$ cells per well. Briefly, cells were incubated for 1 h at 37°C with either $Q\beta(ZZ)_{42}@CD_{13}$, $Q\beta(ZZ)_{42}@CD_{13}$ + anti-ErbB2/$HER2_{21}$, or fresh DMEM. The final particle concentration was 5 nM for all treated wells. Cells were rinsed twice with PBS and either dosed with fresh media containing 1, 10, or 100 μM 5-FC (for all particle-treated cells); 1, 10, or 100 μM 5-FU; or left untreated.

After 24 h, cells were rinsed twice with PBS and incubated with 1 mM 3-(4,5-dimethylthiazol-2-yl)-2,5-diphenyltetrazolium bromide (MTT) in fresh DMEM for 2 h at 37°C. Media was removed and 200 µL DMSO was added to dissolve formazan crystals. After thorough mixing, absorbance was measured at 540 nm using a microplate reader (Thermo Fisher Scientific).

*Colony formation assay*

Colony formation assay was performed to determine if SSEA-5-labeled Qβ$(ZZ)_{42}$@$CD_{13}$ VLPs selectively kill hPSCs in the presence of 5-FC. Vehicle- or VLP-treated cells were harvested and plated at $1x10^5$ cells/$cm^2$ onto a feeder layer of irradiated MEF ($2.5x10^4$ cells/$cm^2$). Cells were cultured with conditioned medium from MEFs and hbFGF (8 ng/mL) for 10 more days until colonies were visible. The cells were then fixed for the detection of hPSCs by immunocytochemistry.

*qRT-PCR*

RNA was extracted from vehicle- and VLP-treated cells (n=3/group) 3 days after the VLP treatment, using Aurum total RNA mini kit (Bio-Rad) as per manufacturer's instructions. Cells were lysed in 350 µL lysis buffer supplemented with 1% β-mercaptoethanol then stored at -80ºC until further processing. Samples were reverse-transcribed using 100 U of Superscript III enzyme and random primers in 20 µL reaction mixture containing Vilo reaction buffer as per manufacturer's instructions (SuperScript® VILO™ cDNA Synthesis Kit by Life Technologies). Samples were processed in a Bio-Rad thermal cycler with following temperature cycles: 25ºC for 10 min, 42ºC for 2 h and 25ºC for 5 min. The reaction mixture was then diluted 5 times before further use for real-time PCR (qPCR). Human specific PCR primers (**Appendix I**) for the genes examined

were retrieved from open access websites (http://primerdepot.nci.nih.gov/ or http://pga.mgh.harvard.edu/primerbank/). Thermocycler reaction was set up as follows using the: initial denaturation step at 95ºC for 10 min, 40 cycles of two-steps with 15 s of denaturation at 95ºC followed by 1 min of annealing at 60ºC using Applied Biosystems 7500 real-time PCR systems. All iTaq SyBr green samples were normalized to the level of the housekeeping gene GAPDH. Relative expression levels compared to control samples were presented as fold changes calculated by the 2−ΔΔCt method. Data are presented as mean ± SD. Relative expression of stem cell marker genes in both vehicle and VLP-treated samples was compared to normal cardiomyocytes cultures and 1% spiked cardiomyocytes at Day 0 (before 5-FC treatment).

*$Ca^{2+}$ imaging*

Live cell imaging of intracellular $Ca^{2+}$ transient was performed to assess functional characteristic of cardiomyocytes as described previously.[38,39] Cultured cells were dissociated using Trypsin/EDTA, seeded onto Matrigel-coated 25x25x1 mm glass coverslips (~ 25,000 cells per coverslip), allowed to adhere overnight and then maintained in RPMI/B27 medium until they recovered beating activity. Cells were incubated for 15 min at 37°C in 2 mL RPMI/B27 medium containing 5 µM Fluo-4, AM, a cell permeant-fluorescent $Ca^{2+}$ dye (Thermo Fisher, F14201) for cytosolic loading. After 15 min, cells were placed in a stimulation chamber on an Olympus FV1000 inverted confocal IX81 microscope, where they were eluted for 5 min at 37 °C in Tyrode's solution (148 mM NaCl, 4 mM KCl, 0.5 mM $MgCl_2 \cdot 6H_2O$, 0.3 mM $NaPH_2O_4 \cdot H_2O$, 5 mM HEPES, 10 mM D-Glucose, 1.8 mM $CaCl_2 \cdot H_2O$, pH adjusted to 7.4 with NaOH) to allow for dye de-esterification. Cells were then continuously bathed in 37 °C Tyrode's solution while field-

stimulated (MyoPacer EP Field Stimulator, IonOptix) at 1 Hz, 32 V. Fluo-4 was excited by the 488 nm line of an argon laser and emitted fluorescence was captured at >505 nm. Recordings were acquired in line-scan (X-T) mode at a sampling rate of ≥500 lines per second and a pixel size of 0.155 μm. Lines were preferentially positioned in the center of the cell. Recordings of line-scan $Ca^{2+}$ transients at 40x magnification were processed and exported using FV10-ASW 3.0 microscopy software (Olympus). Analysis of recordings was performed with Clampfit 10.0 software (Molecular Devices). Transient amplitude data are presented as ΔF/F0, where ΔF= fluorescence (F) – basal fluorescence (F0).

*Immunocytochemistry*

Immunocytochemical analyses were done to evaluate presence of hPSCs and cardiomyocyte phenotype as described previously.[40] Cells were dissociated using Trypsin/EDTA and plated on a Matrigel-coated 96 well plate at density of 50,000 cells per well, and cultured until they recovered beating activity before fixation. Cells were washed with PBS and fixed in 4% (vol/vol) paraformaldehyde (Sigma) at room temperature for 15 min then permeabilized in cold methanol for 2 min at room temperature. Cells were then blocked in 5% normal goat serum (NGS) in PBS at 4°C for 1 h and incubated with primary antibodies in 3% NGS overnight at 4°C. After the incubation with the primary antibodies, the cells were washed twice with PBS to get rid of unbound primary antibodies. Cells were then incubated with the corresponding conjugated secondary antibodies (Table S2) at room temperature for 1 h in the dark, washed twice with PBS. Vectorshield mounting medium containing DAPI (Vector Laboratories, H-1200) was used to counterstain nuclei. Cells were imaged using a phase contrast and epifluorescence inverted microscope (Zeiss AxioVert A1) equipped with Zeiss AxioCam digital camera system. Images were

processed and exported using Zeiss AxioVision LE imaging software and image merging was performed in Adobe Photoshop.

*Video-based analysis of contractility*

Contractility of cardiomyocytes was recorded using a phase contrast inverted microscope (Zeiss AxioVert A1) equipped with Zeiss AxioCam digital camera system, 20x magnification, 30 s for each sample, 20 ms interval between frames. Video were processed and exported using Zeiss AxioVision LE imaging software. Video-based analysis of contractility parameters was performed with Matlab R2016b software as described.[41]

*Flow cytometry*

MDA-MB-435, MDA-MB-231, HT-29, and HEK-293 cells were grown to 90% confluence, detached with Accutase, pelleted, and re-suspended in FACS buffer. Approximately 5 x $10^5$ cells were aliquoted for each sample. Qβ particles were added directly to the cell suspensions at a final concentration of 10 nM and incubated at 4°C for 2 h. Cells were washed twice with FACS buffer and fixed with 2% paraformaldehyde for 15 min at room temperature. Following two additional washes, cells were re-suspended in FACS buffer and stored at 4°C until analysis. Cell populations were gated for live cells and 10,000 events were collected using a BD LSRFortessa cell analyzer (BD Biosciences). Data analysis was performed using FlowJo® software (FlowJo, LLC).

*Statistics*

For calcium imaging analysis and video-based analysis of contractility, significant differences between vehicle- and VLP-treated cells were assessed by two-sample *t*-test. All data were expressed as mean ± SD and $p$ values less than 0.05 were considered as significant.

## 3.4. Results and Discussion

### *3.4.1. Antibody-directed elimination of tumorigenic stem cells*

VLPs are named here as previously described: for example, Qβ$(ZZ)_n$@$EGFP_m$ denotes a Qβ VLP in which an average of *n* of the 180 capsid protein subunits have the ZZ domain appended to the C-terminus for display on the external surface, and an average of *m* copies of the EGFP protein are encapsidated inside the particle.[11] In addition, if the surface ZZ domain on the VLPs is bound to an antibody, a + sign appears followed by the antibody's abbreviation. EGFP packaging was engineered by co-transformation of *E. coli* cells with two plasmids, one [designated pET28-CP@EGFP] coding for both the standard capsid protein (CP) and EGFP fused to the Rev peptide to assist in packaging,[11] and the other [pCDF-CP(ZZ)] coding for the CP-ZZ fusion (**Figure 1A**). IPTG-triggered expression from both plasmids routinely yielded particles in a yield of 10-15 mg per L of culture with $n = 60$ and $m = 4$ (**Figure 1B,C**). Characterization by dynamic light scattering revealed a homogeneous hydrodynamic radius ($R_h$) of 17.2 nm, somewhat larger than the wild-type VLP (14 nm), as expected. Antibody SSEA-5, identified by Weissman, Drukker, and colleagues as a binder of an hPSC-specific fucosylated H-1-type carbohydrate antigen,[42] was mixed with these particles to give Qβ$(ZZ)_{60}$@$EGFP_4$+$SSEA\text{-}5_{30}$, which showed an increase in apparent $R_h$ to 21.2 nm (**Figure 1D**), consistent with the presence of

no more than a single layer of IgG antibodies on the particle surface. Multiple angle light scattering (MALS) analysis indicated an increase in particle molecular weight from 3.2 MDa to 5.5 MDa, corresponding to occupancy of approximately half of the ZZ domains by IgG molecules (**Figure 1E**).

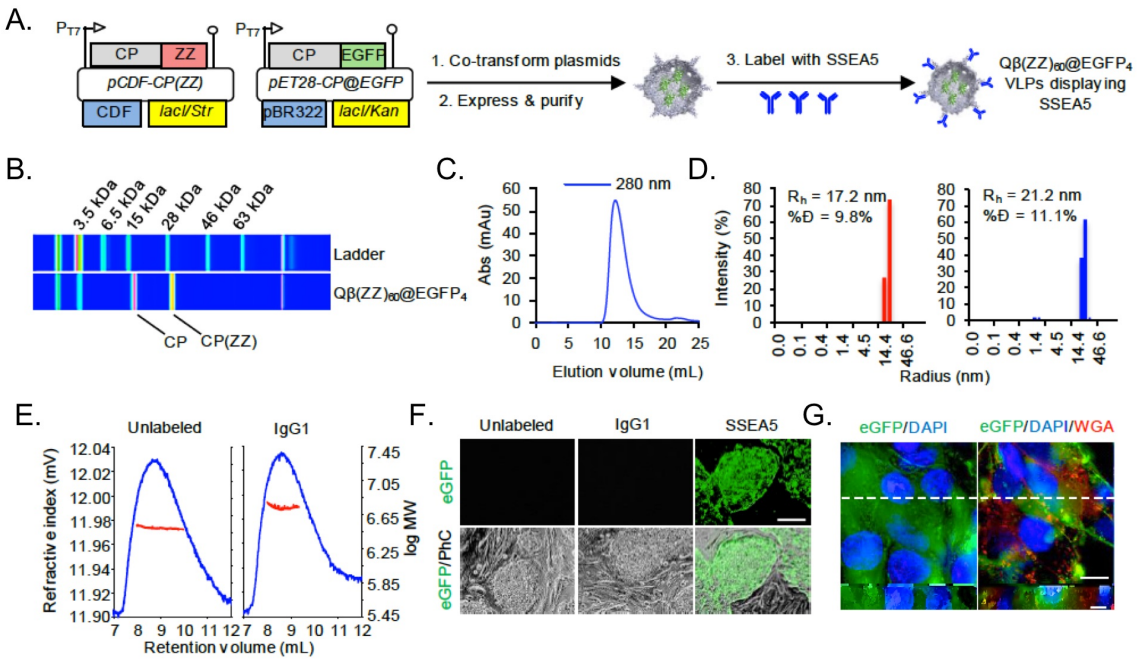


**Figure 1.** SSEA-5-labeled Qβ(ZZ)$_{60}$@EGFP$_4$ VLPs selectively deliver EGFP intracellularly to hPSCs. **(A)** Schematic of Qβ(ZZ)$_{60}$@EGFP$_4$ viral coat protein expression and particle assembly, followed by VLP labeling with SSEA-5 antibodies. (**B**) Denaturing electrophoretic analysis of Qβ(ZZ)$_{60}$@EGFP$_4$ VLPs. (**C**) Fast protein liquid chromatography analysis of Qβ(ZZ)$_{60}$@EGFP$_4$ VLPs. (**D**) Dynamic light scattering histograms of Qβ(ZZ)$_{60}$@EGFP$_4$ VLPs (red) and Qβ(ZZ) $_{60}$@EGFP$_4$+SSEA-5$_{30}$ VLPs (blue); %Đ = % dispersity; $R_h$ = hydrodynamic radius. (**E**) Multiple angle light scattering curves show the change in refractive index (blue peak) of the VLPs as a function of the elution volume through a size-exclusion column. A comparison between the log MW (red trace) of unlabeled (left) and antibody-labeled (right) VLPs indicates approximately half of the ZZ domains are occupied by antibodies. (**F**) Representative microscopy images of hPSC colonies grown on mouse embryonic fibroblasts incubated with 8 nM unlabeled, IgG1-labeled, or SSEA-5-labeled Qβ(ZZ)$_{60}$@EGFP$_4$ VLPs for 30 min at 37°C. Only hPSCs treated with SSEA-5-labeled Qβ(ZZ)$_{60}$@EGFP$_4$ showed detectable EGFP fluorescence. Scale bars = 100 µm. (**G**) Live-cell deconvolution fluorescence microscopy of hPSCs incubated for 30 min at 37°C with 8 nM Qβ(ZZ)$_{60}$@EGFP$_4$+SSEA-5$_{30}$, blue DAPI nuclear probe, and membrane-specific red wheat germ agglutinin (WGA). Left = EGFP and DAPI only; right = EGFP, DAPI, and WGA. XY optical sections are shown above orthogonal YZ cross-sections corresponding to the white dashed line in the XY plane. Cross-sections show prominent cytoplasmic co-localization of EGFP and DAPI along with punctate expression of the membrane-specific WGA dye. XY plane scale bars = 15 µm; YZ scale bars = 5 µm.

$Q\beta(ZZ)_{60}$@$EGFP_4$+SSEA-$5_{30}$ particles were incubated (5, 10, and 15 nM in particle, 37°C) with hESC colonies cultured on mouse embryonic fibroblasts (MEFs). After 30 min, EGFP was detected in all the undifferentiated stem cell colonies at all particle concentrations (**Figure 2A,B**). To confirm the antibody-directed nature of EGFP delivery, a blinded experiment was performed in which hESC colonies were again cultured on MEFs and incubated for 30 min at 37°C with 8 nM of unlabeled, IgG1-labeled (κ isotype control), or SSEA-5 labeled $Q\beta(ZZ)_{60}$@$EGFP_4$. Since mouse embryonic fibroblasts do not express the SSEA-5 binding motif, they were used as a negative cell control. After 30 min, the excess particle-containing supernatant was removed, and the cells were rinsed before imaging. Fluorescence images showed green fluorescent stem cell colonies in the wells treated with $Q\beta(ZZ)_{60}$@$EGFP_4$+SSEA-$5_{30}$ particles, but virtually no green fluorescence in either the MEFs or the hESCs treated with the unlabeled $Q\beta(ZZ)_{60}$@$EGFP_4$ or $Q\beta(ZZ)_{60}$@$EGFP_4$+IgG1 isotype control particles (**Figure 1F)**. In addition, live-cell deconvolution fluorescence microscopy with three-dimensional optical sectioning showed substantial diffuse and intracellular EGFP distribution when live hESC colonies were incubated with DAPI as a nuclear probe (blue), a membrane-specific wheat germ agglutinin dye (WGA; red), and 8 nM of $Q\beta(ZZ)_{60}$@$EGFP_4$+SSEA-$5_{30}$ particles (green; **Figure 1G**). These results demonstrate that $Q\beta(ZZ)_{60}$@$EGFP_4$+SSEA-$5_{30}$ particles selectively target, and appear to be taken up by, undifferentiated stem cells while exhibiting negligible non-specific binding.

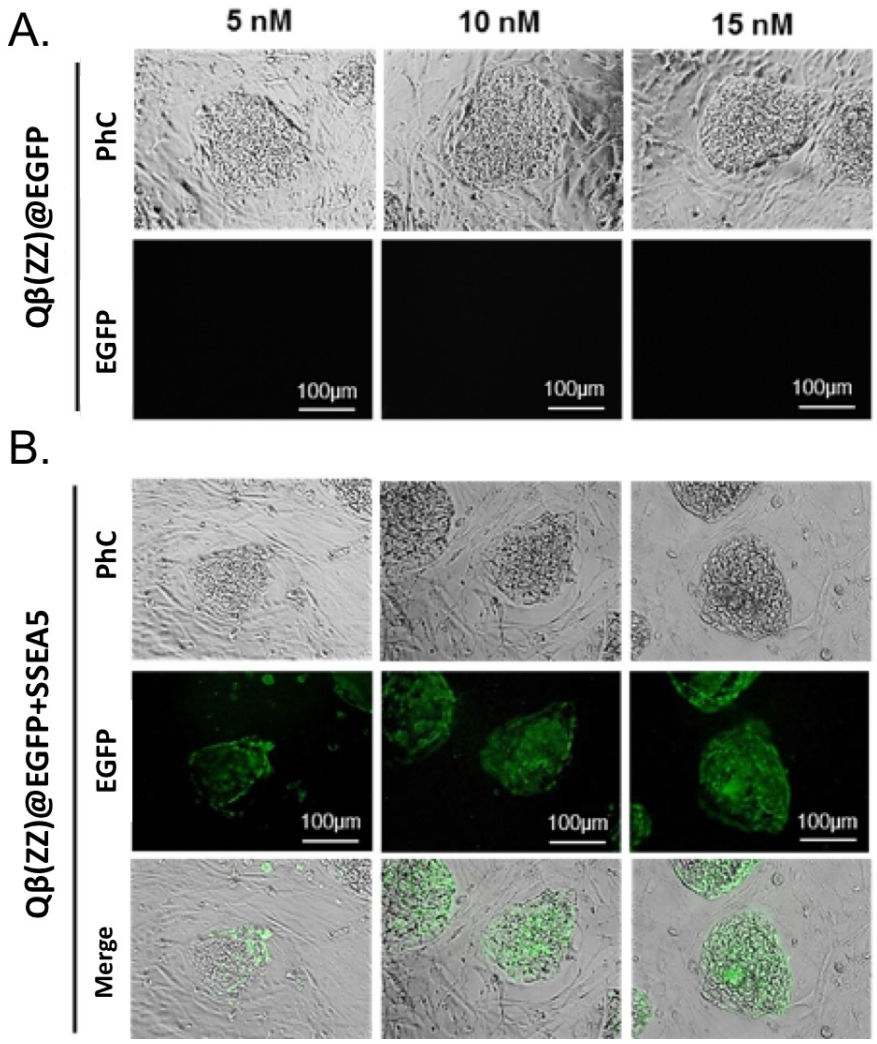


**Figure 2.** Qβ(ZZ) virus-like particles bearing the SSEA-5 antibody selectively target EGFP to undifferentiated cells in a dose-dependent manner. Fluorescence microscopy images show human induced pluripotent stem cell colonies grown on mouse embryonic fibroblasts that were incubated for 30 minutes at 37°C with 5, 10, and 15 nM of **(A)** EGFP-encapsidated Qβ(ZZ) particles bearing no antibody (i.e. Qβ(ZZ)@EGFP) or **(B)** GFP-encapsidated Qβ(ZZ) particles bearing the SSEA-5 antibody (i.e. Qβ(ZZ)@EGFP+SSEA5).

Targeted VLPs with cytotoxic capability were generated as above, replacing the packaged EGFP protein with a thermostable variant of yeast cytosine deaminase (CD).[43] The resulting $Q\beta(ZZ)_{42}@CD_{13}$ particles were addressed with SSEA-5 in the same manner, resulting in very similar yield and physical parameters as the EGFP-containing particles

(**Figure. 3A-D**). The cytotoxic activity of the CD-containing particles was verified first on monocultures of hiPSCs and hESCs, which were incubated for 24 h with titrating concentrations of either 8 nM Qβ$(ZZ)_{42}$@$CD_{13}$+SSEA-$5_{21}$ VLPs in the presence of the prodrug 5-fluorocytosine (5-FC), or its product, 5-fluorouracil (5-FU), alone as a positive cytotoxicity control. Survival percentages for each treatment were determined using a tetrazolium salt-based assay and decreased in a dose-dependent manner in both hPSCs and hESCs (**Figure 3E**). The mean $EC_{50}$ values of 5-FC in the presence of CD-containing particles and 5-FU alone for hESCs and hiPSCs were similar (approximately 1.5 μM), with negligible cell survival observed at 100 μM of either small molecule. To test targeting specificity, monocultures of primary human fibroblasts (hDFs) were treated for 24 h with 8 nM Qβ$(ZZ)_{42}$@$CD_{13}$+SSEA-$5_{21}$ VLPs and either 5-FC or 5-FU at 0.1 μM to 2 mM. 5-FU was found to kill these differentiated cells with efficiency comparable to the killing of stem cells, but no dose-dependent cell death was observed in the presence of 5-FC and the SSEA-5-coated particles containing packaged CD (**Figure 3F**).

The use of this system requires the elimination of residual undifferentiated hPSCs in a mixed population. Thus, co-cultures of hPSC colonies and MEFs were treated for 15 h with 8 nM of unlabeled, IgG1-labeled (isotype control), and SSEA-5-labeled Qβ$(ZZ)_{42}$@$CD_{13}$ VLPs in the presence of 100 μM 5-FC, and 100 μM of 5-FU as a positive control. Subsequent staining with ethidium homodimer-1 (a specific red marker of dead cells) and a green fluorescent antibody against the hPSC-specific TRA-1-60 surface marker gave the results shown in **Figure 3G**. Negligible cell death was induced by unlabeled and isotype control-labeled Qβ$(ZZ)_{42}$@$CD_{13}$ VLPs in the presence of 5-FC; in these cases,

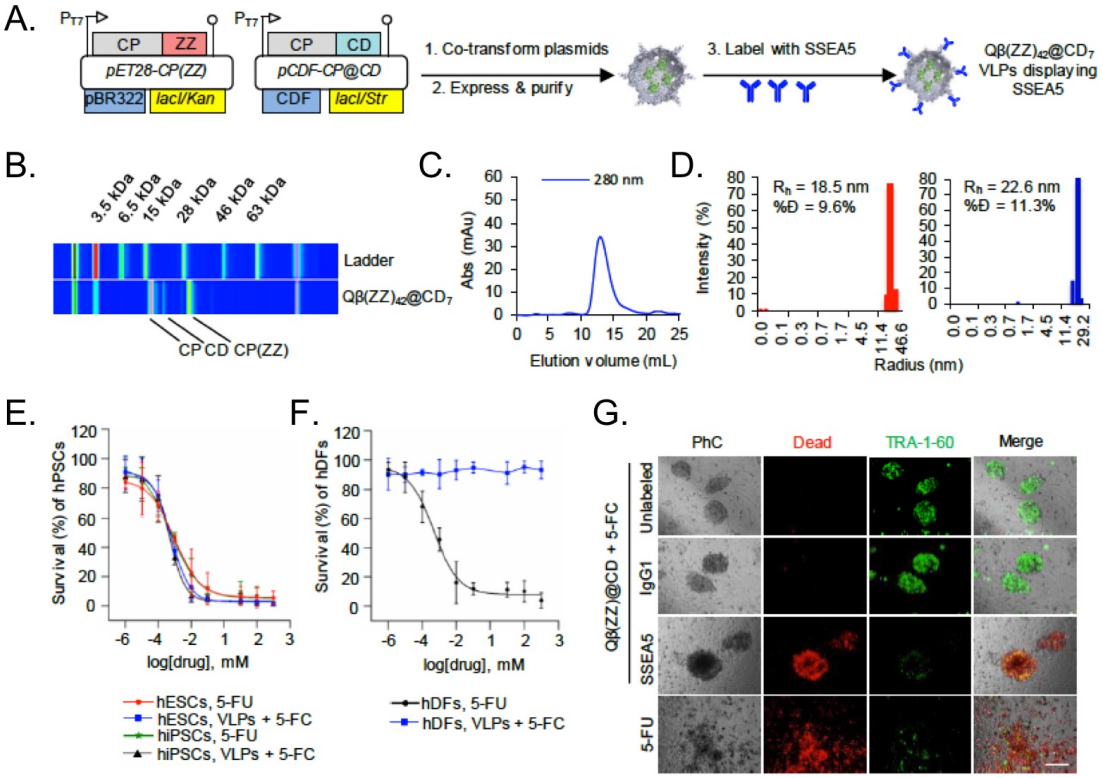


**Figure 3.** SSEA-5-labeled Qβ(ZZ)$_{42}$@CD$_{13}$ VLPs selectively kill hPSCs in the presence of 5-FC. (**A**) Schematic of Qβ(ZZ)$_{42}$@CD$_{13}$ viral coat protein expression and particle assembly, followed by VLP labeling with SSEA-5 antibodies. (**B**) Denaturing electrophoretic, (**C**) FPLC, and (**D**) dynamic light scattering analyses of Qβ(ZZ)$_{42}$@CD$_{13}$ VLPs. (%Đ = % dispersity; $R_h$ = hydrodynamic radius). (**E**) $EC_{50}$ curves showing dose-dependent decreases in human induced pluripotent stem cell (hiPSC) and human embryonic stem cell (hESC) survival after 24 h treatment with both 8 nM Qβ(ZZ)$_{42}$@CD$_{13}$+SSEA-5$_{21}$ VLPs in the presence of the prodrug 5-fluorocytosine (5-FC) or the cytotoxin 5-fluorouracil (5-FU). (**F**) $EC_{50}$ curves show dose-dependent decreases in human dermal fibroblast (hDF) survival percentages after 24 h treatment with 5-FU, but negligible cell death after treatment with 8 nM Qβ(ZZ)$_{42}$@CD$_{13}$+SSEA-5$_{21}$ VLPs in the presence of 5-FC. (**G**) Representative microscopy images show co-cultures of hPSC colonies and MEFs that were treated for 15 h with 8 nM of unlabeled, IgG1-labeled (isotype control), and SSEA-5-labeled Qβ(ZZ)$_{42}$@CD$_{13}$ VLPs in the presence of 100 µM 5-FC as test conditions, and 100 µM 5-FU as a positive control. Red fluorescence indicates dead cells and green fluorescence indicates expression of the pluripotent stem cell-specific TRA-1-60 marker.

hPSC colonies remained intact with bright, flat morphology and abundant TRA-1-60 expression. In contrast, hPSC colonies in co-cultures treated with Qβ$(ZZ)_{42}$@$CD_{13}$+SSEA-$5_{21}$ and 5-FC showed extensive ethidium staining, a dark, barely adherent, mounted morphology, and minimal detection of TRA-1-60, likely due to antibody binding to loose fragments of dead hPSC membranes. The surrounding MEFs were unaffected, demonstrating the specificity of VLP-mediated hPSC killing. Co-cultures treated with 5-FU exhibited indiscriminate cell death.

Currently it is still unclear what stages of hPSC-derived cardiomyocytes are most efficacious for therapeutic application. Clinical application of this methodology may require the killing of undifferentiated cells at an early stage to selectively eliminate residual hPSCs without affecting cardiomyocyte differentiation. To test this, such treatment (8 nM VLPs for 1 h + 100 μM 5-FC for 24 h) was performed at differentiation day 8 or 9 (**Figure 4A**). From initial $1x10^6$ cells seeded, at least 200-300 colonies with stem cell morphology and positive for the pluripotent stem cell marker TRA-1-60 were detected in cells expanded from progenitors treated with vehicle as a control. In contrast, no hPSC colonies were detected in otherwise identical cultures treated with the antibody-directed VLPs + prodrug (**Figure 4B**).

To examine if the treatment affected cardiomyocyte differentiation, we maintained the treated cells in RPMI/B27 medium, monitored cell morphology, and examined the expression of cardiomyocyte genes. At differentiation day 14, beating cardiomyocytes were observed in cultures derived from cells that were treated with either the VLPs or vehicle. Similar to cells derived from control cultures, the majority of the cells derived

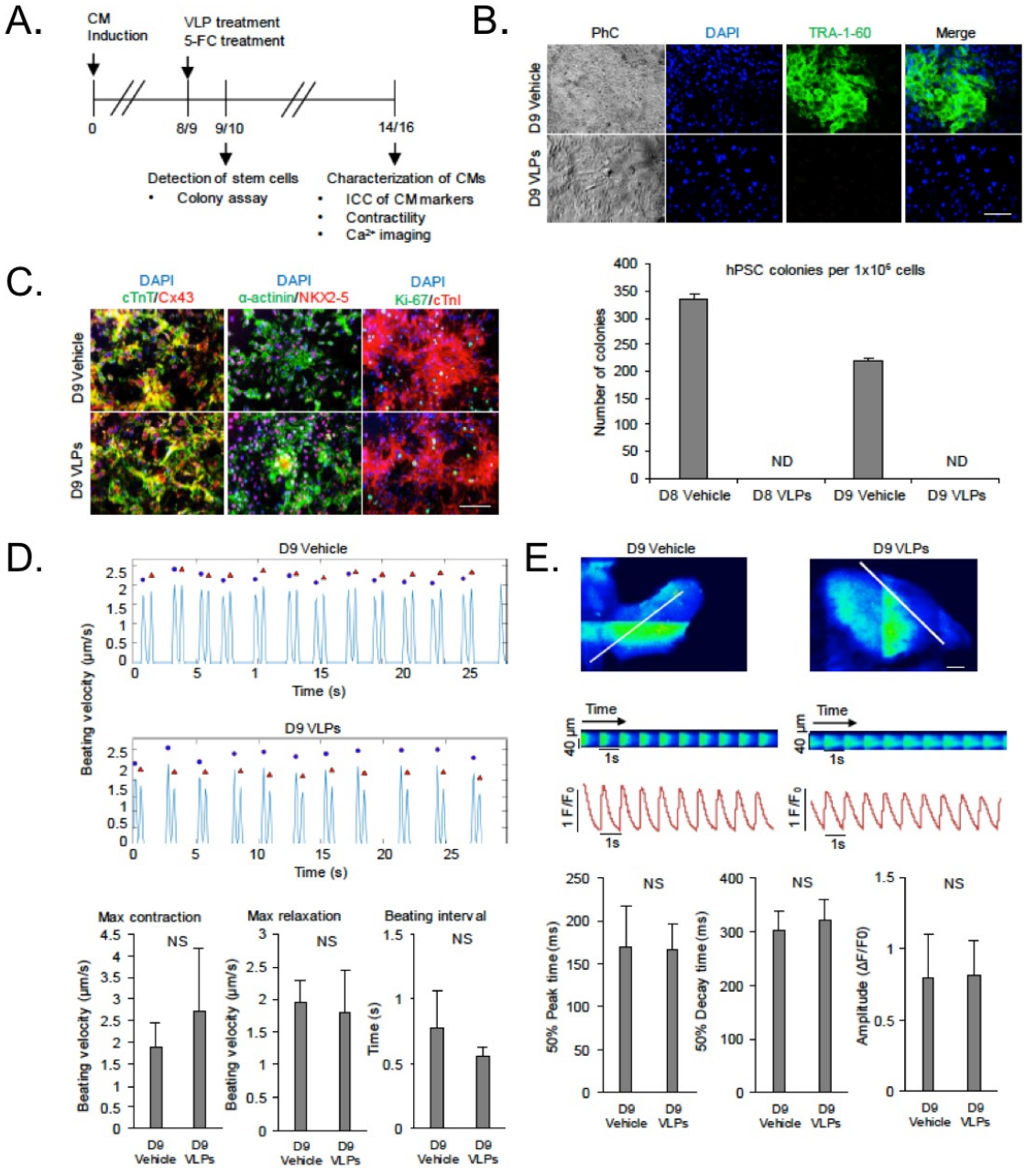


**Figure 4.** SSEA-5-labeled Qβ(ZZ)$_{42}$@CD$_{13}$ VLPs selectively kill residual hPSCs during CM differentiation in the presence of 5-FC. (**a**) Schematic of experimental design for treatments of cardiac progenitors with VLPs. (**b**) Colony assay for the detection of undifferentiated hPSCs. (top panels: blue, DAPI nuclear stain; green, TRA-1-60; scale bars = 100 μm). ND = not detected. (**c**) Expression of cardiomyocyte proteins. Scale bars = 100 μm. (**d**) Video-based analysis of contractility. Contraction parameters are presented as mean ± standard deviation of n=3 biological samples. (**e**) $Ca^{2+}$ transient analyses. Scale bars = 5 μm. $Ca^{2+}$ transient parameters are presented as mean ± standard deviation of n=20 cells. NS = no significant difference between groups (p value >0.05).

from the VLP-treated cultures were positive for cardiac transcription factor NKX2-5, gap junction protein connexin 43, and cardiac structural proteins including cardiac troponin I, cardiac troponin T and α-actinin as detected by immunocytochemistry (**Figure 4C**). In addition, these cells also expressed similar levels of Ki-67, a marker associated with cells at active phases of cell cycle (**Figure 4C**).

The contractility of cardiomyocytes derived from VLP-treated cultures was found to be indistinguishable from that of vehicle-treated control cultures by video-based analysis (**Figure 4D**), including maximum contraction, maximum relaxation, and beating intervals. Furthermore, intracellular $Ca^{2+}$ transients (observed with the aid of calcium indicator dye Fluo-4) of cardiomyocytes derived from VLP-treated cultures were also very similar in $Ca^{2+}$ transient amplitude, 50% peak time, and 50% decay time to those from control cultures (**Figure 4E**). These results suggest that the VLP-based elimination of residual hPSCs from early-stage differentiation cultures did not significantly affect cardiomyocyte differentiation.

To mimic a high level of residual hPSCs in a differentiation culture at the late stage, we co-cultured 1-5% undifferentiated hPSCs with late-stage cardiomyocyte differentiation culture from hPSCs, as commonly used to evaluate specific elimination of stem cells in a mixed population. The co-culture was treated with the prodrug-converting VLPs (8 nM) for 1 h and then with 5-FC (100 μM) for 24 h (**Figure 5A**). Immediately after these treatments or following further culture, the presence of hPSCs and cardiomyocytes was examined by staining with antibodies against markers for stem cells (TRA-1-60) and cardiomyocytes (α-actinin). As expected, TRA-1-60-positive hPSC colonies/cells were detectable in co-cultures treated with vehicle at all time points examined. The amount of

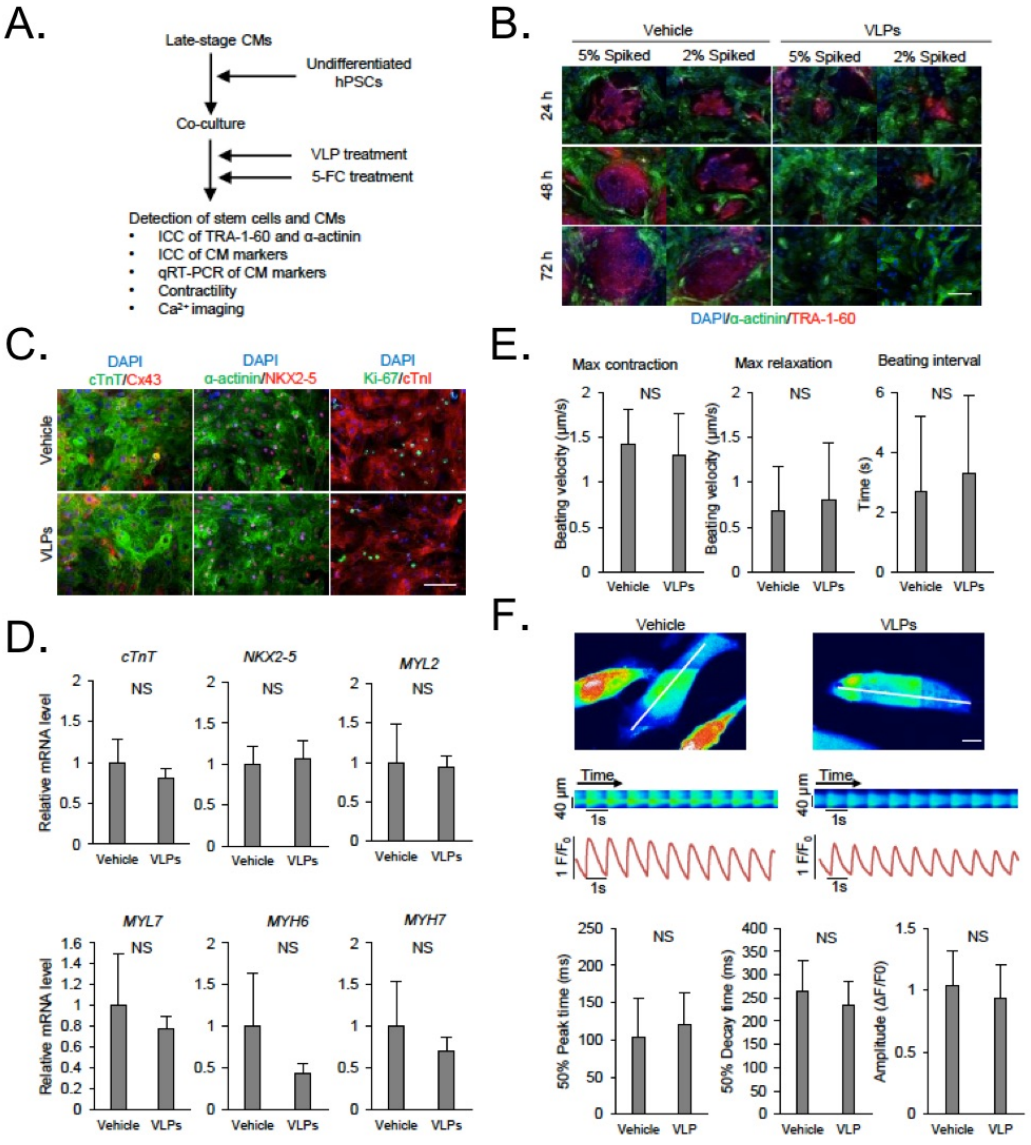


**Figure 5.** SSEA-5-labeled Qβ(ZZ)$_{42}$@CD$_{13}$ VLPs selectively kill hPSCs in co-cultures of hPSC and cardiomyocytes in the presence of 5-FC. (**A**) Schematic of experimental design for the VLP treatment for co-cultures of hPSCs and cardiomyocytes. (**B**) Detection of hPSCs and cardiomyocytes in co-cultures. hPSC-specific marker TRA-1-60 (red); cardiomyocyte-associated protein α-actinin (green). Scale bars = 100 μm. (**C**) Detection of cardiomyocyte proteins. Scale bars = 100 μm. (**D**) Detection of the expression of cardiomyocyte genes by qRT-PCR. Data are presented as mean ± standard deviation of n=3 biological samples. (**E**) Video-based analysis of contractility. Contraction parameters are presented as mean ± standard deviation of n=6 biological samples. (**F**) $Ca^{2+}$ transient analyses. Representative line-scan images show calcium transients in vehicle- and VLP-treated cells in co-cultures from the area indicated by the white lines. Scale bars = 5 μm. $Ca^{2+}$ transient parameters are presented as mean ± standard deviation of n=22 cells. NS = no significant difference between groups (p value>0.05).

TRA-1-60 positive cells decreased overtime in the VLP-treated cultures, and the signal for TRA-1-60 was undetectable 3 days after the VLP treatment (**Figure 5B**). In contrast, the signal for α-actinin was detectable in the majority of TRA-1-60 negative cells in all cultures and was comparable in the vehicle- and VLP-treated cultures (**Figure 5B**). These results suggest that the VLP treatment can specifically eliminate undifferentiated hPSCs in the mixture.

To determine if the VLP + prodrug treatment affected molecular and functional properties of cardiomyocytes, the expression of cardiomyocyte genes, cardiomyocyte contractility and intracellular $Ca^{2+}$ transients were examined after the co-cultures were treated with vehicle or VLP + 5-FC. In both vehicle- and VLP-treated co-cultures, beating cells were observed, which expressed cardiomyocyte transcription factor NKX2-5, connexin 43, cardiac troponin I, cardiac troponin T, α-actinin, and proliferation marker Ki-67 to similar extents (**Figure 5C**). In addition, the expression levels of genes associated with cardiomyocytes (*cTnT*, *NKX2-5*, *MYH6*, *MYH7*, *MYL2* and *MYL7*) were comparable between the vehicle- and VLP-treated samples (**Figure 5D**). Measurements of cardiac contractility were also similar between vehicle- and VLP-treated cells with no significant differences observed in maximum contraction, maximum relaxation, and beating interval as analyzed by a video-based method (**Figure 5E**). Key parameters of intracellular $Ca^{2+}$ transient recordings were similar between vehicle- and VLP-treated cells (**Figure 5F**). These results suggest that the VLP treatment does not alter molecular and functional characteristics of hPSC-derived cardiomyocytes.

*3.4.2. Antibody-guided targeting of HER2+ cancers*

Given the high selectivity and efficacy of the Qβ(ZZ) platform at targeting hPSCs, we sought to further expand the utility of this technology by directing cytotoxic activity against cancer cell populations expressing ErbB2/HER2. $Q\beta(ZZ)_{32}$(Alexa Fluor 488)$_{20}$ + anti-ErbB2/HER2$_{16}$, $Q\beta(ZZ)_{32}$(Alexa Fluor 488)$_{20}$ + isotype control, and $Q\beta(ZZ)_{32}$(Alexa Fluor 488)$_{20}$ particles were incubated (10 nM, 4°C) with MDA-MB-435 (melanoma), HT-29 (colorectal), and MDA-MB-231 (breast) carcinoma cells, respectively. HEK-293 (kidney) cells were treated as a negative control line in the same manner . After 2 hours, specific staining was observed for all cancer cell lines screened by flow cytometry, but no staining was observed for HEK-293 cells (**Figure 6A-D**). Interestingly, staining correlated with the reported levels of ErbB2/HER2 expression in each cell line. MDA-MB-435 and HT-29 cell lines have both been reported to express high levels of ErbB2/HER2 on their surface,[44,45] and these cell lines both showed the highest level of staining by VLPs displaying anti-ErbB2/HER2 antibodies, with MDA-MB-435 showing the highest signal over background (**Figure 6A,B**). MDA-MB-231 cells have been consistently reported as a HER2-negative cell line;[44] however, there are also reports in the literature showing moderate surface expression of HER2.[46,47] Consistent with these observations, MDA-MB-231 cells displayed significantly lower staining by $Q\beta(ZZ)_{32}$(Alexa Fluor 488)$_{20}$ + anti-ErbB2/HER2$_{16}$ that was only slightly above background (**Figure 6C**). HEK-293 cells displayed no significant binding over background (**Figure 6D**). In all cases, unlabeled VLPs or VLPs labeled with an isotype control antibody showed levels of non-specific binding that varied among cell lines.

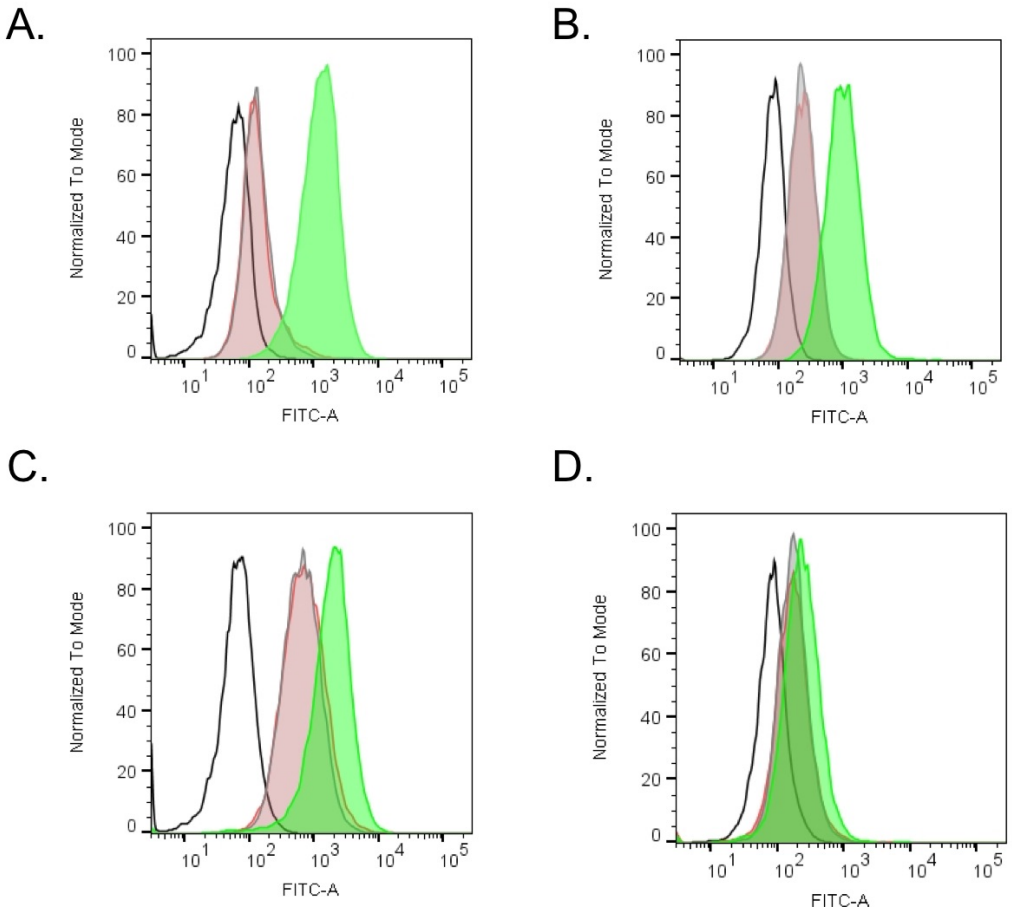


**Figure 6.** Flow cytometry histograms illustrating binding of Qβ$(ZZ)_{32}$(Alexa Fluor 488)$_{20}$ + anti-ErbB2/HER2$_{16}$ to cells expressing HER2. **(A)** MDA-MB-435, **(B)** HT-29, **(C)** MDA-MB-231, and **(D)** HEK-293 cells were all incubated for 2 h at 4°C under the following treatments: Qβ$(ZZ)_{32}$(Alexa Fluor 488)$_{20}$ + anti-ErbB2/HER2$_{16}$ (green), Qβ$(ZZ)_{32}$(Alexa Fluor 488)$_{20}$ + isotype control (grey), Qβ$(ZZ)_{32}$(Alexa Fluor 488)$_{20}$ (red), or DMEM (open). Total particle concentration was 10 nM for all treated cells. Histograms representative of two replicate experiments.

Specific binding was also confirmed by fluorescence microscopy, which showed staining of MDA-MB-435 and HT-29 cells and virtually no detectable fluorescence in HEK-293 cells **(Figure 7)**. Furthermore, the particles primarily appear to localize to the membrane of the target cell populations, although internalization of VLPs may occur with cells cultured at physiological temperatures.

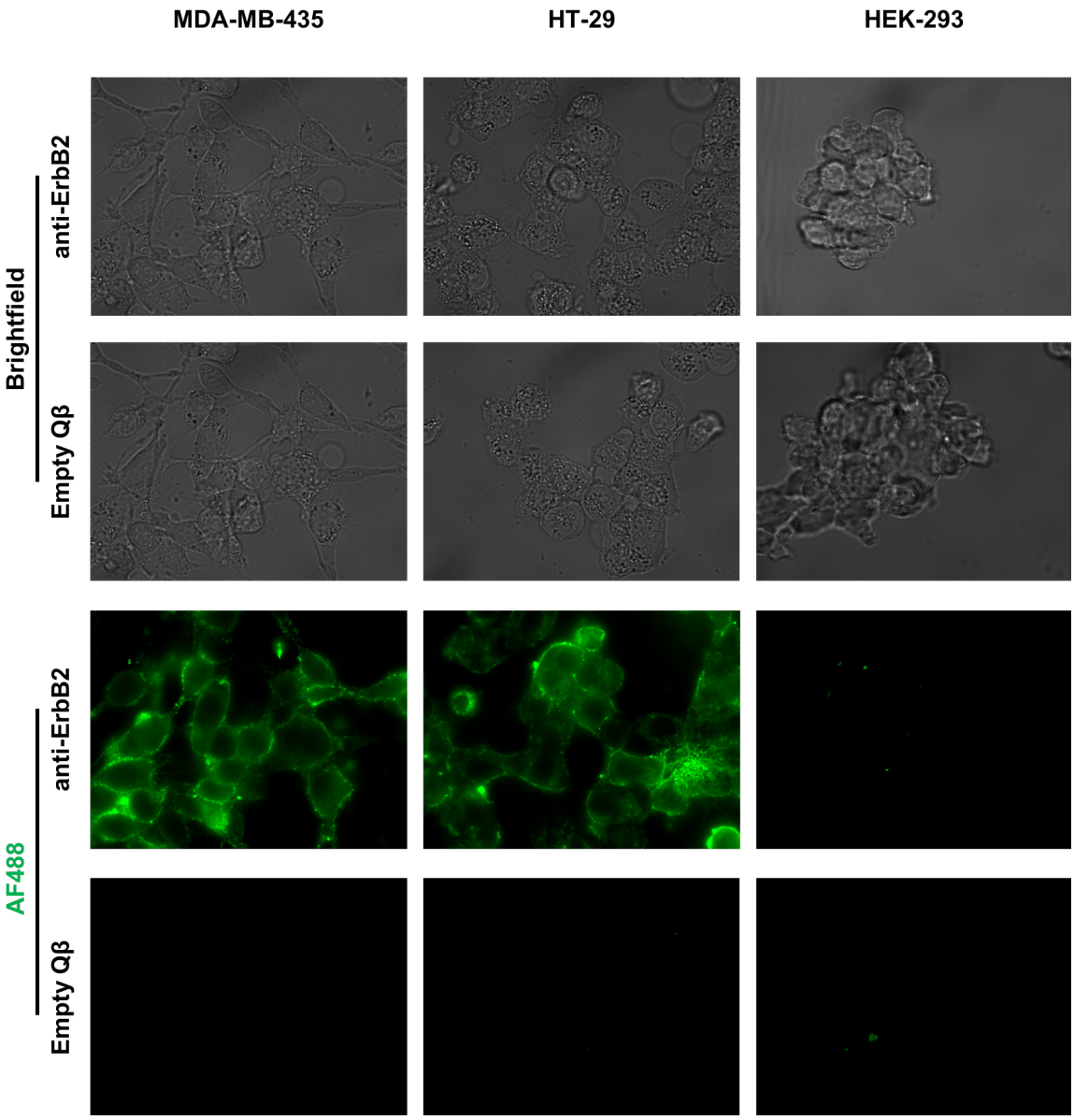


**Figure 7.** Analysis of cellular targeting by fluorescence microscopy. MDA-MB-435, HT-29, and HEK-293 cells were incubated with either 10 nM Qβ$(ZZ)_{32}$(Alexa Fluor 488)$_{20}$ + anti-ErbB2/HER2$_{16}$ (upper panels) or 10 nM Qβ$(ZZ)_{32}$(Alexa Fluor 488)$_{20}$ (lower panels) for 2 h at 4°C. Brightfield images are shown in the first two rows; corresponding fluorescence images are shown in the bottom two rows. Threshold for fluorescence images were set against background from Qβ$(ZZ)_{32}$(Alexa Fluor 488)$_{20}$ staining in ImageJ software.

Finally, we investigated if these particles could effectively mediate conversion of 5-FC to induce selective cell death in the same manner as was used in the removal of hPSCs earlier in this chapter. MDA-MB-435 cells were treated with Qβ$(ZZ)_{42}$@$CD_{13}$ particles (5 nM, 37°C) for 1 hour and subsequently dosed with increasing concentrations of 5-FC (1-100 μM). There was no observed cytotoxicity for cells treated with untargeted VLPs, suggesting that the non-specific binding of particles observed with flow cytometry is negligible and does not impact the specificity of this treatment. Particles bearing the anti-ErbB2/HER2 antibody induced noticeable levels of cytotoxicity with increasing dosing of the prodrug 5-FC; furthermore, the degree of cell death was comparable to that observed with comparable dosing of 5-FU, suggesting the targeted particles are efficiently converting the administered prodrug to the toxic product **(Figure 8)**. These preliminary studies suggest that this platform may serve as a viable method for selectively targeting cancers overexpressing HER2 or other membrane-bound markers.

### 3.5. Conclusions

In summary, we found that the genetic display of antibody-binding Z-domains on the surface of virus-like particles allowed for the generation of a modular platform for therapeutic delivery that was highly efficient and selective for the target cell population. The marriage of genetic engineering to mediate antibody display on the particle surface with the ability to encapsulate prodrug-converting enzymes on the interior provided for a powerful therapeutic platform that can be applied in numerous contexts. Our initial proof-of-concept study focused on the elimination of residual pluripotent stem cells in cardiomyocyte differentiation cultures.

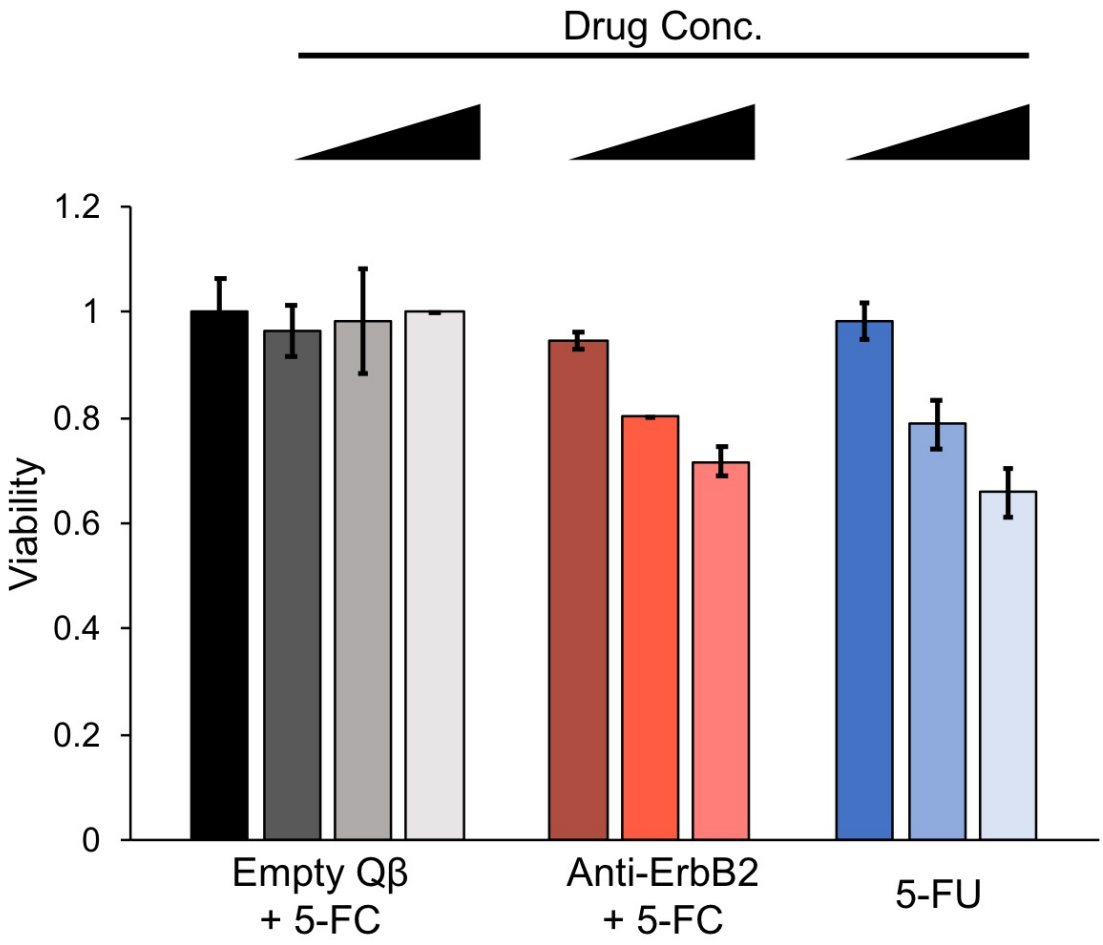


**Figure 8.** Anti-ErbB2/HER2-labeled VLPs selectively target and kill cancer cells expressing HER2 in an antibody-dependent fashion. MDA-MB-435 cells were treated with 5 nM Qβ$(ZZ)_{42}$@$CD_{13}$ + anti-ErbB2/$HER2_{21}$ or 5 nM Qβ$(ZZ)_{42}$@$CD_{13}$ for 1 h, followed by incubation with 1, 10, or 100 μM 5-FC for 24 h. As a control, cells were separately treated with the same doses of 5-FU. Viability of cells was assessed by MTT assay following treatments and absorbance was related to that of untreated cells (black bar; left) to calculate cell viability.

Overall, VLPs encapsulating prodrug-converting enzymes were able to selectively kill tumorigenic stem cells in mixed differentiation cultures without harming surrounding fibroblast cells. Operationally, this method for the targeted elimination of stem cells is simple to perform, requiring no gene transfection or editing and only a simple medium change. The resulting stem cell-derived cardiomyocytes were seemingly unaffected by

this treatment, rendering it an interesting possibility for improving the safety of stem cell-based therapies. We extended the potential applications of this platform by substituting the targeting antibody on the particle surface to direct VLPs against cancer cells expressing HER2. Similar levels of selective targeting were observed against cells displaying moderate-to-high levels of HER2, demonstrating the modular utility of this platform in its ability to be directed against different cell populations by simple exchange of the targeting antibody. Furthermore, these particles mediated selective killing of cancer cells expressing HER2, thereby demonstrating the potential utility of this technology in multiple clinical settings.

The technology developed in this chapter has broad applications in the realm of targeted therapeutics. This platform benefits from the selectivity of the displayed antibody while concurrently raising the associated level of safety by linking the toxic payload to enzymatic conversion. The combination of cytotoxic efficiency and selectivity in this system derives from the production of only small amounts of toxic molecule overall, yet high enough concentrations at the target cells by virtue of localized delivery and enzymatic turnover to mediate cytotoxicity. In addition, the VLP protects the cargo enzymes from degradation by proteases and other factors, and the particles can be produced easily and at large scale. The work presented here highlights the similarities in VLP construct design to generate materials for diverse functional applications.

### 3.6. References

(1) Strebhardt, K.; Ullrich, A. Paul Ehrlich's Magic Bullet Concept: 100 Years of Progress. *Nat. Rev. Cancer* **2008**, *8*, 473–480.

(2) Chari, R. V. J. Targeted Delivery of Chemotherapeutics: Tumor-Activated Prodrug Therapy. *Adv. Drug Deliv. Rev.* **1998**, *31*, 89–104.

(3) Hamblett, K. J.; Senter, P. D.; Chace, D. F.; Sun, M. M. C.; Lenox, J.; Cerveny, C. G.; Kissler, K. M.; Bernhardt, S. X.; Kopcha, A. K.; Zabinski, R. F.; *et al.* Effects of Drug Loading on the Antitumor Activity of a Monoclonal Antibody Drug Conjugate. *Clin. Cancer Res.* **2004**, *10*, 7063.

(4) Zhang, K. E.; Rossin, R.; Hagooly, A.; Chen, Z.; Welch, M. J.; Wooley, K. L. Folate-Mediated Cell Uptake of Shell-Crosslinked Spheres and Cylinders. *J. Polym. Sci. Part A Polym. Chem.* **2008**, *46*, 7578–7583.

(5) Vachutinsky, Y.; Oba, M.; Miyata, K.; Hiki, S.; Kano, M. R.; Nishiyama, N.; Koyama, H.; Miyazono, K.; Kataoka, K. Antiangiogenic Gene Therapy of Experimental Pancreatic Tumor by sFlt-1 Plasmid DNA Carried by RGD-Modified Crosslinked Polyplex Micelles. *J. Control. Release* **2011**, *149*, 51–57.

(6) Chattopadhyay, N.; Cai, Z.; Pignol, J.-P.; Keller, B.; Lechtman, E.; Bendayan, R.; Reilly, R. M. Design and Characterization of HER-2-Targeted Gold Nanoparticles for Enhanced X-Radiation Treatment of Locally Advanced Breast Cancer. *Mol. Pharm.* **2010**, *7*, 2194–2206.

(7) ElSohly, A. M.; Netirojjanakul, C.; Aanei, I. L.; Jager, A.; Bendall, S. C.; Farkas, M. E.; Nolan, G. P.; Francis, M. B. Synthetically Modified Viral Capsids as Versatile Carriers for Use in Antibody-Based Cell Targeting. *Bioconjug. Chem.* **2015**, *26*, 1590–1596.

(8) Aanei, I. L.; ElSohly, A. M.; Farkas, M. E.; Netirojjanakul, C.; Regan, M.; Taylor Murphy, S.; O'Neil, J. P.; Seo, Y.; Francis, M. B. Biodistribution of Antibody-MS2 Viral Capsid Conjugates in Breast Cancer Models. *Mol. Pharm.* **2016**, *13*, 3764–3772.

(9) Kickhoefer, V. A.; Han, M.; Raval-Fernandes, S.; Poderycki, M. J.; Moniz, R. J.; Vaccari, D.; Silvestry, M.; Stewart, P. L.; Kelly, K. A.; Rome, L. H. Targeting Vault Nanoparticles to Specific Cell Surface Receptors. *ACS Nano* **2009**, *3*, 27–36.

(10) Brown, S. D.; Fiedler, J. D.; Finn, M. G. Assembly of Hybrid Bacteriophage Q-Beta Virus-Like Particles. *Biochemistry* **2009**, *47*, 11155–11157.

(11) Fiedler, J. D.; Brown, S. D.; Lau, J.; Finn, M. G. RNA-Directed Packaging of Enzymes within Virus-Like Particles. *Angew. Chemie Int. Ed.* **2010**, *49*, 9648–9651.

(12) Rhee, J.-K.; Hovlid, M. L.; Fiedler, J. D.; Brown, S. D.; Manzenrieder, F.; Kitagishi, H.; Nycholat, C.; Paulson, J. C.; Finn, M. G. Colorful Virus-like Particles: Fluorescent Protein Packaging by the QB Capsid. *Biomacromolecules* **2011**, *12*, 3977–3981.

(13) Nilsson, B.; Moks, T.; Jansson, B.; Abrahmsen, L.; Elmblad, A.; Holmgren, E.;

Henrichson, C.; Jones, T. A.; Uhlen, M. A Synthetic IgG-Binding Domain Based on Staphylococcal Protein A. *Protein Eng.* **1987**, *1*, 107–113.

(14) Gauthier, M.; Maury, Y.; Peschanski, M.; Martinat, C. Human Pluripotent Stem Cells for Genetic Disease Modeling and Drug Screening. *Regen. Med.* **2011**, *6*, 607–622.

(15) Rajamohan, D.; Matsa, E.; Kalra, S.; Crutchley, J.; Patel, A.; George, V.; Denning, C. Current Status of Drug Screening and Disease Modelling in Human Pluripotent Stem Cells. *BioEssays* **2013**, *35*, 281–298.

(16) Bajada, S.; Mazakova, I.; Richardson, J. B.; Ashammakhi, N. Updates on Stem Cells and Their Applications in Regenerative Medicine. *J Tissue Eng Regen Med* **2008**, *2*, 169–183.

(17) Christou, Y. A.; Moore, H. D.; Shaw, P. J.; Monk, P. N. Embryonic Stem Cells and Prospects for Their Use in Regenerative Medicine Approaches to Motor Neurone Disease. *Neuropathology and Applied Neurobiology*, 2007, *33*, 485–498.

(18) Tabar, V.; Studer, L. Pluripotent Stem Cells in Regenerative Medicine: Challenges and Recent Progress. *Nat Rev Genet* **2014**, *15*.

(19) Malecki, M. "Above All, Do No Harm": Safeguarding Pluripotent Stem Cell Therapy against Iatrogenic Tumorigenesis. *Stem Cell Res. Ther.* **2014**, *5*, 73.

(20) Malecki, M.; LaVanne, C.; Alhambra, D.; Dodivenaka, C. Safeguarding Stem Cell-Based Regenerative Therapy against Iatrogenic Cancerogenesis: Transgenic Expression of DNASE1, DNASE1L3, DNASE2, DFFB Controlled by POLA1 Promoter in Proliferating and Differentiation Resisting Human Autologous Pluripotent Induced S. *J Stem Cell Res Ther.* **2013**, *9*.

(21) Lee, M. O.; Moon, S. H.; Jeong, H. C.; Yi, J. Y.; Lee, T. H.; Him, S. H.; Rhee, Y. H.; Lee, S. H.; Oh, S. J.; Lee, M. Y.; *et al.* Inhibition of Pluripotent Stem Cell-Derived Teratoma Formation by Small Molecules. *Proc Natl Acad Sci U S A* **2014**, *110*.

(22) Li, W.; Xiang, A. P. Safeguarding Clinical Translation of Pluripotent Stem Cells with Suicide Genes. *Organogenesis* **2013**, *9*.

(23) Schuldiner, M.; Itskovitz-Eldor, J.; Benvenisty, N. Selective Ablation of Human Embryonic Stem Cells Expressing a "Suicide" Gene. *Stem Cells* **2003**, *21*.

(24) Hara, A.; Aoki, H.; Taguchi, A.; Niwa, M.; Yamada, Y.; Kunisada, T.; Mori, H. Neuron-like Differentiation and Selective Ablation of Undifferentiated Embryonic Stem Cells Containing Suicide Gene with Oct-4 Promoter. *Stem Cells Dev* **2008**, *17*.

(25) Chen, F.; Cai, B.; Gao, Y.; Yuan, X.; Cheng, F.; Wang, T.; Jiang, M.; Zhou, Y.; Lahn, B. T.; Li, W.; *et al.* Suicide Gene-Mediated Ablation of Tumor-Initiating Mouse Pluripotent Stem Cells. *Biomaterials* **2013**, *34*.

(26) Wu, C.; Hong, S. G.; Winkler, T.; Spencer, D. M.; Jares, A.; Ichwan, B.; Nicolae, A.; Guo, V.; Larochelle, A.; Dunbar, C. E. Development of an Inducible Caspase-9 Safety Switch for Pluripotent Stem Cell–based Therapies. *Mol. Ther. - Methods Clin. Dev.* **2014**, *1*, 14053.

(27) Zhong, B.; Watts, K. L.; Gori, J. L.; Wohlfahrt, M. E.; Enssle, J.; Adair, J. E.; Kiem, H. P. Safeguarding Nonhuman Primate iPS Cells with Suicide Genes. *Mol. Ther.* **2011**, *19*, 1667–1675.

(28) Sanna, V.; Pala, N.; Sechi, M. Targeted Therapy Using Nanotechnology: Focus on Cancer. *International Journal of Nanomedicine*, 2014, *9*, 467–483.

(29) Boku, N. HER2-Positive Gastric Cancer. *Gastric Cancer*, 2014, *17*, 1–12.

(30) Slamon, D. Use of Chemotherapy Plus a Monoclonal Antibody Against Her2 for Metastatic Breast Cancer That Overexpesses HER2. *N Engl J Med* **2001**, *344*, 783–792.

(31) Teplinsky, E.; Muggia, F. Targeting HER2 in Ovarian and Uterine Cancers: Challenges and Future Directions. *Gynecol. Oncol.* **2014**, *135*, 364–370.

(32) Pokorski, J. K.; Hovlid, M. L.; Finn, M. G. Cell Targeting with Hybrid Qb Virus-Like Particles Displaying Epidermal Growth Factor. *ChemBioChem* **2011**, *12*, 2441–2447.

(33) Yu, J.; Vodyanik, M. A.; Smuga-Otto, K.; Antosiewicz-Bourget, J.; Frane, J. L.; Tian, S.; Nie, J.; Jonsdottir, G. A.; Ruotti, V.; Stewart, R.; *et al.* Induced Pluripotent Stem Cell Lines Derived from Human Somatic Cells. *Science (80-. ).* **2007**, *318*, 1917–1920.

(34) Thomson, J. A.; Itskovitz-eldor, J.; Shapiro, S. S.; Waknitz, M. A.; Swiergiel, J. J.; Marshall, V. S.; Jones, J. M. Embryonic Stem Cell Lines Derived from Human Blastocysts. *Science (80-. ).* **1998**, *282*, 1145–1147.

(35) Xu, C.; Inokuma, M. S.; Denham, J.; Golds, K.; Kundu, P.; Gold, J. D.; Carpenter, M. K. Feeder-Free Growth of Undifferentiated Human Embryonic Stem Cells. *Nat. Biotechnol.* **2001**, *19*, 971–974.

(36) Laflamme, M. A.; Chen, K. Y.; Naumova, A. V.; Muskheli, V.; Fugate, J. A.; Dupras, S. K.; Reinecke, H.; Xu, C.; Hassanipour, M.; Police, S.; *et al.* Cardiomyocytes Derived from Human Embryonic Stem Cells in pro-Survival

Factors Enhance Function of Infarcted Rat Hearts. *Nat. Biotechnol.* **2007**, *25*, 1015–1024.

(37) Jha, R.; Xu, R.-H.; Xu, C. Efficient Differentiation of Cardiomyocytes from Human Pluripotent Stem Cells with Growth Factors. *Methods Mol. Biol.* **2015**, *1299*, 115–131.

(38) Nguyen, D. C.; Hookway, T. A.; Wu, Q.; Jha, R.; Preininger, M. K.; Chen, X.; Easley, C. A.; Spearman, P.; Deshpande, S. R.; Maher, K.; *et al.* Microscale Generation of Cardiospheres Promotes Robust Enrichment of Cardiomyocytes Derived from Human Pluripotent Stem Cells. *Stem Cell Reports* **2014**, *3*, 260–268.

(39) Preininger, M. K.; Jha, R.; Maxwell, J. T.; Wu, Q.; Singh, M.; Wang, B.; Dalal, A.; Mceachin, Z. T.; Rossoll, W.; Hales, C. M.; *et al.* A Human Pluripotent Stem Cell Model of Catecholaminergic Polymorphic Ventricular Tachycardia Recapitulates Patient-Specific Drug Responses. *Dis. Model. Mech.* **2016**, *9*, 927–939.

(40) Jha, R.; Wu, Q.; Singh, M.; Preininger, M. K.; Han, P.; Ding, G.; Cho, H. C.; Jo, H.; Maher, K. O.; Wagner, M. B.; *et al.* Simulated Microgravity and 3D Culture Enhance Induction, Viability, Proliferation and Differentiation of Cardiac Progenitors from Human Pluripotent Stem Cells. *Sci. Rep.* **2016**, *6*.

(41) Huebsch, N.; Loskill, P.; Mandegar, M. A.; Marks, N. C.; Sheehan, A. S.; Ma, Z.; Mathur, A.; Nguyen, T. N.; Yoo, J. C.; Judge, L. M.; *et al.* Automated Video-Based Analysis of Contractility and Calcium Flux in Human-Induced Pluripotent Stem Cell-Derived Cardiomyocytes Cultured over Different Spatial Scales. *Tissue Eng. Part C Methods* **2015**, *21*, 467–479.

(42) Tang, C.; Lee, A. S.; Volkmer, J. P.; Sahoo, D.; Nag, D.; Mosley, A. R.; Inlay, M. A.; Ardehali, R.; Chavez, S. L.; Pera, R. R.; *et al.* An Antibody against SSEA-5 Glycan on Human Pluripotent Stem Cells Enables Removal of Teratoma-Forming Cells. *Nat Biotechnol* **2011**, *29*.

(43) Korkegian, A.; Black, M. E.; Baker, D.; Stoddard, B. L. Computational Thermostabilization of an Enzyme. *Science (80-. ).* **2005**, *308*, 857–860.

(44) Subik, K.; Lee, J. F.; Baxter, L.; Strzepek, T.; Costello, D.; Crowley, P.; Xing, L.; Hung, M. C.; Bonfiglio, T.; Hicks, D. G.; *et al.* The Expression Patterns of ER, PR, HER2, CK5/6, EGFR, KI-67 and AR by Immunohistochemical Analysis in Breast Cancer Cell Lines. *Breast Cancer Basic Clin. Res.* **2010**, *4*, 35–41.

(45) Li, S.; Buchbinder, E.; Wu, L.; Bjorge, J. D.; Fujita, D. J.; Zhu, S. EGFR and HER2 Levels Are Frequently Elevated in Colon Cancer Cells. *Discov. Reports* **2014**, *1*, 1–8.

(46) Hathaway, H. J.; Butler, K. S.; Adolphi, N. L.; Lovato, D. M.; Belfon, R.; Fegan,

D.; Monson, T. C.; Trujillo, J. E.; Tessier, T. E.; Bryant, H. C.; *et al.* Detection of Breast Cancer Cells Using Targeted Magnetic Nanoparticles and Ultra-Sensitive Magnetic Field Sensors. *Breast Cancer Res.* **2011**, *13*, R108–R108.

(47) Raab, S.; Steinbacher, J.; Schmiedel, B. J.; Kousis, P. C.; Steinle, A.; Jung, G.; Grosse-Hovest, L.; Salih, H. R. Fc-Optimized NKG2D–Fc Constructs Induce NK Cell Antibody-Dependent Cellular Cytotoxicity against Breast Cancer Cells Independently of HER2/neu Expression Status. *J. Immunol.* **2014**, *193*, 4261–4272.

# Chapter 4: Chemical modification of Qβ VLPs to alter trafficking

## 4.1. Abstract

The lungs are an organ where macrophages (MΦ) are present in high abundance in order to intercept invading microorganisms that gain access through the mucosal surfaces of the airways. Several bacterial pathogens have evolved the capacity to evade the innate immune response by establishing infections within pulmonary MΦ upon phagocytosis, leading to prolonged disease that can be fatal if left untreated. These infections are often difficult to control as the compounds administered for treatment do not accumulate within the infected cells at therapeutically relevant concentrations. Macrolide antibiotics, such as azithromycin and clarithromycin, are well-known to accumulate in phagocytic cells and have been shown to preferentially distribute in tissues where these populations of cells reside. In this study, we employed this class of molecules as targeting ligands to direct a virus-like particle (VLP) platform to lung-resident MΦ as a proof-of-concept for the development of an intracellular drug delivery vehicle. We first prepared a series of VLP-macrolide conjugates and assessed their uptake in RAW 264.7 MΦ cells. Enhanced uptake was observed for all conjugates tested relative to particles without macrolide, with azithromycin displaying the greatest effect; distinct differences in uptake were also observed depending on the macrocycle structure and orientation on the particle surface. Activation of MΦ cells was stimulated by particle uptake and biased towards an M2b phenotype. We next investigated the ability of azithromycin to direct VLPs to the lungs in mice, and VLPs were found to significantly accumulate in the lungs within 2 hours. The results of this study indicate that this new

class of bioconjugate could serve as an effective platform for intracellular drug delivery in the context of pulmonary infections.

### 4.2. Introduction

As evidenced in the previous chapter, genetic engineering of virus-like particle (VLP) platforms offers a powerful methodology for developing targeted therapeutics; however, chemical modification represents an equally promising strategy for materials development. While antibodies offer highly selective targeting capabilities, their target repertoire is not all-encompassing. Although it is possible to generate antibodies against any number of specific targets through protein engineering or focused immunological design,[1,2] many cell types do not possess protein or glycan surface signatures that are wholly unique from other cells. When considering that a specific protein or glycan target needs to be recognized in its native conformation for successful antibody targeting, the selection of reagents may become even more limited.[3] In this sense, small molecule conjugations may provide a useful alternative should an antibody target be unavailable to mediate therapeutic delivery.

The display of small molecules on the surface of nanoparticles has been explored previously for applications to mediate cell uptake and targeting. Manchester and colleagues specifically studied the derivatization of cowpea mosaic virus (CPMV) with folic acid and subsequent targeting of tumors bearing the folate receptor, which is frequently upregulated in various cancers.[4] Other small molecules that bind specifically to the extracellular domains of cancer-related proteins have been employed in similar fashion. Anisamide-conjugated liposomes have been explored for the delivery of doxorubicin to human prostate cancer cells overexpressing sigma receptors.[5]

Carbohydrates can also serve as effective targeting ligands, although increased valency of the targeting species is often required as individual ligand-receptor interactions are too weak to stimulate effective responses. Efficient and selective delivery to the liver was achieved using a bicyclic derivative of galactosamine to target the asialoglycoprotein receptor (ASGPR) on hepatocytes but required the use of di- or tri-valent analogues to achieve efficient cargo uptake.[6] The polyvalent display of mannose-based ligands has also been used to target DC-SIGN, a C-type lectin receptor preferentially expressed on dendritic cells, to direct the enhanced uptake of vaccine nanoparticles.[7] As evidenced, small molecules can be employed to direct the targeting and trafficking of nanoparticles to various tissues and cell types; the work discussed in this chapter will focus on the chemical functionalization of VLPs for selective delivery to macrophages.

Macrophages are an incredibly versatile class of immune cells that are distributed throughout the body and perform critical roles in preventing infection and disease, and they are largely localized to tissues where infection or accumulation of foreign particles is most likely to occur.[8] The lungs are one such locale whereby inhaled pathogens can gain direct access for establishing an infection, and macrophages play a critical role in mediating immune responses to prevent this occurrence.[9,10] Numerous intracellular pathogens, such as *Mycobacterium tuberculosis*[11] and *Legionella pneumophila*,[12] usurp the phagocytic activity of macrophages and use the cells as an established breeding ground for prolonged infection.[13] These types of infections are often difficult to treat as administered drugs do not accumulate in macrophages at therapeutic levels;[14] however,

advances in nanotechnology now allow for the controlled design and preparation of targeted drug delivery vehicles for addressing specific cell populations.[14,15]

Virus-like particles are a class of nanomaterials that provide robust utility, as evidenced by their applications in materials science[16,17] and medicine.[18,19] VLPs are often highly stable towards extremes of temperature,[20,21] pH,[20] and solvent composition,[22] making them amenable to a wide variety of chemical modifications while retaining the biocompatibility of a protein. Indeed, previous studies have explored the attachment of glycans,[23] peptides,[24] and polymers[25] to the surface of VLPs for applications in cellular targeting. VLPs have also been shown to be amenable to modifications on the interior of the capsid for the encapsulation of proteins[26] and therapeutic small molecules,[27] further demonstrating their capacity as a platform for drug delivery.

Certain macrolide antibiotics, such as azithromycin and clarithromycin, have been shown to accumulate extensively within lung and liver tissues, leading to more than 100-fold enrichment in these tissues relative to the bloodstream.[28–30] The ability of these molecules to gain entry into phagocytic cells is causal to this effect, but the mechanism that mediates macrolide uptake is still uncertain. Current studies suggest macrolides may engage the mannose receptor, which is ubiquitously expressed on macrophages; however, there is evidence that an uncharacterized active transport system for macrolides may also exist.[31]

Polyvalent display of azithromycin and clarithromycin on gold nanorods was previously shown to promote enhanced uptake in RAW 264.7 macrophages for application as nanotherapeutics in cancer therapy, indicating that these macrocycles can influence the trafficking of nanoscale constructs.[32] Dreaden and coworkers showed that

macrolide-functionalized gold nanorods induced a cytotoxic phenotype in macrophages capable of eliminating cancer cells in co-culture even in the absence of irradiation. This study did not investigate the cytokine profiles associated with the observed phenotype, albeit numerous studies have previously shown that gold nanostructures stimulate inflammatory cytokine production in macrophages.[33,34] In the work presented here, we have further explored the use of macrolide antibiotics as targeting ligands by conjugation to the surface of VLPs derived from the bacteriophage Qβ, a 28-nm icosahedral virus that has been previously studied as a vehicle for drug delivery.[19,35] A series of Qβ conjugates (**3-9**) displaying different macrocycles was prepared, and the uptake of these conjugates in RAW 264.7 macrophages was quantified by fluorescence microscopy. Phenotypic changes and cytokine production in the macrophages were also investigated as a function of VLP treatment to more fully assess responses. Finally, we investigated the ability of azithromycin to direct Qβ particles to macrophage populations in the lung as a proof-of-concept for pulmonary drug delivery.

### 4.3. Materials and Methods

*Cell Culture*

All cell culture reagents were purchased from Invitrogen, unless otherwise indicated. RAW 264.7 macrophage cell line (ATCC) was cultured in phenol red-free Dulbecco's modified Eagle's medium (DMEM) supplemented with 10% fetal bovine serum (FBS), GlutaMAX (2 mM), sodium pyruvate (1 mM), penicillin (100 units/mL), and streptomycin (100 μg/mL). Cells were maintained at 37°C in a humidified incubator with 5% $CO_2$.

*Protein Production and Characterization of VLPs*

The Qβ VLPs were produced and characterized following previously published protocols.[23] Briefly, electrocompetent ClearColi BL21(DE3) *E. coli* cells (Lucigen) were transformed with either pET28 plasmid vector harboring the viral coat protein (CP) gene or bicistronic pCDF vector harboring the CP gene and the mCherry gene. Cells were plated on selective SOB agar. After 24 h, isolated colonies were selected into SOB media (1% NaCl; 25 mL) containing appropriate antibiotic and grown overnight at 37°C. Cultures were diluted into selective SOB media (1% NaCl; 500 mL) the following day and grown at 37°C until cells reached mid-log phase growth ($O.D._{600} \sim 0.9$). Protein expression was induced by the addition of IPTG to a final concentration of 1 mM, and cultures were maintained at 30°C for 16 h before cells were harvested by centrifugation at 6,000 rpm for 10 min. Cells were lysed using a probe sonicator (10 min total, 75 W, 5 sec intervals) in an ice bath. Cell lysates were clarified by centrifugation at 14,000 rpm for 10 min, and supernatant collected. VLPs were precipitated by the addition of 30% $(NH_4)_2SO_4$ (w/v) at 4°C for 2 h, and precipitate was pelleted by centrifugation at 14,000 rpm for 10 min. The resulting pellet was dissolved in 1x TBS and extracted with *n*-BuOH:$CHCl_3$ (1:1, v/v) to remove lipids and aggregates. The samples were centrifuged at 14,000 rpm for 10 min, and the aqueous phase collected and subsequently loaded onto 10-40% sucrose density gradients. VLPs were purified by centrifugation at 28,000 rpm for 4 h, and VLP bands were isolated from the gradient via syringe. Particles were pelleted by centrifugation at 68,000 rpm for 2 h, and pellets were dissolved in 0.1M potassium phosphate buffer.

The protein concentration of the VLP samples was determined by Bradford assay using BSA standards. Samples were characterized by FPLC size-exclusion chromatography (Superose 6 10/300 GL) monitored by absorbance at 280 nm, dynamic light scattering (Wyatt Dynapro plate reader), microfluidic gel electrophoresis (Agilent 2100 Bioanalyzer with Series II Protein 80 chips), and mass spectrometry (Agilent 6230B TOF LC/MS). All conjugations were performed as described and characterized using these same methods.

*Synthesis of VLP-Macrolide Conjugates*

**Qβ@mCherry-$(N_3)_{135}$:** A solution of Qβ@mCherry (0.36 mL from 10 mg/mL stock solution in 0.1M $KPO_4$, pH 7.4, 0.255 μmol subunit, 1.02 μmol reactive amines) was cooled in an ice bath. To this solution was added 10.2 μL NHS-$PEG_{12}$-$N_3$ (100 mM stock solution in DMSO, ~ 4 equiv per reactive amine). The tube was gently inverted to mix reagents and incubated overnight at 4°C. The degree of acylation was quantified by LC-ESI-TOF analysis (135 per particle, 0.75 per subunit). Particles were purified using PD-10 prepacked Sephadex columns (GE Healthcare) according to manufacturer's instructions. Particles were further concentrated to 7.7 mg/mL using Amicon Ultra-4 centrifugal filters with 100 kDa molecular weight cutoff.

**Qβ@mCherry-$(N_3)_{170}$:** A solution of Qβ@mCherry (1.5 mL from 10 mg/mL stock solution in 0.1M $KPO_4$, pH 7.4, 1.06 μmol subunit, 4.25 μmol reactive amines) was cooled in an ice bath. To this solution was added 54 μL NHS-$PEG_{12}$-$N_3$ (100 mM stock solution in DMSO, 5 equiv per reactive amine). The tube was gently inverted to mix reagents and incubated overnight at 4°C. The degree of acylation was quantified by LC-ESI-TOF analysis (170 per particle, 0.95 per subunit). Particles were purified using PD-

10 prepacked Sephadex columns (GE Healthcare) according to manufacturer's instructions. Particles were further concentrated to 7.7 mg/mL using Amicon Ultra-4 centrifugal filters with 100 kDa molecular weight cutoff.

**Conjugate 3**: **Qβ@mCherry-(Clarith1)$_{30}$(HPG)$_{120}$:** A solution of Qβ@mCherry-($N_3$)$_{170}$ (200µl from 7.7 mg/mL stock solution in 0.1M $KPO_4$, pH 7.4, 0.109 µmol subunit, 96 nmol reactive azide) was diluted with 33 µl of DMSO. To this solution was added a mixture of 49.7 µL of 10 mM macrolide (5 equiv to reactive azide) and 7.95 µL of 50 mM HPG (4 equiv to reactive azide) in one portion. The tube was slowly inverted to create a homogenous solution. The reaction mixture turned cloudy and opaque. Subsequently, 24.9 µL of 40 mM $CuSO_4$ (10 equiv to azide) was added along with 24.9 µL of 200 mM THPTA (50 equiv to azide) in a single portion along with 19.9 µL of 500 mM aminoguanidine (100 equiv to azide). The tube was again slowly inverted to mix all components and the reaction was initiated by the addition of 19.9 µL of 500 mM sodium ascorbate (100 equiv to azide). After mixing, the reaction was incubated at 55 °C for 3 hours. The reaction mixture was purified by centrifugal filtration against 0.1M $KPO_4$ (3 x 15 mL, dilution >10,000x, 4000x *g*, 4 °C, 7 min runs) using Amicon Ultra-4 centrifugal filters with 100 kDa MWCO and was concentrated to ~2.5 mg/mL. The sample was sterile filtered through a 0.22 µm PVDF syringe filter, and the total protein content was quantified by Bradford assay using BSA standards. Recovery of protein was approximately 30 %. The extent of modification was determined by LC-ESI-TOF and the quality of the sample was further checked with electrophoresis. The final modified particles were composed of >95% intact particles as determined by DLS and FPLC.

**Note:** Some of the particles were modified more heavily than 30 macrolides, but they precipitated overnight. Clarithromycin derivatives displayed marked solubility issues.

**Conjugate 4: Qβ@mCherry-(Clarith2)$_{60}$(HPG)$_{90}$**: A solution of Qβ@mCherry-($N_3$)$_{170}$ (200 µl from 7.7 mg/mL stock solution in 0.1M $KPO_4$, pH 7.4, 0.109 µmol subunit, 96 nmol reactive azide) was diluted with 33 µl of DMSO. To this solution was added a mixture of 49.7 µL of 10 mM macrolide (5 equiv to reactive azide) and 7.95 µL of 50 mM HPG (4 equiv to reactive azide) in one portion. The tube was slowly inverted to create a homogenous solution. The reaction mixture turned cloudy and opaque. Subsequently, 24.9 µL of 40 mM $CuSO_4$ (10 equiv to azide) was added along with 24.9 µL of 200 mM THPTA (50 equiv to azide) in a single portion and 19.9 µL of 500 mM aminoguanidine (100 equiv to azide). The tube was again slowly inverted to mix all components and the reaction was initiated by the addition of 19.9 µL of 500 mM sodium ascorbate (100 equiv to azide). After mixing, the reaction was incubated at 55 °C for 3 hours. The reaction mixture was purified by centrifugal filtration against 0.1M $KPO_4$ (3 x 15 mL, dilution >10,000x, 4000x *g*, 4 °C, 7 min runs) using Amicon Ultra-4 centrifugal filters with 100 kDa MWCO and was concentrated to ~2.5 mg/mL. The sample was sterile filtered through a 0.22 µm PVDF syringe filter, and the total protein content was quantified by Bradford assay using BSA standards. Recovery of protein was approximately 40 %. The extent of modification was determined by LC-ESI-TOF and the quality of the sample was further checked with electrophoresis. The final modified particles were composed of >95% intact particles as determined by DLS and FPLC.

**Conjugate 5: Qβ@mCherry-(TriKeto)$_{90}$(HPG)$_{70}$**: A solution of Qβ@mCherry-($N_3$)$_{170}$ (200 µl from 7.7 mg/mL stock solution in 0.1M $KPO_4$, pH 7.4, 0.109 µmol subunit, 96

nmol reactive azide) was diluted with 33 µl of DMSO. To this solution was added a mixture of 49.7 µL of 10 mM macrolide (5 equiv to reactive azide) and 7.95 µL of 50 mM HPG (4 equiv to reactive azide) in one portion. The tube was slowly inverted to create a homogenous solution. The reaction mixture turned cloudy and opaque. Subsequently, 24.9 µL of 40 mM $CuSO_4$ (10 equiv to azide) was added along with 24.9 µL of 200 mM THPTA (50 equiv to azide) in a single portion and 19.9 µL of 500 mM aminoguanidine (100 equiv to azide). The tube was again slowly inverted to mix all components and the reaction was initiated by addition of 19.9 µL of 500 mM sodium ascorbate (100 equiv to azide). After mixing, the reaction incubated at 55 °C for 3 hours. The reaction mixture was purified by centrifugal filtration against 0.1M $KPO_4$ (dilution >10,000x, 4,000x *g*, 4 °C, 7 min runs) using Amicon Ultra-4 centrifugal filters with 100 kDa MWCO and was concentrated to ~2.5 mg/mL concentration. The sample was sterile filtered through a 0.22 µm PVDF syringe filter, and the total protein content was quantified by Bradford assay using BSA standards. Recovery of protein was approximately 60 %. The extent of modification was determined by LC-ESI-TOF and the quality of the sample was further checked with electrophoresis. The final modified particles were composed of >95% intact particles as determined by DLS and FPLC.

**<u>Conjugate 6</u>: Qβ@mCherry-(TriKeto)$_{180}$**: A solution of Qβ@mCherry-$(N_3)_{170}$ (100 µL from 8.5 mg/mL stock solution in 0.1M $KPO_4$, pH 7.4, 60.2 nmol subunit, 85.6 nmol reactive azide) was diluted with 33 µL of DMSO. To this solution was added 42.3 µL of 10 mM macrolide (5 equiv to reactive azide). The tube was slowly inverted to create a homogenous solution. The reaction mixture turned cloudy and opaque. Subsequently, 8.57 µL of 200 mM $CuSO_4$ (20 equiv to azide) was added along with 8.57 µL of 1M

THPTA (100 equiv to azide) in a single portion and 17.1 μL of 500 mM aminoguanidine (100 equiv to azide). The tube was again slowly inverted to mix all components and the reaction was initiated by the addition of 17.1 μL sodium ascorbate (100 equiv to azide). After mixing, the reaction was incubated at 55 °C for 3 hours. The reaction mixture was purified by centrifugal filtration against 0.1M $KPO_4$ (dilution >10,000x, 14,000x *g*, 4 °C, 3 min runs) using Amicon Ultra-0.5 centrifugal filters with 100 kDa MWCO and concentrated to ~2.5 mg/mL. The sample was sterile filtered through a 0.22 μm PVDF syringe filter, and the total protein content was quantified by Bradford assay using BSA standards. Recovery of protein was approximately 50 %. The extent of modification was determined by LC-ESI-TOF and the quality of the sample was further checked with electrophoresis. The final modified particles were composed of >95% intact particles as determined by DLS and FPLC.

**Conjugate 7: Qβ@mCherry-(Azith1)$_{90}$(HPG)$_{40}$**: A solution of Qβ@mCherry-$(N_3)_{135}$ (30 μl from 8.5 mg/mL stock solution in 0.1M $KPO_4$, pH 7.4, 18.9 nmol subunit, 17 nmol reactive azide) was diluted with 5 μl of DMSO. To this solution was added a mixture of 7 μL of 10 mM macrolide (5 equiv to reactive azide) and 0.83 μL of 50 mM HPG (4 equiv to reactive azide) in one portion. The tube was slowly inverted to create a homogenous solution. The reaction mixture turned cloudy and opaque. Subsequently, 3.48 μL of 40 mM $CuSO_4$ (10 equiv to azide) was added along with 3.48 μL of 200 mM THPTA (50 equiv to azide) in a single portion and 2.78 μL of 500 mM aminoguanidine (100 equiv to azide). The tube was again slowly inverted to mix all components and the reaction was initiated by addition of 2.78 μL of 500 mM sodium ascorbate (100 equiv to azide). After mixing, the reaction was incubated at 55 °C for 3 hours. The reaction mixture was

purified by centrifugal filtration against 0.1M $KPO_4$ (dilution >10,000x, 14,000x *g*, 4 °C, 3 min runs) using Amicon Ultra-0.5 centrifugal filters with 100 kDa MWCO and concentrated to ~2.5 mg/mL. The sample was sterile filtered through a 0.22 μm PVDF syringe filter, and the total protein content was quantified by Bradford assay using BSA standards. Recovery of protein was approximately 50 %. The extent of modification was determined by LC-ESI-TOF and the quality of the sample was further checked with electrophoresis. The final modified particles were composed of >95% intact particles as determined by DLS and FPLC.

**Conjugate 8: Qβ@mCherry-$(Azith2)_{50}(HPG)_{110}$**: A solution of Qβ@mCherry-$(N_3)_{170}$ (200 μl from 7.7 mg/mL stock solution in 0.1M $KPO_4$, pH 7.4, 0.109 μmol subunit, 96 nmol reactive azide) was diluted with 28 μl of DMSO. To this solution was added a mixture of 55 μL of 10 mM macrolide (5.5 equiv to reactive azide) and 5 μL of 50 mM HPG (2.5 equiv to reactive azide) in one portion. The tube was slowly inverted to create a homogenous solution. The reaction mixture turned cloudy and opaque. Subsequently, 24.9 μL of 40 mM $CuSO_4$ (10 equiv to azide) was added along with 24.9 μL of 200 mM THPTA (50 equiv to azide) in a single portion and 19.9 μL of 500 mM aminoguanidine (100 equiv to azide). The tube was again slowly inverted to mix all components and the reaction was initiated by the addition of 19.9 μL of 500 mM sodium ascorbate (100 equiv to azide). After mixing, the reaction was incubated at 55 °C for 3 hours. The reaction mixture was purified by centrifugal filtration against 0.1M $KPO_4$ (3 x 15 mL, dilution >10,000x, 4,000x *g*, 4 °C, 7 min runs) using Amicon Ultra-4 centrifugal filters with 100 kDa MWCO and was concentrated to ~2.5 mg/mL concentration. The sample was sterile filtered through a 0.22 μm PVDF syringe filter, and the total protein content was

quantified by Bradford assay using BSA standards. Recovery of protein was approximately 60 %. The extent of modification was determined by LC-ESI-TOF and the quality of the sample was further checked with electrophoresis. The final modified particles were composed of >95% intact particles as determined by DLS and FPLC.

**Conjugate 9: Qβ@mCherry-(Azith2)$_{145}$**: A solution of Qβ@mCherry-($N_3$)$_{170}$ (150 µl from 7.7 mg/mL stock solution in 0.1M $KPO_4$, pH 7.4, 77 nmol subunit, 70 nmol reactive azide) was diluted with 20 µl of DMSO. To this solution was added a mixture of 49 µL of 10 mM macrolide (7 equiv to reactive azide). The tube was slowly inverted to create a homogenous solution. The reaction mixture turned cloudy and opaque. After this 1.74 µL of 250 mM $CuSO_4$ (10 equiv to azide) was added along with 1.74 µL of 1.25 M THPTA (50 equiv to azide) in a single portion and 14 µL of 500 mM aminoguanidine (100 equiv to azide). The tube was again slowly inverted to mix all components and the reaction was initiated by the addition of 14 µL of 500 mM sodium ascorbate (100 equiv to azide). After mixing, the reaction was incubated at 55 °C for 3 hours. The reaction mixture was purified by centrifugal filtration against 0.1M $KPO_4$ (3 x 15 mL, dilution >10,000x, 4,000x *g*, 4 °C, 7 min runs) using Amicon Ultra-4 centrifugal filters with 100 kDa MWCO and was concentrated to ~2.5 mg/mL concentration. The sample was sterile filtered through a 0.22 µm PVDF syringe filter, and the total protein content was quantified by Bradford assay using BSA standards. Recovery of protein was approximately 60 %. The extent of modification was determined by LC-ESI-TOF and the quality of the sample was further checked with electrophoresis. The final modified particles were composed of >95% intact particles as determined by DLS and FPLC.

**Conjugate 10: Qβ@mCherry-(tolyl)$_{115}$(HPG)$_{55}$**: A solution of Qβ@mCherry-($N_3$)$_{170}$ (200 µl from 7.7 mg/mL stock solution in 0.1M $KPO_4$, pH 7.4, 0.109 µmol subunit, 96 nmol reactive azide) was diluted with 33 µl of DMSO. To this solution was added a mixture of 49.7 µL of 10 mM *p*-tolylacetylene (5 equiv to reactive azide) and 7.95 µL of 50 mM HPG (4 equiv to reactive azide) in one portion. The tube was slowly inverted to create a homogenous solution. The reaction mixture was clear after mixing. Subsequently, 24.9 µL of 40 mM $CuSO_4$ (10 equiv to azide) was added along with 24.9 µL of 200 mM THPTA (50 equiv to azide) in a single portion and 19.9 µL of 500 mM aminoguanidine (100 equiv to azide). The tube was again slowly inverted to mix all components and the reaction was initiated by the addition of 19.9 µL of 500 mM sodium ascorbate (100 equiv to azide). After mixing, the reaction was incubated at 55 °C for 3 hours. The reaction mixture was purified by centrifugal filtration against 0.1M $KPO_4$ (3 x 15 mL, dilution >10,000x, 4,000x *g*, 4 °C, 7 min runs) using Amicon Ultra-4 centrifugal filters with 100 kDa MWCO and was concentrated to ~2.5 mg/mL concentration. The sample was sterile filtered through a 0.22 µm PVDF syringe filter, and the total protein content was quantified by Bradford assay using BSA standards. Recovery of protein was approximately 80 %. The extent of modification was determined by LC-ESI-TOF and the quality of the sample was further checked with electrophoresis. The final modified particles were composed of >95% intact particles as determined by DLS and FPLC.

**Conjugate 9-IR800CW: Qβ-(Azith2)$_{153}$(HPG)$_{75}$**: A solution of wild-type Qβ (250 µL from 10 mg/mL stock solution in 0.1M $KPO_4$, pH 7.4, 352 nmol subunit, 1.4 µmol reactive amines) was diluted with 148 µL 0.1M $KPO_4$ and reacted with 102 µL IRDye® 800CW NHS ester (1 mg/mL stock solution in DMSO, 0.25 equiv per protein subunit).

The tube was gently inverted to mix reagents, sealed with foil, and incubated overnight at 4°C. The reaction mixture was purified by centrifugal filtration against 0.1M $KPO_4$ (3 x 15 mL, dilution >10,000x, 4000x *g*, 4 °C, 7 min runs) using Amicon Ultra-4 centrifugal filters with 100 kDa MWCO and was concentrated to ~5 mg/mL. Dye loading was assessed by absorbance measurements and calculations using the molar extinction coefficient for the dye ($\varepsilon_{IRDye}$ = 270,000 $M^{-1}cm^{-1}$; 24 dye molecules per particle). Particles were subsequently reacted with 28.2 μL NHS-$PEG_{12}$-$N_3$ (100 mM stock solution in DMSO, ~4 equiv per reactive amine) overnight at 4°C and purified by centrifugal filtration against 0.1M $KPO_4$ (3 x 15 mL, dilution >10,000x, 4000x *g*, 4 °C, 7 min runs) using Amicon Ultra-4 centrifugal filters with 100 kDa MWCO. Degree of acylation was quantified by ESI-TOF analysis (237 per particle, 1.3 per subunit) and protein concentration was determined by Bradford assay using BSA standards. Finally, a solution of particles (125 μL from 5.53 mg/mL stock solution in 0.1M $KPO_4$, pH 7.4, 48.7 nmol subunit, 64.3 nmol reactive azide) was diluted with 13 μL DMSO. To this solution was added a mixture of 30.5 μL of 10 mM macrolide (5 equiv to reactive azide) and 3 μL of 50 mM HPG (2.5 equiv to reactive azide) in one portion. The tube was slowly inverted to create a homogenous solution. The reaction mixture turned cloudy and opaque. After this 0.76 μL of 400 mM $CuSO_4$ (5 equiv to azide) was added along with 15.3 μL of 100 mM THPTA (25 equiv to azide) in a single portion and 9 μL of 200 mM aminoguanidine (30 equiv to azide). The tube was again slowly inverted to mix all components and the reaction was initiated by the addition of 3.7 μL of 500 mM sodium ascorbate (30 equiv to azide). After mixing, the reaction was incubated at 55 °C for 3 hours. The reaction mixture was purified by centrifugal filtration against 0.1M $KPO_4$

(dilution >10,000x, 14,000x *g*, 4 °C, 3 min runs) using Amicon Ultra-0.5 centrifugal filters with 100 kDa MWCO and was concentrated to ~1.5 mg/mL concentration. The sample was sterile filtered through a 0.22 μm PVDF syringe filter, and the total protein content was quantified by Bradford assay using BSA standards. Recovery of protein was approximately 60 %. The extent of modification was determined by ESI-TOF HRMS. The final modified particles were composed of >95% intact particles as determined by DLS.

**Conjugate 10-IR800CW: Qβ-(tolyl)$_{130}$**: A solution of wild-type Qβ (2 mL from 3.5 mg/mL stock solution in 0.1M $KPO_4$, pH 7.4, 496 nmol subunit, 1.98 μmol reactive amines) was diluted reacted with 248 μL IRDye® 800CW NHS ester (1 mg/mL stock solution in DMSO, 0.5 equiv per protein subunit). The tube was gently inverted to mix reagents, sealed with foil, and incubated overnight at 4°C. The reaction mixture was purified by centrifugal filtration against 0.1M $KPO_4$ (3 x 15 mL, dilution >10,000x, 4000x *g*, 4 °C, 7 min runs) using Amicon Ultra-4 centrifugal filters with 100 kDa MWCO and was concentrated to ~5 mg/mL. Dye loading was assessed by absorbance measurements and calculations using the molar extinction coefficient for the dye ($\varepsilon_{IRDye}$ = 270,000 $M^{-1}cm^{-1}$; 20 dye molecules per particle). Particles were subsequently reacted with 28.2 μL NHS-$PEG_{12}$-$N_3$ (100 mM stock solution in DMSO, ~4 equiv per reactive amine) overnight at 4°C and purified by centrifugal filtration against 0.1M $KPO_4$ (3 x 15 mL, dilution >10,000x, 4000x *g*, 4 °C, 7 min runs) using Amicon Ultra-4 centrifugal filters with 100 kDa MWCO. Degree of acylation was quantified by ESI-TOF analysis (135 per particle, 0.75 per subunit) and protein concentration was determined by Bradford assay using BSA standards. Finally, a solution of particles (400 μL from 3.4

mg/mL stock solution in 0.1M $KPO_4$, pH 7.4, 96.3 nmol subunit, 72.2 nmol reactive azide) was diluted with 250 μL DMSO. To this solution was added 12.6 μL of 50 mM 4-ethynyltoluene (9 equiv to reactive azide). The tube was slowly inverted to create a homogenous solution. The reaction mixture turned cloudy and opaque. After this 2.8 μL of 250 mM $CuSO_4$ (10 equiv to azide) was added along with 2.8 μL of 1.25 M THPTA (50 equiv to azide) in a single portion and 2.9 μL of 2.4 M aminoguanidine (100 equiv to azide). The tube was again slowly inverted to mix all components and the reaction was initiated by the addition of 7 μL of 1 M sodium ascorbate (100 equiv to azide). After mixing, the reaction was incubated at 55 °C for 3 hours. The reaction mixture was purified by centrifugal filtration against 0.1M $KPO_4$ (dilution >10,000x, 14,000x *g*, 4 °C, 3 min runs) using Amicon Ultra-0.5 centrifugal filters with 100 kDa MWCO and was concentrated to ~1.5 mg/mL concentration. The sample was sterile filtered through a 0.22 μm PVDF syringe filter, and the total protein content was quantified by Bradford assay using BSA standards. Recovery of protein was approximately 70 %. The extent of modification was determined by ESI-TOF HRMS. The final modified particles were composed of >95% intact particles as determined by DLS.

*Live-Cell Microscopy and Fluorescence Imaging*

RAW 264.7 cells were grown to 80% confluence and seeded onto 8-chambered microscope slides at 1:10 dilution. After 24 h, cells were treated with Qβ conjugates (2.5 nM) and incubated for 24 h at 37°C in a humidified incubator with 5% $CO_2$. At each respective time point, cells were rinsed twice with fresh DMEM and subsequently imaged on an Eclipse Ti-U fluorescence microscope (Nikon) equipped with a 60x oil immersion objective. Images were analyzed using ImageJ software. Cells were manually

selected by freeform drawing, and the area integrated density was calculated for each selection. Background fluorescence was calculated in the same manner as an average from three randomly selected points in the image where no cells were present. The corrected fluorescence per cell (CFPC) was calculated using the following equation:

$$CFPC = Integrated\ Density - (Area\ of\ cell * Mean\ background\ fluorescence)$$

*Nitrite Assay*

Nitrite production in RAW 264.7 cells was quantified using a Griess assay (Thermo Fisher Scientific). Briefly, RAW 264.7 cells were seeded in 12-well plates ($2x10^5$ cells/well) and maintained 24 h prior to treatment with Qβ conjugates (2.5 nM), azithromycin (150 nM), clarithromycin (150 nM), dendrimer-AZM (12.5 nM), dendrimer-CLA (12.5 nM), or LPS (100 ng/mL). At 24 h post-treatment, 75 µL of cell culture supernatant was transferred to a 96-well plate for analysis in duplicate. Samples were diluted in 65 µL sterile water, and 10 µL Griess Reagent added to each sample. Griess Reagent was prepared by mixing together equal volumes of *N*-(1-naphthyl)ethylenediamine and sulfanilic acid. Samples were incubated at room temperature for 30 min and absorbance was measured at 548 nm on a microplate reader (Thermo Fisher Scientific). Nitrite concentrations in samples were calculated from standard curve using the nitrite standard provided by the manufacturer.

*Arginase Assay*

Arginase activity in RAW 264.7 cells was quantified using the QuantiChrom arginase assay kit (BioAssay Systems) following the manufacturer's protocol. Briefly, RAW 264.7 cells were seeded in 12-well plates ($2x10^5$ cells/well) and maintained 24 h prior to treatment with Qβ conjugates (2.5 nM), azithromycin (150 nM), clarithromycin

(150 nM), dendrimer-AZM (12.5 nM), dendrimer-CLA (12.5 nM), or LPS (100 ng/mL). At 24 h post-treatment, cells were harvested for each sample, washed with PBS, and centrifuged at 1,000x *g* for 10 min. Cell pellets were lysed for 10 min using 150 µL of 10mM Tris-HCl (pH 7.4) containing cOmplete™ EDTA-free protease inhibitor tablet (Roche) and 0.4% (w/v) Triton X-100 (Sigma). Lysates were centrifuged for 10 min at 14,000x *g* and supernatant collected for assay. 50 µL urea standard (1 mM; $O.D._{standard}$) and 50 µL sterile water ($O.D._{water}$) were added to separate wells of a 96-well plate, while 40 µL of each sample was added to 2 separate wells. One of the sample wells was left untouched ($O.D._{blank}$) while 10 µL of 5x substrate buffer was added to the other sample well ($O.D._{sample}$). The plate was incubated at 37 °C for 1 h, after which 200 µL urea reagent (prepared from equal volumes of kit reagents A and B) was added to all wells followed by 10 µL of 5x substrate buffer to the $O.D._{blank}$ wells. The plate was incubated at room temperature for 1 h and absorbance was measured at 430 nm on a microplate reader (Thermo Fisher Scientific). Arginase activity was calculated using the following equation:

$$Arginase\ activity = \frac{(O.D._{sample} - O.D._{blank})}{(O.D._{standard} - O.D._{water})} \times 10.4\ (U/L)$$

*Cytokine Analysis*

Cytokine production was measured in culture supernatants using ELISA kits (PeproTech) according to the manufacturer's protocol. Culture supernatants were analyzed in duplicate from the same samples as used for the nitrite and arginase assays.

*Mice and Biodistribution Analysis*

CD-1 IGS mice (8-12 weeks) were purchased from Charles River Laboratories and maintained in the animal facility of the Georgia Institute of Technology. All animal

care and experimental procedures were approved by the Institutional Care and Use Committee of the Georgia Institute of Technology. Mice were administered 50 μg VLP conjugates labeled with IRDye® 800cw (LI-COR, Inc.; see Supplemental Methods) via tail vein injection and returned to cage for 2h or 24 h ($n$=2 per time point), after which mice were imaged using an IVIS Spectrum CT imaging cabinet (Bruker). Mice were subsequently euthanized and tissues collected for *ex vivo* imaging and quantitative analysis.

Liver and lung tissues were harvested from mice treated with VLP conjugates labeled with IRDye® 800cw (LI-COR, Inc.) at 2 h or 24 h ($n$ = 2). Tissues were rinsed twice with chilled 1x PBS and blotted dry, after which samples were imaged *ex vivo* using an IVIS Spectrum CT imaging cabinet (Bruker). All image analysis was performed in Living Image software. Regions of interest (ROIs) were manually set around each tissue sample, and the total radiant efficiency was calculated for each ROI.

## 4.4. Results and Discussion

### *4.4.1. Particle design and characterization*

Qβ VLPs were prepared from recombinant expression in *E. coli*, either as wild-type particles or engineered to encapsulate mCherry (designated Qβ@mCherry) as previously described.[36] To prepare Qβ conjugates with macrolide ligands, variants of azithromycin **(Azith1, Azith2)**, clarithromycin **(Clarith1, Clarith2)**, and a tricyclic ketolide **(TriKeto)** were synthesized bearing an alkyne functional group to allow for attachment to the VLP by the copper(I)-catalyzed azide-alkyne cycloaddition (CuAAC) reaction. Qβ VLPs, which display 720 amine groups on their surface,[37] were prepared through acylation with an excess of *N*-hydroxysuccinimide ester **1** to install azide

**Scheme 1.** Conjugation of macrolides to Qβ VLPs via CuAAC.

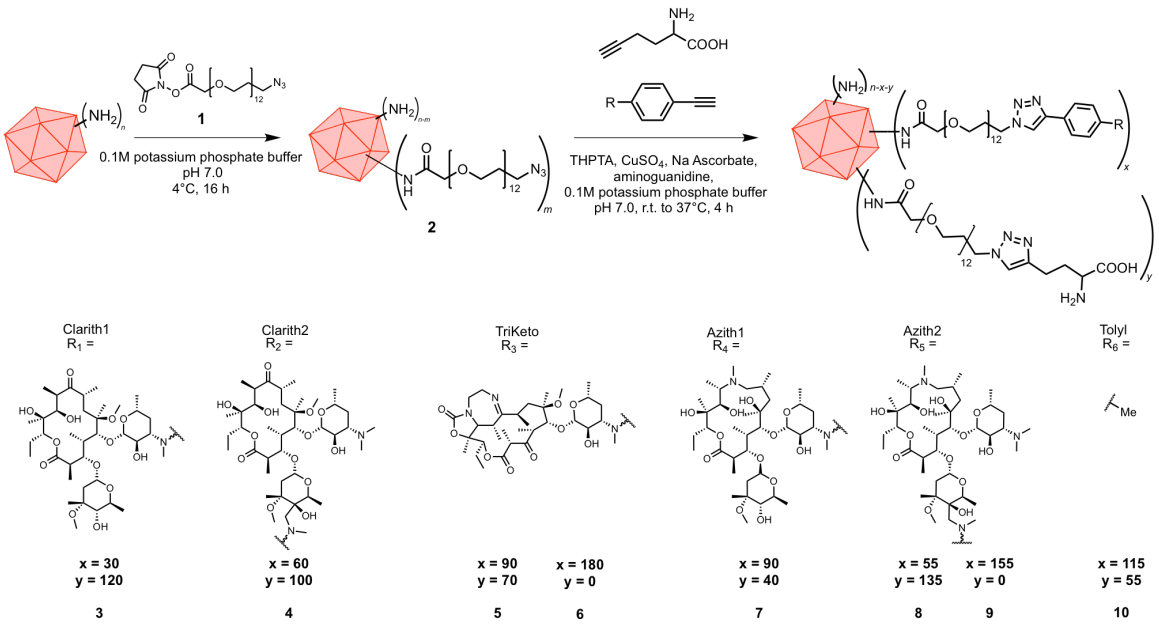


functionalities. After purification away from the excess small molecules, the azide-functionalized VLPs were reacted with **Clarith1** and homopropargylglycine (**HPG**; to yield **3**), **Clarith2** and **HPG** (to yield **4**), **TriKeto** and **HPG** (to yield **5**), **TriKeto** alone (to yield **6**), **Azith1** and **HPG** (to yield **7**), **Azith2** and **HPG** (to yield **8**), **Azith2** alone (to yield **9**) or 4-ethynyltoluene and **HPG** (to yield negative control particle **10**; **Scheme 1**). Loadings ranging from 30-150 modifications could be achieved with 5 equivalents of alkyne per reactive azide group **(Scheme 1)**, but the solubility of VLP conjugates decreased dramatically with increased loading density. **HPG** was simultaneously conjugated to the particles to offset the decreased solubility of the VLP conjugates.

The conjugates were characterized by liquid chromatography coupled to an electrospray ionization time-of-flight (ESI-TOF) mass spectrometer, which revealed labeling of an average of one azide per subunit for **2**, and subsequent attachment of macrolides and **HPG** on **3-10 (Figure 1)**. The average loading for each species was determined by the relative intensities of the corresponding peaks in the mass spectra.

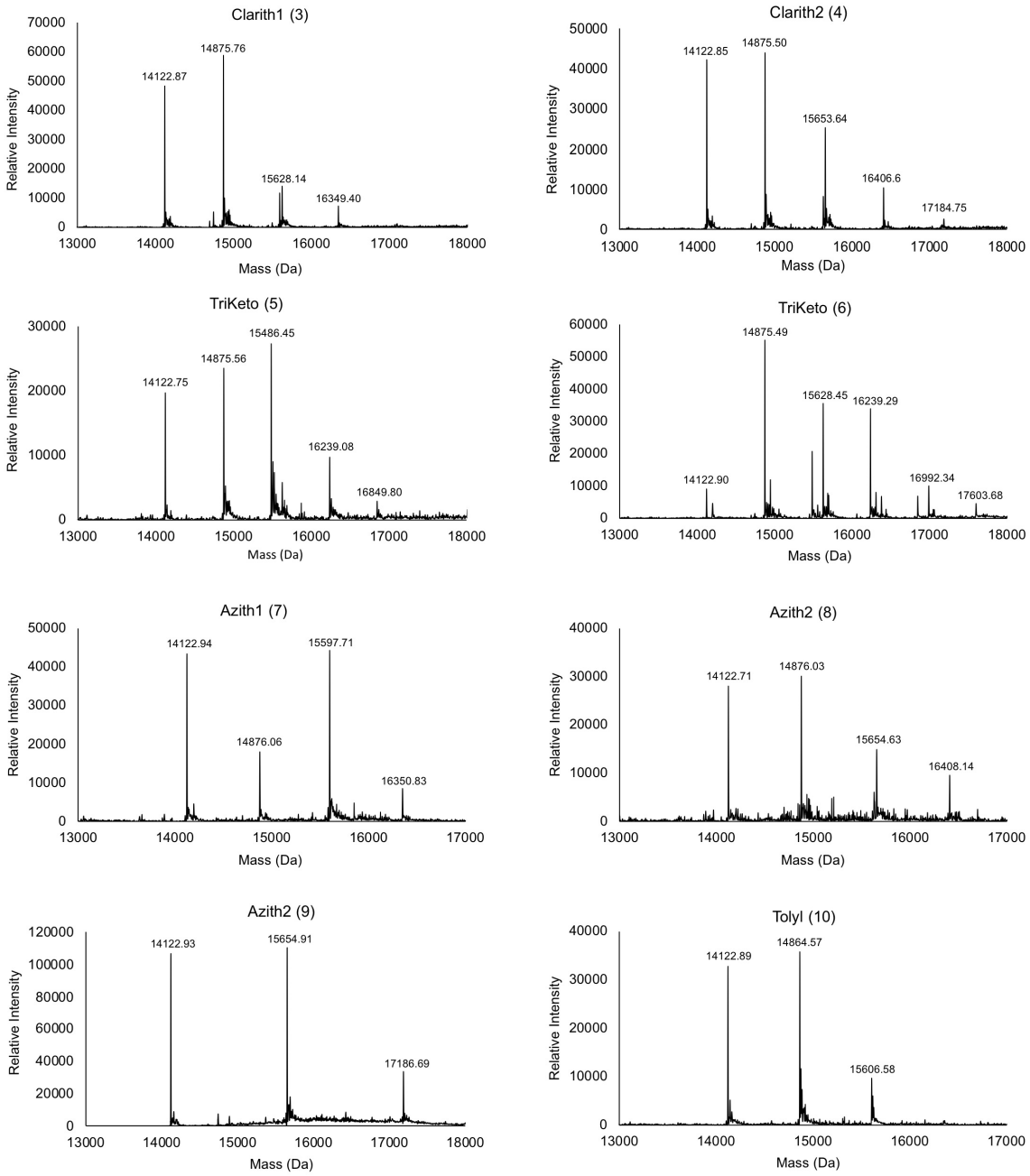


**Figure 1**. Deconvolved high-resolution LC-MS spectra for Qβ-macrolide conjugates.

Electrophoretic analysis further confirmed the level of modification with macrolides. Size exclusion chromatography, electrophoretic analysis, and dynamic light scattering gave data characteristic of intact monodisperse particles for **3-10 (Figures 2 and 3)**. The

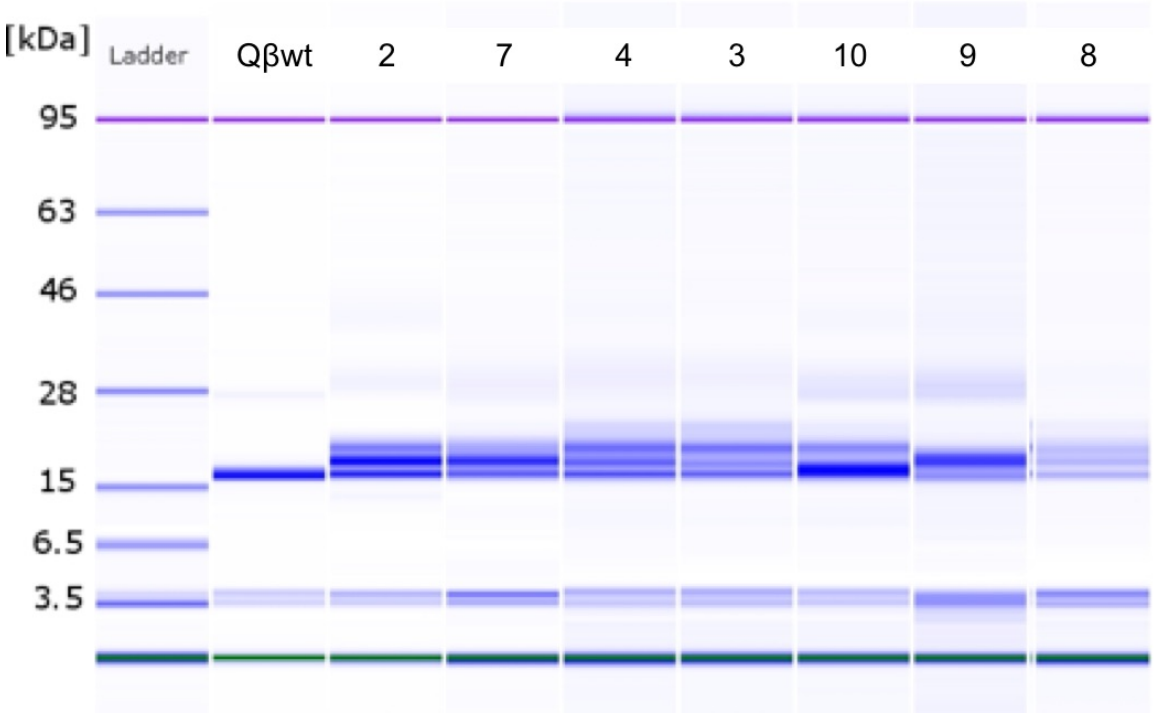


**Figure 2.** Electrophoretic analysis of Qβ-macrolide conjugates under denaturing conditions. Labels at the top of each lane denote the identity of each respective sample.

A.

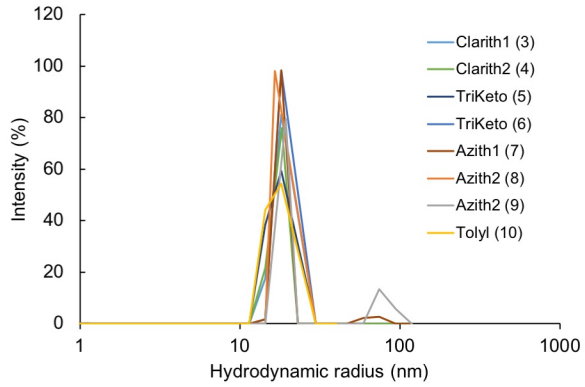


B.

| Conjugate | $R_h$ (nm) | Pd (%) |
|---|---|---|
| Clarith1 (3) | 17.6 | 8.3 |
| Clarith2 (4) | 17.4 | 9.1 |
| TriKeto (5) | 16.8 | 11.1 |
| TriKeto (6) | 18.2 | 2.6 |
| Azith1 (7) | 17.1 | 10 |
| Azith2 (8) | 16.5 | 11.5 |
| Azith2 (9) | 19.3 | 10.4 |
| Tolyl (10) | 16.5 | 11.5 |

**Figure 3.** DLS analysis of Qβ-macrolide conjugates. (**A**) Histogram overlay showing the hydrodynamic radius ($R_h$) for indicated samples. (**B**) Table listing of $R_h$ and percent polydispersity for Qβ-macrolide conjugates.

hydrodynamic radii of the macrolide conjugates were slightly larger than that for unmodified VLPs (~ 14 nm), mostly attributed to interactions of the attached macrocycles with the solvent.

*4.4.2. Assessment of macrophage uptake and activation*

The multivalent attachment of azithromycin, clarithromycin, and the tricyclic ketolide have all been previously shown to promote enhanced uptake of gold nanorods by macrophages in a ligand-dependent manner.[32] In order to further investigate this phenomenon using a different nanoparticle platform, we first chose to quantify the uptake of macrolide-labeled Qβ@mCherry VLPs by RAW 264.7 macrophages. All VLP-macrolide conjugates screened (**3**-**9**) showed significant accumulation in macrophages over the course of 24 h relative to control particles (**10; Figure 4A, B**). Interestingly, **4 (Clarith2)** and **8 (Azith2)** displayed significantly greater uptake compared to **3 (Clarith1)** and **7 (Azith1)**, respectively, despite only differing by the point of attachment on the macrocycle to the VLP. These differences in uptake were attributed to steric hindrance of key functionalities on the macrocycle that are important for the mechanism of macrolide uptake in phagocytic cells. In particular, the tertiary amine that serves as the point of attachment in **3** and **7** might play a key role, as it is distal to the VLP surface in **4** and **8**, and studies to explore these structural influences on the mechanism of uptake are ongoing.

Comparison of azithromycin (**8**, **9**) and ketolide (**5**, **6**) particles revealed a sharp dependence of uptake on the density of macrolide display for the former but not the latter (**Figure 5**). This could derive, wholly or in part, from at least three potential effects: (i) a heretofore unappreciated polyvalent effect for azithromycin interaction with a cell-surface receptor for active transport into phagocytic cells,[31] (ii) a change in the physical properties of the particle with the difference in azithromycin, but not ketolide, density so as to enhance passive uptake, or (iii) differences in P-glycoprotein (P-gp) mediated efflux

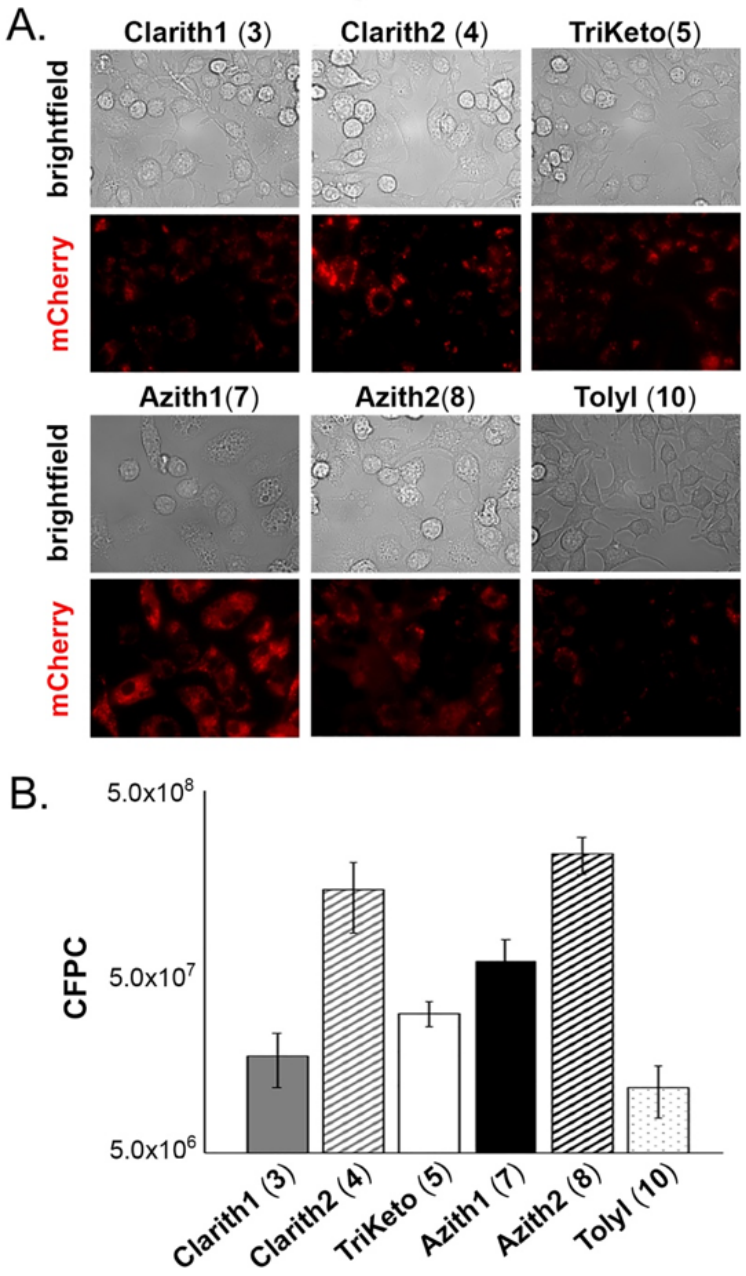


**Figure 4.** VLPs modified with macrolides show enhanced uptake in RAW 264.7 macrophages. **(A)** Representative microscopy images of RAW 264.7 macrophages after 24 h. Upper panels, brightfield. Lower panels, mCherry fluorescence. **(B)** Quantification of VLP uptake as measured by the corrected fluorescence per cell. Bars represent the average +/- standard error ($n$ = 20).

of particles. P-gp has been shown to play a significant role in the accumulation and cellular trafficking of macrolide antibiotics, and a previous study showed that uptake and

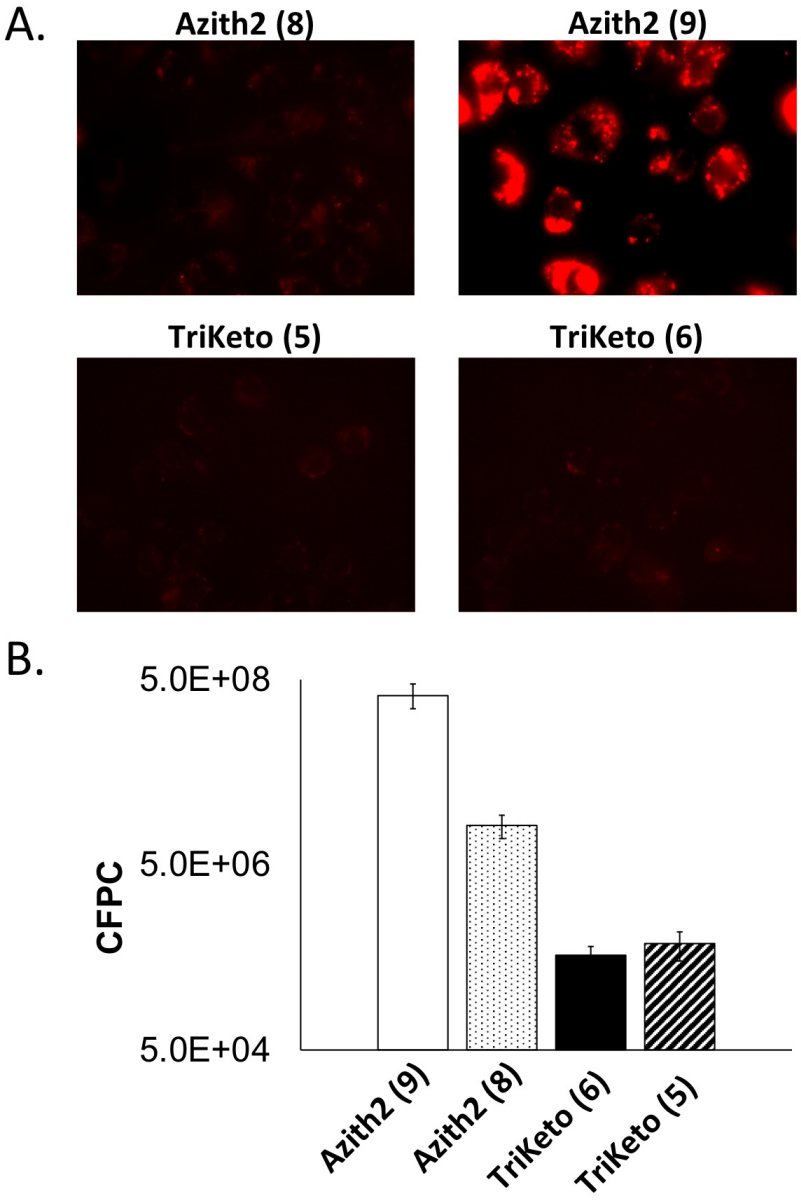


**Figure 5.** Density-dependent uptake of VLP-macrolide conjugates. **(A)** Representative fluorescence microscopy images of RAW 264.7 macrophages after 24 h showing intense punctate staining with increased loading of azithromycin on Qβ VLPs. **(B)** Quantification of VLP uptake as measured by the corrected fluorescence per cell. Bars represent the average +/- standard error ($n$ = 20).

efflux of gold nanorods modified with azithromycin and clarithromycin, but not the tricyclic ketolide, occurred in a P-gp-dependent manner,[38] corresponding with the expected binding affinities of each molecule for the transporter.[39] In this case, a higher

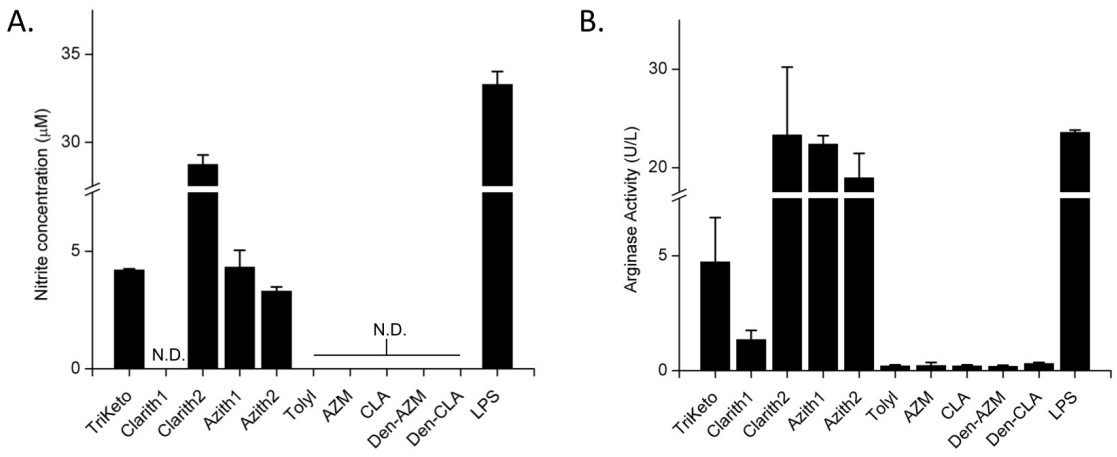


**Figure 6.** Analysis of MΦ polarization as a function of arginine metabolism in cells treated with Qβ-macrolide conjugates after 24 h. (**A**) Quantification of nitrite production as a by-product of nitric oxide synthase activity, indicative of M1 polarization. (**B**) Quantification of arginase activity, indicative of M2 polarization. Cells were dosed with VLP-macrolide conjugates (1.3-5 nM in particle), free macrolides (150 nM), dendrimer species (12.5 nM in dendrimer), or LPS (100 ng/mL), respectively. Data are presented as mean +/- standard error from two individual experiments. N.D. = not detected.

density of azithromycin display would have to inhibit either P-gp transport or recycling. Studies to distinguish among these possibilities have not yet been performed.

We next chose to investigate if the polyvalent display of macrolides on the particle surface influenced macrophage polarization. In order to assess the effects of valency, VLP conjugates were compared against free macrolide (azithromycin, clarithromycin) and macrolide-modified dendrimer species (**Den-AZM**, **Den-CLA**). Activated macrophages are typically polarized towards an M1 (Th1) phenotype or an M2 (Th2) phenotype, although there is evidence that suggests these states are not mutually exclusive.[40] Polarization along either axis can be categorized in part by monitoring arginine metabolism through cellular activities of arginase (M2) or nitric oxide synthase (M1), as well as by characteristic cytokine profiles.[41] RAW 264.7 macrophages treated

with macrolide-labeled VLPs displayed signals that were not consistent with polarization towards any of the known macrophage phenotypes **(Table 1)**.

**Table 1.** Summary of MΦ polarization states and profiles from VLP-treated cells.

| | **Nitrite** | **Arginase** | **TNF-α** | **IL-6** | **IL-10** | **IL-12** |
|---|---|---|---|---|---|---|
| M1 | High | Low | High | High | Low | High |
| M2a | Low | High | Low | Low | High | Low |
| M2b | Medium/High | High | High | High | High | Low |
| M2c | Low | High | Low | Low | High | Low |
| **Macrolide conjugate treatment** | | | | | | |
| **3** (**Clarith1**) | Low | Low | High | Low | High | Low |
| **4** (**Clarith2**) | High | High | High | High | High | Low |
| **5** (**TriKeto**) | Medium | Medium | High | Low | Medium | Low |
| **7** (**Azith1**) | Medium | High | High | High | High | Low |
| **8** (**Azith2**) | Medium | High | High | Low | High | Low |
| Den-AZM/CLA | Low | Low | Low | Low | Low | Low |
| Free AZM/CLA | Low | Low | Low | Low | Low | Low |
| **10** (**Tolyl**) | Low | Low | Low | Low | Low | Low |
| LPS | High | High | High | Medium | High | High |

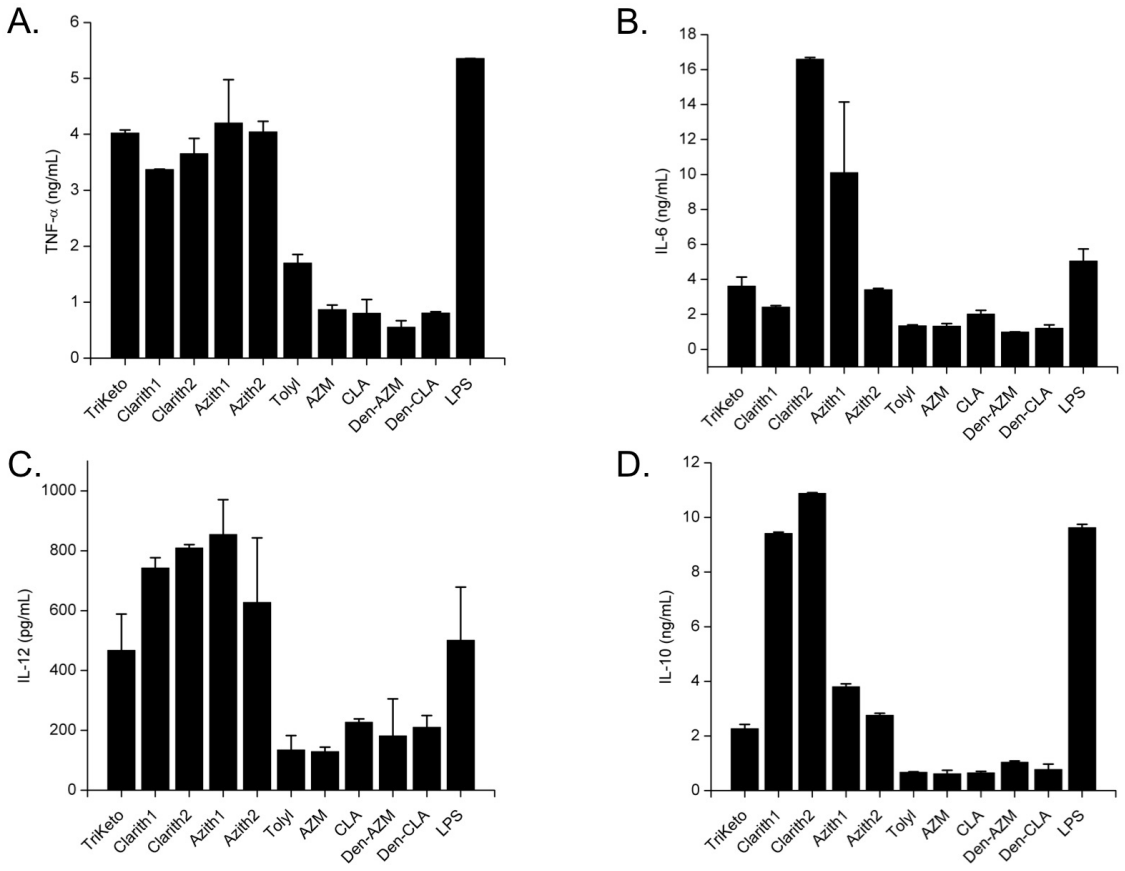


**Figure 7.** Elevated cytokine production in RAW 264.7 MΦ cells treated with VLP-macrolide conjugates after 24 hours. (**A**) TNF-α, (**B**) IL-6, (**C**) IL-12, and (**D**) IL-10 were all measured by ELISA after dosing with VLP-macrolide conjugates (1.3-5 nM in particle), free macrolides (150 nM), dendrimer species (12.5 nM in dendrimer), or LPS (100 ng/mL), respectively. Macrolide concentration was normalized across all samples to 150 nM. Data are presented as mean +/- standard error from two individual experiments.

Conjugates **4 (Clarith2)**, **5 (TriKeto)**, **7 (Azith1)**, and **8 (Azith2)** all induced significant nitrite levels after 24 h relative to cells treated with free macrolides or dendrimers (**Figure 6A**), typically a signature of M1 macrophages. Interestingly, **4** (**Clarith2**) induced significant nitrite production, whereas **3** (**Clarith1**) did not stimulate any detectable levels. Control particle **10 (Tolyl)** did not elicit a detectable response. Conjugates **4** (**Clarith2**), **7 (Azith1)**, and **8 (Azith2)** also induced significant arginase activity, seemingly indicative of a mixed activation state among these cell populations.

Conjugates **3 (Clarith1)** and **5 (TriKeto)** induced much lower but detectable levels of arginase activity; control molecules, including unconjugated particles (**10**; **Tolyl**), free macrolides and macrolide-modified dendrimers, stimulated no increase in arginase activity compared to the untreated cells (**Figure 6B**). Cytokine levels were screened and also did not correlate well with any known phenotype among macrophages treated with VLP-macrolide conjugates. Conjugates **3 (Clarith1)**, **4 (Clarith2)**, **5 (TriKeto)**, **7 (Azith1)**, and **8 (Azith2)** all stimulated significant production of TNF-α after 24 h relative to cells treated with conjugate **10 (Tolyl)**, free macrolides, or dendrimers (**Figure 7A)**. Interestingly, only conjugates **4 (Clarith2)** and **7 (Azith1)** stimulated significant production of IL-6, while conjugates **3 (Clarith1)**, **5 (TriKeto)**, and **8 (Azith2)** gave rise to levels that were notably diminished but still significant (**Figure 7B**). Macrophages treated with conjugates **3**-**9** also produced significant levels of IL-12 relative to control-treated cells, although the amount of IL-12 produced was significantly lower than that of other cytokines (**Figure 7C**). Despite the increased production of these cytotoxic molecules, macrophages treated with these conjugates did not exhibit killing activity against cancer cells, as was shown previously with macrolide-functionalized gold nanorods.[32] Interestingly, conjugates **3 (Clarith1)** and **4 (Clarith2)** gave rise to significant IL-10 production; conjugates **5 (TriKeto)**, **7 (Azith1)**, and **8 (Azith2)** all stimulated levels that were much lower but still higher than control-treated cells (**Figure 7D**). Production of IL-10 in conjunction with IL-6 and TNF-α has been observed with polarization towards the M2b subset;[42] however, it is likely that the polarization of these macrophage populations is highly dynamic, and that these cells experience phenotypic changes over time. It is possible that these cells are in an intermediary activation state

between the M1 and M2a phenotypes, which is consistent with their mixed phenotypic signatures and cytokine profiles.[43] Extensive investigations of this phenomenon will further elucidate the effect of these conjugates on macrophages.

*4.4.3. Trafficking of modified particles in mice*

Finally, we investigated the trafficking of dye-labeled VLPs modified with azithromycin (**Azith2; 9)** in mice to determine if attachment of the macrocycle could direct particles to tissues where the free macrolides are known to accumulate. Previous studies have shown that azithromycin accumulates in macrophages, leading to greater than 100-fold enrichment in the lungs and liver compared to circulation.[28–30] Indeed, we found that **9 (Azith2)** particles showed significant accumulation in lung tissue after 2 h compared to control particles (**10; Tolyl**), where no signal was detected after 2 h (**Figure 8A, C**). Qβ VLPs do not naturally traffic to the lung, indicating that the conjugated macrolide is directing particles to accumulate in lung-resident macrophages. Particles were also found in the livers of both cohorts after 2 h, with mice administered **9 (Azith2)** displaying significantly higher signal in tissue compared to mice administered **10** (**Tolyl; Figure 8A, D**). After 24 h, no signal could be detected in the lungs of mice from either cohort, and signals from the livers in both cohorts were equivalent (**Figure 8B**).

**4.5. Conclusions**

As there are several pathogenic organisms known to establish infections within pulmonary macrophages (i.e., *M. tuberculosis*, *L. pneumophila*),[11,12] intracellular drug delivery would be highly beneficial for the treatment of persistent lung infections. In this study, we demonstrated the ability of macrolide antibiotics to function as targeting ligands to direct a virus-like particle platform to the lungs for selective accumulation in

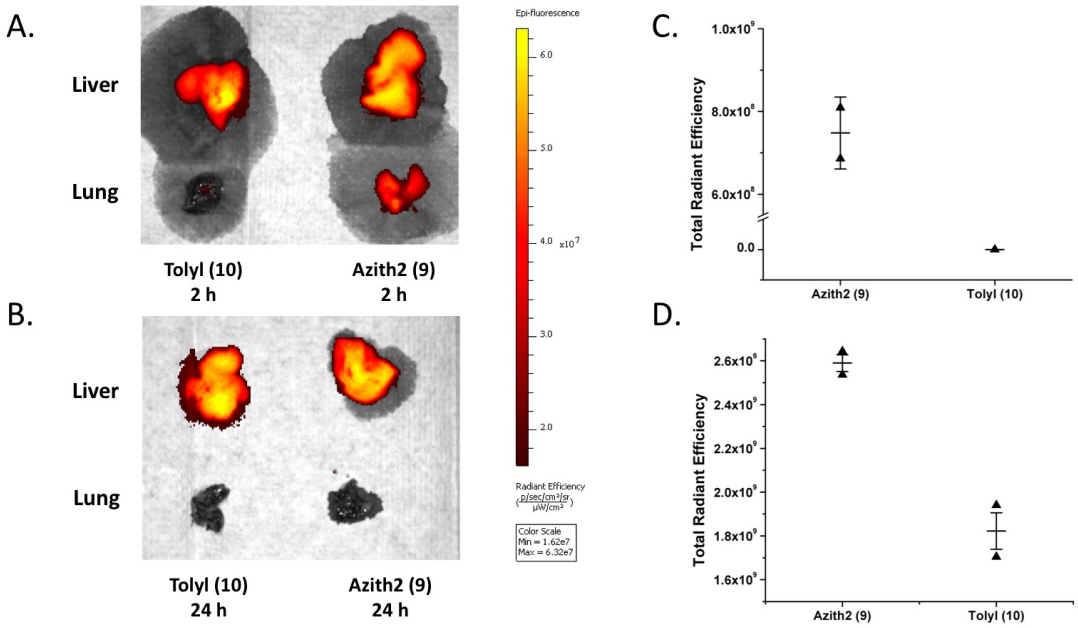


**Figure 8**. Quantitative imaging of Qβ-azithromycin conjugates trafficking to the lungs and liver. (**A**) Representative image of isolated liver (top) and lung tissue (bottom) from mice administered Qβ-azithromycin (**9**) or Qβ-tolyl (**10**) after 2 h. Image shows accumulation only in lungs for mice administered **9**. Azithromycin also promotes increased uptake in the liver relative to control particles. (**B**) Representative image of isolated liver (top) and lung tissue (bottom) from mice administered Qβ-azithromycin (**9**) or Qβ-tolyl (**10**) after 24 h. No fluorescence was detected in the lungs of mice from either cohort and fluorescence in the liver was equivalent. (**C**) Quantitative analysis ex vivo of lung tissue fluorescence 2 h after intravenous administration of **9** or **10**, respectively. (**D**) Quantitative analysis ex vivo of liver tissue fluorescence 2 h after intravenous administration of **9** or **10**, respectively.

pulmonary macrophages. Azithromycin promoted the highest uptake by macrophages *in vitro* among all of the ligands tested, and the uptake was found to be dependent on both the orientation of the macrolide on the particle surface as well as the density of surface coverage. These findings are consistent with the existence of an active transport system for macrolides in phagocytic cells[31] and also correlate with observations for P-gp-dependent trafficking in macrophages.[38] The differential responses in cellular uptake based on the attachment point to the macrocycle suggest that specific functional groups must be accessible for receptor engagement, and increased uptake corresponding to

macrolide density also suggests that specific ligand-receptor engagement is occurring. Investigations to further characterize the mechanism of uptake with the Qβ platform are ongoing. Furthermore, we found that the polyvalent display of macrolides on the surface of Qβ VLPs potentiates macrophage activation with metabolic and cytokine signatures that do not wholly match any of the canonical activation states.[40] Activation and polarization were not observed with the treatment of free macrolides; display on a dendrimer scaffold, albeit at lower valency; or with Qβ bearing a tolyl group. This stands in contrast to the earlier report by Dreaden and colleagues showing that macrolide-functionalized gold nanorods stimulated a cytotoxic phenotype.[32] It should be noted, however, that the platforms from that study were modified with ~ 1000 macrolides, significantly higher than the degrees of functionalization achieved in this work. Given the disparity in both loadings and platform properties, it is unclear whether macrophage activation is potentiated solely by polyvalent display of macrolides or if uptake of the display platform is governing these phenomena. Further studies are ongoing to investigate the factors governing macrophage activation in this context. Most importantly, we found that polyvalent display of azithromycin on the VLP surface directs particles to pulmonary macrophages within a few hours of administration, which could allow Qβ VLPs to be used as drug delivery agents for pulmonary infections. The conjugation of small molecule drugs to both the interior and exterior of VLPs has been well-documented,[44–46] and efforts to screen delivery of these Qβ-macrolide conjugates to patient-derived macrophages are currently ongoing with the hopes of transitioning this platform towards clinical applications. To our knowledge, this is the first example of a macrolide-nanoparticle conjugate being applied for cellular targeting *in vivo* and

represents potential for the development of a novel pulmonary drug delivery platform. This work further exemplifies the diverse modification strategies that can be employed for the development of targeted VLP platforms, particularly if a motif accessible by gene engineering is not available.

### 4.6. References


(1) Chames, P.; Baty, D. Antibody Engineering and Its Applications in Tumor Targeting and Intracellular Immunization. *FEMS Microbiology Letters*, 2000, *189*, 1–8.

(2) Hamakubo, T.; Kusano-Arai, O.; Iwanari, H. Generation of Antibodies against Membrane Proteins. *Biochim. Biophys. Acta - Proteins Proteomics* **2014**, *1844*, 1920–1924.

(3) Forsström, B.; Bisławska Axnäs, B.; Rockberg, J.; Danielsson, H.; Bohlin, A.; Uhlen, M. Dissecting Antibodies with Regards to Linear and Conformational Epitopes. *PLoS One* **2015**, *10*.

(4) Destito, G.; Yeh, R.; Rae, C. S.; Finn, M. G.; Manchester, M. Folic Acid-Mediated Targeting of Cowpea Mosaic Virus Particles to Tumor Cells. *Chem. Biol.* **2007**, *14*, 1152–1162.

(5) Banerjee, R.; Tyagi, P.; Li, S.; Huang, L. Anisamide-Targeted Stealth Liposomes: A Potent Carrier for Targeting Doxorubicin to Human Prostate Cancer Cells. *Int. J. Cancer* **2004**, *112*, 693–700.

(6) Sanhueza, C. A.; Baksh, M. M.; Thuma, B.; Roy, M. D.; Dutta, S.; Préville, C.; Chrunyk, B. A.; Beaumont, K.; Dullea, R.; Ammirati, M.; *et al.* Efficient Liver Targeting by Polyvalent Display of a Compact Ligand for the Asialoglycoprotein Receptor. *J. Am. Chem. Soc.* **2017**, *139*, 3528–3536.

(7) Cruz, L. J.; Tacken, P. J.; Pots, J. M.; Torensma, R.; Buschow, S. I.; Figdor, C. G. Comparison of Antibodies and Carbohydrates to Target Vaccines to Human Dendritic Cells via DC-SIGN. *Biomaterials* **2012**, *33*, 4229–4239.

(8) Wynn, T. A.; Chawla, A.; Pollard, J. W. Macrophage Biology in Development, Homeostasis and Disease. *Nature* **2013**, *496*, 445–455.

(9) Morales-Nebreda, L.; Misharin, A. V; Perlman, H.; Budinger, G. R. S. The Heterogeneity of Lung Macrophages in the Susceptibility to Disease. *Eur. Respir. Rev.* **2015**, *24*, 505.

(10) Martin, T. R.; Frevert, C. W. Innate Immunity in the Lungs. *Proc. Am. Thorac. Soc.* **2005**, *2*, 403–411.

(11) Daniel, T. M. The History of Tuberculosis. *Respir. Med.* **2006**, *100*, 1862–1870.

(12) Phin, N.; Parry-Ford, F.; Harrison, T.; Stagg, H. R.; Zhang, N.; Kumar, K.; Lortholary, O.; Zumla, A.; Abubakar, I. Epidemiology and Clinical Management of Legionnaires' Disease. *Lancet Infect. Dis.* **2014**, *14*, 1011–1021.

(13) Mitchell, G.; Chen, C.; Portnoy, D. A. Strategies Used by Bacteria to Grow in Macrophages. *Microbiol. Spectr.* **2016**, *4*, 10.1128/microbiolspec.MCHD-0012-2015.

(14) Lee, W.-H.; Loo, C.-Y.; Traini, D.; Young, P. M. Nano- and Micro-Based Inhaled Drug Delivery Systems for Targeting Alveolar Macrophages. *Expert Opin. Drug Deliv.* **2015**, *12*, 1009–1026.

(15) Gagliardi, M. Biomimetic and Bioinspired Nanoparticles for Targeted Drug Delivery. *Ther. Deliv.* **2017**, *8*, 289–299.

(16) Abedin, M. J.; Liepold, L.; Suci, P.; Young, M.; Douglas, T. Synthesis of a Crosslinked Branched Polymer Network in the Interior of a Protein Cage. *J. Am. Chem. Soc.* **2009**, *131*, 4346–4354.

(17) Maassen, S. J.; van der Ham, A. M.; Cornelissen, J. J. L. M. Combining Protein Cages and Polymers: From Understanding Self-Assembly to Functional Materials. *ACS Macro Lett.* **2016**, *5*, 987–994.

(18) Galaway, F. A.; Stockley, P. G. MS2 Viruslike Particles: A Robust, Semisynthetic Targeted Drug Delivery Platform. *Mol. Pharm.* **2013**, *10*, 59–68.

(19) Chen, Z.; Li, N.; Chen, L.; Lee, J.; Gassensmith, J. J. Dual Functionalized Bacteriophage Qβ as a Photocaged Drug Carrier. *Small* **2016**, *12*, 4563–4571.

(20) Caldeira, J. C.; Peabody, D. S. Thermal Stability of RNA Phage Virus-Like Particles Displaying Foreign Peptides. *J. Nanobiotechnology* **2011**, *9*, 22.

(21) Ashcroft, A. E.; Lago, H.; Macedo, J. M. B.; Horn, W. T.; Stonehouse, N. J.; Stockley, P. G. Engineering Thermal Stability in RNA Phage Capsids via Disulphide Bonds. *J Nanosci Nanotechnol* **2005**, *5*, 2034–2041.

(22) Johnson, H. R.; Hooker, J. M.; Francis, M. B.; Clark, D. S. Solubilization and Stabilization of Bacteriophage MS2 in Organic Solvents. *Biotechnol. Bioeng.* **2007**, *97*, 224–234.

(23) Rhee, J.-K.; Baksh, M.; Nycholat, C.; Paulson, J. C.; Kitagishi, H.; Finn, M. G.

Glycan-Targeted Virus-like Nanoparticles for Photodynamic Therapy. *Biomacromolecules* **2012**, *13*, 2333–2338.

(24) Hovlid, M. L.; Lau, J. L.; Breitenkamp, K.; Higginson, C. J.; Laufer, B.; Manchester, M.; Finn, M. G. Encapsidated Atom-Transfer Radical Polymerization in Qbeta Virus-like Nanoparticles. *ACS Nano* **2014**, *8*, 8003–8014.

(25) Pokorski, J. K.; Breitenkamp, K.; Liepold, L. O.; Qazi, S.; Finn, M. G. Functional Virus-Based Polymer-Protein Nanoparticles by Atom Transfer Radical Polymerization. *J. Am. Chem. Soc.* **2011**, *133*, 9242–9245.

(26) Fiedler, J. D.; Brown, S. D.; Lau, J.; Finn, M. G. RNA-Directed Packaging of Enzymes within Virus-Like Particles. *Angew. Chemie Int. Ed.* **2010**, *49*, 9648–9651.

(27) Ashley, C. E.; Carnes, E. C.; Phillips, G. K.; Durfee, P. N.; Buley, M. D.; Lino, C. A.; Padilla, D. P.; Phillips, B.; Carter, M. B.; Willman, C. L.; *et al.* Cell-Specific Delivery of Diverse Cargos by Bacteriophage MS2 Virus-like Particles. *ACS Nano* **2011**, *5*, 5729–5745.

(28) Hand, W. L.; Hand, D. L. Characteristics and Mechanisms of Azithromycin Accumulation and Efflux in Human Polymorphonuclear Leukocytes. *Int. J. Antimicrob. Agents* **2001**, *18*, 419–425.

(29) Steel, H. C.; Theron, A. J.; Cockeran, R.; Anderson, R.; Feldman, C. Pathogen- and Host-Directed Anti-Inflammatory Activities of Macrolide Antibiotics. *Mediators of Inflammation*, 2012, *2012*.

(30) Wildfeuer, A.; Laufen, H.; Zimmermann, T. Uptake of Azithromycin by Various Cells and Its Intracellular Activity under in Vivo Conditions. *Antimicrob. Agents Chemother.* **1996**, *40*, 75–79.

(31) Bosnar, M.; Kelnerić, Ž.; Munić, V.; Eraković, V.; Parnham, M. J. Cellular Uptake and Efflux of Azithromycin, Erythromycin, Clarithromycin, Telithromycin, and Cethromycin. *Antimicrob. Agents Chemother.* **2005**, *49*, 2372–2377.

(32) Dreaden, E. C.; Mwakwari, S. C.; Austin, L. A.; Kieffer, M. J.; Oyelere, A. K.; El-Sayed, M. A. Small Molecule-Gold Nanorod Conjugates Selectively Target and Induce Macrophage Toxicity towards Breast Cancer Cells. *Small* **2012**, *8*, 2819–2822.

(33) Bartneck, M.; Keul, H. A.; Singh, S.; Czaja, K.; Bornemann, J.; Bockstaller, M.; Moeller, M.; Zwadlo-Klarwasser, G.; Groll, J. Rapid Uptake of Gold Nanorods by Primary Human Blood Phagocytes and Immunomodulatory Effects of Surface Chemistry. *ACS Nano* **2010**, *4*, 3073–3086.

(34) Cho, W. S.; Cho, M.; Jeong, J.; Choi, M.; Cho, H. Y.; Han, B. S.; Kim, S. H.; Kim, H. O.; Lim, Y. T.; Chung, B. H.; *et al.* Acute Toxicity and Pharmacokinetics of 13 Nm-Sized PEG-Coated Gold Nanoparticles. *Toxicol. Appl. Pharmacol.* **2009**, *236*, 16–24.

(35) Pokorski, J. K.; Hovlid, M. L.; Finn, M. G. Cell Targeting with Hybrid Qb Virus-Like Particles Displaying Epidermal Growth Factor. *ChemBioChem* **2011**, *12*, 2441–2447.

(36) Rhee, J.-K.; Hovlid, M. L.; Fiedler, J. D.; Brown, S. D.; Manzenrieder, F.; Kitagishi, H.; Nycholat, C.; Paulson, J. C.; Finn, M. G. Colorful Virus-like Particles: Fluorescent Protein Packaging by the QB Capsid. *Biomacromolecules* **2011**, *12*, 3977–3981.

(37) Golmohammadi, R.; Fridborg, K.; Bundule, M.; Valegard, K.; Liljas, L. The Crystal Structure of Bacteriophage QB at 3.5A Resolution. *Structure* **1996**, *4*, 543–554.

(38) Dreaden, E. C.; Raji, I. O.; Austin, L. A.; Fathi, S.; Mwakwari, S. C.; Humphries IV, W. H.; Kang, B.; Oyelere, A. K.; El-Sayed, M. A. P-Glycoprotein-Dependent Trafficking of Nanoparticle-Drug Conjugates. *Small* **2014**, *10*, 1719–1723.

(39) Raub, T. J. P-Glycoprotein Recognition of Substrates and Circumvention through Rational Drug Design. *Mol. Pharm.* **2006**, *3*, 3–25.

(40) Martinez, F. O.; Gordon, S. The M1 and M2 Paradigm of Macrophage Activation: Time for Reassessment. *F1000Prime Rep.* **2014**, *6*.

(41) Mosser, D. M.; Edwards, J. P. Exploring the Full Spectrum of Macrophage Activation. *Nat. Rev. Immunol.* **2008**, *8*, 958–969.

(42) Weagel, E.; Smith, C.; Liu, P. G.; Robinson, R.; O'Neill, K. Macrophage Polarization and Its Role in Cancer. *J. Clin. Cell. Immunol.* **2015**, *6*, 4–11.

(43) Melton, D. W.; McManus, L. M.; Gelfond, J. A. L.; Shireman, P. K. Temporal Phenotypic Features Distinguish Polarized Macrophages in Vitro. *Autoimmunity* **2015**, *48*, 161–176.

(44) Aljabali, A. A. A.; Shukla, S.; Lomonossoff, G. P.; Steinmetz, N. F.; Evans, D. J. CPMV-DOX Delivers. *Mol. Pharm.* **2013**, *10*, 3–10.

(45) Galaway, F. A.; Stockley, P. G. MS2 Viruslike Particles: A Robust, Semisynthetic Targeted Drug Delivery Platform. *Mol. Pharm.* **2013**, *10*, 59–68.

(46) Czapar, A. E.; Steinmetz, N. F. Plant Viruses and Bacteriophages for Drug Delivery in Medicine and Biotechnology. *Curr. Opin. Chem. Biol.* **2017**, *38*, 108–

116.

# Chapter 5: Investigating the immune response to hybrid protein-polymer VLPs

## 5.1. Abstract

Covalent attachment of polymeric species to the surface of proteins and nanoparticles has proven to be a critical aspect in the development of effective biomedical platforms capable of avoiding immune surveillance. The most widely-employed polymer for these applications has been poly(ethylene glycol) (PEG), yet recent evidence has suggested that more advanced polymer architectures significantly improve the *in vitro* and *in vivo* properties of protein-polymer hybrid materials. Moreover, there has been limited research directly investigating the performance of PEG against these more advanced polymer architectures. In this work, we describe the assembly and characterization of a series of virus-like particle (VLP)-polymer conjugates (poly(oligo(ethylene glycol) methacrylate) and poly(methacrylamido glucopyranose)), and the subsequent investigation of their ability to shield from antibody recognition as functions of polymer loading density, polymer chain length, polymer architecture, and conjugation site. Increasing chain length and loading density were both found to significantly diminish antibody recognition of the VLP conjugates; the conformation adopted by different polymer architectures was also found to greatly influence antibody recognition. A direct comparison of these conjugates against PEGylated VLPs *in vivo* showed that all formulations gave rise to similar antibody titers that were significantly diminished relative to unmodified particles. Interestingly, the quality of the antibody response was impacted by the properties of the conjugate, with differences in observed affinity and avidity showing a complex dependence on loading density, chain length, and architecture.

## 5.2. Introduction

The covalent attachment of hydrophilic polymer chains to the surface of biomolecules and nanoparticles has allowed for the development of hybrid macromolecular assemblies with unique properties that are finding increased use in the field of biomedicine.[1–4] Conjugation of linear poly(ethylene glycol) (PEG) has been widely used to dampen the immunogenicity of proteins and other materials,[5,6] and all of the protein-polymer hybrid drugs currently approved by the FDA are PEGylated conjugates.[7] Furthermore, attachment of polymers has also been shown to improve the circulation lifetime of proteins, which is a critical factor for advancing protein-based therapeutics into the clinic.[8–10] Protein-polymer hybrids are typically generated using either "graft-to"[11,12] or "graft-from"[13,14] methodologies. The former relies on the total synthesis of the desired polymer prior to conjugation,[15] while the latter involves direct growth of the polymer chain from the protein surface after installation of an initiator moiety.[16,17] While the "graft-from" approach offers high yielding reactions, grafting a preformed polymer onto a protein often allows for a more defined material as the polymer can be more readily characterized prior to attachment. Coverage of the polymer on the biomolecule is often lower, however, due to the inherent difficulty of covalently ligating two large molecules at relatively low concentrations.[11]

Recent examples in the literature indicate that advanced polymer architectures provide significant advantages at protecting and stabilizing conjugate proteins and reducing clearance rates compared to linear PEG chains.[18–21] Controlled radical polymerizations (CRPs), such as atom-transfer radical polymerization (ATRP) and reversible-addition fragmentation chain-transfer (RAFT), typically yield polymers with

brush-type architectures and are commonly employed methodologies in the development of protein-polymer materials due to their compatibility with aqueous conditions.[17,22–24] Brush polymer architectures have recently been shown to impart greater shielding capabilities than linear PEG when conjugated to the model therapeutic protein L-asparaginase,[25] exemplifying the impact of polymer architecture on the biomedical properties of protein-polymer materials.

In addition to polymer architecture, several other structural features of conjugate assembly have also been shown to influence recognition by the immune system. Rats administered PEGylated adenovirus developed significantly lower immunoglobulin levels with increasing degrees of polymer modification, resulting in improved efficacy for therapeutic applications.[26] Furthermore, the chain length of the conjugate polymers has been shown to influence the immune response against protein-based therapeutics. Cowpea mosaic virus (CPMV) was modified with PEG, and cellular uptake was found to be significantly inhibited with increasing molecular weight of the PEG chains.[27] Despite these and other numerous reports investigating different factors governing the immune response to protein-polymer conjugates, to our knowledge there has not been a comprehensive study examining all of these components on a singular platform.

Icosahedral virus-like particles (VLPs) represent emerging platforms for applications in biomedicine ranging from drug delivery and imaging to vaccine development.[28–31] Their structural stability, monodispersity, and periodicity make them ideal for the development of well-defined delivery vehicles using a variety of different chemical modifications.[32,33] In addition to modifying the particle surface, the interior of VLPs has also been addressed for the packaging of drugs,[34] therapeutic proteins,[35,36] and

polymers[37,38] for different biomedical applications. Despite these extensive efforts in developing VLPs as therapeutics, recognition by the immune system remains a significant hindrance towards implementing VLPs in clinical applications. Due to their size and repetitive organization, VLPs are readily recognized by components of both the innate and adaptive immune system,[39] which limits the efficacy of repetitive treatment regimens. However, cellular uptake and protein-protein interactions involved in these processes can be mitigated by the covalent attachment of polymeric species to the particle surface.

The immune response against protein-polymer hybrids is likely influenced by a combination of factors relating to the global structure and composition of the conjugate hybrid material. Prior research efforts have focused on evaluating a single aspect of these structures (i.e., density, chain length, conformation) rather than simultaneously investigating all of these factors. This study describes the investigation of all of these aspects using a series of polymers conjugated to VLPs derived from the bacteriophage Qβ, a 28-nm particle with well-defined structure known to atomic resolution.[40] In addition, we directly compared structural features of these conjugates to PEGylated VLPs by assessing their ability to block antibody recognition. We further investigated the performance of these materials *in vivo*, and we found that their ability to shield particles from the immune system was on par with that of PEGylated conjugates. Surprisingly, despite eliciting similar IgG titers, the quality of the antibody response was impacted by the structural organization and composition of the polymer conjugates. This data represents the first comprehensive evaluation of structural features in a defined set of protein-polymer materials and how those features impact protein-protein interactions and recognition by the immune system. Furthermore, these data suggest that more advanced polymer architectures rival PEG with

respect to immunological shielding and could serve in the development of biomedical materials with novel properties without sacrificing *in vivo* performance.

## 5.3. Materials and Methods

*Protein purification and characterization*

The Qβ VLPs were prepared as described in previously published protocols.[41] Briefly, chemically competent BL21(DE3) *E. coli* cells were transformed with pET28 vector harboring the viral coat protein (CP) gene. Cells were plated on selective SOB agar and grown overnight. After 24 h, a single colony was selected for inoculation into SOB media (25 mL; $Kan^+$) for overnight outgrowth at 37°C. Cultures were diluted into selective SOB media (500 mL; $Kan^+$) the following day and maintained at 37°C until mid-log phase growth was achieved ($O.D._{600} \sim 0.9$). Protein expression was subsequently induced by the addition of IPTG to a final concentration of 1 mM, and cultures were maintained at 30°C for 16 h. Cells were harvested by centrifugation at 6,000 rpm for 10 min, and pellets were suspended in 1x TBS for lysis using a probe sonicator (10 min total, 75 W, 5 sec intervals) in an ice bath. Lysates were clarified by centrifugation at 14,000 rpm for 10 min, and VLPs precipitated from the collected supernatant by the addition of 30% $(NH_4)_2SO_4$ (w/v) at 4°C for 1 h. Precipitate was pelleted by centrifugation at 14,000 rpm for 10 min, and the resulting pellet was dissolved in 1x TBS. Proteins were extracted from lipids and aggregates with *n*-BuOH:$CHCl_3$ (1:1; v/v) and subsequent centrifugation at 14,000 rpm for 10 min. The aqueous phase was collected and loaded onto 10-40% sucrose density gradients, where VLPs were further purified by centrifugation at 28,000 rpm for 4 h. VLPs were isolated from gradient via syringe and pelleted by centrifugation at 68,000 rpm for 2 h. Pellets were dissolved in 0.1M $KPO_4$ buffer and subsequently characterized.

Protein concentration of all VLP samples was determined by Bradford assay with BSA as standards. Samples were characterized by FPLC size-exclusion chromatography (Superose 6 10/300 GL) monitored by absorbance at 280 nm, dynamic light scattering (Wyatt Dynapro plate reader), and mass spectrometry (Agilent 6230B TOF LC/MS). All conjugations were performed, and products characterized as described in subsequent sections.

*VLP-polymer conjugate synthesis*

Qβ-$(PEG_4\text{-}N_3)_{600}$: A solution of wild-type Qβ VLPs (0.2 mL from 25 mg/mL stock solution in 0.1M $KPO_4$, pH 7.4, 0.352 μmol subunit, 1.41 μmol reactive amines) was diluted with 660 μL 0.1M $KPO_4$ and cooled in an ice bath. To this solution was added 140 μL NHS-$PEG_4\text{-}N_3$ (100 mM stock solution in DMSO, ~ 10 equiv per reactive amine). The tube was gently inverted to mix reagents and incubated for 16 h at 4°C. Particles were purified using PD-10 prepacked Sephadex columns (GE Healthcare) according to manufacturer's instructions. Particles were further concentrated to 5.2 mg/mL using Amicon Ultra-4 centrifugal filters with 100 kDa molecular weight cutoff. The degree of acylation was quantified by ESI-TOF analysis (600 per particle, 3.3 per subunit).

Qβ-POEGMA13-L: A solution of Qβ-$(PEG_4\text{-}N_3)_{600}$ (25 μL from 7.3 mg/mL stock solution in 0.1M $KPO_4$, pH 7.4, 12.9 nmol subunit, 42.5 nmol reactive azide) was diluted with 3.33 μL 0.1M $KPO_4$. To this solution was added 10 μL of **3** (300 mg/mL in DMSO; 0.2 equiv per reactive azide). The tube was gently inverted to create a homogenous solution. Subsequently, 2.2 μL of 100 mM $CuSO_4$ (5 equiv to azide) and 22 μL of 100 mM THPTA (50 equiv to azide) were added in a single portion, followed by the addition of 6.5 μL of 200 mM aminoguanidine (30 equiv to azide). The tube was again gently inverted to mix

all components and the reaction was initiated by the addition of 2.6 μL of 500 mM sodium ascorbate (30 equiv to azide). After mixing, the reaction was incubated at 50°C for 16 h. The reaction mixture was purified by centrifugal filtration against 0.1M $KPO_4$ using Amicon Ultra-4 centrifugal filters with 100 kDa MWCO and concentrated to 2.5 mg/mL. The sample was filtered through a 0.22 μm PTFE sterile syringe filter, and the total protein content was quantified by Bradford assay using BSA standards. Recovery of protein was approximately 95%. The extent of modification was determined by SEC-MALS analysis and NAGE; the final modified particles were composed of >95% intact particles as determined by DLS and FPLC analysis.

Qβ-POEGMA13-M: A solution of Qβ-$(PEG_4\text{-}N_3)_{600}$ (25 μL from 7.3 mg/mL stock solution in 0.1M $KPO_4$, pH 7.4, 12.9 nmol subunit, 42.5 nmol reactive azide) was diluted with 3.33 μL 0.1M $KPO_4$. To this solution was added 6.7 mg of **3** dissolved in 10 μL DMSO (2 equiv per reactive azide). The tube was gently inverted to create a homogenous solution. Subsequently, 2.2 μL of 100 mM $CuSO_4$ (5 equiv to azide) and 22 μL of 100 mM THPTA (50 equiv to azide) were added in a single portion, followed by the addition of 6.5 μL of 200 mM aminoguanidine (30 equiv to azide). The tube was again gently inverted to mix all components and the reaction was initiated by the addition of 2.6 μL of 500 mM sodium ascorbate (30 equiv to azide). After mixing, the reaction was incubated at 50°C for 16 h. The reaction mixture was purified by centrifugal filtration against 0.1M $KPO_4$ using Amicon Ultra-4 centrifugal filters with 100 kDa MWCO and concentrated to 2.5 mg/mL. The sample was filtered through a 0.22 μm PTFE sterile syringe filter, and the total protein content was quantified by Bradford assay using BSA standards. Recovery of protein was approximately 95%. The extent of modification was determined by SEC-MALS analysis

and NAGE; the final modified particles were composed of >95% intact particles as determined by DLS and FPLC analysis.

Qβ-POEGMA13-H: A solution of Qβ-$(PEG_4\text{-}N_3)_{600}$ (192 μL from 5.2 mg/mL stock solution in 0.1M $KPO_4$, pH 7.4, 70.3 nmol subunit, 0.232 μmol reactive azide) was diluted with 3.33 μL 0.1M $KPO_4$. To this solution was added 13.3 mg of **3** dissolved in 100 μL DMSO (4.3 equiv per reactive azide). The tube was gently inverted to create a homogenous solution. Subsequently, 11.9 μL of 100 mM $CuSO_4$ (5 equiv to azide) and 59.5 μL of 100 mM THPTA (25 equiv to azide) were added in a single portion, followed by the addition of 33.25 μL of 200 mM aminoguanidine (30 equiv to azide). The tube was again gently inverted to mix all components and the reaction was initiated by the addition of 66.5 μL of 100 mM sodium ascorbate (30 equiv to azide). After mixing, the reaction was incubated at 50°C for 16 h. The reaction mixture was purified by centrifugal filtration against 0.1M $KPO_4$ using Amicon Ultra-4 centrifugal filters with 100 kDa MWCO and concentrated to 1.3 mg/mL. The sample was filtered through a 0.22 μm PTFE sterile syringe filter, and the total protein content was quantified by Bradford assay using BSA standards. Recovery of protein was approximately 95%. The extent of modification was determined by SEC-MALS analysis, and the final modified particles were composed of >95% intact particles as determined by DLS and FPLC analysis.

Qβ-POEGMA38: A solution of Qβ-$(PEG_4\text{-}N_3)_{600}$ (192 μL from 5.2 mg/mL stock solution in 0.1M $KPO_4$, pH 7.4, 70.3 nmol subunit, 0.232 μmol reactive azide) was diluted with 36.6 μL 0.1M $KPO_4$. To this solution was added 27.2 mg of **4** dissolved in 100 μL DMSO (4.3 equiv per reactive azide). The tube was gently inverted to create a homogenous solution. Subsequently, 11.9 μL of 100 mM $CuSO_4$ (5 equiv to azide) and 59.5 μL of 100

mM THPTA (25 equiv to azide) were added in a single portion, followed by the addition of 33.25 μL of 200 mM aminoguanidine (30 equiv to azide). The tube was again gently inverted to mix all components and the reaction was initiated by the addition of 66.5 μL of 100 mM sodium ascorbate (30 equiv to azide). After mixing, the reaction was incubated at 50°C for 16 h. The reaction mixture was purified by centrifugal filtration against 0.1M $KPO_4$ using Amicon Ultra-4 centrifugal filters with 100 kDa MWCO and concentrated to 1 mg/mL. The sample was filtered through a 0.22 μm PTFE sterile syringe filter, and the total protein content was quantified by Bradford assay using BSA standards. Recovery of protein was approximately 95%. The extent of modification was determined by SEC-MALS analysis, and the final modified particles were composed of >95% intact particles as determined by DLS and FPLC analysis.

Qβ-POEGMA57: A solution of Qβ-$(PEG_4\text{-}N_3)_{600}$ (192 μL from 5.2 mg/mL stock solution in 0.1M $KPO_4$, pH 7.4, 70.3 nmol subunit, 0.232 μmol reactive azide) was diluted with 36.6 μL 0.1M $KPO_4$. To this solution was added 40.0 mg of **5** dissolved in 100 μL DMSO (4.3 equiv per reactive azide). The tube was gently inverted to create a homogenous solution. Subsequently, 11.9 μL of 100 mM $CuSO_4$ (5 equiv to azide) and 59.5 μL of 100 mM THPTA (25 equiv to azide) were added in a single portion, followed by the addition of 33.25 μL of 200 mM aminoguanidine (30 equiv to azide). The tube was again gently inverted to mix all components and the reaction was initiated by the addition of 66.5 μL of 100 mM sodium ascorbate (30 equiv to azide). After mixing, the reaction was incubated at 50°C for 16 h. The reaction mixture was purified by centrifugal filtration against 0.1M $KPO_4$ using Amicon Ultra-4 centrifugal filters with 100 kDa MWCO and concentrated to 1.2 mg/mL. The sample was filtered through a 0.22 μm PTFE sterile syringe filter, and the

total protein content was quantified by Bradford assay using BSA standards. Recovery of protein was approximately 95%. The extent of modification was determined by SEC-MALS analysis, and the final modified particles were composed of >95% intact particles as determined by DLS and FPLC analysis.

Qβ-PMAG: A solution of Qβ-$(PEG_4\text{-}N_3)_{600}$ (192 μL from 5.2 mg/mL stock solution in 0.1M $KPO_4$, pH 7.4, 70.3 nmol subunit, 0.232 μmol reactive azide) was diluted with 36.6 μL 0.1M $KPO_4$. To this solution was added 13.5 mg of **6** dissolved in 100 μL DMSO (4 equiv per reactive azide). The tube was gently inverted to create a homogenous solution. Subsequently, 11.9 μL of 100 mM $CuSO_4$ (5 equiv to azide) and 59.5 μL of 100 mM THPTA (25 equiv to azide) were added in a single portion, followed by the addition of 33.25 μL of 200 mM aminoguanidine (30 equiv to azide). The tube was again gently inverted to mix all components and the reaction was initiated by the addition of 66.5 μL of 100 mM sodium ascorbate (30 equiv to azide). After mixing, the reaction was incubated at 50°C for 16 h. The reaction mixture was purified by centrifugal filtration against 0.1M $KPO_4$ using Amicon Ultra-4 centrifugal filters with 100 kDa MWCO and concentrated to 2 mg/mL. The sample was filtered through a 0.22 μm PTFE sterile syringe filter, and the total protein content was quantified by Bradford assay using BSA standards. Recovery of protein was approximately 95%. The extent of modification was determined by SEC-MALS analysis, and the final modified particles were composed of >95% intact particles as determined by DLS and FPLC analysis.

Qβ-mPEG: A solution of Qβ-$(PEG_4\text{-}N_3)_{600}$ (192 μL from 5.2 mg/mL stock solution in 0.1M $KPO_4$, pH 7.4, 70.3 nmol subunit, 0.232 μmol reactive azide) was diluted with 36.6 μL 0.1M $KPO_4$. To this solution was added 9.1 mg of **7** dissolved in 100 μL DMSO (4 equiv

per reactive azide). The tube was gently inverted to create a homogenous solution. Subsequently, 11.9 μL of 100 mM $CuSO_4$ (5 equiv to azide) and 59.5 μL of 100 mM THPTA (25 equiv to azide) were added in a single portion, followed by the addition of 33.25 μL of 200 mM aminoguanidine (30 equiv to azide). The tube was again gently inverted to mix all components and the reaction was initiated by the addition of 66.5 μL of 100 mM sodium ascorbate (30 equiv to azide). After mixing, the reaction was incubated at 50°C for 16 h. The reaction mixture was purified by centrifugal filtration against 0.1M $KPO_4$ using Amicon Ultra-4 centrifugal filters with 100 kDa MWCO and concentrated to 6.8 mg/mL. The sample was filtered through a 0.22 μm PTFE sterile syringe filter, and the total protein content was quantified by Bradford assay using BSA standards. Recovery of protein was approximately 85%. The extent of modification was determined by SEC-MALS analysis, and the final modified particles were composed of >95% intact particles as determined by DLS and FPLC analysis.

*SEC-MALS analysis*

Samples were diluted to 0.1 mg/mL in 0.1M $KPO_4$ buffer (pH 7.4) and injected onto a Superose 6 10/300 GL size exclusion column (GE Healthcare) using an Agilent HPLC to maintain a 0.4 mL/min flow rate during analysis. Samples were detected using a UV-Vis detector (Agilent), a Viscotek SEC-MALS 20 multi-angle light scattering detector (Malvern), and a Viscotek VE3580 refractometer (Malvern). The average molecular weight, $M_w$, was calculated with OmniSEC 5.0 software and plotted across the elution peak. The degree of modification for the polymer-labeled samples was related to the measured difference in $M_w$ between the sample and starting material divided by the average molecular weight of the respective polymer chain.

*Sandwich ELISA*

Anti-Qβ IgY (10 μg/mL) was plated overnight at 4°C. Plate was washed thrice with PBS-Tween 20 (0.05% Tween; PBST) and blocked with 3% BSA in PBST for 2 h at RT. Plate was aspirated and VLP-polymer conjugates were added in triplicate from 0.01-100 μg/mL and incubated for 1 h at RT. Plate was washed thrice with PBST and mouse anti-Qβ IgG monoclonal antibody (1:2500, Clone 5D6; Abbiotec, Inc.) incubated for 1 h at RT. Plate was washed thrice with PBST and anti-mouse IgG HRP-conjugate reporter antibody (1:2500; Pierce) incubated for 1 h at RT, followed by a final washing with PBST and development with TMB substrate (1-Step™ Ultra TMB; Thermo Fisher Scientific). Development was quenched by the addition of 1M $H_2SO_4$ and absorbance measured at 405 nm on microplate reader (Thermo Fisher Scientific).

*Mice and immunizations*

CD-1 IGS mice (8-12 weeks) were purchased from Charles River Laboratories and maintained in the animal facility of the Georgia Institute of Technology. All animal care and experimental procedures were approved by the Institutional Care and Use Committee of the Georgia Institute of Technology. Mice were administered 10 μg VLP-polymer conjugates via subcutaneous injection at days 0, 14, and 28. Blood was collected via submandibular bleed on days 7, 21, and 35 for serum analysis. Mice were maintained until day 70 for subsequent blood collection prior to sacrifice.

*ELISA analysis*

Qβ WT (1 μg/mL) was plated overnight at 4°C. Plate was washed thrice with PBST and blocked with 3% BSA in PBST for 2 h at RT. Serum dilutions were prepared in master plate using 3% BSA in PBST and added to assay plate to give final dilutions from 1:500-

1:128000, which were incubated for 1 h at RT. Plate was washed thrice with PBST and incubated with anti-mouse IgG HRP-conjugate reporter antibody (1:2500, Abbiotec, Inc.) for 1 h at RT. A final washing with PBST was followed by development with TMB substrate (1-Step™ Ultra TMB; Thermo Fisher Scientific) and quenching with 1M $H_2SO_4$. Absorbance was measured at 405 nm on a microplate reader (Thermo Fisher Scientific).

*Avidity ELISA*

Plates were prepared as described for standard ELISA analysis. After blocking with 3% BSA in PBST, serum was added to assay plate at a final dilution of 1:8000, which was incubated for 1 h at RT. Plate was washed thrice with PBST and incubated with increasing concentrations of NaSCN (0-5 M) in PBS for 15 min at RT. Plate was washed thrice and analysis continued as described for standard ELISA.

## 5.4. Results and Discussion

### *5.4.1. Conjugate synthesis and characterization*

To prepare protein-polymer hybrids from the icosahedral Qβ VLPs, a series of poly(oligo(ethylene glycol) methacrylate (POEGMA) and poly(methacrylamido glucopyranose) (PMAG) polymer chains (**3**-**6**) was prepared by RAFT polymerization as previously described.[42] The resulting polymers were found to be rather water-soluble and not detrimental to the stability of the protein nanoparticle upon covalent attachment. Each polymer was synthesized with a terminal alkyne to allow for conjugation to the VLP by the robust copper(I)-catalyzed azide-alkyne cycloaddition (CuAAC) reaction using the accelerating ligand **8** (THPTA).[43] The VLP, which bears a total of 720 amino groups on the surface, was acylated with a molar excess of *N*-hydroxysuccinimide ester **1**. After purification from the excess small molecule, the azidated VLP was addressed with

**Scheme 1:** Preparation of Qβ-polymer conjugates.

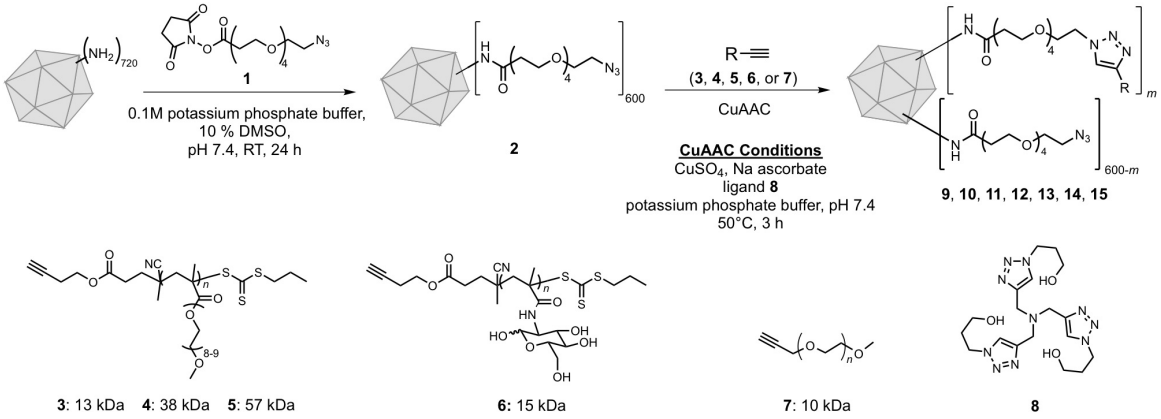


polymers **3-7** to yield conjugates **9-15**, respectively **(Scheme 1**). Heating of the reaction was found to be necessary in order to achieve reasonable levels of attachment to the VLP, presumably due to steric hindrance. The resulting conjugates were characterized by size exclusion chromatography coupled with multi-angle light scattering (SEC-MALS), which allowed for quantification of polymer labeling through calculation of the absolute molecular weight of the hybrid species. The Qβ conjugates were labeled with ~36, ~59, ~93, ~38, ~33, ~78, and ~92 chains to yield Qβ-POEGMA13-L, Qβ-POEGMA13-M, Qβ-POEGMA13-H, Qβ-POEGMA38, Qβ-POEGMA57, Qβ-PMAG, and Qβ-mPEG, respectively (**Table 1**). The alphabetic notation following POEGMA13 was used to denote conjugates with low, moderate, and high loadings of the same polymer chain. Despite variations in loading density, polymer chains were conjugated to VLPs at similar mass loadings for conjugates **11-15** (**Table 1**). The lower loadings observed with the higher molecular weight species were attributed to decreased reactivity of the larger polymers due to steric crowding, and higher loadings could not be achieved in significant yield.

The radius of gyration ($R_g$) for each conjugate was also calculated from SEC-MALS analysis and related to the conformation adopted by the polymer chains on the particle surface. For conjugates **9**, **12**, and **13**, the $R_g$ was measured at 18.9 nm, 22.1 nm,

**Table 1:** SEC-MALS analysis of Qβ-polymer conjugates

| Conjugate | Polymer | $M_n$ (Da) | $R_g$ (nm) | Modifications |
|---|---|---|---|---|
| **9** | Q$\beta$-POEGMA13-L | 3.40x10$^6$ | 18.9 | 36 |
| **10** | Q$\beta$-POEGMA13-M | 3.69x10$^6$ | 20.1 | 59 |
| **11** | Q$\beta$-POEGMA13-H | 4.12x10$^6$ | 18.1 | 93 |
| **12** | Q$\beta$-POEGMA38 | 4.35x10$^6$ | 22.1 | 38 |
| **13** | Q$\beta$-POEGMA57 | 4.79x10$^6$ | 23.0 | 33 |
| **14** | Q$\beta$-PMAG | 4.08x10$^6$ | 17.5 | 78 |
| **15** | Q$\beta$-mPEG | 3.84x10$^6$ | 18.2 | 92 |

and 23.0 nm, respectively; the contribution by the conjugate polymer chains scaled with the degree of polymerization ($N$) as $R_g \sim N^{0.47}$, indicative of more swollen polymer conformations.[44] Interestingly, there was a distinct change in $R_g$ with increasing degrees of modification for conjugates **9**-**11**, with $R_g$ increasing to 20.1 nm for conjugate **10** and contracting to 18.1 nm for conjugate **11**. Decreases in $R_g$ were even more pronounced for conjugates **14** (17.5 nm) and **15** (18.2 nm), with sizes scaling as $R_g \sim N^{0.31}$ and $R_g \sim N^{0.28}$, indicative of dense globular conformations. The decrease in $R_g$ observed for the most heavily modified VLPs (**11**, **14**, and **15**) suggests that the polymer chains may be interacting and associating into more tightly packed structures. This observation may extend to the free polymer chains in solution, as species with lower $R_g$ would exhibit decreased steric hindrance during conjugation and allow for a higher degree of modification.

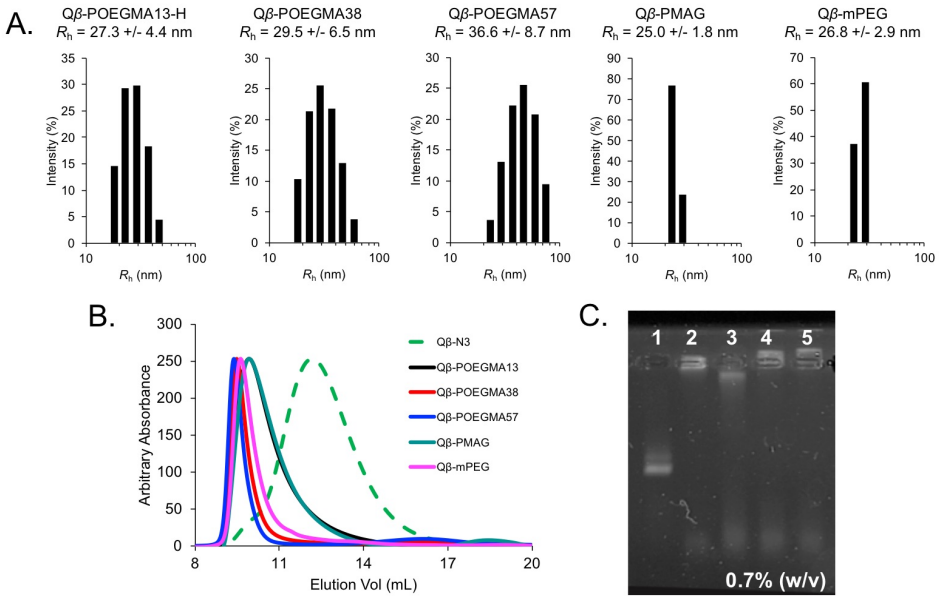


**Figure 1.** Characterization of Qβ-polymer conjugates. (**A**) DLS histograms of Qβ-polymer conjugates. Rh = hydrodynamic radius. (**B**) Comparative SEC traces of Qβ-polymer conjugates relative to starting material (**2**; dashed trace). (**C**) Native agarose gel (0.7 % w/v) of intact Qβ-polymer conjugates. Unmodified particles (lane 1) migrate into the gel because of the endogenous RNA packaged inside of the VLP during assembly; modified particles (lanes 2-5) show significantly hindered migration into the gel. Lane 1: Qβ-$PEG_4$-$N_3$; Lane 2: Qβ-PMAG; Lane 3: Qβ-POEGMA13-H; Lane 4: Qβ-POEGMA38; Lane 5: Qβ-POEGMA57. Gel stained with SYBR Safe Gel Stain.

Size-exclusion chromatography, dynamic light scattering, and gel electrophoretic analysis were all characteristic of intact hybrid particles for conjugates **9-15** (**Figure 1A-C**). Modified particles displayed significant increases in hydrodynamic radius from ~15 nm for unmodified Qβ VLPs to ~ 25-35 nm, with differences in radii between conjugates likely a result of the varying chain lengths and architectures. The hydrodynamic radii were noticeably larger than the radii of gyration obtained from SEC-MALS analysis, as $R_g$ is inherently dependent upon shape. All hybrid VLP conjugates displayed significant decreases in elution volume as measured by size-exclusion chromatography, indicative of larger molecular weight species (**Figure 1A,B**). Native agarose gel electrophoresis (NAGE) displayed significant retention of all modified species within the gel wells, while

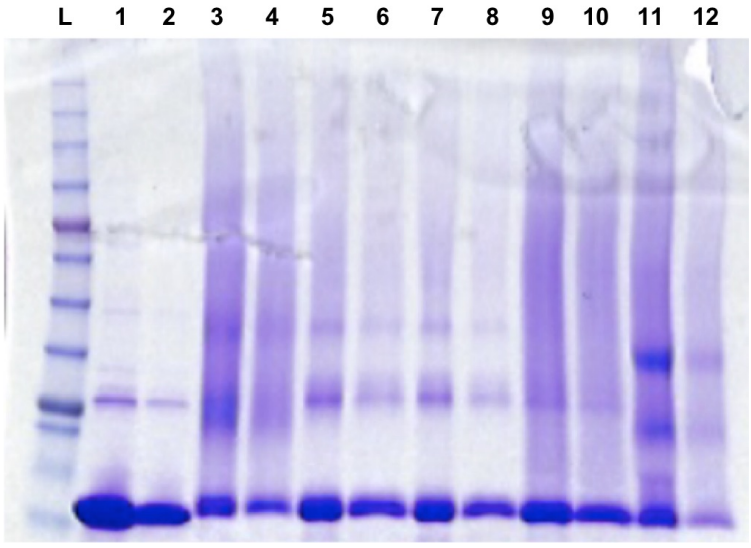


**Figure 2.** SDS-PAGE analysis of Qβ-polymer conjugates. L: ladder; Lanes 1-2: unmodified Qβ; Lanes 3-4: Qβ-POEGMA13-H; Lanes 5-6: Qβ-POEGMA38; Lanes 7-8: Qβ-POEGMA57; Lanes 9-10: Qβ-PMAG; Lanes 11-12: Qβ-mPEG. Even-numbered lanes loaded with 10 μg; odd-numbered lanes loaded with 5 μg. Gel stained with Coomassie Blue.

unmodified VLPs migrated farther into the gel as they were unhindered by the bulk of the conjugated chains (**Figure 1C**). Analysis by SDS-PAGE also showed distinct smearing of higher molecular weight species for all Qβ conjugates, which is typically observed for high molecular weight protein-polymer hybrids (**Figure 2**). To ensure that these observations were due to covalent attachment of polymer chains rather than nonspecific association with the particle surface, reaction mixtures of Qβ VLPs and polymers were incubated without the addition of a reducing agent to initiate the CuAAC reaction. Particles purified from these mixtures did not show an increase in hydrodynamic radius, and all displayed migration patterns in NAGE consistent with unmodified VLPs (**Figure 3A,B**).

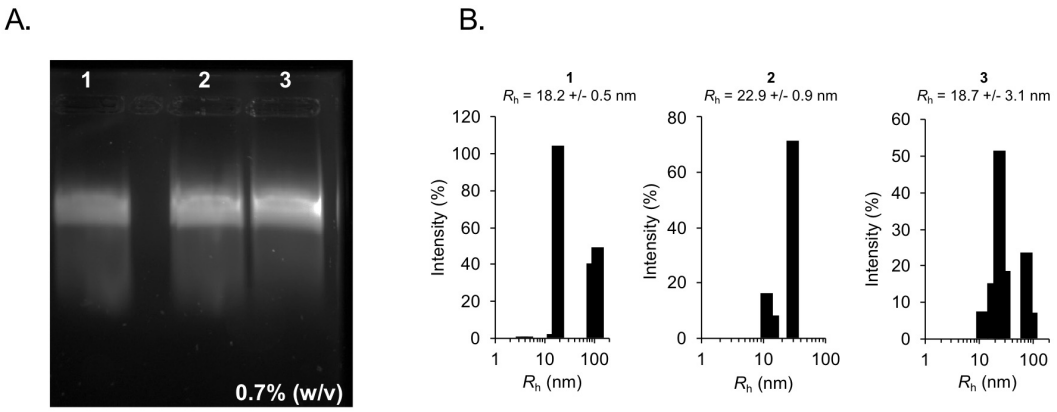


**Figure 3.** Analysis of POEGMA control reactions without addition of sodium ascorbate. Native agarose gel (0.7%) analysis (left) of POEGMA control reactions. Equivalent migration distance into gel indicates a lack of modification by polymer species. Gel stained with SYBR Safe Gel Stain. DLS histograms of POEGMA control reactions (right). Rh = hydrodynamic radius. Observed radii consistent with azidated VLP size. Sample 1: Qβ+ **3**; Sample 2: Qβ+**4**; Sample 3: Qβ+**5**.

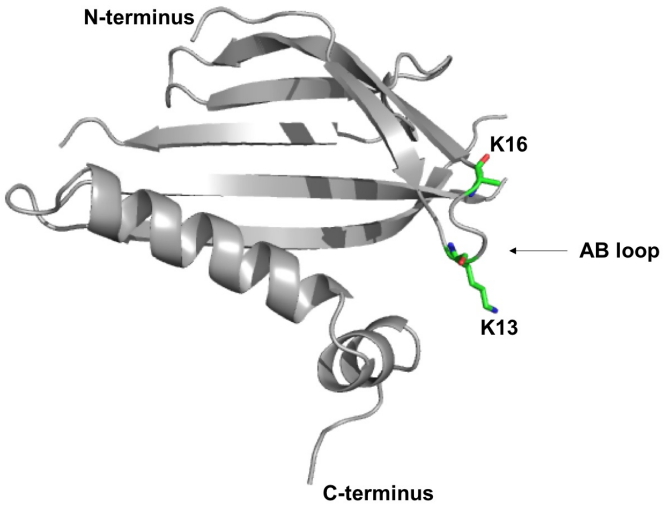


**Figure 4.** Cartoon representation of the Qβ coat protein monomer. The flexible AB loop is highlighted, and lysine residues 13 and 16 are shown in green. The side chain of lysine 16 is not resolved in the crystal structure. PDB ID: 1QBE.

*5.4.2. Assessment of conjugate properties on antibody binding*

We first chose to investigate the ability of the conjugated polymers to block recognition of the Qβ VLP by monoclonal antibodies generated against two different variants of the viral coat protein (wild-type and K13Q/K16Q). Lysine-13 and lysine-16 both reside in the flexible AB loop of the coat protein structure (**Figure 4)**, which is predicted to be the dominant epitope for display and recognition by the immune system on major histocompatibility complex class II (MHC-II) molecules.[45] Immunization of mice with Qβ VLPs comprised of the wild-type coat protein allowed for the generation of B-cell hybridomas from which mAb 11A1 was identified; immunizations with the K13Q/K16Q mutant VLP allowed for selection of mAb 5D6. Interestingly, mAb 5D6 was capable of recognizing both the wild-type and mutant VLPs, whereas mAb 11A1 solely recognized particles comprised of the wild-type protein. This disparity suggests that the epitope recognized by mAb 11A1 lies within the AB loop, whereas the epitope recognized by mAb 5D6 lies elsewhere on the particle.

Recognition of Qβ-POEGMA conjugates **9**, **12**, and **13** was assessed by sandwich ELISA using mAbs 11A1 and 5D6, with significant differences observed between the performance of the two antibodies (**Figure 5A,B**). Both mAbs showed significant binding to unmodified Qβ VLPs, with 5D6 displaying significantly stronger binding compared to 11A1 (**Figure 6**). VLPs modified with POEGMA polymers **3**-**5** showed diminished binding by 5D6 that correlated with increasing molecular weight of the conjugated polymer chain (**Figure 5A**), consistent with previous observations that increasing the chain length of a common polymer architecture diminished the immunogenicity of protein conjugates.[27] Interestingly, mAb 11A1 binding was completely abolished by the attachment of

POEGMA chains of any size (**Figure 5B**). This result further supported the hypothesis that mAbs 11A1 and 5D6 recognize discrete epitopes on the particle surface. As the polymer chains are conjugated to Qβ VLPs at the lysine residues (**Scheme 1**), the complete abrogation of binding by 11A1 further indicates that this mAb recognizes an epitope in the exposed AB loop as this would be a site directly blocked by polymer attachment at either lysine-13 or lysine-16 (**Figure 4**).

We next investigated how the density of polymer loading influenced recognition of the Qβ VLP by mAb 5D6. Recognition of Qβ-POEGMA conjugates **9**-**11** was assessed by sandwich ELISA, and significant inhibition of antibody binding was observed with increasing density of polymer chains on the Qβ particle surface (**Figure 5C**). Qβ-POEGMA13-L did not significantly inhibit binding of mAb 5D6 (> 95% recognition relative to wild-type VLPs), whereas increasing the POEGMA loading to ~ 59 (Qβ-POEGMA13-M) and ~ 93 (Qβ-POEGMA13-H) modifications resulted in 53% and 18% relative recognition, respectively. This result correlated with previous observations that increasing coverage of polymer chains on a viral particle surface served to dampen the immunogenicity of the platform.[26]

In addition to investigating the effect of polymer density, we also studied the effects of polymer architecture on antibody recognition. A linear mPEG chain (**7**) was compared against the brush-type POEGMA (**3**) and the linear glycopolymer PMAG (**6**) conjugated at equivalent densities to Qβ VLPs, and recognition of the VLPs by mAb 5D6 was evaluated by sandwich ELISA (**Figure 5D**). Particles modified with mPEG (**15**) and POEGMA13 (**11**) displayed significant inhibition of antibody binding compared to recognition of wild-type VLPs, with Qβ-POEGMA13-H showing equivalent ability to

block recognition compared to Qβ-mPEG (18% vs. 24% of signal relative to wild-type, respectively). Interestingly, Qβ-PMAG displayed significantly poorer performance in blocking recognition of the VLP (78%), despite similar coverage density and molecular weight of the polymer chain. These observations are consistent with previous reports that

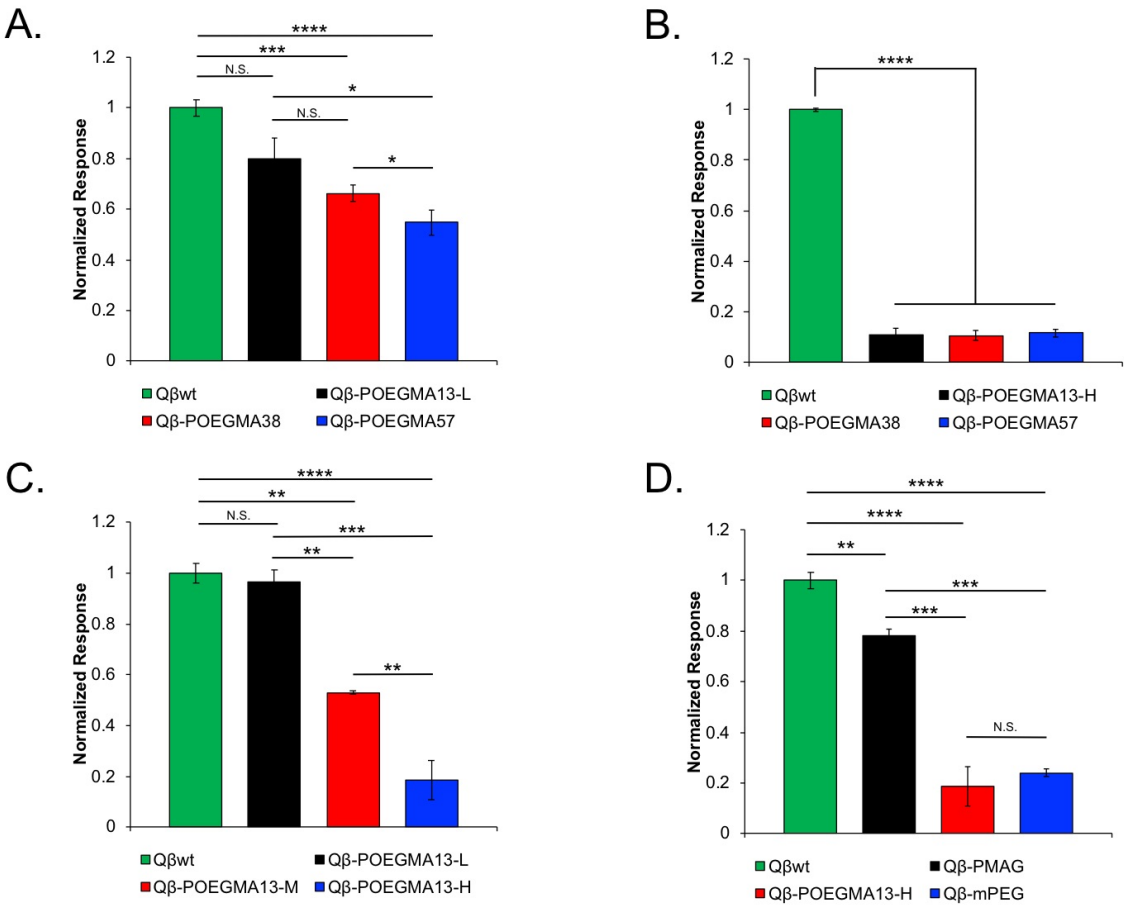


**Figure 5.** Analysis of Qβ-polymer conjugate properties that influence antibody recognition *in vitro*. (**A**) ELISA response using mAb 5D6 for detection of Qβ-POEGMA conjugates as a function of increasing polymer molecular weight. (**B**) ELISA response using mAb 11A1 for detection of Qβ-POEGMA conjugates. Differential response between mAb 5D6 and mAb 11A1 demonstrates the impact of differential epitope blocking by polymer attachment. (**C**) ELISA response using mAb 5D6 for detection of Qβ-POEGMA conjugates as a function of polymer loading density. (**D**) ELISA response using mAb 5D6 for detection of Qβ-polymer conjugates as a function of polymer architecture. Results are normalized to recognition of unmodified VLP at 1 μg/mL for all assays. Data are mean value from 3 independent replicates +/- standard error. Statistical analysis performed using Student's *t*-test. $p \leq 0.0001$: ****; $p \leq 0.001$: ***; $p \leq 0.01$: **; $p \leq 0.05$: *; N.S. = not significant.

polymer architecture and conformation on the particle surface influence the ability of antibodies to bind to protein conjugates.[20,21] Furthermore, our analysis of $R_g$ for the conjugate polymers suggested that conjugates **11**, **14**, and **15** would adopt compact

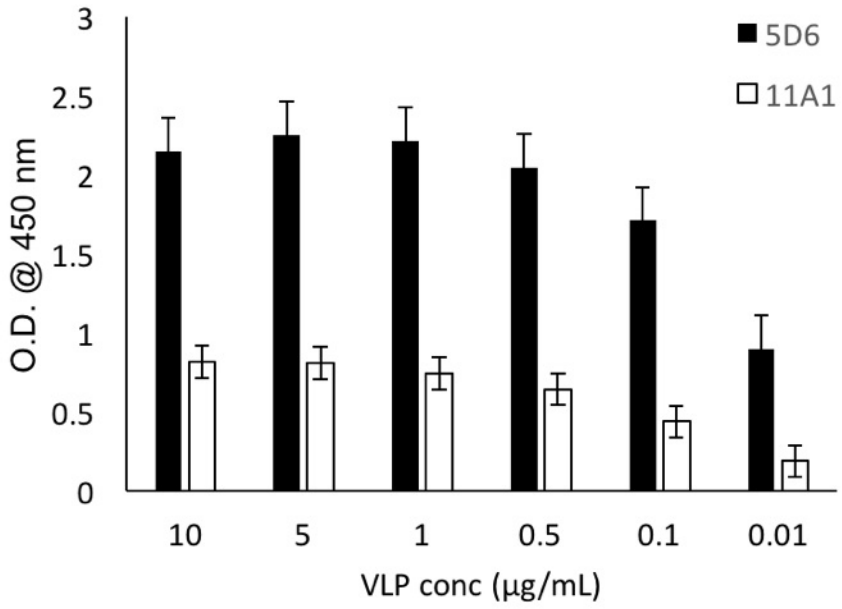


**Figure 6.** Comparative binding analysis between mAbs 5D6 and 11A1 against unmodified Qβ VLPs.

structures on the VLP surface, but there are clearly distinct differences in how these structural conformations relate to shielding of the particle surface.

*5.4.3. Evaluation of antibody responses in mice*

To this point, we had investigated various components of polymer structure and conjugate composition individually; however, recognition by the immune system is likely a complex interplay between features of protein-polymer materials. In order to address this, we finally chose to investigate the performance of the protein-polymer conjugates *in*

*vivo* to determine if attachment of the polymers could effectively dampen the immune response to the VLP. For this study, female CD-1 mice ($n$=4) were immunized with 10 µg of each VLP conjugate and received two subsequent 10 µg immunizations in weeks 2 and 4, respectively (**Figure 7A**). Based on the *in vitro* performance tests, Qβ-POEGMA13-H was selected from the POEGMA13 conjugates for testing *in vivo*. Serum

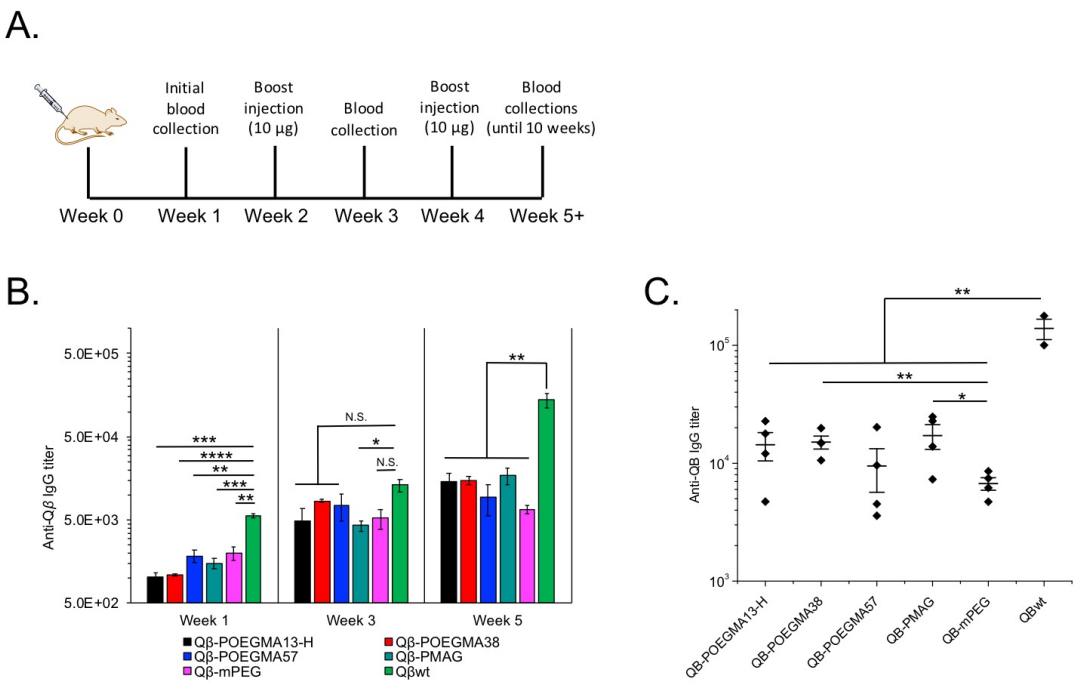


**Figure 7.** Analysis of Qβ-polymer conjugate immunogenicity *in vivo*. (**A**) Schematic of immunization schedule. (**B**) IgG titers against the unmodified Qβ particle in mice immunized with indicated polymer conjugates. Sera analyzed from weeks 1, 3, and 5 of study following immunizations. The data was fit and solved using a Generalized Reduced Gradient algorithm, and the titer was calculated as the mid-point of the corresponding curve fit. Bars represent mean value for each group +/- standard error ($n$ = 4). (**C**) Endpoint IgG titers against unmodified Qβ particle. Sera analyzed from week 5 of study following final immunization. Lines represent mean value for each group +/- standard error ($n$ = 4). All statistical analysis performed using Student's $t$-test. $p \leq 0.0001$: ****; $p \leq 0.001$: ***; $p \leq 0.01$: **; $p \leq 0.05$: *; N.S. = not significant.

samples were obtained in weeks 1, 3, and 5; and serum IgG antibody titers specific to the Qβ VLP were measured by ELISA against the unconjugated wild-type particle (**Figure**

**7B,C**). Antibodies specific to the Qβ VLP were generated in all cohorts, but development of antibody responses in all groups immunized with polymer conjugates was significantly delayed relative to cohorts immunized with the wild-type particle (**Figure 7B**). Following a second immunization, IgG titers remained lower in all mice immunized with polymer conjugates but not significantly (**Figure 7B**). Endpoint titer analysis following a third

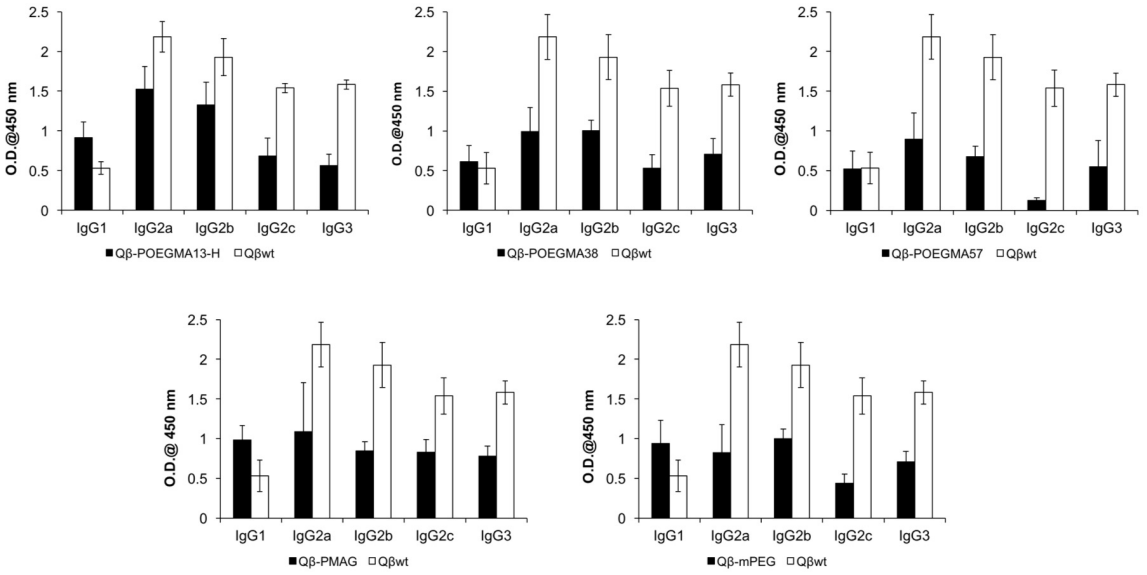


**Figure 8.** IgG subclass distribution for Qβ conjugates. Each data set compares IgG subclasses from mice immunized with Qβ polymer conjugates (black) and mice immunized with unmodified Qβ particles (white). Bars represent mean value for each data set +/- standard error ($n$ = 4).

immunization revealed a significant increase in the IgG titer in cohorts immunized with the wild-type particle, whereas titers remained much lower in all groups treated with polymer conjugates (**Figure 7C**). Analysis of the different IgG subclasses revealed that, while overall titers were lower, the distribution remained unchanged relative to mice immunized with unlabeled VLPs (**Figure 8**). Despite differing performances in blocking antibody recognition *in vitro*, all Qβ polymer conjugates gave rise to similar IgG titers

with Qβ-mPEG displaying the lowest (6,720). While the series of Qβ-POEGMA conjugates (**11-13)** displayed decreasing recognition by mAb 5D6 with increasing length of the polymer chain *in vitro*, IgG titers among these cohorts were statistically equivalent (**Figure 7C**). Interestingly, Qβ-PMAG also gave rise to equivalent IgG titers (17,175) despite its poor performance in blocking antibody recognition *in vitro*.

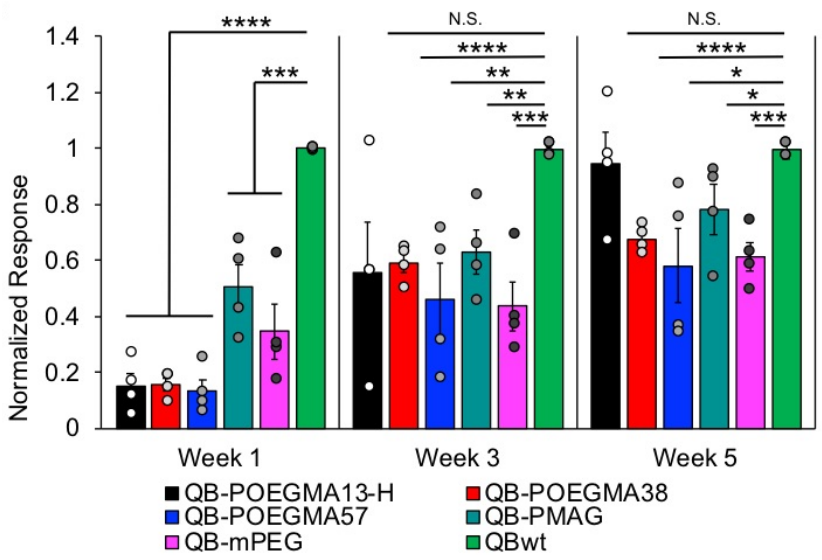


**Figure 9.** Normalized ELISA response against unmodified Qβ particle from mice immunized with indicated polymer conjugates. Sera analyzed from week 5 of study at 1:8000 dilution. Results are normalized to recognition of unmodified VLP by sera from mice immunized with unmodified Qβ particle. Bars represent mean value for each group +/- standard error ($n$ = 4). All statistical analysis performed using Student's $t$-test. $p \leq 0.0001$: ****; $p \leq 0.001$: ***; $p \leq 0.01$: **; $p \leq 0.05$: *; N.S. = not significant.

Although the IgG titers among cohorts immunized with VLP-polymer conjugates were statistically equivalent, there were distinct differences in antibody performance that were consistent with observations from the *in vitro* assays. Antibody recognition of Qβ VLPs was assessed at a normalized serum dilution for each cohort, and recognition of the

particle was compared to serum from mice immunized with unlabeled VLPs (**Figure 9**). Interestingly, mice immunized with Qβ-POEGMA (**11-13**) displayed significantly lower seroreactivity compared to serum from mice immunized with unlabeled VLPs following the initial immunization (**Figure 9**). Reactivity increased with subsequent immunizations but remained significantly lower than in mice receiving unmodified particles. Surprisingly, following the final immunization, serum from mice immunized with Qβ-POEGMA13-H displayed equivalent recognition compared to serum from mice immunized with unlabeled

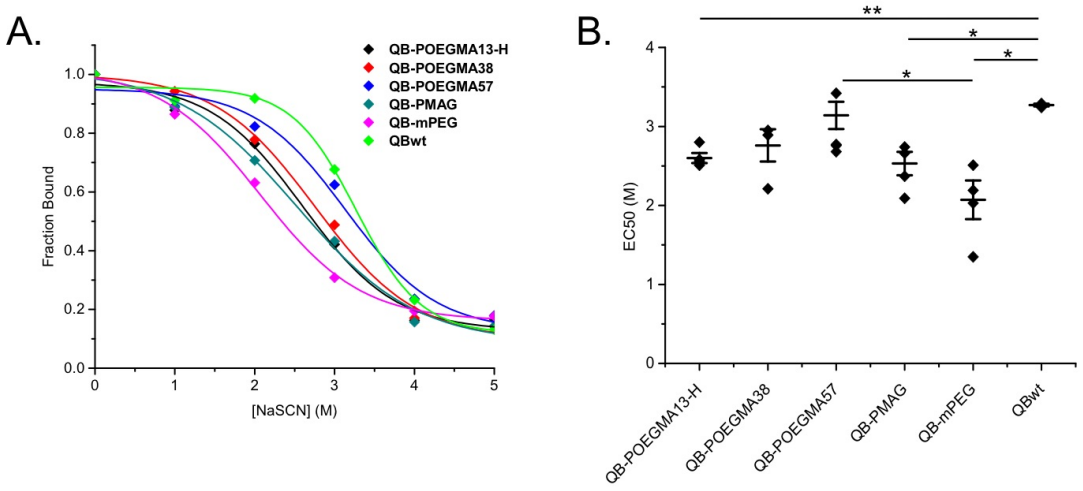


**Figure 10.** Avidity analyses of polyclonal sera against unmodified Qβ particles. **(A)** Avidity of serum IgG responses assessed by NaSCN-displacement ELISA. **(B)** $EC_{50}$ determined from sigmoidal dose response regression analysis. Lines represent mean value for each group +/- standard error ($n = 4$). All statistical analysis performed using Student's *t*-test. $p \leq 0.0001$: ****; $p \leq 0.001$: ***; $p \leq 0.01$: **; $p \leq 0.05$: *; N.S. = not significant.

VLPs (~ 95% relative to wild-type); serum from mice immunized with Qβ-POEGMA38 and Qβ-POEGMA57 showed significantly lower response levels (68% and 58%, respectively). Serum from mice immunized with Qβ-PMAG and Qβ-mPEG showed significantly reduced responses to the particle following the initial immunization, although not as marked as mice immunized with the Qβ-POEGMA conjugates. These responses increased following subsequent immunizations but remained significantly lower than the

response to unlabeled VLPs (78% and 61% relative to wild-type, respectively). This variation in recognition of the Qβ VLP despite mice from all cohorts exhibiting similar IgG titers seemed to indicate functional differences among the antibody repertoires generated, which correlated with weaker responses as the polymer chain length increased (**Figure 11A, B)**.

In order to investigate these differences further, we next analyzed the functional affinity (avidity) of the polyclonal sera from each cohort. The chaotropic agent sodium thiocyanate (NaSCN) was used to displace serum antibodies in a standard ELISA run at a

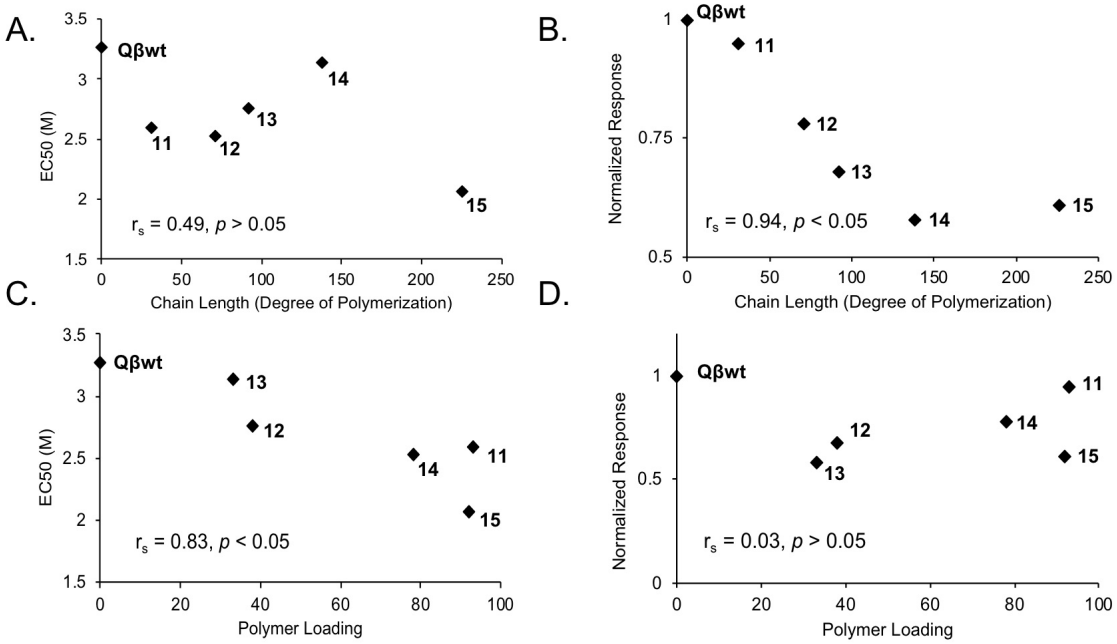


**Figure 11.** Spearman correlation analysis of polymer loading and chain length with $EC_{50}$ values and seroreactivity for Qβ conjugates. Correlation of chain length with $EC_{50}$ **(A)** and seroreactivity **(B)**. Correlation of polymer loading with $EC_{50}$ **(C)** and seroreactivity **(D)**. Individual points represent the mean value measured for the indicated polymer conjugate.

normalized serum dilution, and the $EC_{50}$ (concentration of NaSCN needed to decrease O.D. by 50%) was calculated for each cohort. All cohorts immunized with polymer conjugates generated lower avidity antibody responses against the Qβ VLP relative to

mice immunized with unlabeled particles (**Figure 10A,B**),with Qβ-PMAG and Qβ-mPEG giving rise to antibody responses with significantly lower avidities. Surprisingly, Qβ-POEGMA conjugates **9-11** showed a trend of increasing avidity with increasing chain length of the conjugate POEGMA polymer despite an overall decrease in seroreactivity. This observation could be rationalized as a function of polymer loading and epitope accessibility, as there was a definitive correlation between the number of polymer modifications and avidity (**Figure 11C, D**). Overall, polymer attachment dampened the immunogenicity of the Qβ VLPs *in vivo*, but there were distinctive differences in the function of the antibody populations generated.

*5.4.4. Discussion*

Despite the advantages that have been demonstrated by the conjugation of polymers to protein-based therapeutics, there have been relatively few advancements of protein-polymer hybrid materials into the clinic since the advent of PEGylation. While PEG has been effective at limiting recognition of conjugate proteins by the immune system and prolonging circulation in the bloodstream, more complex polymer architectures have been shown to have improved properties in these respects; these represent opportunities for the development of novel materials that could expand the application of protein-polymer materials in the clinic and possibly supplant PEG as the polymer of choice in biomedical applications. Despite this mounting evidence, studies on the influence that protein-polymer conjugate structure and composition have on this behavior have remained limited in scope. We show in this work a comprehensive assessment of these structural and organizational features that play clear roles in governing antigen recognition and the quality of antibody

responses, and we further explore direct comparisons to PEGylated conjugates both *in vitro* and *in vivo*.

The Qβ VLP proved a robust platform for developing hybrid polymer materials in a controlled manner that could be systematically evaluated as: 1) its organized periodic structure provided for well-defined sites of attachment and 2) its inherently immunogenic nature allowed for the shielding capacity of the conjugate polymers to be directly assessed *in vivo*. Synthesis of VLP-polymer conjugates could be readily achieved for all polymers tested, although the difficulties of ligating the larger molecular weight POEGMA species to the VLP surface were apparent as the loadings of conjugates **12** and **13** were substantially lower. Despite the lower polymer loading, the increased chain length of these species allowed for the VLP conjugates to possess similar mass loadings to the conjugates prepared with the lower molecular weight polymer species.

As several features of protein-polymer hybrid structure and composition have been implicated as factors governing immune recognition, we first set out to collectively characterize the impact of polymer loading density, polymer chain length, and polymer architecture on the ability of antibodies to recognize the Qβ particle. To accomplish this, we leveraged the immunogenic nature of Qβ VLPs to generate two different mAbs (clones 5D6 and 11A1) that recognized distinct epitopes on the particle surface. Indeed, these two antibodies displayed markedly different recognition capabilities when compared against Qβ-POEGMA conjugates of increasing chain lengths. Recognition by clone 5D6 was progressively inhibited with increasing chain length of the POEGMA conjugates, with a maximum of 45% knockdown in binding. Interestingly, binding by clone 11A1 was completely abrogated for all three polymer conjugates. Given the striking difference in

performance between the two mAbs, we believe the site of polymer conjugation on the protein surface to be a key determinant in governing protein-protein interactions and epitope accessibility. Our previous observation that clone 5D6 was capable of recognizing VLPs derived from both the wild-type coat protein as well as a double mutant (K13Q/K16Q), whereas clone 11A1 only recognized the wild-type protein, suggested that not only did the antibodies recognize distinct epitopes but that the epitope for 11A1 was located on the flexible AB loop. As all of the polymer conjugates were synthesized through attachment at the lysine residues on the particle surface, any degree of polymer modification at lysine-13 or lysine-16 would directly block epitope accessibility in the loop. This observation suggests that the site of polymer conjugation may play a crucial role in governing protein-protein interactions and recognition of protein-polymer materials by the immune system.

The density of polymer loading has been previously found to influence the immune response against viral capsids, with increased loadings of PEG resulting in diminished antibody responses and cellular uptake.[27] In this vein, we analyzed Qβ-POEGMA conjugates with mAb 5D6 in order to assess the impact from density of functionalization on subsequent antibody recognition. These Qβ-POEGMA conjugates were modified with POEGMA **3** at increasing levels of functionalization (36, 59, and 93 modifications, respectively), and antibody binding was significantly inhibited with increased polymer loading. As clone 5D6 recognizes an epitope distinct from the AB loop, direct blocking of antibody binding due to the conjugation site is unlikely; however, these polymer chains extend into solution above the VLP surface and increasing the number of modifications

likely impedes accessibility of the Qβ particle through either steric repulsion or the presence of a hydration shell around the surface.

More recently, studies have shown that the conformation of polymer chains conjugated to nanoparticle surfaces also influences protein-protein interactions and immune recognition.[20,21] The conformation adopted by the conjugate polymer is inherently related to the architecture of the polymer chain (i.e., branched vs. linear) as well as interactions between the extended polymer chains in solution. Intramolecular association of polymer chains was clearly evident in more heavily modified conjugates (**11**, **14**, **15**), as there was a small but marked decrease in their $R_g$ (17-18 nm) compared to conjugates with fewer modifications (22-23 nm). This higher degree of modification would have resulted in a denser array of polymer chains on the VLP surface, likely allowing for association between these chains into more tightly packed globular domains. This correlated well with predictions from Flory's theory, where the $R_g$ for the polymer chains scaled with exponents indicative of densely packed globular conformations.[44] Interestingly, these conjugates exhibited markedly different performance in blocking antibody recognition despite similar polymer loadings and molecular weights. Qβ-PMAG only inhibited antibody recognition by ~20%, while Qβ-POEGMA13-H and Qβ-mPEG both abolished binding by ~80%, suggesting clear differences in conformation between polymer architectures. It is possible that multiple hydrogen-bonding events between the carbohydrate moieties in **14** promote association between the polymer chains, whereas POEGMA and PEG adopt less compact structures in solution, allowing for greater coverage of the VLP surface. Further studies to investigate the conformations adopted by these polymer chains when conjugated to the Qβ particle are currently ongoing.

Our evaluation of these structural features *in vitro* provided a comprehensive analysis of individual components on the same protein platform, but nothing to address the simultaneous influence of multiple features on immune recognition. To fully explore the impact of structure and composition on recognition by the immune system and relate these findings with our *in vitro* analysis, we finally analyzed the antibody response against the Qβ VLP in mice administered multiple doses of conjugates **11**-**15**. The administration of doses was set to reflect a scenario whereby a patient would be administered several rounds of treatment to gauge if recognition by the immune system could be inhibited during this time period. Indeed, all protein-polymer conjugates resulted in significantly lower anti-Qβ IgG antibody titers, but there were only slight differences in titer between conjugates. Interestingly, the initial development of an antibody response was significantly delayed relative to the response against unmodified particles. Following a second immunization, titers began to approach levels generated by unlabeled VLPs; however, titers did not increase significantly after a third dose while mice administered unlabeled particles experienced a much larger increase. Although class switching does occur, it appears that memory recall is significantly reduced as repeated dosing did not result in significant increases in titer compared to unlabeled particles. This would seem to indicate that, despite differences in conjugate structure and composition, the modifications tested were sufficient to limit protein-protein interactions and cellular uptake of particles *in vivo*, thereby mitigating the humoral response against the VLP.

Despite similar antibody titers among mice immunized with polymer conjugates, there were distinct differences in the performance of these antibody populations. All Qβ-POEGMA conjugates (**11-13**) displayed lower responses than either Qβ-PMAG (**14**) or

Qβ-mPEG (**15**) in a normalized test for seroreactivity following a single injection. Following secondary immunizations, stronger responses against the particle were developed; however, these responses remained significantly lower than those against wild-type VLPs. Interestingly, responses in mice immunized with both Qβ-PMAG and Qβ-mPEG showed only a moderate increase in signal. This would suggest that affinity maturation occurs at differential rates between Qβ-PMAG, Qβ-mPEG, and Qβ-POEGMA conjugates; and further experiments to investigate this phenomenon are warranted to fully understand the onset of immune responses to protein-polymer materials. Although *in vitro* tests suggested that Qβ-POEGMA13-H (**11**) would demonstrate the greatest shielding capacity, this conjugate surprisingly gave rise to antibodies with comparable reactivity to unlabeled particles following a third immunization. Antibody recognition progressively decreased with increasing chain lengths of POEGMA conjugated to the VLP, thus indicating that polymer chain length may play a critical role in governing the quality of antibody responses against conjugate proteins. However, weaker antibody responses observed with Qβ-PMAG and Qβ-mPEG suggest that the conformation adopted by conjugate polymer chains also plays a key role in the immune response.

To further investigate the quality of antibody responses in immunized mice, we investigated the observed avidity of the polyclonal antibody population in sera against Q$\beta$ VLPs. Interestingly, the avidity of the antibodies generated against the particle decreased with increasing density of functionalization. It is likely that epitope accessibility is more limited in conjugates that are more heavily modified as the polymer chains cover more of the particle surface area, which could play a fundamental role in governing the diversity and affinity of the antibodies comprising the polyclonal population. Interestingly, when

comparing avidity and seroreactivity for Qβ-POEGMA conjugates **11-13**, opposing trends were observed. While the relative recognition of the particle decreased with increasing polymer chain length, the avidity increased. This could suggest that the polyclonal populations may fundamentally differ in terms of epitope diversity, such that the Qβ conjugates bearing more POEGMA chains give rise to a less diverse population of antibodies with higher affinity; whereas conjugates bearing fewer POEGMA chains give rise to a more diverse population of antibodies with lower affinities. However, Qβ-mPEG gave rise to an antibody population with both low avidity as well as diminished seroreactivity, suggesting that the density of polymer loading is not the sole determining factor on the quality of the antibody response. Studies to fully identify differences in the antibody populations arising after exposure to these conjugates, such as differences in antibody affinities or epitope diversity, could provide significant insight into protein-polymer material design and are currently in progress.

### 5.5. Conclusions

When analyzed collectively, the data from this study suggests a complex interplay among the structural features of protein-polymer materials that influence recognition by the immune system. Complete abrogation of the immune response against a nanoparticle carrier is well beyond our current technology, yet the results from this study provide an understanding of the structural features that influence immune recognition and subsequent antibody responses. The degree of modification and the chain length of the conjugate polymer appear to significantly influence the antibody populations generated against the VLP, and further studies will serve to elucidate the mechanisms governing these phenomena. While Qβ-mPEG produced the weakest overall response, the

POEGMA and PMAG conjugates gave rise to similar titers and levels of seroreactivity in most cases. This shows that, while our understanding of the structure-function relationship for protein-polymer hybrid materials is incomplete, advanced polymer architectures can be used to generate novel materials without sacrificing the performance gained from PEGylation, and these materials could serve to develop the next generation of biomaterials for clinical applications.

### 5.6. References


(1) Kaleem, K.; Erhan, S.; Chertok, F. Novel Materials from Protein–polymer Grafts. *Nature* **1987**, *325*, 328.

(2) Katre, N. V. The Conjugation of Proteins with Polyethylene Glycol and Other Polymers: Altering Properties of Proteins to Enhance Their Therapeutic Potential. *Adv. Drug Deliv. Rev.* **1993**, *10*, 91–114.

(3) Duncan, R. The Dawning Era of Polymer Therapeutics. *Nat. Rev. Drug Discov.* **2003**, *2*, 347.

(4) Rother, M.; Nussbaumer, M. G.; Renggli, K.; Bruns, N. Protein Cages and Synthetic Polymers: A Fruitful Symbiosis for Drug Delivery Applications, Bionanotechnology and Materials Science. *Chem. Soc. Rev.* **2016**, *45*, 6213–6249.

(5) Pasut, G.; Veronese, F. M. State of the Art in PEGylation: The Great Versatility Achieved after Forty Years of Research. *J. Control. Release* **2012**, *161*, 461–472.

(6) Jevševar, S.; Kunstelj, M.; Porekar, V. G. PEGylation of Therapeutic Proteins. *Biotechnol. J.* **2010**, *5*, 113–128.

(7) Alconcel, S. N. S.; Baas, A. S.; Maynard, H. D. FDA-Approved Poly(ethylene Glycol)-Protein Conjugate Drugs. *Polym. Chem.* **2011**, *2*, 1442–1448.

(8) Suk, J. S.; Xu, Q.; Kim, N.; Hanes, J.; Ensign, L. M. PEGylation as a Strategy for Improving Nanoparticle-Based Drug and Gene Delivery. *Adv. Drug Deliv. Rev.* **2016**, *99*, 28–51.

(9) Kim, K.-P.; Cha, J.-D.; Jang, E.-H.; Klumpp, J.; Hagens, S.; Hardt, W.-D.; Lee, K.-Y.; Loessner, M. J. PEGylation of Bacteriophages Increases Blood Circulation Time and Reduces T-Helper Type 1 Immune Response. *Microb. Biotechnol.* **2008**, *1*, 247–257.

(10) Bruckman, M. A.; Randolph, L. N.; VanMeter, A.; Hern, S.; Shoffstall, A. J.; Taurog, R. E.; Steinmetz, N. F. Biodistribution, Pharmacokinetics, and Blood Compatibility of Native and PEGylated Tobacco Mosaic Virus Nano-Rods and -Spheres in Mice. *Virology* **2014**, *449*, 163–173.

(11) Hansson, S.; Trouillet, V.; Tischer, T.; Goldmann, A. S.; Carlmark, A.; Barner-Kowollik, C.; Malmström, E. Grafting Efficiency of Synthetic Polymers onto Biomaterials: A Comparative Study of Grafting-from versus Grafting-To. *Biomacromolecules* **2013**, *14*, 64–74.

(12) Isarov, S. A.; Lee, P. W.; Pokorski, J. K. "Graft-To" protein/polymer Conjugates Using Polynorbornene Block Copolymers. *Biomacromolecules* **2016**, *17*, 641–648.

(13) Averick, S.; Simakova, A.; Park, S.; Konkolewicz, D.; Magenau, A. J. D.; Mehl, R. A.; Matyjaszewski, K. ATRP under Biologically Relevant Conditions: Grafting from a Protein. *ACS Macro Lett.* **2012**, *1*, 6–10.

(14) Wallat, J. D.; Rose, K. A.; Pokorski, J. K. Proteins as Substrates for Controlled Radical Polymerization. *Polym. Chem.* **2014**, *5*, 1545–1558.

(15) Heredia, K. L.; Maynard, H. D. Synthesis of Protein-Polymer Conjugates. *Org. Biomol. Chem.* **2007**, *5*, 45–53.

(16) Bontempo, D.; Maynard, H. D. Streptavidin as a Macroinitiator for Polymerization: In Situ Protein−Polymer Conjugate Formation. *J. Am. Chem. Soc.* **2005**, *127*, 6508–6509.

(17) Pokorski, J. K.; Breitenkamp, K.; Liepold, L. O.; Qazi, S.; Finn, M. G. Functional Virus-Based Polymer-Protein Nanoparticles by Atom Transfer Radical Polymerization. *J. Am. Chem. Soc.* **2011**, *133*, 9242–9245.

(18) Nguyen, T. H.; Kim, S.-H.; Decker, C. G.; Wong, D. Y.; Loo, J. A.; Maynard, H. D. A Heparin-Mimicking Polymer Conjugate Stabilizes Basic Fibroblast Growth Factor. *Nat. Chem.* **2013**, *5*, 221.

(19) Fuhrmann, G.; Grotzky, A.; Lukic, R.; Matoori, S.; Luciani, P.; Yu, H.; Zhang, B.; Walde, P.; Schluter, A. D.; Gauthier, M. A.; *et al.* Sustained Gastrointestinal Activity of Dendronized Polymer-Enzyme Conjugates. *Nat Chem* **2013**, *5*, 582–589.

(20) Lee, K. L.; Shukla, S.; Wu, M.; Ayat, N. R.; El Sanadi, C. E.; Wen, A. M.; Edelbrock, J. F.; Pokorski, J. K.; Commandeur, U.; Dubyak, G. R.; *et al.* Stealth Filaments: Polymer Chain Length and Conformation Affect the in Vivo Fate of PEGylated Potato Virus X. *Acta Biomater.* **2015**, *19*, 166–179.

(21) Lee, P. W.; Isarov, S. A.; Wallat, J. D.; Molugu, S. K.; Shukla, S.; Sun, J. E. P.;

Zhang, J.; Zheng, Y.; Dougherty, M. L.; Konkolewicz, D.; *et al.* Polymer Structure and Conformation Alter the Antigenicity of Virus-like Particle-Polymer Conjugates. *J. Am. Chem. Soc.* **2016**.

(22) Li, H.; Li, M.; Yu, X.; Bapat, A. P.; Sumerlin, B. S. Block Copolymer Conjugates Prepared by Sequentially Grafting from Proteinsvia RAFT. *Polym. Chem.* **2011**, *2*, 1531–1535.

(23) Averick, S.; Mehl, R. A.; Das, S. R.; Matyjaszewski, K. Well-Defined Biohybrids Using Reversible-Deactivation Radical Polymerization Procedures. *J. Control. Release* **2015**, *205*, 45–57.

(24) Pelegri-O'Day, E. M.; Maynard, H. D. Controlled Radical Polymerization as an Enabling Approach for the Next Generation of Protein–Polymer Conjugates. *Acc. Chem. Res.* **2016**, *49*, 1777–1785.

(25) Liu, M.; Johansen, P.; Zabel, F.; Leroux, J. C.; Gauthier, M. A. Semi-Permeable Coatings Fabricated from Comb-Polymers Efficiently Protect Proteins in Vivo. *Nat Commun* **2014**, *5*, 5526.

(26) Eto, Y.; Yoshioka, Y.; Ishida, T.; Yao, X.; Morishige, T.; Narimatsu, S.; Mizuguchi, H.; Mukai, Y.; Okada, N.; Kiwada, H.; *et al.* Optimized PEGylated Adenovirus Vector Reduces the Anti-Vector Humoral Immune Response against Adenovirus and Induces a Therapeutic Effect against Metastatic Lung Cancer. *Biol. Pharm. Bull.* **2010**, *33*, 1540–1544.

(27) Steinmetz, N. F.; Manchester, M. PEGylated Viral Nanoparticles for Biomedicine: The Impact of PEG Chain Length on VNP Cell Interactions In Vitro and Ex Vivo. *Biomacromolecules* **2009**, *10*, 784–792.

(28) Pokorski, J. K.; Steinmetz, N. F. The Art of Engineering Viral Nanoparticles. *Mol. Pharm.* **2011**, *8*, 29–43.

(29) Zhang, L.; Qiu, W.; Crooke, S.; Li, Y.; Abid, A.; Xu, B.; Finn, M. G.; Lin, F. Development of Autologous C5 Vaccine Nanoparticles to Reduce Intravascular Hemolysis in Vivo. *ACS Chem. Biol.* **2017**, *12*, 539–547.

(30) Pokorski, J. K.; Hovlid, M. L.; Finn, M. G. Cell Targeting with Hybrid Qb Virus-Like Particles Displaying Epidermal Growth Factor. *ChemBioChem* **2011**, *12*, 2441–2447.

(31) Prasuhn, D. E.; Yeh, R. M.; Obenaus, A.; Manchester, M.; Finn, M. G. Viral MRI Contrast Agents: Coordination of Gd by Native Virions and Attachment of Gd Complexes by Azide-Alkyne Cycloaddition. *Chem. Commun.* **2007**, 1269–1271.

(32) Pushko, P.; Pumpens, P.; Grens, E. Development of Virus-Like Particle

Technology from Small Highly Symmetric to Large Complex Virus-Like Particle Structures. *Intervirology* **2013**, *56*, 141–165.

(33) Smith, M. T.; Hawes, A. K.; Bundy, B. C. Reengineering Viruses and Virus-like Particles through Chemical Functionalization Strategies. *Curr. Opin. Biotechnol.* **2013**, *24*, 620–626.

(34) Ashley, C. E.; Carnes, E. C.; Phillips, G. K.; Durfee, P. N.; Buley, M. D.; Lino, C. A.; Padilla, D. P.; Phillips, B.; Carter, M. B.; Willman, C. L.; *et al.* Cell-Specific Delivery of Diverse Cargos by Bacteriophage MS2 Virus-like Particles. *ACS Nano* **2011**, *5*, 5729–5745.

(35) Sánchez-Sánchez, L.; Tapia-Moreno, A.; Juarez-Moreno, K.; Patterson, D. P.; Cadena-Nava, R. D.; Douglas, T.; Vazquez-Duhalt, R. Design of a VLP-Nanovehicle for CYP450 Enzymatic Activity Delivery. *J. Nanobiotechnology* **2015**, *13*, 66.

(36) Qazi, S.; Miettinen, H. M.; Wilkinson, R. A.; McCoy, K.; Douglas, T.; Wiedenheft, B. Programmed Self-Assembly of an Active P22-Cas9 Nanocarrier System. *Mol. Pharm.* **2016**, *13*, 1191–1196.

(37) Abedin, M. J.; Liepold, L.; Suci, P.; Young, M.; Douglas, T. Synthesis of a Crosslinked Branched Polymer Network in the Interior of a Protein Cage. *J. Am. Chem. Soc.* **2009**, *131*, 4346–4354.

(38) Hovlid, M. L.; Lau, J. L.; Breitenkamp, K.; Higginson, C. J.; Laufer, B.; Manchester, M.; Finn, M. G. Encapsidated Atom-Transfer Radical Polymerization in Qβ Virus-like Nanoparticles. *ACS Nano* **2014**, *8*, 8003–8014.

(39) Bachmann, M. F.; Jennings, G. T. Vaccine Delivery: A Matter of Size, Geometry, Kinetics and Molecular Patterns. *Nat. Rev. Immunol.* **2010**, *10*, 787–796.

(40) Golmohammadi, R.; Fridborg, K.; Bundule, M.; Valegard, K.; Liljas, L. The Crystal Structure of Bacteriophage QB at 3.5A Resolution. *Structure* **1996**, *4*, 543–554.

(41) Fiedler, J. D.; Higginson, C.; Hovlid, M. L.; Kislukhin, A. A.; Castillejos, A.; Manzenrieder, F.; Campbell, M. G.; Voss, N. R.; Potter, C. S.; Carragher, B.; *et al.* Engineered Mutations Change the Structure and Stability of a Virus-Like Particle. *Biomacromolecules* **2012**, *13*, 2339–2348.

(42) Zheng, J.; Jung, S.; Schmidt, P. W.; Lodge, T. P.; Reineke, T. M. 2-Hydroxyethylcellulose and Amphiphilic Block Polymer Conjugates Form Mechanically Tunable and Nonswellable Hydrogels. *ACS Macro Lett.* **2017**, *6*, 145–149.

(43) Hong, V.; Presolski, S. I.; Ma, C.; Finn, M. G. Analysis and Optimization of Copper-Catalyzed Azide–Alkyne Cycloaddition for Bioconjugation. *Angew. Chemie Int. Ed.* **2009**, *48*, 9879–9883.

(44) Flory, P. J. *Principles of Polymer Chemistry*; Cornell University Press: New York, 1953.

(45) Polonskaya, Z.; Deng, S.; Sarkar, A.; Kain, L.; Comellas-Aragones, M.; McKay, C. S.; Kaczanowska, K.; Holt, M.; McBride, R.; Palomo, V.; *et al.* T Cells Control the Generation of Nanomolar-Affinity Anti-Glycan Antibodies. *J. Clin. Invest.* **2017**, *127*, 1491–1504.

# Chapter 6: Genetic modification of PP7 VLPs to dampen phagocytic uptake

## 6.1. Abstract

Virus-like particles (VLPs) represent useful nanoscale platforms for engineering delivery vehicles in biomedicine. Particles derived from the bacteriophage PP7 are particular useful in this context as they are incredibly stable and remarkably tolerant of genetically encoded peptide extensions from the N-or C-termini of the coat protein subunits. Their incredible tolerance towards genetic manipulation allows for quantitative display of peptide extensions from each subunit, which can be precisely tuned by employment of an assembly-competent single chain dimer of the coat protein to generate particles with 50% fewer extensions. Despite their genetic and structural plasticity, VLP platforms remain limited in clinical employment due to their immunogenic structural properties which can promote adaptive immune responses and rapid clearance from the bloodstream. Previously, the display of a minimal peptide (Self) derived from CD47 on polystyrene nanoparticles was shown to inhibit phagocytic uptake and increase circulation half-lives in the bloodstream. In this work, we chose to explore the utility of the Self peptide in mitigating recognition of PP7 VLPs by genetically encoding the Self peptide as a C-terminal extension of the single chain coat protein dimer. Particles were tolerant of the peptide extension and could be produced in high yields without the need for subunit co-expression. Display of the Self peptide significantly inhibited particle uptake by RAW 264.7 macrophages *in vitro*, and immunized mice generated IgG titers moderately lower than those treated with unmodified PP7 particles. Overall, the display of the Self peptide on PP7 can be precisely tuned and shows promise for inhibiting

phagocytic uptake (and presumably clearance) of particles, which would expand their utility as platforms for delivery in medicine.

## 6.2. Introduction

The immune system has evolved to clear invading pathogenic organisms and dying cells from the body through a variety of cellular mechanisms; these responses also mediate the clearance of foreign materials (i.e., nanoparticles, virus-like particles (VLPs), etc.) that are typically employed in drug delivery or other therapeutic applications.[1,2] As noted in the introductory chapter, the size and periodic organization of VLPs are key determinants for interactions at the biological interface and can serve to stimulate complement deposition or pattern recognition receptor (PRR) engagement.[3–5] Likewise, synthetic nanocarriers are often comprised of unnatural materials or chemical linkages that the body recognizes as foreign.

The field of drug delivery has primarily employed the chemical conjugation of polymeric species (namely, PEG) to the surface of nanoparticles and protein therapeutics in order to combat phagocytic clearance and recognition by the immune system.[6–8] These conjugate polymers mimic the glycocalyx of a healthy cell, thereby disrupting protein-protein interactions and inhibiting immune-mediated clearance of the therapeutic species. However, the bulk of the attached polymer chains often reduces the activity of biologics[9] and can also hinder therapeutic uptake by diseased cells.[10] Furthermore, as discussed in Chapter 5, the properties of the attached polymer species as well as the degree to which the therapeutic is modified can directly influence the resulting immune response, making predictive design of these materials challenging. As was evidenced in previous chapters regarding the modification of VLPs to mediate cellular targeting, the ability to

manipulate protein-based therapeutics at the genetic level also offers an alternative approach for evading immune-mediated clearance.

The glycoprotein CD47 has been identified as a "marker of self" in mice[11] and is ubiquitously expressed on cell membranes in humans and other mammals.[12] Lindberg and colleagues were the first to demonstrate the biological role of CD47 in a blood transfusion study using $CD47^{-/-}$ mice.[13] These mice were found to be completely viable; however, if red blood cells (RBCs) from the $CD47^{-/-}$ mice were transfused into wild-type ($CD47^{+/+}$) mice, macrophages cleared them from circulation within hours. The native binding partner of CD47 is signal regulatory protein alpha (SIRPα), an inhibitory receptor that is abundantly expressed on leukocytes and monocytes.[14] Lindberg and colleagues demonstrated that the CD47-SIRPα interaction was responsible for inhibiting macrophage uptake of RBCs, while inhibition or absence of this interaction promoted rapid clearance.[11]

The role and potential application of CD47 in the inhibition of phagocytic clearance was further explored by Discher and colleagues, who showed that display of human CD47 on microparticles prevented uptake by macrophages.[15] They further developed the potential for CD47 to be explored in therapeutic delivery applications by minimizing the domain to a 21-amino acid peptide (Self) derived from the most prominent contacting residues in the hCD47-SIRPα crystal structure.[16,17] Polystyrene nanoparticles displaying the Self peptide showed delayed clearance from the circulation which subsequently enhanced delivery of the particles to tumors.[16] This study was the first to demonstrate display of a minimal component of CD47 on a nanoparticle for the inhibition of immune-mediated clearance *in vivo*.

In addition to its role in regulating phagocytic uptake and clearance, CD47-SIRPα signaling is also a key component that governs immune cell activation. Sarfati and co-workers identified the CD47-SIRPα signaling axis as a crucial checkpoint in dendritic cell and monocyte activation, as ligation of CD47 inhibited both cytokine production and maturation of these cell subsets.[18] Furthermore, CD47 ligation also inhibited cellular responsiveness to IL-12 and the maturation of naïve T-cells.[19,20] The results of these studies clearly implicate CD47-SIRPα signaling as an important element governing not only phagocytic clearance but also recognition and stimulation of adaptive immunity.

The engineered display of peptides on the surface of VLPs has been investigated previously for applications in the development of vaccines and other biomimetic scaffolds. Chackerian and Peabody have extensively explored the development of MS2 and PP7 platforms for the display of disease-associated peptide epitopes, specifically through incorporation of extensions in the AB-loop of the viral coat protein.[21–23] Single-chain dimer variants of both MS2 and PP7 were generated and shown to have increased stability relative to analogous particles comprised of coat protein monomers.[21] These particles were shown to be tolerant to the incorporation of 6-10 amino acid peptides into the AB-loop, which has typically been shown to destabilize VLP structures; however, the VLP could only tolerate incorporation into a single subunit of the fused dimer.[23,24] Chackerian and colleagues employed these particles for the affinity selection of epitopes as well as the display of viral peptides for the development of vaccines. Despite the enhanced stability of these constructs and their tolerance of peptide insertions, the display of peptides as N-or C-terminal extensions of a fused dimer has not been explored **(Figure 1)**.

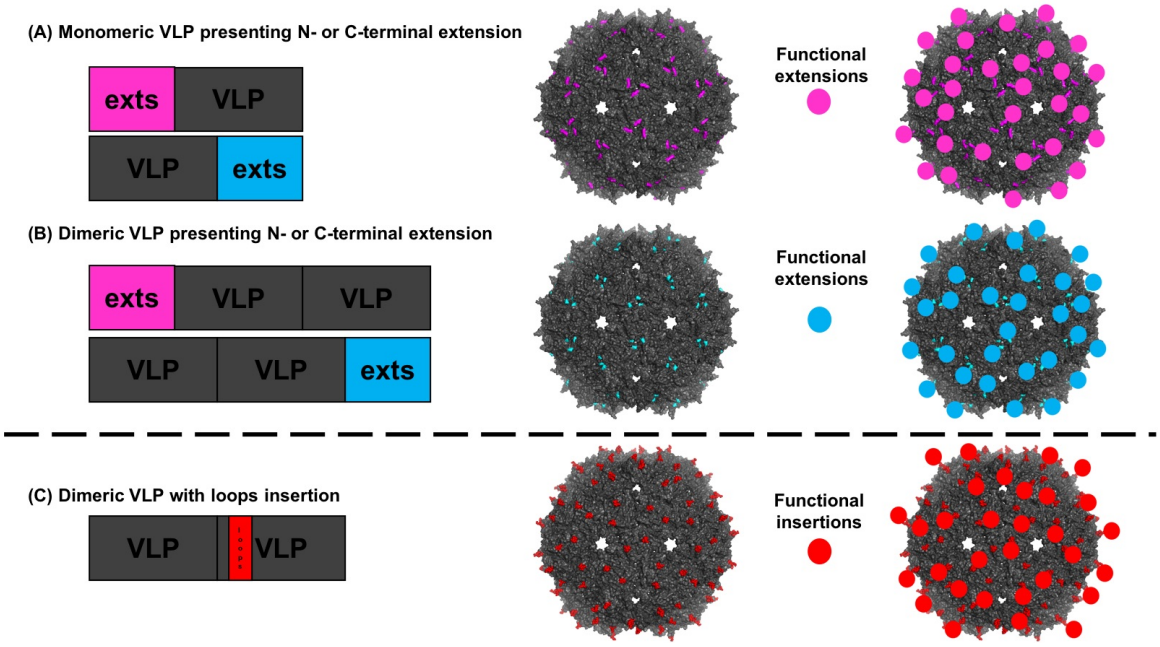


**Figure 1.** Genetic modification of VLP particles to present extensions/insertions. (A) Functional peptide extensions fused onto PP7 monomeric coat protein as either N- or C-terminal extensions, which allows for presentation of 180 copies. (B) Functional peptide extensions fused onto PP7 single-chain coat protein dimers as either N- or C-terminal extensions, which allows for presentation of 90 copies. (C) Functional peptides fused onto PP7 monomeric coat protein via insertion into the AB loop, which allows for presentation of 90 copies. Depending on the intrinsic properties of the functional peptide, not all peptides can be readily fused using the strategies shown.

In this work, we sought to investigate the generation of PP7 VLPs comprised of a single-chain dimer displaying a C-terminal extension of the Self peptide identified by Discher and colleagues. While Douglas and coworkers have previously explored the display of the Self peptide on the surface of P22 VLPs, this display was facilitated by fusing the peptide to the trimeric decoration protein (Dec) from bacteriophage L,[25] which binds tightly to the P22 capsid.[26] Although display in this fashion did mitigate particle uptake by phagocytic cells, our system provides for direct covalent linkage of the inhibitory peptide to the VLP surface. PP7 VLPs produced in our system could be isolated in high yields with 90 copies of the Self peptide displayed on the surface

(although there is mounting evidence that particles formed from single-chain dimer extensions adopt $T = 4$ geometry, equating to 120 displayed peptides). Display of the Self peptide significantly inhibited uptake of PP7 VLPs by macrophages *in vitro* relative to unmodified particles, but immunization with these particles gave rise to comparable IgG titers in mice. Overall, the results of this study suggest that genetic display of the Self peptide could serve to mitigate phagocytic uptake and clearance of VLP delivery platforms and extend the range of their applications.

## 6.3. Materials and Methods

*Molecular Cloning and Construct Design*

To construct the expression plasmid for PP7-Self in this work, an existing expression vector for the PP7 fused dimer (pET28-PP72) was modified. Briefly, the coding sequence for the Self peptide (GNYTSEVTELTREGETIIELK) was codon-optimized for expression in *E. coli* with a serine-to-cysteine mutation introduced at the fifth position to mitigate aggregation of VLPs during expression and purification. To incorporate this sequence as a C-terminal extension of the fused dimer, a Q5 Site-Directed Mutagenesis Kit (New England Biolabs) was used with forward primer 5'-GGATCCATGTCGAAAACCAT-3' and reverse primer 5'-TTATTTTAACTCGATAATAGTTTCTCCTTCGCGGGTTAACTCCGTAACTTCGGAGGTGTAATTGCCGGCGCCGCTTTCGCTCGCGCCACCGCGGCCCA-3', where the coding sequence for the Self peptide is underlined.

*Protein Production and Characterization*

PP7 VLPs were expressed and purified following protocols previously established for the purification of Qβ VLPs. Briefly, chemically competent BL21(DE3) *E. coli* cells

were transformed with a pET28 plasmid harboring the gene for either the PP7 coat protein single-chain dimer or the single-chain dimer bearing C-terminal peptide fusions as indicated (Self or scrSelf). Cells were plated on selective SOB agar, and, after 18 h, selective SOB media (25 mL) was inoculated with a single colony and grown overnight at 37°C. After 24 h, this culture was diluted into selective SOB media (500 mL) and grown at 37°C until the optical density ($O.D._{600}$) reached mid-log phase (~ 0.9). Expression was induced by the addition of IPTG (1 mM) and cultures were maintained at 30°C for 16 h. Cells were harvested by centrifugation at 6,000 rpm for 10 min, and dried cells were re-suspended in 1x TBS prior to lysis using a probe sonicator (10 min total, 75 W, 5 sec intervals) in an ice bath. Lysate was clarified by centrifugation at 14,000 rpm for 10 min, and proteins were precipitated from supernatant by the addition of 30% $(NH_4)_2SO_4$ (w/v) at 4°C for 2 h. Precipitate was pelleted by centrifugation at 14,000 rpm for 10 min and was re-suspended in 1x TBS prior to extraction with *n*-BuOH:$CHCl_3$ (1:1, v/v) to remove aggregates and lipids. Mixture was separated by centrifugation at 14,000 rpm for 10 min, and aqueous phase was collected and immediately loaded onto 10-40% sucrose density gradient. VLPs were purified by centrifugation at 28,000 rpm for 4 h, and bands corresponding to intact particles were extracted via syringe. Particles were pelleted by ultracentrifugation at 68,000 rpm for 2 h, and the resulting pellets were dissolved in 0.1M potassium phosphate buffer.

The protein concentration of the VLP samples was determined by Bradford assay using BSA standards. Particles were characterized by dynamic light scattering (Wyatt Dynapro plate reader), FPLC size-exclusion chromatography (Superose 6 10/300 GL) monitoring the absorbance at 280 nm, microfluidic gel electrophoresis (Agilent 2100

Bioanalyzer with Series II Protein 80 chips), and mass spectrometry (Agilent 6230B TOF LC/MS).

*Cell Culture*

All cell culture reagents were purchased from Invitrogen. RAW 264.7 macrophage cells (ATCC) were cultured in phenol red-free Dulbecco's modified Eagle's medium (DMEM) supplemented with 5% fetal bovine serum (FBS), GlutaMAX (2 mM), sodium pyruvate (1 mM), penicillin (100 U/mL), and streptomycin (100 μg/mL). Cells were maintained in a humidified incubator at 37°C with 5% $CO_2$ atmosphere.

*Live-Cell Microscopy and Fluorescence Imaging*

RAW 264.7 macrophages were cultured to 80% confluence and seeded onto chambered microscope slides (ibidi) at 1:10 dilution. After 24 h, cells were treated with PP7 VLPs (10 or 20 nM) labeled with Alexa Fluor 488 and incubated for 6 h, 12 h, and 24 h at 37°C in a humidified incubator with 5% $CO_2$. At each respective time point, cells were rinsed twice with 1x PBS and imaged on an Eclipse Ti-U fluorescence microscope (Nikon) equipped with a 60x oil immersion objective. Images were subsequently analyzed with ImageJ software. To calculate the corrected fluorescence per cell (CFPC), cells were manually selected by freeform drawing, and the area integrated density was calculated. Background fluorescence was calculated in the same manner as an average of three points were no cells were present. Calculations of the CFPC were made using the following equation:

$$CFPC = Integrated\ density - (Area\ of\ cell * Mean\ background\ fluorescence)$$

*Mice and Immunizations*

Female CD-1 IGS mice (8-12 weeks) were obtained from Charles River Laboratories and maintained in the animal facility of the Georgia Institute of Technology. All animal care and experimental procedures were approved by the Institutional Animal Care and Use Committee of the Georgia Institute of Technology. Mice were administered 10 μg VLP by subcutaneous injection at days 0, 14, and 28. Blood was collected via submandibular bleed at days 7, 21, and 35 for serum antibody analysis. Mice were maintained until day 50 for continued analysis prior to sacrifice.

*ELISA*

Wild-type PP7 (single-chain dimer; 1 μg/mL) VLPs were plated overnight at 4°C. Plate was washed thrice with PBST and blocked with 3% BSA in PBST for 2 h at room temperature. Serum dilutions were prepared in a master plate using 3% BSA in PBST as diluent and transferred to the assay plate to give final dilutions of 1:500-1:128000, which were incubated for 1 h at room temperature. Plate was washed thrice with PBST and incubated with anti-mouse IgG HRP-conjugate reporter antibody (1:2500, Abbiotec, Inc.) for 1 h at room temperature. A final washing with PBST was followed by development with TMB substrate (1-Step™ Ultra TMB; Thermo Fisher Scientific) and quenching with 1M $H_2SO_4$. Absorbance was measured at 405 nm on a microplate reader (Thermo Fisher Scientific).

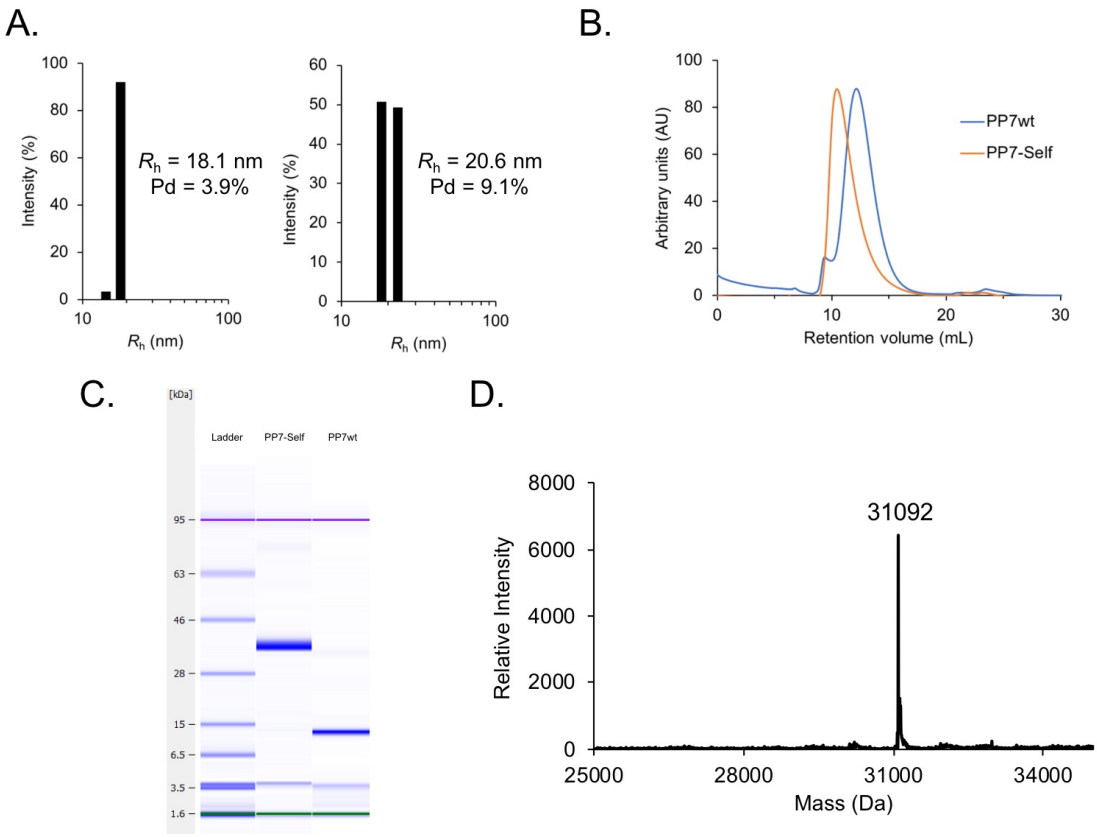


**Figure 2.** Characterization of PP7-Self and PP7wt particles. **(A)** Dynamic light scattering measurements of PP7wt particles (left) and PP7-Self particles (right). Particles displaying the peptide extension have a slightly larger radius than unmodified VLPs. **(B)** FPLC elution profile for PP7wt (blue) and PP7-Self (orange) showing particles are intact and greater than 95% pure. PP7-Self VLPs display shorter retention times indicative of larger molecular species. **(C)** Denaturing electrophoretic analysis of PP7wt and PP7-Self VLPs showing single distinct protein species comprising both samples, respectively. **(D)** High-resolution mass spectrometry analysis of PP7-Self, revealing a single protein species with the predicted mass.

## 6.4. Results and Discussion

### *6.4.1. Particle design and characterization*

To prepare VLP constructs bearing the Self peptide, a codon-optimized sequence for the Self peptide was appended to the 3'-end of the gene encoding for the single chain PP7 coat protein dimer. This strategy allowed for every dimeric unit to display exactly one copy of the peptide extension, equating to 90 copies on the entire particle surface.

Expression of this construct in *E. coli* generated monodisperse particles that could be isolated in high yields (30 mg/L). Size-exclusion chromatography, dynamic light scattering, and gel electrophoretic analysis were all characteristic of intact, monodisperse particles for preparations of PP7wt and PP7-Self **(Figure 2A-C)**. Particles displaying the peptide extension showed an increase in their hydrodynamic radius relative to PP7wt particles (~ 21 versus ~ 18 nm), indicative of the uniform display of the Self peptide on the particle surface **(Figure 2A)**. In addition, PP7-Self particles displayed a slight but distinct decrease in elution volume relative to PP7wt as measured by size-exclusion chromatography, which is also indicative of larger particles **(Figure 2B)**. Electrophoretic analysis of PP7wt and PP7-Self showed a single band at the corresponding molecular weight for each respective species (~ 13 kDa for PP7wt versus ~ 31 kDa for PP7-Self), demonstrating that the fused-dimer bearing the Self peptide extension was the sole component mediating particle assembly **(Figure 2C)**. Analysis by mass spectrometry further confirmed that PP7-Self particles were comprised of solely the fused-dimer bearing the Self peptide extension **(Figure 2D)**. This stands in contrast to our previous work with the Qβ VLP, which requires co-expression of the subunit bearing the peptide extension together with the unmodified coat protein for assembly of hybrid particles. The disadvantage of the Qβ platform with this respect is a lack of control over the number of extensions incorporated, whereas the PP7 fused-dimer constructs bearing terminal extensions allow for precise control based on the geometry of particle assembly.

*6.4.2. Assessment of macrophage uptake*

Following successful assembly and characterization of the PP7-Self VLPs, we sought to test if display of the Self peptide was sufficient to inhibit particle uptake by

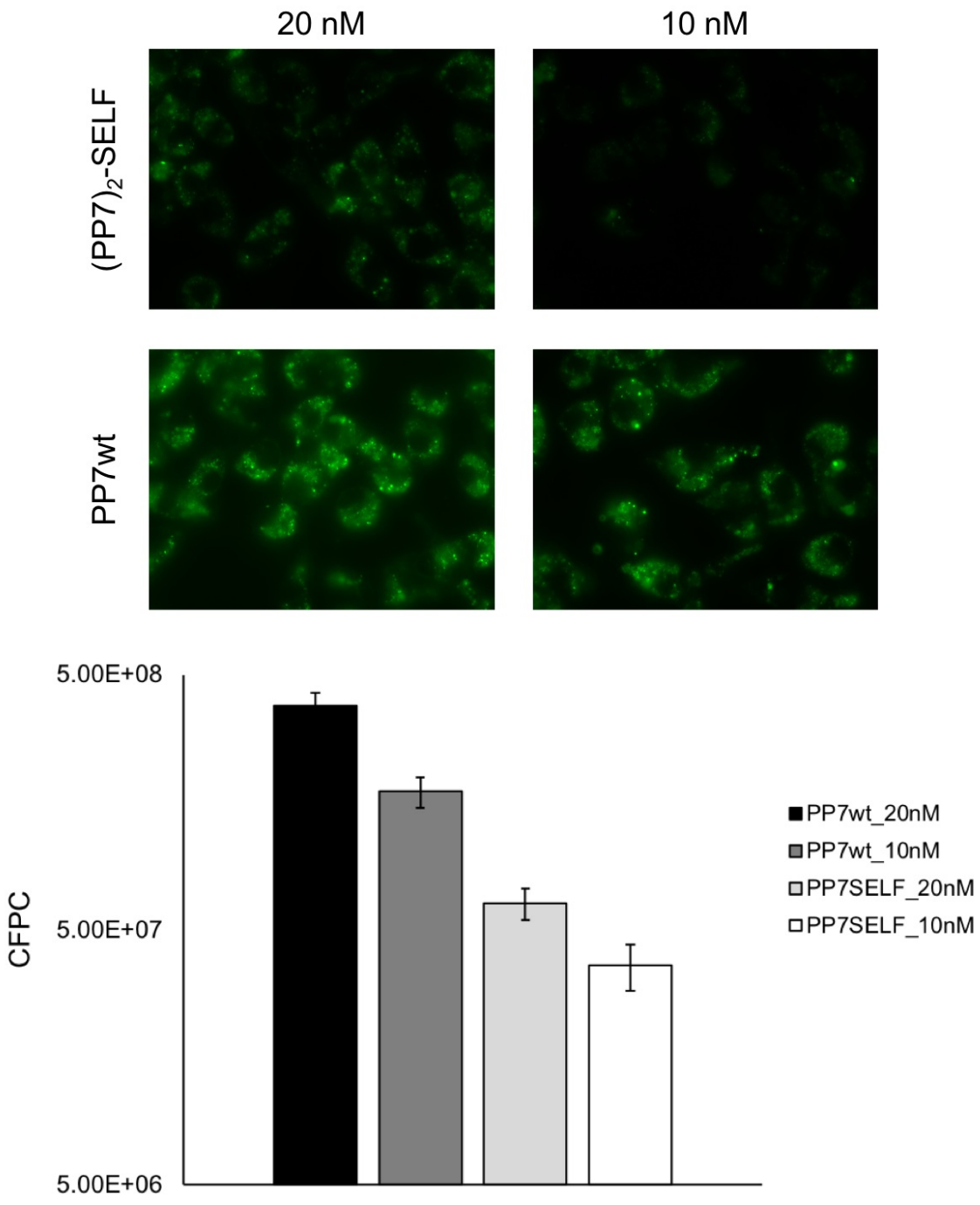


**Figure 3.** Uptake of PP7wt and PP7-Self VLPs in RAW 264.7 macrophages. (Upper panels) Representative microscopy images of macrophages after incubation with PP7wt or PP7-Self VLPs (10 nM and 20 nM) for 24 h. (Lower panel) Quantification of VLP uptake as measured by the corrected fluorescence per cell. Bars represent the average +/- standard error ($n$ = 15).

phagocytic cells as first reported by Discher. VLPs were first labeled with Alexa Fluor 488 in order to visualize particle uptake by fluorescence microscopy, and RAW 264.7 macrophages were subsequently incubated with either PP7wt or PP7-Self (10 nM and 20 nM) for 24 hours. Significant uptake by macrophages was observed in a dose-dependent manner for PP7wt, with punctate staining indicative of phagocytic uptake and localization of particles into endosomal compartments **(Figure 3)**. In contrast, uptake of PP7-Self was significantly inhibited at both concentrations tested, indicating that display of the Self peptide on the surface of the VLP was able to inhibit phagocytic uptake **(Figure 3)**. PP7-Self particles that were phagocytosed also exhibited punctate staining, further supporting that particle uptake was mediated by the same process but inhibited by signaling through the CD47-SIRPα axis.

*6.4.3. Evaluation of humoral immune response*

To further explore the ability of the Self peptide to mitigate cellular recognition of particles, we next tested the humoral immune response generated against PP7-Self relative to PP7wt VLPs. Female CD-1 mice ($n = 4$) were initially immunized subcutaneously with 10 μg of either PP7-Self or PP7wt particles, followed by two subsequent immunizations at the same dose. Following the initial immunization, mice immunized with PP7-Self displayed lower titers than mice immunized with PP7wt, but the difference in titers was not significant **(Figure 4)**. Interestingly, IgG titers against the coat protein increased but remained significantly lower in mice administered PP7-Self relative to PP7wt following a second immunization **(Figure 4)**.

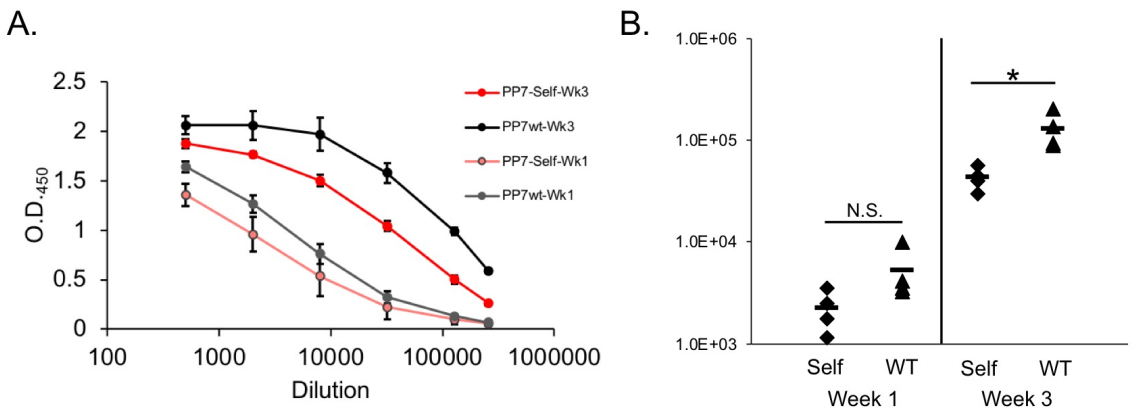


**Figure 4.** Total IgG titers against PP7wt and PP7-Self. **(A)** Average titer curves for anti-PP7 total IgG in sera collected 7 days post-immunization with either PP7wt or PP7-Self ($n$ = 4). **(B)** Individual titers from mice immunized with PP7wt or PP7-Self. The data was fit and solved using four parameter logistic regression analysis, and the titer was calculated as the mid-point of the corresponding curve fit. Lines represent mean value for each group; symbols represent individual mice ($n$ = 4).

### 6.5. Conclusions

The PP7 particle represents a very robust platform for engineering drug delivery vehicles as it can more readily accommodate genetic manipulation and display of large peptide domains from the N- or C-termini. Expression of monomeric PP7 fusions is capable of generating particles displaying a peptide from each subunit (180), while the fused dimer construct can be used to finely tune display in a more controlled fashion than co-expression of hybrid subunits, which was employed in previous chapters with the Qβ platform. Display of the Self peptide was capable of mitigating the uptake of VLPs by macrophages *in vitro* and had a moderate effect on the generation of a humoral immune response against PP7, as measured by total IgG antibody titers. While the Self peptide may not be capable of completely shielding particles from the immune system, it does appear to have potent efficacy at inhibiting phagocytosis, which could translate into useful applications for prolonged systemic delivery. Phagocytic clearance is one of the

primary mechanisms by which nanoscale particles are removed from circulation, so if these results translate to clearance studies *in vivo*, it will provide a useful platform for applications in drug delivery.

### 6.6. References


(1) Gustafson, H. H.; Holt-Casper, D.; Grainger, D. W.; Ghandehari, H. Nanoparticle Uptake: The Phagocyte Problem. *Nano Today*, 2015, *10*, 487–510.

(2) Storm, G.; Belliot, S. O.; Daemen, T.; Lasic, D. D. Surface Modification of Nanoparticles to Oppose Uptake by the Mononuclear Phagocyte System. *Advanced Drug Delivery Reviews*, 1995, *17*, 31–48.

(3) Bachmann, M. F.; Jennings, G. T. Vaccine Delivery: A Matter of Size, Geometry, Kinetics and Molecular Patterns. *Nat. Rev. Immunol.* **2010**, *10*, 787–796.

(4) Link, A.; Zabel, F.; Schnetzler, Y.; Titz, A.; Brombacher, F.; Bachmann, M. F. Innate Immunity Mediates Follicular Transport of Particulate but Not Soluble Protein Antigen. *J. Immunol.* **2012**, *188*, 3724–3733.

(5) Zaiss, A.-K.; Cotter, M. J.; White, L. R.; Clark, S. A.; Wong, N. C. W.; Holers, V. M.; Bartlett, J. S.; Muruve, D. A. Complement Is an Essential Component of the Immune Response to Adeno-Associated Virus Vectors. *J. Virol.* **2008**, *82*, 2727–2740.

(6) Suk, J. S.; Xu, Q.; Kim, N.; Hanes, J.; Ensign, L. M. PEGylation as a Strategy for Improving Nanoparticle-Based Drug and Gene Delivery. *Adv. Drug Deliv. Rev.* **2016**, *99*, 28–51.

(7) Jevševar, S.; Kunstelj, M.; Porekar, V. G. PEGylation of Therapeutic Proteins. *Biotechnol. J.* **2010**, *5*, 113–128.

(8) Pasut, G.; Veronese, F. M. State of the Art in PEGylation: The Great Versatility Achieved after Forty Years of Research. *J. Control. Release* **2012**, *161*, 461–472.

(9) Gong, Y.; Leroux, J. C.; Gauthier, M. A. Releasable Conjugation of Polymers to Proteins. *Bioconjugate Chemistry*, 2015, *26*, 1179–1181.

(10) Hong, R. L.; Huang, C. J.; Tseng, Y. L.; Pang, V. F.; Chen, S. T.; Liu, J. J.; Chang, F. H. Direct Comparison of Liposomal Doxorubicin with or without Polyethylene Glycol Coating in C-26 Tumor-Bearing Mice: Is Surface Coating with Polyethylene Glycol Beneficial? *Clin. Cancer Res.* **1999**, *5*, 3645–3652.

(11) Oldenborg, P.-A.; Zheleznyak, A.; Fang, Y.-F.; Lagenaur, C. F.; Gresham, H. D.;

Lindberg, F. P. Role of CD47 as a Marker of Self on Red Blood Cells. *Science (80-. ).* **2000**, *288*, 2051.

(12) Bentley, A. A.; Adams, J. C. The Evolution of Thrombospondins and Their Ligand-Binding Activities. *Mol. Biol. Evol.* **2010**, *27*, 2187–2197.

(13) Oldenborg, P. A.; Zheleznyak, A.; Fang, Y. F.; Lagenaur, C. F.; Gresham, H. D.; Lindberg, F. P. Role of CD47 as a Marker of Self on Red Blood Cells. *Science (80-. ).* **2000**, *288*, 2051–2054.

(14) Brown, E. J.; Frazier, W. A. Integrin-Associated Protein (CD47) and Its Ligands. *Trends Cell Biol.* **2001**, *11*, 130–135.

(15) Tsai, R. K.; Discher, D. E. Inhibition Of "self" engulfment through Deactivation of Myosin-II at the Phagocytic Synapse between Human Cells. *J. Cell Biol.* **2008**, *180*, 989–1003.

(16) Rodriguez, P. L.; Harada, T.; Christian, D. A.; Pantano, D. A.; Tsai, R. K.; Discher, D. E. Minimal "Self" peptides That Inhibit Phagocytic Clearance and Enhance Delivery of Nanoparticles. *Science (80-. ).* **2013**, *339*, 971–975.

(17) Hatherley, D.; Graham, S. C.; Turner, J.; Harlos, K.; Stuart, D. I.; Barclay, A. N. Paired Receptor Specificity Explained by Structures of Signal Regulatory Proteins Alone and Complexed with CD47. *Mol. Cell* **2008**, *31*, 266–277.

(18) Demeure, C. E.; Tanaka, H.; Mateo, V.; Rubio, M.; Delespesse, G.; Sarfati, M. CD47 Engagement Inhibits Cytokine Production and Maturation of Human Dendritic Cells. *J. Immunol.* **2000**, *164*, 2193–2199.

(19) Avice, M.-N.; Rubio, M.; Sergerie, M.; Delespesse, G.; Sarfati, M. CD47 Ligation Selectively Inhibits the Development of Human Naive T Cells into Th1 Effectors. *J. Immunol.* **2000**, *165*, 4624–4631.

(20) Latour, S.; Tanaka, H.; Demeure, C.; Mateo, V.; Rubio, M.; Brown, E. J.; Maliszewski, C.; Lindberg, F. P.; Oldenborg, A.; Ullrich, A.; *et al.* Bidirectional Negative Regulation of Human T and Dendritic Cells by CD47 and Its Cognate Receptor Signal-Regulator Protein- : Down-Regulation of IL-12 Responsiveness and Inhibition of Dendritic Cell Activation. *J. Immunol.* **2001**, *167*, 2547–2554.

(21) Peabody, D. S.; Manifold-Wheeler, B.; Medford, A.; Jordan, S. K.; do Carmo Caldeira, J.; Chackerian, B. Immunogenic Display of Diverse Peptides on Virus-like Particles of RNA Phage MS2. *J Mol Biol* **2008**, *380*.

(22) Chackerian, B.; Caldeira, J. D.; Peabody, J.; Peabody, D. S. Peptide Epitope Identification by Affinity Selection on Bacteriophage MS2 Virus-Like Particles. *J Mol Biol* **2011**, *409*.

(23) Caldeira, J. D.; Medford, A.; Kines, R. C.; Lino, C. A.; Schiller, J. T.; Chackerian, B.; Peabody, D. S. Immunogenic Display of Diverse Peptides, Including a Broadly Cross-Type Neutralizing Human Papillomavirus L2 Epitope, on Virus-like Particles of the RNA Bacteriophage PP7. *Vaccine* **2010**, *28*.

(24) Peabody, D. S. Subunit Fusion Confers Tolerance to Peptide Insertions in a Virus Coat Protein. *Arch Biochem Biophys* **1997**, *347*.

(25) Schwarz, B.; Madden, P.; Avera, J.; Gordon, B.; Larson, K.; Miettinen, H. M.; Uchida, M.; LaFrance, B.; Basu, G.; Rynda-Apple, A.; *et al.* Symmetry Controlled, Genetic Presentation of Bioactive Proteins on the P22 Virus-like Particle Using an External Decoration Protein. *ACS Nano* **2015**, *9*, 9134–9147.

(26) Gilcrease, E. B.; Winn-Stapley, D. A.; Hewitt, F. C.; Joss, L.; Casjens, S. R. Nucleotide Sequence of the Head Assembly Gene Cluster of Bacteriophage L and Decoration Protein Characterization. *J Bacteriol* **2005**, *187*, 2050–2057.

# Chapter 7: Conclusion

## 7.1. Comprehensive Discussion

The overarching theme of the work presented in this thesis was the chemical and genetic engineering of virus-like particle platforms for vaccine design and drug delivery. In this final chapter, the key findings of this thesis will be summarized and a discussion on future directions of study will follow.

Chapter 2 focused on the genetically-encoded display of peptide epitopes on Qβ VLPs for applications in vaccine development. For this study, our efforts were focused on the treatment of complement-mediated autoimmune disorders, such as paroxysmal nocturnal hemoglobinuria (PNH),[1] in an effort to leverage the inherent immunogenicity of the Qβ platform to break tolerance against a self-antigen. Furthermore, patients suffering from PNH and other hemolytic pathologies have limited therapeutic options, so a more effective (and cheaper) alternative would be a tremendous benefit in the clinic.[2] Our efforts found that immunization with a homologous xenoprotein of complement component 5 (C5) generated high IgG titers in mice, but these antibodies failed to cross-react with the native C5 protein. After failing to generate a cross-reactive immune response with this vaccine, we next identified 12 potential immunogenic peptides in the native mouse C5 protein and prepared a mosaic protein comprised of these epitopes interspersed with a known tolerance-breaking peptide (PADRE).[3] Immunization with this construct gave rise to cross-reactive antibody responses that mapped to a dominant peptide epitope on the surface of the C5 protein. Finally, we designed Qβ VLPs to display this peptide epitope as a C-terminal extension of the coat protein and assembled

hybrid particles for immunization. Complement activity was significantly diminished, but not abolished, in mice receiving the Qβ vaccine, and clinical indicators of disease in a PNH mouse model were undetectable following immunization. These studies build on previous efforts employing the Qβ VLP as a vaccine platform against self-antigens[4–7] but is the first such study to engineer the display of the antigen as a genetic fusion rather than through chemical conjugation. Furthermore, the vaccine was well-tolerated in mice, and the results of this study show great promise at progressing forward into clinical applications.

Chapter 3 described the production and application of Qβ VLPs displaying genetically-encoded protein extensions for applications in cellular targeting and therapeutic delivery. Incorporation of the Fc-binding Z-domain[8] as a C-terminal extension of the coat protein allowed for the production of particles that could be targeted against specific cell surface markers by virtue of antibodies arrayed on the particle surface. As a proof-of-concept, we first chose to focus our efforts in this area on the selective elimination of human pluripotent stem cells (hPSCs) *in vitro*. Residual hPSCs in transplantation cultures are one of the primary hindrances towards advancing stem cell therapies forward into the clinic, as the immortal nature of these cells can lead to the formation of teratomas *in vivo*.[9–11] Leveraging the specificity of antibodies as targeting moieties, we first labeled VLPs with antibodies against a glycan target (SSEA-5) that is specifically expressed on the surface of undifferentiated hPSCs.[12] Particles bearing this antibody were capable of selectively targeting hPSC colonies co-cultured with dermal fibroblasts even at low nanomolar concentrations; given the high selectivity of this system, we next encapsulated cytosine deaminase within the VLP to mediate targeted

prodrug therapy.[13] Administration of these particles followed by treatment with the prodrug 5-fluorocytosine (5-FC) induced cell death only in the hPSCs, with no detectable cell death in the surrounding fibroblasts. Finally, to test this system as it would be applied in a clinical setting, hPSCs were differentiated into cardiomyocytes, and the differentiation culture was treated with the VLP/prodrug in the same manner. No residual stem cells were detected following treatment, and differentiated cardiomyocytes exhibited no negative side effects from exposure to the treatment.

This platform proved to be incredibly modular, allowing for simple exchange of packaged proteins and/or displayed antibodies to mediate different functions or delivery to different cell types. Another avenue that was explored using this technology was the selective targeting of cancer cells expressing HER2, a common cancer marker that has been well-validated with antibody-based therapeutics.[14–16] Display of antibodies against HER2 allowed for the selective delivery of Qβ VLPs to these cells; furthermore, delivery of cytosine deaminase *in vitro* also mediated prodrug-induced cytotoxicity in a selective manner. The modularity of this platform shows great promise at translating into several realms of clinically relevant applications.

The first two chapters of this work focused on the power of genetic manipulation to mediate display of peptide and protein domains on the surface of Qβ VLPs for different applications in medicine; Chapter 4 detailed the chemical modification of VLPs with small molecules to modulate cellular uptake and trafficking. Macrolide antibiotics have been well-documented to accumulate in phagocytic cells, which has directed their distribution into tissues from the bloodstream.[17,18] In this work, we developed a series of Qβ macrolide conjugates in order to enhance uptake in macrophages and direct particles

to the lungs as a proof-of-concept for pulmonary drug delivery. VLP-macrolide conjugates showed enhanced uptake by macrophages *in vitro*, with particles displaying azithromycin exhibiting the greatest effect. Macrophages treated with these conjugates exhibited activations towards an M2b phenotype,[19] indicating that these materials may have some therapeutic potential in altering macrophage activation states; this stands in contrast to previous reports with macrolide-modified gold nanorods, which were shown to stimulate activation towards a cytotoxic phenotype in macrophages.[20] More importantly, azithromycin-modified VLPs accumulated in the lungs within 2 hours of systemic administration, demonstrating these materials could potentially be employed as agents for pulmonary drug delivery through a route other than inhalation.

While the development of targeted therapeutics is an admirable goal, one must not overlook the innate defenses of the body that work to clear foreign materials, including drug delivery vehicles, from systemic circulation. The attachment of hydrophilic polymer chains to the surface of protein-based therapeutics has been commonly employed to mitigate recognition by the immune system and prolong circulation lifetimes,[21–23] but there have been no comprehensive studies investigating the performance of these materials in relation to (polyethylene)glycol (PEG). Chapter 5 details efforts to fully characterize the immune response to protein-polymer hybrid materials using Qβ VLPs modified with different polymer architectures (POEGMA, PMAG, PEG) at different chain lengths and densities. Initial screenings with monoclonal antibodies against the coat protein *in vitro* showed decreased recognition with increasing chain length as well as polymer loading. The humoral immune response *in vivo* is much more complex, yet still bears distinct correlations with polymer chain length as well as degree of modification.

Mice immunized with these conjugates developed significantly lower titers than mice immunized with unmodified VLPs; however, the apparent seroreactivity (or observed strength of binding) decreased with increasing polymer chain length. Furthermore, VLPs bearing more polymer chains gave rise to antibodies with weaker avidities, suggesting that the epitope repertoire may be influenced by surface accessibility in these constructs. The results from this survey will help inform on the design of polymer-modified materials, as well as the overall factors governing antibody responses to protein-polymer materials.

Finally, Chapter 6 returned to the use of genetically-encoded peptide domains in order to accomplish shielding of PP7 VLPs from phagocytic uptake. The body is capable of discriminating foreign materials by recognition of CD47 on the surface of its own cells,[24] and this interaction have been exploited to prolong the circulation of microparticles *in vivo* using a minimal peptide (Self) from the CD47 binding interface.[25] Building on this study, we sought to genetically display the Self peptide on the surface of PP7 VLPs in a controllable fashion, as PP7 offers a greater tolerance to the incorporation of genetic extensions and can display peptides on every subunit if needed.[26] Particles displaying the Self peptide exhibited decreased uptake by macrophages *in vitro*, but these constructs failed to significantly diminish antibody responses generated against PP7 in immunized mice. Overall, it appears that display of the Self peptide may be useful for mitigating phagocytic clearance but does not have an effect on the generation of an adaptive response against the VLP.

## 7.2. Future Directions

Collectively, the body of work detailed in this thesis presents many interesting and exciting opportunities for further exploration. The vaccines developed in Chapter 2 proved to be very effective at giving rise to C5-specific antibody responses that were capable of ameliorating C5 activity and hemoglobinuria. In order to fully establish the safety of this vaccine, a challenge study with a non-lethal dose of bacteria should be conducted to definitively ensure that innate immunity has not been compromised due to knockdown of C5 activity. Pursuant to translating this technology into the clinic, particles displaying human homologs of the same peptide epitopes identified in this study could also be designed and screened through *in vitro* immunization of human peripheral mononuclear cells before eventually translating into clinical studies.[27] Finally, the ability of Qβ VLPs to serve as an effective vaccine platform against genetically encoded self-antigens presents many opportunities to apply this design strategy in treating other autoimmune disorders.

The platform developed in Chapter 3 for the targeted delivery of prodrug-converting enzymes offers a number of different avenues for exploration. As a direct supplement to the work conducted in these initial studies, an assessment of teratoma formation *in vivo* could be conducted by transplanting differentiated cardiomyocytes into mice following treatment of the differentiation culture with SSEA-5-targeted VLPs and subsequent dosing with 5-FC. With respect to targeting HER2-positive cancers, validation of specific killing in co-culture can be screened, followed by application of targeted killing in established mouse tumor models. As previously mentioned, the modularity of this system lends itself to numerous applications in targeting disease – the

ability to exchange the targeting antibody on the particle surface and the enzyme packaged on the interior allows for the generation of particles with a wide range of biological activities that can be delivered to various cell types.

The Qβ-macrolide conjugates developed in Chapter 4 offer an interesting platform for applications in pulmonary drug delivery. Confirmation of delivery to pulmonary macrophages via histological studies should be undertaken, but more importantly, loading of these particles with a drug and screening for the treatment of respiratory infections could prove to be incredibly useful for clinical applications. Most drug delivery routes for addressing the lung involve inhalation,[28] with very few reports of systemic administration for delivery to the lung. Further study on the activation state of treated macrophages *in vivo* would be highly beneficial, as this data would inform on the potential of these conjugates to modulate the immunological fate of these cells.

In addition to having the ability to specifically deliver particles to tissues or cells as desired, shielding these constructs from recognition and clearance by the immune system is another important goal. The efficacy of drug delivery vehicles depends largely on their ability to circulate for prolonged periods of time, in addition to directing delivery to a specific subset of cells. Our survey of different polymer architectures covalently conjugated to the Qβ VLP could be greatly supplemented through structural analysis of the attached polymer chains and determination of their conformation in solution. Furthermore, the distinct differences in the antibody responses generated *in vivo* warrant a more in-depth study of the antibody repertoires and how they correlate with the physical properties of the protein-polymer conjugates. Isolation of individual B-cells and determination of epitope diversity and affinities in the population will help further

elucidate the influence of polymer chain length and loading density on the humoral response against protein conjugates.

Our exploratory studies displaying the Self peptide on PP7 VLPs to mitigate phagocytosis showed promising results that can be readily explored for applications in drug delivery. The tolerance for PP7 for peptide extensions will allow the correlation between peptide display density and phagocytosis to be explored *in vitro*, and it will be extremely interesting to see if these particles display extended circulation half-lives *in vivo* due to their inhibition of phagocytic uptake.

Finally, it will be incredibly interesting to combine multiple facets of these studies into the development of Qβ VLPs with novel properties. It will be paramount to combine the targeting moieties discussed in Chapters 3 and 4 with polymer modifications (Chapter 5) to reduce particle clearance and immunogenicity while imparting targeting capabilities. It is worth noting that the chemical attachment of targeting molecules (such as macrolides) can be accomplished on the pendant ends of polymer chains equipped with the proper functionalities, so that polymer modification does not impede the targeting moiety. Furthermore, the ability to genetically display Self peptides on the surface of the VLP in order to mitigate clearance (Chapter 6) leaves reactive functional groups on the coat protein fully addressable for modification with therapeutics or other molecular cargo.

Overall, the work detailed in each chapter of this thesis is focused in a unique area that can address individual problems in medicine, but when brought together, the results lay the foundation for even greater work to be accomplished in the future.

## 7.3. References


(1) Risitano, A. M. Paroxysmal Nocturnal Hemoglobinuria and Other Complement-Mediated Hematological Disorders. *Immunobiology* **2012**, *217*, 1080–1087.

(2) Coyle, D.; Cheung, M. C.; Evans, G. A. Opportunity Cost of Funding Drugs for Rare Diseases: The Cost-Effectiveness of Eculizumab in Paroxysmal Nocturnal Hemoglobinuria. *Med. Decis. Mak.* **2014**, *34*, 1016–1029.

(3) Del Guercio, M. F.; Alexander, J.; Kubo, R. T.; Arrhenius, T.; Maewal, A.; Appella, E.; Hoffman, S. L.; Jones, T.; Valmori, D.; Sakaguchi, K.; *et al.* Potent Immunogenic Short Linear Peptide Constructs Composed of B Cell Epitopes and Pan DR T Helper Epitopes (PADRE) for Antibody Responses in Vivo. *Vaccine* **1997**, *15*, 441–448.

(4) Röhn, T. A.; Jennings, G. T.; Hernandez, M.; Grest, P.; Beck, M.; Zou, Y.; Kopf, M.; Bachmann, M. F. Vaccination against IL-17 Suppresses Autoimmune Arthritis and Encephalomyelitis. *Eur. J. Immunol.* **2006**, *36*, 2857–2867.

(5) Röhn, T. A.; Bachmann, M. F. Vaccines against Non-Communicable Diseases. *Current Opinion in Immunology*, 2010, *22*, 391–396.

(6) Spohn, G.; Schori, C.; Keller, I.; Sladko, K.; Sina, C.; Guler, R.; Schwarz, K.; Johansen, P.; Jennings, G. T.; Bachmann, M. F. Preclinical Efficacy and Safety of an Anti-IL-1β Vaccine for the Treatment of Type 2 Diabetes. *Mol. Ther. - Methods Clin. Dev.* **2014**, *1*, 14048.

(7) Tissot, A. C.; Spohn, G.; Jennings, G. T.; Shamshiev, A.; Kurrer, M. O.; Windak, R.; Meier, M.; Viesti, M.; Hersberger, M.; Kundig, T. M.; *et al.* A VLP-Based Vaccine against Interleukin-1a Protects Mice from Atherosclerosis. *Eur. J. Immunol.* **2013**, *43*, 716–722.

(8) Braisted, A. C.; Wells, J. A. Minimizing a Binding Domain from Protein A. *Proc. Natl. Acad. Sci. USA* **1996**, *93*, 5688–5692.

(9) Lee, M. O.; Moon, S. H.; Jeong, H. C.; Yi, J. Y.; Lee, T. H.; Him, S. H.; Rhee, Y. H.; Lee, S. H.; Oh, S. J.; Lee, M. Y.; *et al.* Inhibition of Pluripotent Stem Cell-Derived Teratoma Formation by Small Molecules. *Proc Natl Acad Sci U S A* **2014**, *110*.

(10) Zhong, B.; Watts, K. L.; Gori, J. L.; Wohlfahrt, M. E.; Enssle, J.; Adair, J. E.; Kiem, H. P. Safeguarding Nonhuman Primate iPS Cells with Suicide Genes. *Mol. Ther.* **2011**, *19*, 1667–1675.

(11) Malecki, M. "Above All, Do No Harm": Safeguarding Pluripotent Stem Cell Therapy against Iatrogenic Tumorigenesis. *Stem Cell Res. Ther.* **2014**, *5*, 73.

(12) Tang, C.; Lee, A. S.; Volkmer, J.-P. P.; Sahoo, D.; Nag, D.; Mosley, A. R.; Inlay, M. A.; Ardehali, R.; Chavez, S. L.; Pera, R. R.; *et al.* An Antibody against SSEA-5 Glycan on Human Pluripotent Stem Cells Enables Removal of Teratoma-Forming Cells. *Nat. Biotechnol.* **2011**, *29*, 829–834.

(13) Fiedler, J. D.; Brown, S. D.; Lau, J.; Finn, M. G. RNA-Directed Packaging of Enzymes within Virus-Like Particles. *Angew. Chemie Int. Ed.* **2010**, *49*, 9648–9651.

(14) Teplinsky, E.; Muggia, F. Targeting HER2 in Ovarian and Uterine Cancers: Challenges and Future Directions. *Gynecol. Oncol.* **2014**, *135*, 364–370.

(15) Tagliabue, E.; Balsari, A.; Campiglio, M.; Pupa, S. M. HER2 as a Target for Breast Cancer Therapy. *Expert Opin. Biol. Ther.* **2010**, *10*, 711–724.

(16) Subik, K.; Lee, J. F.; Baxter, L.; Strzepek, T.; Costello, D.; Crowley, P.; Xing, L.; Hung, M. C.; Bonfiglio, T.; Hicks, D. G.; *et al.* The Expression Patterns of ER, PR, HER2, CK5/6, EGFR, KI-67 and AR by Immunohistochemical Analysis in Breast Cancer Cell Lines. *Breast Cancer Basic Clin. Res.* **2010**, *4*, 35–41.

(17) Bosnar, M.; Kelnerić, Ž.; Munić, V.; Eraković, V.; Parnham, M. J. Cellular Uptake and Efflux of Azithromycin, Erythromycin, Clarithromycin, Telithromycin, and Cethromycin. *Antimicrob. Agents Chemother.* **2005**, *49*, 2372–2377.

(18) Hand, W. L.; Hand, D. L. Characteristics and Mechanisms of Azithromycin Accumulation and Efflux in Human Polymorphonuclear Leukocytes. *Int. J. Antimicrob. Agents* **2001**, *18*, 419–425.

(19) Martinez, F. O.; Gordon, S. The M1 and M2 Paradigm of Macrophage Activation: Time for Reassessment. *F1000Prime Rep.* **2014**, *6*.

(20) Dreaden, E. C.; Mwakwari, S. C.; Austin, L. A.; Kieffer, M. J.; Oyelere, A. K.; El-Sayed, M. A. Small Molecule-Gold Nanorod Conjugates Selectively Target and Induce Macrophage Toxicity towards Breast Cancer Cells. *Small* **2012**, *8*, 2819–2822.

(21) Han, J.; Zhao, D.; Li, D.; Wang, X.; Jin, Z.; Zhao, K. Polymer-Based Nanomaterials and Applications for Vaccines and Drugs. *Polymers* , 2018, *10*.

(22) Storm, G.; Belliot, S. O.; Daemen, T.; Lasic, D. D. Surface Modification of Nanoparticles to Oppose Uptake by the Mononuclear Phagocyte System. *Advanced Drug Delivery Reviews*, 1995, *17*, 31–48.

(23) Rother, M.; Nussbaumer, M. G.; Renggli, K.; Bruns, N. Protein Cages and Synthetic Polymers: A Fruitful Symbiosis for Drug Delivery Applications, Bionanotechnology and Materials Science. *Chem. Soc. Rev.* **2016**, *45*, 6213–6249.

(24) Oldenborg, P. A.; Zheleznyak, A.; Fang, Y. F.; Lagenaur, C. F.; Gresham, H. D.; Lindberg, F. P. Role of CD47 as a Marker of Self on Red Blood Cells. *Science (80-. ).* **2000**, *288*, 2051–2054.

(25) Rodriguez, P. L.; Harada, T.; Christian, D. A.; Pantano, D. A.; Tsai, R. K.; Discher, D. E. Minimal "Self" peptides That Inhibit Phagocytic Clearance and Enhance Delivery of Nanoparticles. *Science (80-. ).* **2013**, *339*, 971–975.

(26) Caldeira, J. C.; Peabody, D. S. Stability and Assembly in Vitro of Bacteriophage PP7 Virus-like Particles. *J Nanobiotechnology* **2007**, *5*, 10.

(27) Tomimatsu, K.; Shirahata, S. Antigen-Specific in Vitro Immunization: A Source for Human Monoclonal Antibodies. *Methods Mol. Biol.* **2014**, *1060*, 297–307.

(28) Lee, W.-H.; Loo, C.-Y.; Traini, D.; Young, P. M. Nano- and Micro-Based Inhaled Drug Delivery Systems for Targeting Alveolar Macrophages. *Expert Opin. Drug Deliv.* **2015**, *12*, 1009–1026.

## Appendix A

## Complete list of primers

Note: All sequences listed in 5' to 3' directionality

**Primers for molecular cloning**

**C5-F:**

TCTACTGGATCCGCTTTCAACGAATGCTGC

**C5-R:**

TCTACTCTCGAGTTACAGCTGTTTACGTTTCGG

**P2-PADRE-F:**

TCTACTCCATGGCAAAATTAGAGACTGTTACTTTAGGTAACATCGGGAAAGA

TGGA

**P2-PADRE-R:**

TCTACTCTCGAGTTAGCTACCGCTGGTGCTTTCTTCTTTGCTCGGTTTATAGCT

TGCACCGGATCCTGCTGCT

**P2-SCR-R:**

ATTTCTCTCGAGTTATTTGCTATAGCTTTTGCTGGTTTCTTCGCTACCTGCCGG

GCTACCGGATCCTGCTGCTGCTTTCAG

**PP7-SELF-F:**

GGATCCATGTCGAAAACCAT

**PP7-SELF-R:**

TTATTTTAACTCGATAATAGTTTCTCCTTCGCGGGTTAACTCCGTAACTTCGGA

GGTGTAATTGCCGGCGCCGCTTTCGCTCGCGCCACCGCGGCCCA

**Primers for qRT-PCR**

**cTnT-F:**

GCGGGTCTTGGAGACTTTCT

**cTnT-R:**

TTCGACCTGCAGGAGAAGTT

**NKX2-5-F:**

CTGTCTTCTCCAGCTCCACC

**NKX2-5-R:**

TTCTATCCACGTGCCTACAGC

**MYH6-F:**

CTTCTCCACCTTAGCCCTGG

**MYH6-R:**

GCTGGCCCTTCAACTACAGA

**MYH7-F:**

CGCACCTTCTTCTCTTGCTC

**MYH7-R:**

GAGGACAAGGTCAACACCCT

**MYL2-F:**

CGTTCTTGTCAATGAAGCCA

**MYL2-R:**

CAACGTGTTCTCCATGTTCG

**MYL7-F:**

CTTGTAGTCGATGTTCCCCG

**MYL7-R:**

TCAAGCAGCTTCTCCTGACC

**GAPDH-F:**

CTGGGCTACACTGAGCACC

**GAPDH-R:**

AAGTGGTCGTTGAGGGCAATG

## Appendix B

## Coding regions for protein production

The sequences listed in this section were inserted into plasmid backbones for expression (as indicated in the main text) using restriction enzymes and standard molecular cloning techniques. Coding sequences for extensions are underlined.

**Qβ coat protein:**

ATGGCAAAATTAGAGACTGTTACTTTAGGTAACATCGGGAAAGATGGAAAAC
AAACTCTGGTCCTCAATCCGCGTGGGGTAAATCCCACTAACGGCGTTGCCTC
GCTTTCACAAGCGGGTGCAGTTCCTGCGCTGGAGAAGCGTGTTACCGTTTCGG
TATCTCAGCCTTCTCGCAATCGTAAGAACTACAAGGTCCAGGTTAAGATCCA
GAACCCGACCGCTTGCACTGCAAACGGTTCTTGTGACCCATCCGTTACTCGCC
AGGCATACGCTGACGTGACCTTTTCGTTCACGCAGTATAGTACCGATGAGGA
ACGAGCTTTTGTTCGTACAGAGCTTGCTGCTCTGCTCGCTAGTCCTCTGCTGA
TCGATGCTATTGATCAGCTGAACCCAGCGTATTAA

**C5 cleavage site (C-terminal extension):**

ATGGCAAAATTAGAGACTGTTACTTTAGGTAACATCGGGAAAGATGGAAAAC
AAACTCTGGTCCTCAATCCGCGTGGGGTAAATCCCACTAACGGCGTTGCCTC
GCTTTCACAAGCGGGTGCAGTTCCTGCGCTGGAGAAGCGTGTTACCGTTTCGG
TATCTCAGCCTTCTCGCAATCGTAAGAACTACAAGGTCCAGGTTAAGATCCA
GAACCCGACCGCTTGCACTGCAAACGGTTCTTGTGACCCATCCGTTACTCGCC
AGGCATACGCTGACGTGACCTTTTCGTTCACGCAGTATAGTACCGATGAGGA
ACGAGCTTTTGTTCGTACAGAGCTTGCTGCTCTGCTCGCTAGTCCTCTGCTGA
TCGATGCTATTGATCAGCTGAACCCAGCGTATGCATATGGCGGTGGATCCGCT
TTCAACGAATGCTGCACCATCGCTAACAAAATCCGTAAAGAATCTCCGCACA
AACCGGTTCAGCTGGGTCGTATCCACATCAAAACCCTGCTGCCGGTTATGAA
AGCTGACATCCGTTCTTACTTCCCGGAATCTTGGCTGTGGGAAATCCACCGTG
TTCCGAAACGTAAACAGCTGTAA

**PADRE-P2 (C-terminal extension):**

ATGGCAAAATTAGAGACTGTTACTTTAGGTAACATCGGGAAAGATGGAAAAC
AAACTCTGGTCCTCAATCCGCGTGGGGTAAATCCCACTAACGGCGTTGCCTC
GCTTTCACAAGCGGGTGCAGTTCCTGCGCTGGAGAAGCGTGTTACCGTTTCGG
TATCTCAGCCTTCTCGCAATCGTAAGAACTACAAGGTCCAGGTTAAGATCCA
GAACCCGACCGCTTGCACTGCAAACGGTTCTTGTGACCCATCCGTTACTCGCC
AGGCATACGCTGACGTGACCTTTTCGTTCACGCAGTATAGTACCGATGAGGA

ACGAGCTTTTGTTCGTACAGAGCTTGCTGCTCTGCTCGCTAGTCCTCTGCTGA
TCGATGCTATTGATCAGCTGAACCCAGCGTATGCATATGGCGGTGCGAAATTT
GTGGCGGCGTGGACCCTGAAAGCGGCGGCGGGCAGCGGCGCGAGCTATAAA
CCGAGCAAAGAAGAAAGCACCAGCGGCAGCTAA

**ZZ-domain (C-terminal extension):**

ATGGCAAAATTAGAGACTGTTACTTTAGGTAACATCGGGAAAGATGGAAAAC
AAACTCTGGTCCTCAATCCGCGTGGGGTAAATCCCACTAACGGCGTTGCCTC
GCTTTCACAAGCGGGTGCAGTTCCTGCGCTGGAGAAGCGTGTTACCGTTTCGG
TATCTCAGCCTTCTCGCAATCGTAAGAACTACAAGGTCCAGGTTAAGATCCA
GAACCCGACCGCTTGCACTGCAAACGGTTCTTGTGACCCATCCGTTACTCGCC
AGGCATACGCTGACGTGACCTTTTCGTTCACGCAGTATAGTACCGATGAGGA
ACGAGCTTTTGTTCGTACAGAGCTTGCTGCTCTGCTCGCTAGTCCTCTGCTGA
TCGATGCTATTGATCAGCTGAACCCAGCGTATGGATCCGGTGGCGCGAGCGA
AAGCGGCGCCATGGTTGACAACAAATTCAACAAAGAACAGCAGAACGCTTTC
TACGAAATCCTGCACCTGCCGAACCTGAACGAAGAACAGCGTAACGCTTTCA
TCCAGTCTCTGAAAGACGACCCGTCTCAGTCTGCTAACCTGCTGGCTGAAGCT
AAAAAACTGAACGACGCTCAGGCTCCGAAAGCCATGGTTGACAACAAATTCA
ACAAAGAACAGCAGAACGCTTTCTACGAAATCCTGCACCTGCCGAACCTGAA
CGAAGAACAGCGTAACGCTTTCATCCAGTCTCTGAAAGACGACCCGTCTCAG
TCTGCTAACCTGCTGGCTGAAGCTAAAAAACTGAACGACGCTCAGGCTCCGA
AATAA

**rev-tagged EGFP:**

ATGGAGCTGACAAGACAGGCACGTCGAAATCGCAGGAGACGATGGCGGGAA
CGTCAAAGGGGCTCGGGTGGCGAGCTCTCGGCCGCCATGGTTTCTAAAGGTG
AAGAACTGTTCACCGGTGTTGTTCCGATCCTGGTTGAACTGGACGGTGACGTT
AACGGTCACAAATTCTCTGTTCGTGGTGAAGGTGAAGGTGACGCTACCAACG
GTAAACTGACCCTGAAATTCATCTGCACCACCGGTAAACTGCCGGTTCCGTG
GCCGACCCTGGTTACCACCCTGACCTACGGTGTTCAGTGCTTCTCTCGTTACC
CGGACCACATGAAACAGCACGACTTCTTCAAATCTGCTATGCCGGAAGGTTA
CGTTCAGGAACGTACCATCTCTTTCAAAGACGACGGTACCTACAAAACCCGT
GCTGAAGTTAAATTCGAAGGTGACACCCTGGTTAACCGTATCGAACTGAAAG
GTATCGACTTCAAAGAAGACGGTAACATCCTGGGTCACAAACTGGAATACAA
CTTCAACTCTCACAACGTTTACATCACCGCTGACAAACAGAAAAACGGTATC
AAAGCTAACTTCAAAATCCGTCACAACGTTGAAGACGGTTCTGTTCAGCTGG
CTGACCACTACCAGCAGAACACCCCGATCGGTGACGGTCCGGTTCTGCTGCC
GGACAACCACTACCTGTCTACCCAGTCTGTTCTGTCTAAAGACCCGAACGAA
AAACGTGACCACATGGTTCTGCTGGAATTCGTTACCGCTGCTGGTATCACCCT
GGGTATGGACGAACTGTACAAATAA

**rev-tagged CD:**

ATGGAGCTGACAAGACAGGCACGTCGAAATCGCAGGAGACGATGGCGGGAA
CGTCAAAGGGGCTCGGGTGGCGAGCTCTCGGCCGCCATGGTTACCGGTGGTA
TGGCTTCTAAATGGGACCAGAAAGGTATGGACATCGCTTACGAAGAAGCTCT
GCTGGGTTACAAAGAAGGTGGTGTTCCAATTGGTGGTTGCCTGATCAACAAC
AAAGACGGTTCTGTTCTGGGTCGTGGTCACAACATGCGTTTCCAGAAAGGTTC
TGCTACCCTGCACGGTGAAATCTCTACCCTGGAAAACTGCGGTCGTCTGGAA
GGTAAAGTTTACAAAGACACCACCCTGTACACCACCCTGTCTCCGTGCGACA
TGTGCACCGGTGCTATCATCATGTACGGTATCCCGCGTTGCGTTATCGGTGAA
AACGTTAACTTCAAATCTAAAGGTGAAAAATACCTGCAGACCCGTGGTCACG
AAGTTGTTGTTGTTGACGACGAACGTTGCAAAAAACTGATGAAACAGTTCAT
CGACGAACGTCCGCAGGACTGGTTCGAAGACATCGGTGAACTCGAGTCTGGT
AAAGAAACCGCTGCTGCGAAATTTGAACGCCAGCACATGGACTCGTCTACTA
GCGCAGCTTAATTAACCTAGGCTGCTGCCACCGCTGAGCAATAA

**rev-tagged mCherry:**

ATGGAGCTGACAAGACAGGCACGTCGAAATCGCAGGAGACGATGGCGGGAA
CGTCAAAGGGGCTCGGGTGGCGAGCTCTCGGCCGCCATGGTGAGCAAGGGC
GAGGAGGATAACATGGCCATCATCAAGGAGTTCATGCGCTTCAAGGTGCACA
TGGAGGGCTCCGTGAACGGCCACGAGTTCGAGATCGAGGGCGAGGGCGAGG
GCCGCCCCTACGAGGGCACCCAGACCGCCAAGCTGAAGGTGACCAAGGGTG
GCCCCCTGCCCTTCGCCTGGGACATCCTGTCCCCTCAGTTCATGTACGGCTCC
AAGGCCTACGTGAAGCACCCCGCCGACATCCCCGACTACTTGAAGCTGTCCT
TCCCCGAGGGCTTCAAGTGGGAGCGCGTGATGAACTTCGAGGACGGCGGCGT
GGTGACCGTGACCCAGGACTCCTCCCTGCAAGACGGCGAGTTCATCTACAAG
GTGAAGCTGCGCGGCACCAACTTCCCCTCCGACGGCCCCGTAATGCAGAAGA
AGACCATGGGCTGGGAGGCCTCCTCCGAGCGGATGTACCCCGAGGACGGCGC
CCTGAAGGGCGAGATCAAGCAGAGGCTGAAGCTGAAGGACGGCGGCCACTA
CGACGCTGAGGTCAAGACCACCTACAAGGCCAAGAAGCCCGTGCAGCTGCCC
GGCGCCTACAACGTCAACATCAAGTTGGACATCACCTCCCACAACGAGGACT
ACACCATCGTGGAACAGTACGAACGCGCCGAGGGCCGCCACTCCACCGGCG
GCATGGACGAGCTGTACAAGTAA

**PP7 coat protein (fused dimer):**

ATGTCGAAAACCATCGTCCTGTCCGTGGGCGAAGCAACCCGCACCCTGACCG
AAATCCAATCTACCGCAGACCGCCAAATCTTTGAAGAAAAAGTGGGTCCGCT
GGTCGGTCGTCTGCGTCTGACCGCCTCTCTGCGTCAGAACGGCGCGAAAACG
GCCTATCGCGTCAATCTGAAACTGGATCAAGCAGACGTGGTTGATTGCAGCA
CCTCTGTTTGTGGTGAACTGCCGAAAGTGCGTTATACGCAGGTTTGGTCACAT
GACGTCACCATTGTGGCAAACTCGACGGAAGCTAGTCGCAAATCCCTGTACG
ATCTGACCAAATCCCTGGTGGCGACCTCTCAAGTGGAAGACCTGGTGGTGAA

CCTGGTGCCGCTGGGCCGCGCATATGGCGGTTCGAAAACCATCGTCCTGTCC
GTGGGCGAAGCAACCCGCACCCTGACCGAAATCCAATCTACCGCAGACCGCC
AAATCTTTGAAGAAAAAGTGGGTCCGCTGGTCGGTCGTCTGCGTCTGACCGC
CTCTCTGCGTCAGAACGGCGCGAAAACGGCCTATCGCGTCAATCTGAAACTG
GATCAAGCAGACGTGGTTGATTGCAGCACCTCTGTTTGTGGTGAACTGCCGA
AAGTGCGTTATACGCAGGTTTGGTCACATGACGTCACCATTGTGGCAAACTC
GACGGAAGCTAGTCGCAAATCCCTGTACGATCTGACCAAATCCCTGGTGGCG
ACCTCTCAAGTGGAAGACCTGGTGGTGAACCTGGTGCCGCTGGGCCGCTAA

**Self peptide (C-terminal extension):**

ATGTCGAAAACCATCGTCCTGTCCGTGGGCGAAGCAACCCGCACCCTGACCG
AAATCCAATCTACCGCAGACCGCCAAATCTTTGAAGAAAAAGTGGGTCCGCT
GGTCGGTCGTCTGCGTCTGACCGCCTCTCTGCGTCAGAACGGCGCGAAAACG
GCCTATCGCGTCAATCTGAAACTGGATCAAGCAGACGTGGTTGATTGCAGCA
CCTCTGTTTGTGGTGAACTGCCGAAAGTGCGTTATACGCAGGTTTGGTCACAT
GACGTCACCATTGTGGCAAACTCGACGGAAGCTAGTCGCAAATCCCTGTACG
ATCTGACCAAATCCCTGGTGGCGACCTCTCAAGTGGAAGACCTGGTGGTGAA
CCTGGTGCCGCTGGGCCGCGCATATGGCGGTTCGAAAACCATCGTCCTGTCC
GTGGGCGAAGCAACCCGCACCCTGACCGAAATCCAATCTACCGCAGACCGCC
AAATCTTTGAAGAAAAAGTGGGTCCGCTGGTCGGTCGTCTGCGTCTGACCGC
CTCTCTGCGTCAGAACGGCGCGAAAACGGCCTATCGCGTCAATCTGAAACTG
GATCAAGCAGACGTGGTTGATTGCAGCACCTCTGTTTGTGGTGAACTGCCGA
AAGTGCGTTATACGCAGGTTTGGTCACATGACGTCACCATTGTGGCAAACTC
GACGGAAGCTAGTCGCAAATCCCTGTACGATCTGACCAAATCCCTGGTGGCG
ACCTCTCAAGTGGAAGACCTGGTGGTGAACCTGGTGCCGCTGGGCCGCGGTG
GCGCGAGCGAAAGCGGCGCCGGCAATTACACCTCCGAAGTTACGGAGTTAAC
CCGCGAAGGAGAAACTATTATCGAGTTAAAATAA

## Appendix C

## Buffer compositions

**FACS buffer:** 5% fetal bovine serum, 2 mM EDTA in 1x PBS

**10x potassium phosphate buffer (1M):** 107.5 g dibasic potassium phosphate (anhydrous) and 52 g monobasic potassium phosphate (anhydrous) in 1 L of $H_2O$

**1x TBS:** 50 mM Tris-HCl, 150 mM NaCl, pH 7.6

**1x PBS:** 137 mM NaCl, 2.7 mM KCl, 4.3 mM $Na_2HPO_4$, 1.47 mM $KH_2PO_4$, pH 7.4

**PBST:** 1x PBS + 0.1% Tween 20